Constraints on Global Carbon Cycling, Basin Formation, and Early Animal Evolution During the Neoproterozoic and Early Cambrian

CONSTRAINTS ON GLOBAL CARBON CYCLING, BASIN FORMATION, AND EARLY ANIMAL EVOLUTION DURING THE NEOPROTEROZOIC AND EARLY CAMBRIAN

A dissertation presented

by

Emily Frances Smith

to

The Department of Earth and Planetary Sciences

in partial fulfillment of the requirements

for the degree of

Doctor of Philosophy

in the subject of

Earth and Planetary Sciences

Harvard University

Cambridge, Massachusetts

August 2015

CONSTRAINTS ON GLOBAL CARBON CYCLING, BASIN FORMATION, AND EARLY ANIMAL EVOLUTION DURING THE NEOPROTEROZOIC AND EARLY CAMBRIAN

ABSTRACT

Within this dissertation, I document different time intervals during the Neoproterozoic through the early Cambrian (1000 – 525 Ma), one of the most dynamic and non-uniformitarian intervals in the history of the Earth. This thesis focuses on two time periods of change within this time interval: 1) The pre-Cryogenian-Cryogenian transition (~800-635 Ma) and 2) the Ediacaran-Cambrian Transition (~551-525 Ma).

To begin, I use a combination of detailed mapping, regional stratigraphy, and geochronology to reinterpret the depositional and tectonic setting of the ~750-730 Ma Beck Spring Dolomite and its bounding units in Death Valley, California. Instead of being deposited in an interior seaway in a long-lived aulacogen as Rodinia rifted apart, I suggest that this unit was accommodated by strike-slip motion that could have represented a margin-wide event along the west coast of Laurentia. The true rift to drift did not occur until the latest Ediacaran to earliest Cambrian.

Late Ediacaran to early Cambrian datasets from the Great Basin in the western USA are integrated to refine the biological and environmental changes that occur across the Ediacaran-Cambrian Boundary. In my third chapter, two new horizons of exceptionally preserved Ediacaran fauna that include *Conotubus* and *Gaojiashania* are documented. These fossils were previously only known from South China. The *Conotubus* horizon occurs just below the most negative $\delta^{13}C$ values in the basal Cambrian $\delta^{13}C$ excursion, establishing it as the youngest Ediacaran fossil to date. These

fossils are placed into a high-resolution $\delta^{13}C$ chemostratigraphic framework, allowing for regional and global correlation. Three $\delta^{13}C$ chemostratigraphic curves from the Great Basin combined with five sections from Western Mongolia show that instead of a single, rapid $\delta^{13}C$ excursion at the Ediacaran-Cambrian Boundary, there is one broad excursion with more secondary structure than has been previously documented. Together, these data suggest the nadir of the $\delta^{13}C$ excursion is younger than 541 Ma and provide a new framework to interpret Ediacaran-Cambrian biostratigraphy, chemostratigraphy, and U/Pb ash ages globally.

The final chapter focuses on the earliest Cambrian in Southwest Mongolia. By using extensive field data, I construct a basin-wide facies model and age model for the Zavkhan Basin. I place the early Cambrian fossil horizons into this new framework and correlate the composite dataset from Mongolia with others globally. In doing so, I reinterpret the tempo and patterns of evolution during this critical interval in Earth history.

The following chapters cover diverse events in Earth history that better constrain topics ranging from the breakup of the supercontinent Rodinia to environmental change across the Ediacaran-Cambrian Boundary to rates of evolutionary change during the early Cambrian. All of these topics, however, are united by a multidisciplinary approach that combines original field observations with geochemical, geochronological, stratigraphic, and paleontological datasets to constrain the origin and timing of the coevolution of life and the environment in the deep past.

TABLE OF CONTENTS

LIST OF FIGURES

LIST OF TABLES

ACKNOWLEDGEMENTS

During my PhD, I have been supported by an inspiring and generous group of advisors, colleagues, technicians, administrators, and friends. Here is a too-short thanks to many who made my work and my graduate school experience possible, rewarding, and joyful.

I would like to begin by thanking my advisor, Francis Macdonald. After I had spent two years teaching English in Asia, he patiently reintroduced me to rocks. Over the course of my graduate studies, he spent months training me in the field. He answered question after question, sometimes the same one multiple times. He abided by and corrected my sometimes haphazard and flailing approach to research. He gave me the freedom to explore my own research ideas, even when that sometimes resulted in failure. And, with some trepidation, he handed over the keys to Reggie. His seemingly endless scientific creativity, openness, work ethic, and genuine enthusiasm for Earth history have truly inspired me. I want to thank him for being a tremendous advocate for me, I'm sure more times and in more ways than I even realize.

I would like to thank the other members of my oral and dissertation committees, Dan Schrag, Andy Knoll, Sujoy Mukhopadhyay, and Dave Johnston. Sujoy patiently led me through my first graduate class in geochemistry. I greatly appreciated his advice, approachability, and insight. Dan taught me more geochemistry, generously spent time working with me one-on-one, and allowed me open access to his lab. Much of this research would not have been possible without the scientific freedom that he gave me. He has been a shrewd advisor, knowing when I need a boost of confidence and when I need a dose of honest criticism. Andy has always offered an open door to discuss my fossils and

future. His comments are positive and encouraging while still helpful and insightful. Last but not least, I want to thank Dave for always making time to discuss my research, read my personal statements, and support me professionally. They all contributed greatly to my development as a scientist and to this document.

Additionally, Sara Pruss has acted as an unofficial advisor to me. She involved me in her research projects, helped me mentor Smith undergraduates, and always treated me like a colleague. Sara has been a tremendous mentor in a field where female field geologist role models are scarce. I am grateful and lucky to have her as a mentor, colleague, and friend.

This work and my development as a scientist benefitted greatly from others in the Macdonald Group. I owe a big thanks to all of them. Alan has been a source of inspiration, laughs, and verbal harassment. Thanks to him, I can now almost understand Scottish. I know very few biologists who can also identify as capable geochemists and geologists; Erik is one of them. I thank him for his careful questioning and for always taking the time to give me extremely thoughtful feedback. Athena always has a smile on her face and a corny joke to share. Her unapologetic enthusiasm for everything will always be contagious. Justin's critical eye, vivid stories, and tough questions have always been appreciated. Uyanga and I have worked closely for the past five years. From the Taishir to *tsuivan*, she has taught me much in the field and at Harvard. She has helped me navigate odd and unpredictable scenarios in Mongolia and commiserated with me about odd and unpredictable scenarios back here in Cambridge. Her knowledge, quiet strength, grit, and perseverance are inspiring. Much of my work in Mongolia would not have been possible without her and her family's help. I thank Blake for his boundless creativity, his

love of nature, and his pickles and beets. I thank Lyle for his shared enthusiasm of the Beck Mountains, Ediacaran caterpillars, and backgammon. Camille was a fantastic field assistant, diligent lab manager, and the best field camp can-shooter. Sarah and Camille oversaw the thankless, overwhelming job of moving, sorting, and organizing all of our samples in the basement, and I am very grateful to them for that.

There are many other colleagues, friends, and students – far too many to properly thank – that have contributed to this project. I thank Ben Black for his kindness, his odd sense of humor, and help with ArcGIS. Claire Bucholz has been a wonderful colleague and loyal friend. I thank Ryan Petterson, Tony Prave, and Carol Dehler for generously and openly sharing their maps, data, and knowledge of Death Valley with me. Kristin, Cori, Rowan, Zach, Maya, Greg, Andy, JC, Ben K., Ben C., Emma, Frasier, Sarah, Tom, Katie, Lauren, Eileen, Natalya, Phoebe, Ben, Meredith, Yanpeng, Christian, Harriet, Carling, Jacky, Tamara, Erik C., Eric M., Jocelyn, JT, Jenny, Rita, Shannon, Helen, Alex, Hannah, Cristi, Roger, and many more have been very supportive friends and colleagues. I would like to thank my office mates, old and current, for laughs and companionship. Sierra and Kathryn have been patient listeners, eager learners, and the best of friends.

Much of this work would not have been possible without the help of my many field assistants. I was lucky to have such tough and curious ones. For the Mongolia field work, I would like to thank Tanya Petach, Dan Bradley, Sarah Moon, Camille Dwyer, Ellen Smith, Ross Anderson, Gerelt Sarantuya, Jaka Chuluunbaatar, Munkh Delger, Munkh-Erdeen Jugder, Uchral Khuchitbaatar, and Otgo Dandar. I would like to especially thank Tanya Petach for her unwavering enthusiasm and positivity for two field seasons in Mongolia and three years in the Macdonald lab. I would like to thank our

drivers for their knowledge of local roads, their cooking, and their good humor. Mogi always chose the best camps, saved me in a flash flood, and snuck me into a protected national forest; Ama created outstanding meals out of subpar ingredients; and Ulzi always had a joke up his sleeve and helped me fashion sample bags out of plastic sheets when I ran out. For the field work in the western USA, I thank Frances Liu, Athena Eyster, Blake Hodgin for enduring snow storms, blistering heat, rattlesnakes, moths in our food, and the Gold Point mayor/sheriff/bartender with me. Without all of these people with me in the field, I would have been much lonelier, far less productive, and possibly not here to write this dissertation.

Greg Eischeid taught me how to use the Optima during my first year of graduate school, and, together with Sarah Manley, patiently endured four more years of my pestering questions and Optima challenges. I thank Mark Schmitz and Jim Crowley for welcoming me to the Geochronology Lab at Boise State University. Jim spent weeks carefully training me in the meticulous art of mounting, polishing, imaging, and dissolving zircons. I would also like to thank Susannah Porter and John Moore for graciously hosting me in Santa Barbara and very generously teaching me about small shelly fossils.

The Harvard EPS Department has a wonderfully supportive and interactive community, and this wouldn't be the case without the staff. I would like to especially thank Marisa Reilly for all the support she has given the Macdonald Group. Our research program would disintegrate without her. I am endlessly indebted to Sarah Colgan for making sure that I didn't accidentally drop out and for helping me work through the Harvard System, even if I deserved no such help. I would also like to thank Chenoweth

Moffat, Paul Kelley, Maryorie Grande, and all the others who make the EPS Department run so smoothly and work hard to create such a cohesive atmosphere.

I am grateful to the generous funding that made much of this work possible. I thank Harvard EPS and the National Science Foundation Graduate Research Fellowship for funding much of my graduate education and dissertation research. The NASA Astrobiology MIT node generously funded much of the work in Mongolia. I am grateful to the Harvard University Center for the Environment, which provided me with a financial fellowship for three semesters. I am grateful to the Amherst Clarke Fellowship for Geology, which helped buy field gear and provide financial support to some of the visiting Mongolian students.

I am grateful to James W. Hagadorn for inspiring my delight in fossils, the Beastie Boys, and desert adventures. Steve Sauter's enthusiasm for the Amherst Natural History Museum was infectious. He helped instill in me an enthusiasm for the natural world, the history of Amherst geology, and outreach. I thank my Amherst geology friends, especially Ariel Morales, Lidya Tarhan, and Alex Urquhart, for being devoted friends, mapping buddies, bunk mates, and curious learners. Our geology classes would not have been nearly as silly or interesting without you, and I probably would not have gone to graduate school had it not been for the joy you brought to our classes.

My Adams House community has been like family to me for the past three years. The House masters, tutors, elves, students, and staff have made my past three years infinitely richer and have made Cambridge a home away from home for me. Hilary, Yakir, and Fah showed me what it's like to live in wonder of science, notably through soap experiments and yogurt. And Betsy, Pascal, Marius, Maleka, Naomi, Phil, Jen,

Tegan, Andres, Meg, Chip, Aubry, Maryam, Arjun, Naseemah, Dami, Adam, Celeste, Joe, Kris, and Ted reminded me that there's also a huge world outside of science. Additionally, I thank Rachel for being a wonderful listener, roommate, and friend for the entire time I was in Boston. I thank the Palfreys and Sam Houston for generously allowing me to write up my dissertation in the oldest house in Cambridge and the most haunted basement room of Adams.

Thanks to my family for their constant love and support. I thank my parents for passing along their wonder of the natural world. Who knew all the hours spent playing in the backyard creek would lead to something more than perpetually grubby hands and skinned knees? I thank Andrew for always being my best backyard buddy and for his shared love of the outdoors. I thank Ellen for visiting and helping me in Mongolia. Ellen and Warren, I can't wait to see you two fly.

And finally, I owe a huge thanks to my fiancé, Amos. He has smuggled ashes out of China, spent a vacation feigning interest in Snowball Earth strata, and enthusiastically accepted dozens of my rock gifts over the years. He has encouraged me to spend months at a time in the field even though he knew I would rarely check in. I thank him for tolerating and embracing my inconsistencies, moods, wanderings, field gear, and everything else. Even after ten years, he continues to inspire me and help make me a stronger, more compassionate person.

CHAPTER 1: INTRODUCTION

The Neoproterozoic through the early Cambrian (1000 – 525 Ma) was one of the most dynamic and non-uniformitarian intervals in the history of the Earth (Fig. 1.1). Sediments from this time interval preserve changes that include: eukaryotic diversification (Knoll et al., 2006), the rise of the first animals (Love et al., 2009; Narbonne and Gehling, 2003), diversification in macroscopic, complex life (Budd and Jensen, 2000; Conway Morris and Peel, 1995; Erwin et al., 1997; Sepkoski and Schopf, 1992), a major tectonic reorganization (Hoffman, 1991; Li et al., 2008), instability in almost all geochemical cycles, a rise in atmospheric oxygen to near modern levels (Canfield et al., 2007; Scott et al., 2008), and multiple advances of ice sheets into equatorial land masses (Harland, 1964; Hoffman et al., 1998; Kirschvink, 1992). During the Neoproterozoic to early Cambrian, the surficial Earth transitioned from an environment that was in many ways hostile to most life forms to a hospitable one, more like the one that we live in today. The research in this dissertation is an effort to better constrain and understand the feedbacks between and mechanisms for environmental and biological change during this transitional era.

Our understanding of what happened globally during this time period is pieced together from a handful of regional studies. The accuracy of the global picture is limited by the accuracy of geologic data from any individual basin, an understanding of the local biases, and the precision with which these records are integrated. Two regions where expanded strata record these changes are western Mongolia and the western USA.

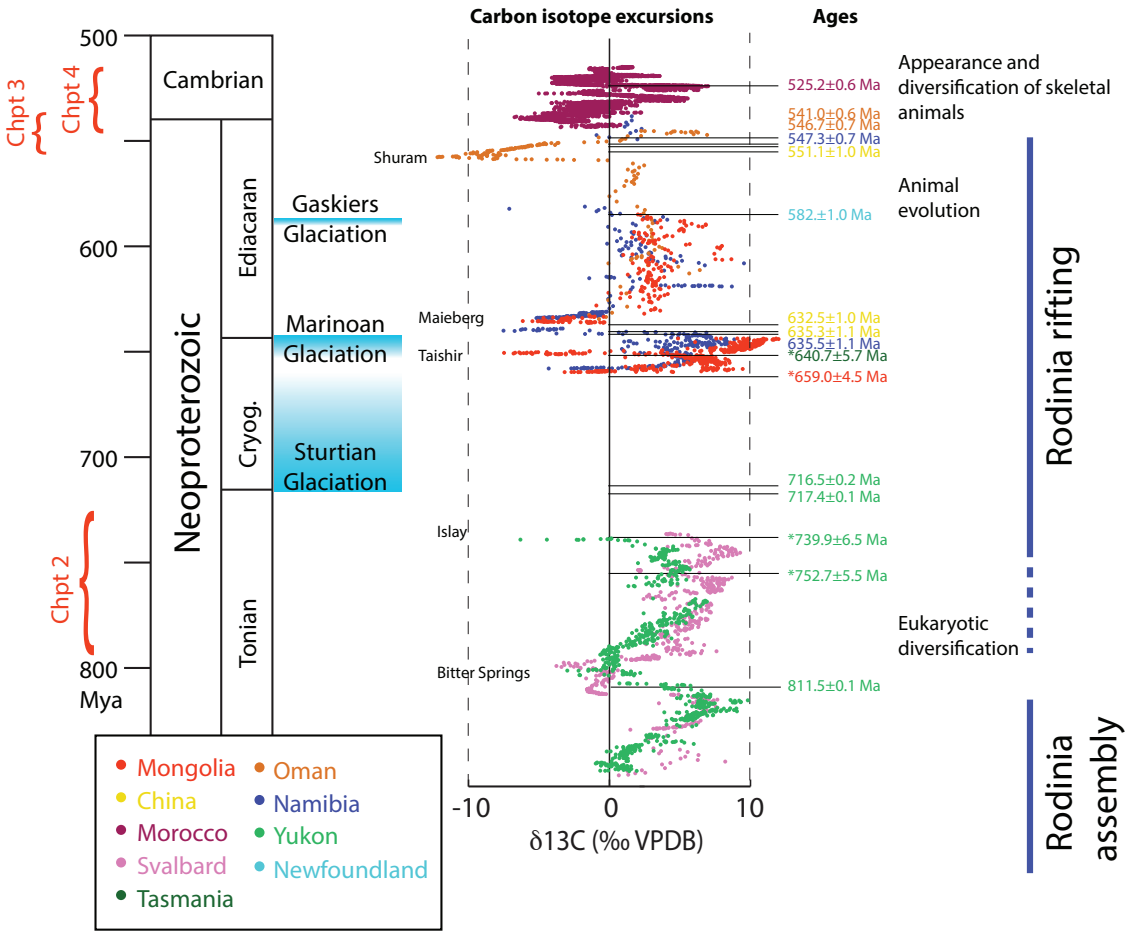

Figure 1.1. Summary timeline of late Proterozoic through early Phanerozoic Earth history

This timeline includes major evolutionary milestones, major glacial events, a composite chemostratigraphic curve (Halverson et al., 2005; Macdonald et al., 2009; Macdonald et al., 2010; Maloof et al., 2005), U/Pb ash and Re/Os (indicated with a star) ages (Bowring et al., 2003; Bowring et al., 2007; Condon et al., 2005; Hoffmann et al., 2004; Kendall et al., 2009; Macdonald et al., 2010; Maloof et al., 2005; Rooney et al., 2015; Strauss et al., 2014), and the timing of the formation and rifting of Rodinia. The time intervals that are the focus of this dissertation are indicated with red brackets on the left side of the figure.

In Mongolia, due to its relatively recent opening to the West, there are still many first order geologic questions to be addressed. The work done there is the culmination of three summer field seasons and months of lab work. It presents a basin-wide facies model that

is necessary to integrate this locality into the global picture. In the western USA, Death Valley and the White Inyo Mountains are two classic areas to study Neoproterozoic and early Paleozoic strata. In both Mongolia and the western USA, I revisited old sites and mapped out new ones to revise the regional stratigraphy and tectonic models for the Neoproterozoic through Cambrian.

Chapter 2 covers the tectonostratigraphic history of the Beck Spring Dolomite and its bounding units, the Horse Thief Springs Fm and Unit KP1 (or the Saratoga Spring Sandstone), which form part of the Pahrump Group, in Death Valley, California. The classic model is that the Pahrump Group, which records deposition from ~1100 to 635 Ma, was deposited in a long-lived aulacogen as the Neoproterozoic supercontinent, Rodinia, rifted apart. Using a combination of geologic mapping, regional stratigraphy, chemostratigraphy, and geochronology, I create new facies, depositional, and tectonic models for these units. The Beck Spring Dolomite and its bounding units were not deposited in a long-lived platform, but rapidly accumulated in a tectonically active basin during a narrow window from ~750-730 Ma. Following this, there was a local orogeny from ~730-660 Ma that can be attributed to local transpression. Thus, I suggest that instead of being deposited during a pulse of long-lived rifting, these units were accommodated by strike-slip motion along the western margin of Laurentia. The true rift to drift transition on this margin is not until the latest Ediacaran, as indicated by the subsidence history of strata along this margin.

In Chapter 3, I fast-forward ~200 million years to the real rift to drift that is recorded in Ediacaran-Cambrian strata in the Great Basin. Mt. Dunfee in Nevada is the only known locality globally that preserves *Cloudina*, other Ediacaran fossils,

Treptichnus pedum, and the basal Cambrian negative carbon isotope excursion in low-grade, thick, nearly continuous carbonate-dominated strata. In this chapter, the first detailed geologic map and composite section of this area are presented, precisely calibrating important biostratigraphic markers in a stratigraphic and chemostratigraphic framework. While mapping and measuring section, two horizons that contain exceptionally preserved Ediacaran body fossils that include *Gaojiashania* and *Conotubus*, were discovered. These two fossils were previously only known from South China. Data from eight sections in the Great Basin the Western Mongolia preserve the latest Ediacaran in expanded carbonate-dominated strata, demonstrating that there is more, globally reproducible secondary structure to the broad negative basal Cambrian carbon isotope excursion. By integrating datasets globally, I present a new biostratigraphic and chemostratigraphic framework for which to interpret and calibrate the Ediacaran-Cambrian transition.

Building on the results from Chapter 3, in Chapter 4 I present integrated datasets from a late Ediacaran to early Cambrian basin in Southwest Mongolia. In this chapter, I present a new geologic map of the Zavkhan Basin, a basin-wide facies model for the late Ediacaran through Cambrian strata in this basin, and a new age model. Using a combination of sequence- and chemostratigraphy, I correlate dozens of sections from across the basin, placing small shelly fossil horizons into a more robust spatial and temporal framework and revising the fossil first appearances of small shelly fossil genera in Mongolia. The integrated datasets from Southwest Mongolia are correlated with sections from Oman, Morocco, and South China, other sections globally with known absolute ages and chemostratigraphy. Using these new global correlations, I replot global

fossil first appearances during the earliest Cambrian. Although there are still three distinct pulses of fossil first appearances, as was shown in previous compilations, I suggest that this pattern is controlled largely by regional sedimentation and taphonomy rather than the rate of taxonomic origination. This chapter establishes the necessary geologic foundation for Mongolia to be a key locality to study the Ediacaran-Cambrian transition. It highlights the fact that, although great strides have been made in constraining relative and absolute environmental and biological changes during this major transition in Earth history, the tempo of origination and mechanisms for biological change are still poorly understood.

Although the data and interpretations from Chapter 2 are separated from those in Chapters 3 and 4 by ~200 million years, they are united by a motivation to understand the mechanisms and feedbacks for environmental, tectonic, and biological change in deep time. They are also united by an approach grounded in the careful collection of extensive field data. This approach allows for laboratory datasets – ranging from geochronological to geochemical to paleontological – to be placed into a geological and stratigraphic context. I have used this approach to construct integrated, basin-wide datasets that can in turn be used to provide insights into the coevolution of life and the environment of the late Proterozoic and early Cambrian Earth.

References

Bowring, S., Myrow, P., Landing, E., Ramezani, J. and Grotzinger, J., 2003. Geochronological constraints on terminal Neoproterozoic events and the rise of Metazoan, EGS-AGU-EUG Joint Assembly, pp. 13219.

Bowring, S.A., Grotzinger, J.P., Condon, D.J., Ramezani, J., Newall, M.J. and Allen, P.A., 2007. Geochronologic constraints on the chronostratigraphic framework of the Neoproterozoic Huqf Supergroup, Sultanate of Oman. American Journal of Science, 307(10): 1097-1145.

Budd, G.E. and Jensen, S., 2000. A critical reappraisal of the fossil record of the bilaterian phyla. Biological Reviews, 75(2): 253-295.

Canfield, D.E., Poulton, S.W. and Narbonne, G.M., 2007. Late-Neoproterozoic deep-ocean oxygenation and the rise of animal life. Science, 315(5808): 92-95.

Condon, D., Zhu, M.Y., Bowring, S., Wang, W., Yang, A.H. and Jin, Y.G., 2005. U-Pb ages from the Neoproterozoic Doushantuo Formation, China. Science, 308(5718): 95-98.

Conway Morris, S. and Peel, J., 1995. Articulated halkieriids from the Lower Cambrian of North Greenland and their role in early protostome evolution. Philosophical Transactions: Biological Sciences: 305-358.

Erwin, D., Valentine, J. and Jablonski, D., 1997. The Origin of Animal Body Plans Recent fossil finds and new insights into animal development are providing fresh perspectives on the riddle of the explosion of animals during the Early Cambrian. American Scientist, 85(2): 126-137.

Halverson, G.P., Hoffman, P.F., Schrag, D.P., Maloof, A.C. and Rice, A.H.N., 2005. Toward a Neoproterozoic composite carbon-isotope record. Geological Society of America Bulletin, 117(9-10): 1181-1207.

Harland, W., 1964. Critical evidence for a great infra-Cambrian glaciation. Geologische Rundschau, 54(1): 45-61.

Hoffman, P.F., 1991. Did the breakout of Laurentia turn Gondwanaland inside-out. Science, 252(5011): 1409-1412.

Hoffman, P.F., Kaufman, A.J., Halverson, G.P. and Schrag, D.P., 1998. A Neoproterozoic snowball earth. science, 281(5381): 1342-1346.

Hoffmann, K.H., Condon, D.J., Bowring, S.A. and Crowley, J.L., 2004. U-Pb zircon date from the Neoproterozoic Ghaub Formation, Namibia: Constraints on Marinoan glaciation. Geology, 32(9): 817-820.

Kendall, B., Creaser, R.A. and Selby, D., 2009. 187Re-187Os geochronology of Precambrian organic-rich sedimentary rocks. Geological Society, London, Special Publications, 326(1): 85-107.

Kirschvink, J.L., 1992. Late Proterozoic low-latitude global glaciation: the snowball Earth.

Knoll, A.H., Javaux, E.J., Hewitt, D. and Cohen, P., 2006. Eukaryotic organisms in Proterozoic oceans. Philosophical Transactions of the Royal Society B: Biological Sciences, 361(1470): 1023-1038.

Li, Z., Bogdanova, S., Collins, A.S., Davidson, A., De Waele, B., Ernst, R., Fitzsimons, I.C., Fuck, R., Gladkochub, D. and Jacobs, J., 2008. Assembly, configuration, and break-up history of Rodinia: a synthesis. Precambrian research, 160(1): 179-210.

Love, G.D., Grosjean, E., Stalvies, C., Fike, D.A., Grotzinger, J.P., Bradley, A.S., Kelly, A.E., Bhatia, M., Meredith, W. and Snape, C.E., 2009. Fossil steroids record the appearance of Demospongiae during the Cryogenian period. Nature, 457(7230): 718-721.

Macdonald, F.A., Jones, D.S. and Schrag, D.P., 2009. Stratigraphic and tectonic implications of a new glacial diamictite-cap carbonate couplet in southwestern Mongolia. Geology, 37: 123-126.

Macdonald, F.A., Schmitz, M.D., Crowley, J.L., Roots, C.F., Jones, D.S., Maloof, A.C., Strauss, J.V., Cohen, P.A., Johnston, D.T. and Schrag, D.P., 2010. Calibrating the cryogenian. Science, 327(5970): 1241-1243.

Maloof, A.C., Schrag, D.P., Crowley, J.L. and Bowring, S.A., 2005. An expanded record of Early Cambrian carbon cycling from the Anti-Atlas Margin, Morocco. Canadian Journal of Earth Sciences, 42(12): 2195-2216.

Narbonne, G.M. and Gehling, J.G., 2003. Life after snowball: the oldest complex Ediacaran fossils. Geology, 31(1): 27-30.

Rooney, A.D., Strauss, J.V., Brandon, A.D. and Macdonald, F.A., 2015. A Cryogenian chronology: Two long-lasting synchronous Neoproterozoic glaciations. Geology, 43(5): 459-462.

Scott, C., Lyons, T., Bekker, A., Shen, Y., Poulton, S., Chu, X. and Anbar, A., 2008. Tracing the stepwise oxygenation of the Proterozoic ocean. Nature, 452(7186): 456-459.

Sepkoski, J. and Schopf, J., 1992. Biotic Diversity and rates of evolution during Proterozoic and earliest Phanerozoic time. The Proterozoic biosphere: a multidisciplinary study. Cambridge University Press, Cambridge: 521-566.

Strauss, J.V., Rooney, A.D., Macdonald, F.A., Brandon, A.D. and Knoll, A.H., 2014. 740 Ma vase-shaped microfossils from Yukon, Canada: Implications for Neoproterozoic chronology and biostratigraphy. Geology, 42(8): 659-662.

CHAPTER 2. TECTONOSTRATIGRAPHIC EVOLUTION OF THE *C.* 780-730 MA BECK SPRING DOLOMITE: BASIN FORMATION IN THE CORE OF RODINIA

A version of this chapter was published in:

[Smith, E. F., Macdonald, F. A., Crowley, J. L., Hodgin, E. B., & Schrag, D. P. (2015). Tectonostratigraphic evolution of the c. 780–730 Ma Beck Spring Dolomite: Basin Formation in the core of Rodinia. *Geological Society, London, Special Publications*, *424*, SP424-6.]

This chapter also incorporates data, figures, and text that are intended for publication at *Geosphere* with coauthors Lyle L. Nelson and Francis A. Macdonald.

Abstract

The Beck Spring Dolomite is a mixed carbonate-siliciclastic succession exposed in Death Valley, California, that was deposited between c. 750 and 730 Ma. Along with its bounding units, the Horse Thief Springs Formation below and unit KP1 of the Kingston Peak Formation above, the Beck Spring Dolomite was deposited in one of the ChUMP (Chuar-Uinta Mountains-Pahrump) basins with subsidence commonly attributed to the nascent rifting of Rodinia. These pre-Sturtian successions preserve eukaryotic microfossil assemblages, diverse microbialites, and large carbon isotope excursions directly below Sturtian-age glacial deposits.

Here we present new geological mapping, measured stratigraphic sections, carbon isotope chemostratigraphy and detrital zircon geochronology from the Beck Spring

Dolomite and its bounding units. The carbon isotope excursion at the top of the Beck Spring Dolomite has previously been attributed to meteoric diagenesis associated with karst breccias, but here we demonstrate that these breccias are instead mass flow deposits that formed during deposition of the Kingston Peak Formation and that the carbon isotope excursion is not only reproducible throughout the basin, but is associated with transgression rather than regression and exposure. In addition, we refine local correlations and discuss the use of chemostratigraphic curves from these units for regional and global correlations.

The Beck Spring Dolomite was deposited during the second of three distinct basin-forming events recorded in the Pahrump Group with basin inversion occurring between each event. The presence of faulting and folding that are sealed by the c. 635 Ma Marinoan age glacial deposits, the character of the lateral facies change, and detrital zircon provenance analyses indicate that the Beck Spring Dolomite fringed a coeval paleo-high to the south in a tectonically active basin. Detrital zircon age distributions in the Beck Spring Dolomite show sharp probability peaks at ~1200, 1400, and 1800 Ma, consistent with local sources to the southwest in the Mojave block rather than from transcontinental rivers.

We suggest that the Horse Thief Spring Fm, the Beck Spring Dolomite, and the Saratoga Spring Sandstone were accommodated by a strike-slip margin and subsequently folded in a transpressional orogenic event that we refer to as the "Saratoga Orogeny". This tectonism generated topography, which we refer to as the "Beck Mountains" that is responsible for the emplacement of large olistoliths (<1 km long) in the overlying glacial deposits of the Kingston Peak Formation (KP2-KP3). Deposition of the Beck Spring

Dolomite and bounding units do not record evidence of incipient rifting of the western margin of Laurentia but instead reflect a distinct, margin-wide tectonothermal event.

2.1. Introduction

The Death Valley region of SE California hosts a 1.5 to 6.0 kilometer-thick, well-exposed Neoproterozoic succession, the Pahrump Group (Figs. 2.1 and 2.2). The classic view is that the three units comprising the group, the Crystal Spring Formation, Beck Spring Dolomite and Kingston Peak Formation, formed in a long-lived aulacogen bounded to the north and south by upland source areas, and that carbonate-dominated units like the Beck Spring Dolomite were deposited during periods of tectonic quiescence (Roberts, 1982; Wright et al., 1976). This model was developed when there were few age constraints on these strata. Nearly a decade later, researchers used ages of basement terrains, Grenville-age orogenic belts and stratigraphic ties to hypothesize the formation and break-up of the supercontinent Rodinia (Dalziel, 1991; Hoffman, 1991; Moores, 1991). Details of the paleogeographic arrangement and components of Rodinia are still debated, but nearly all models place Laurentia at the core of the supercontinent. Thus, Neoproterozoic basin formation in Death Valley is especially important for the reconstruction of Rodinia because it was proximal to both the western and southern margins of Laurentia, and as a result, has the potential to record the Neoproterozoic tectonic evolution of both margins. Over the past few decades, age constraints have been refined and several major unconformities have been recognized within the Pahrump Group, suggesting the strata were deposited during multiple, distinct basin-forming

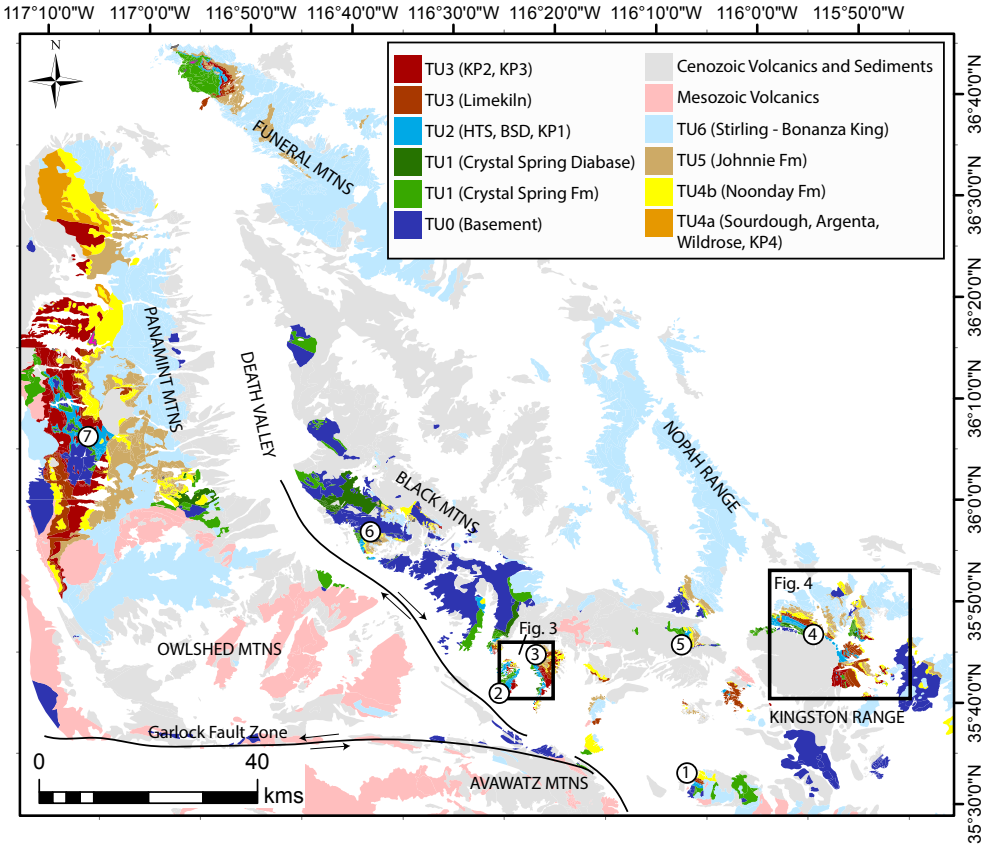

Figure 2.1. Death Valley location map and major faults.
AH, Alexander Hills; BM, lack Mountains; HC, Happy Canyon; KR, Kingston Range; NR, Nopah Range; SH, Silurian Hills; SPH, Saddle Peak Hills; SS, Saratoga Springs (southern Ibex Hills); and SW, Sperry Wash. The areas mapped in Figs. 2.3 and 2.5 are boxed in black. Locations of measured sections are marked with circled numbers that correspond to numbered sections in Fig. 2.5.

Figure 2.2. Schematic stratigraphy of the Pahrump Group in SE Death Valley.
Stratigraphy of the Crystal Spring Formation is modified from Roberts (1982). Basement age populations are from Wooden et al. (2013). HTS = Horse Thief Spring Formation, BSD = Beck Spring Dolomite, J = Johnnie Formation.

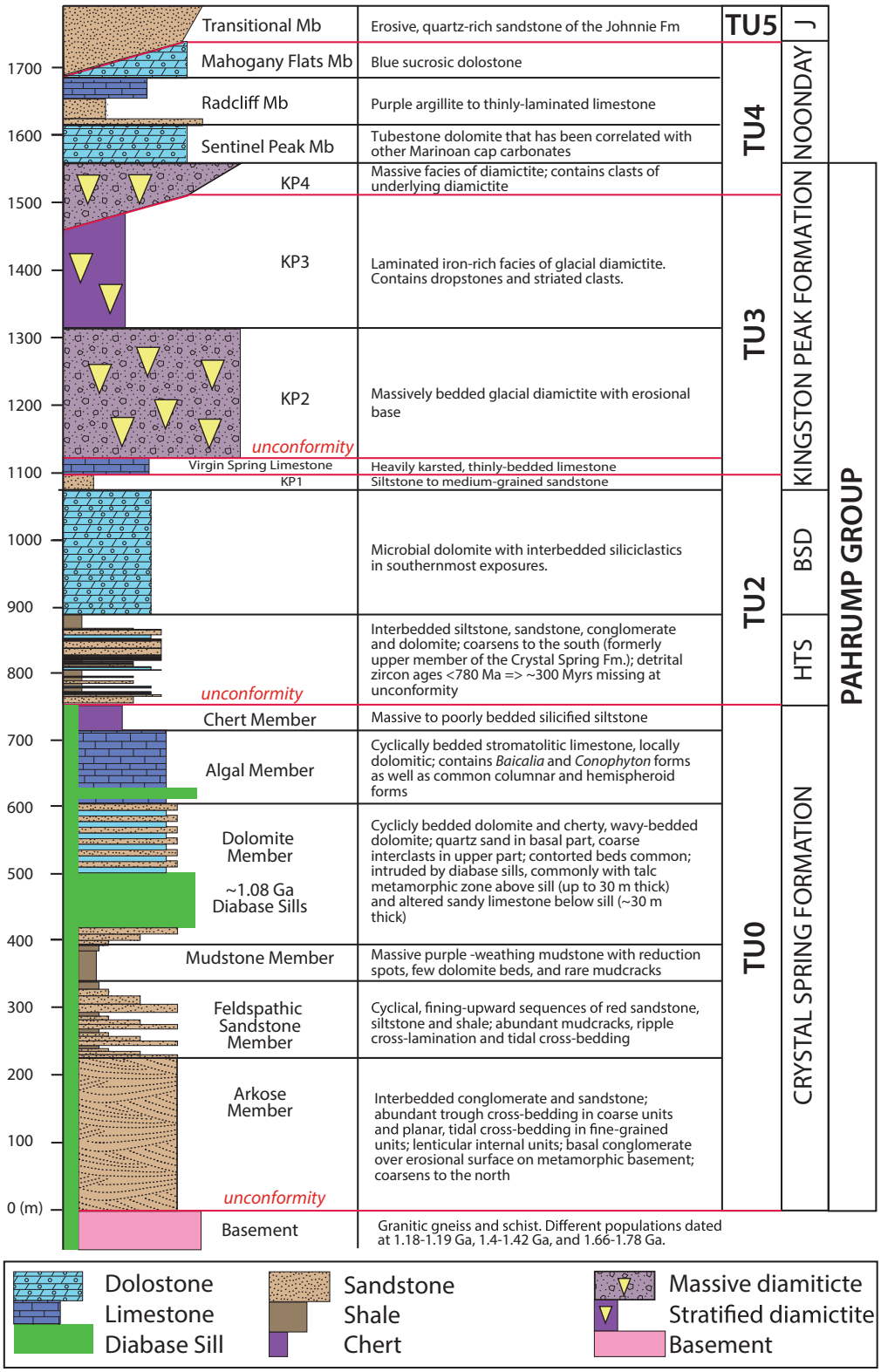

Figure 2.2 (continued).

events and, thus calling into question the long-lived aulacogen model (Heaman and Grotzinger, 1992; Macdonald et al., 2013a; Mahon et al., 2014b; Prave, 1999).

Other western Laurentian successions have been previously attributed to record the rifting of Rodinia, including the Chuar Group in Arizona (Timmons et al., 2001) and the Uinta Mountain Group in Utah (Dehler et al., 2010). These basins are collectively referred to as the ChUMP (Chuar-Uinta Mountains-Pahrump) basins, and are thought to have formed in an extensive interior seaway that formed in the incipient stages of rifting (Dehler et al., 2001; Dehler et al., 2010; Link et al., 1993). The shared features between units in the ChUMP basins include similar fossil assemblages with vase-shaped microfossils (VSMs) in the uppermost stratigraphy (Dehler et al., 2010; Horodyski, 1987; Licari, 1978; Porter and Knoll, 2000), unconformity-bounded successions with age constraints between ~780-730 Ma (Macdonald et al., 2013a; Mahon et al., 2014b), large carbon isotope excursions (Brehm, 2008; Corsetti and Kaufman, 2003; Dehler et al., 2005; Dehler et al., 2010; Dehler et al., 2007; Macdonald et al., 2013a), and pronounced meter-scale cyclicity (Dehler et al., 2001). Similar features and age constraints also have been documented in the Callison Lake dolostone and Coates Lake Group of NW Canada (Jefferson and Parrish, 1989; Macdonald et al., 2010; Rooney et al., 2014; Strauss et al., 2014).

Here, with new and previously published data, we propose an alternative model for the tectonostratigraphic evolution and subsidence mechanisms for the iconic Pahrump Group in Death Valley. This new model integrates geological mapping, measured sections, detrital zircon geochronology and carbon isotope chemostratigraphy of the Beck Spring Dolomite and its encasing strata, the underlying Horse Thief Springs Formation

(previously defined as the upper Member of the Crystal Spring Formation) and the overlying unit KP1 of the Kingston Peak Formation (Macdonald et al., 2013a; Mahon et al., 2014b) from seven localities (Fig. 2.1). These strata are bounded by unconformities, which Macdonald et al. (2013a) used to demarcate Tectonostratigraphic Unit 2 (TU2), a regionally developed package interpreted to record a distinct basin-forming event. To avoid nomenclatural issues we will use TU2 throughout to delineate this succession of rocks.

2.2. Geologic Setting

In Death Valley, the Pahrump Group defines a 1.5 to 4.0 km thick, well-exposed and easily accessible Meso- and Neoproterozoic succession (Hewett, 1940; Noble, 1934). Its basal unit, the Crystal Spring Formation, unconformably overlies 1780-1660 Ma granitic gneisses of the Mojave crustal province (Barth et al., 2000; Strickland et al., 2013; Wasserburg et al., 1959) and 1430-1400 Ma porphyritic quartz monzonite (Labotka et al., 1980). Following the amalgamation of the Mojave basement by 1210-1180 Ma with the intrusion of the AMCG suite of anorthosite, syenite and granite (Wooden et al., 2013), the Death Valley region experienced extension and basin formation. This extension accommodated the emplacement of diabase sills that have been dated at two localities at 1087 ± 3 and 1069 ± 3 Ma with discordant multigrain baddeleyite U-Pb TIMS ages (Heaman and Grotzinger, 1992).

A maximum age constraint on the middle portion of the Pahrump Group (TU2) is provided by the Crystal Spring Diabase. An upper age constraint is provided by the Noonday Formation, the basal member of which has been identified as a basal Ediacaran cap dolostone (Petterson et al., 2011) and has been dated globally at ca. 635 Ma (Calver

et al., 2013; Condon et al., 2005; Hoffmann et al., 2004). Additionally, the Kingston Peak Formation contains glacial deposits that have been correlated to the Sturtian and Marinoan glaciations (Macdonald et al., 2013a; Macdonald et al., 2010; Prave, 1999). Neoproterozoic LA-ICPMS detrital zircon ages (Mahon et al., 2014b) and correlation of pre-Sturtian basins on the western margin of Laurentia suggest a more narrow window of deposition of TU2 between ~750 and 730 Ma (Dehler et al., 2001; Macdonald et al., 2013a; Rooney et al., 2014; Strauss et al., 2014).

Multiple episodes of late Neoproterozoic tectonism are recorded in the Pahrump succession; evidence includes syn-sedimentary normal faults in the middle (KP2) and upper (KP3) parts of the Kingston Peak Formation in SE Death Valley, basalt in the KP2- or KP3-correlative Surprise diamictite in the Panamint Mountains (Macdonald et al., 2013a; Miller, 1985; Prave, 1999), and multiple unconformities throughout the succession including the base of the Noonday Formation, which regionally sits on all of the underlying units, including basement (Prave, 1999; Stewart, 1975; Wright, 1954). Map relations and flute casts indicate that the deepening direction during Kingston Peak time was to the S-SE (Mrofka, 2010; Petterson et al., 2011). Unconformities are also present in the overlying Ediacaran strata, most prominently at the base of and in the uppermost Johnnie Formation (Clapham and Corsetti, 2005; Petterson et al., 2011; Summa, 1993). Based on subsidence curves, passive margin sedimentation did not develop in this area until latest Ediacaran-early Cambrian Wood Canyon time (Armin and Mayer, 1983; Bond et al., 1985; Bond and Kominz, 1984; Fedo and Cooper, 2001; Stewart, 1970). This passive margin was deepening to the NW (Nelson, 1978). Thus, while there is clear evidence for Ediacaran-age rifting, it remains unclear if deposition of

TU2 was accommodated by rifting, transtension, transpression, compression, or dynamic subsidence.

2.3. Previous Studies

Until recently, the Horse Thief Springs Formation, the basal unit of TU2, was included in the Crystal Spring Formation. The base of the Horse Thief Springs Formation is marked by a significant unconformity that was first recognized by Mbuyi and Prave (1993) and described by Macdonald et al., (2013a). Mahon et al. (2014b) elevated the succession between this unconformity and the Beck Spring Dolomite to the formation level and renamed it the Horse Thief Springs Formation.

The sedimentology, stratigraphy, and regional depositional patterns of the Horse Thief Springs Formation were documented by Maud (1979; 1983), Roberts (1982), and Mahon (2012). Maud (1979; 1983) separated the unit into six regionally traceable sequences of dominantly siliciclastic rocks that are each overlain by dolomite, with the final sequence being overlain by the Beck Spring Dolomite. He labeled these sequences A through F. The lower part of the formation preserves enterolithic bedding, which Maud interpreted as evidence for deposition of evaporites in a restricted basin. He also documented karsting on the top surfaces of the dolomite marker beds. The formation coarsens to the S-SW and is thickest in the NW part of the Kingston Range, thinning in all directions from there (Maud, 1979; Maud, 1983). He suggested that the facies character of the interbedded stromatolitic dolostone, siltstone, sandstone, and conglomerate suggest that these record near-shore marine environments. Mahon et al. (2014a) used stratigraphic and detrital zircon data to argue that the Horse Thief Springs Formation marks the intial basin development during the incipient rifting of Rodinia. The

only published $\delta^{13}C$ data from the Horse Thief Springs Formation are low-resolution (10-20 m) $\delta^{13}C$ data from the upper part of the formation in Beck Canyon and at Saratoga Springs (Corsetti and Kaufman, 2003).

Previous studies of the Beck Spring Dolomite focused on the petrology, sedimentology, and stratigraphy of the microbial, carbonate-dominated successions of the Beck Spring Dolomite in the Kingston Range and southern Death Valley area (Gutstadt, 1968; Harwood and Sumner, 2011; Harwood and Sumner, 2012; Loyd and Corsetti, 2010; Marian and Osborne, 1992; Shafer, 1983). In the Alexander Hills and the Kingston Range, the Beck Spring Dolomite is divided into informal sub-members that include a lower laminated facies, a middle microbial, thrombolitic and intraclastic facies, and an upper cherty grainstone facies (Corsetti and Kaufman, 2003; Harwood and Sumner, 2011; Marian, 1979; Marian and Osborne, 1992). The SW exposures of the Beck Spring Dolomite contain siliciclastic units preserved in m-scale parasequences, syn-depositional faults, and soft-sedimentary deformation (Macdonald et al., 2013a; Mahon, 2012; Marian, 1979).

Much detailed work has been done to compare modern microbialites to the Beck Spring Dolomite stromatolites and thrombolites to constrain specific depositional environments, and generally, previous workers have suggested that the unit was deposited on a stable, shallow marine platform in a subtidal to intertidal environment (Harwood and Sumner, 2011; Marian, 1979; Marian and Osborne, 1992; Zempolich et al., 1988). Marian (1979) suggested that this unit was deposited during a period of relatively slow and stable subsidence based on his documentation of a uniform thickness of the unit, however much of this work only documented the carbonate-dominated sections of the

Beck Spring Dolomite in a very narrow region of SE Death Valley. Mahon (2012) and Mahon et al. (2014a) later argued that the Horse Thief Springs Formation and conformably overlying Beck Spring Dolomite were deposited in a basin that was undergoing extensional tectonism.

Carbon isotope chemostratigraphy of the Beck Spring Dolomite was documented in Alexander Hills, the Kingston Range, Saddle Peak Hills, and Saratoga Springs by Corsetti and Kaufman (2003), Prave (1999) and Macdonald et al. (2013a). All of these sampled sections show a "W-shape" chemostratigraphic profile with a large negative carbon isotope excursion at the top of the Beck Spring Dolomite. This excursion has been correlated with the Islay excursion (Hoffman et al., 2012; Strauss et al., 2014). Hurtgen et al. (2004) complemented these carbon isotope studies with a carbonate-associated sulfate isotope study.

The diagenetic history of the carbonate rocks in the Beck Spring Dolomite were described by Tucker (1982; 1983), Zempolich et al. (1988), Kenny and Knauth (2001), and Horodyski and Knauth (1994). The latter two studies describe paleokarst pits containing putative microfossils and brecciated clasts with highly depleted $\delta^{13}C$ values in the Beck Spring Dolomite in the Kingston Range. Importantly, the breccia at the top of the Beck Spring Dolomite is distinct from the intraformational, intraclastic breccia that was documented in the Alexander Hills and Kingston Range (Harwood and Sumner, 2011 and references therein). Horodyski and Knauth (1994) used this Beck breccia and putative microfossils as evidence for terrestrial biota during the Precambrian. Elaborating on this interpretation, Kenny and Knauth (2001) found depleted carbon and oxygen isotope values in a breccia in the eastern Kingston Range and suggested it represented a

terrestrial karst breccia. This interpretation is important because it has fueled not only speculation about the colonization of land, but also the idea that the carbon isotope chemostratigraphy of the Beck Spring Dolomite is compromised by meteoric diagenesis and cannot be used for correlation or interpretation of the Neoproterozoic carbon cycle (e.g. Knauth and Kennedy, 2009).

Undisputed microfossils from the chert and dolomite in the upper part of the Beck Spring Dolomite were described by Cloud et al. (1969), Licari (1978), and Pierce and Cloud (1979). These microfossils were thought to extend into the Cryogenian in Death Valley, but have since been documented as being redeposited (Macdonald et a., 2013a). These microfossils, especially vase-shaped microfossils (VSMs), are significant because, since the early reports of them in Death Valley, they have only been found in TU2-correlative basins and identified as a potential tool for correlation (Bloeser, 1985; Dehler et al., 2007; Porter and Knoll, 2000; Vidal and Ford, 1985), and particular assemblages have been suggested as possible Neoproterozoic index fossils (Strauss et al., 2014).

Overlying the Beck Spring Dolomite is unit KP1, the least studied of the three units in TU2. Historically, KP1 has been placed within the Kingston Peak Formation, due in part to difficulty correlating the glacial stratigraphy in SE Death Valley to that in the Panamint Mountains (Wright, 1954). KP1 consists of siltstone to fine-grained quartz-arkosic sandstone without glaciogenic features. Its gradational contact with the underlying Beck Spring Dolomite (Miller, 1985; Mrofka, 2010; Wright et al., 1992) and the unconformity at its top surface (Macdonald et al., 2013a; Mrofka, 2010) indicate that it is part of the same basin-forming event as the Beck Spring Dolomite (Prave, 1999). When the Pahrump Group stratigraphy is further refined and formalized, we support

Mrofka's (2010) suggestion that unit KP1 be renamed and removed from the Kingston Peak Formation.

In addition to studies of the three TU2 units, we refer to and expand upon the geological mapping and unit descriptions of Kupfer (1960) from the Silurian Hills. More specifically, we refer to his units 4-12, which we correlate with TU2 strata (shown on the left side of the Silurian Hills section in Fig. 2.7).

2.4. Methods

2.4.1. Field work

We mapped the geology and measured stratigraphic sections of TU2 in the Alexander Hills, southern Black Mountains, eastern Kingston Range, central Panamint Mountains, Saddle Peak Hills, Saratoga Springs, and Silurian Hills (Figs. 2.1, 2.3, 2.4, 2.5, and 2.6). TU2 is also exposed in the Funeral Range of northern Death Valley (Fig. 2.1), however, there, the metamorphic grade is too high to preserve sedimentary textures and meaningful stratigraphic thicknesses. Locations were selected with the aim of constructing a basin-wide depositional model across the Death Valley region. The measured sections in Fig. 2.7 are a combination of new and previously published data.

Measured sections and carbon isotopes from Beck Canyon in the Kingston Range and the Saddle Peak Hills were previously published in Macdonald et al. (2013a), however, these sections were re-measured for this study to more closely examine the sedimentology and to better characterize the $\delta^{13}C$ values in the transition beds between the Horse Thief Springs Formation and Beck Spring Dolomite. Also of note is that north of Beck Canyon, the Beck Spring Dolomite is the prominent ridge former (Fig. 2.5), and

Figure 2.3. Geological map of Saratoga Springs and Saddle Peak Hills.
Geological map of Saratoga Springs and Saddle Peak Hills. This area was mapped by F. Macdonald, E. Smith, and the Harvard Field Camp in 2012 and 2013, on the Old Ibex Pass and Saddle Peak Hills 1:24,000 topographic maps with UTM gridlines. Coordinates are marked with crosses and measured sections are marked with red lines. White circles mark locations of measured sections in Fig. 2.7. White triangles mark locations of photos in Figs. 2.8, 2.9, and 2.10.

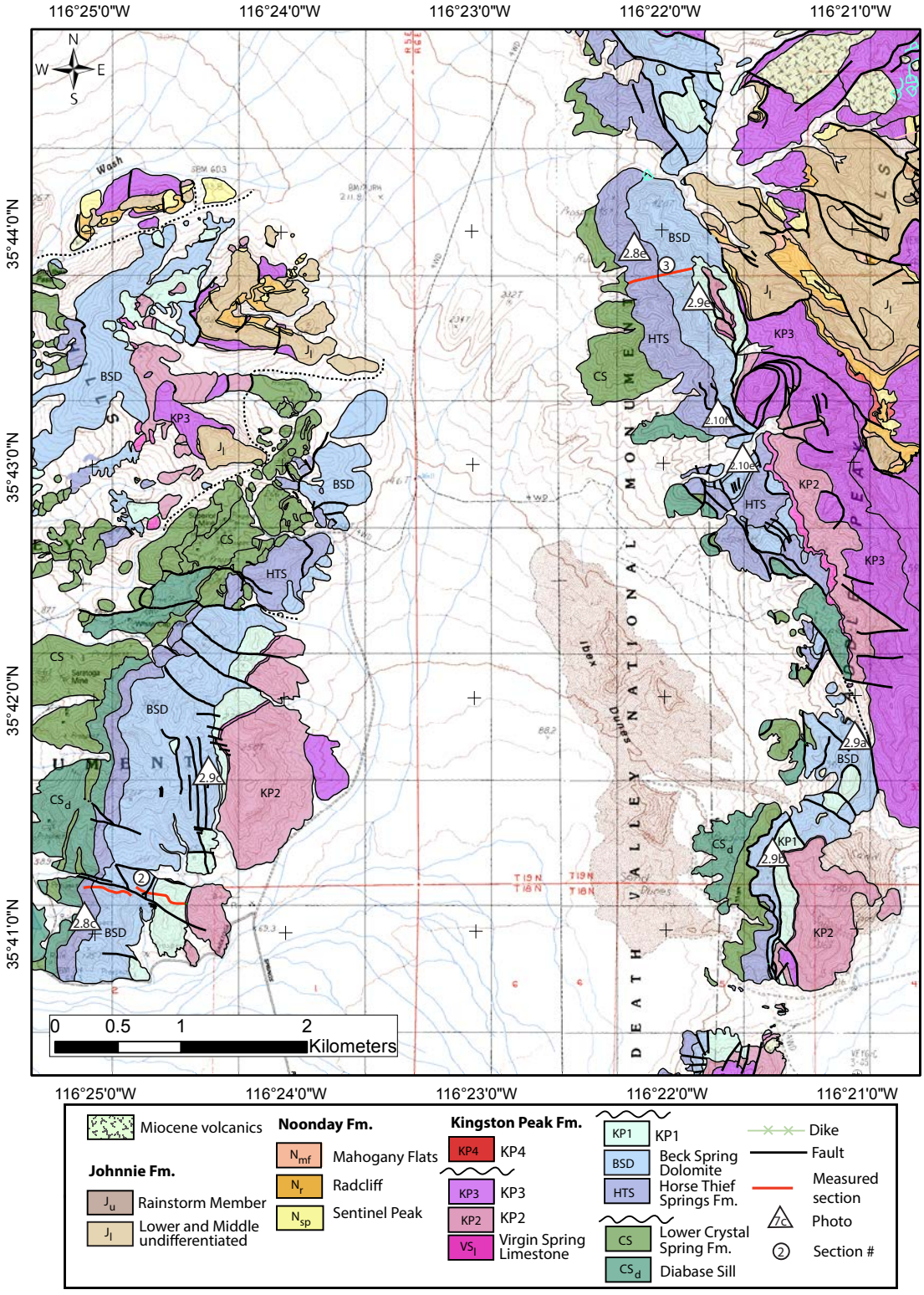

Figure 2.3 (continued).

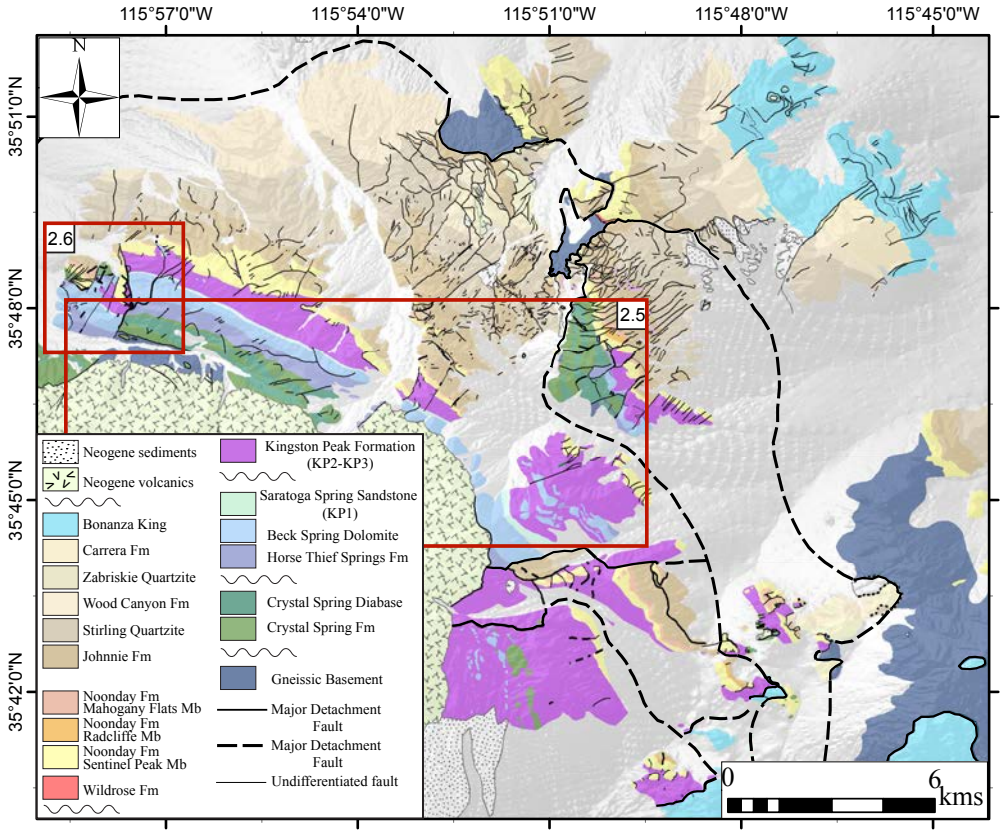

Figure 2.4. Geological map of the Kingston Range

Geological map of the Kingston Range, adapted from Calzia et al., (2000), Macdonald et al., (2013), Smith et al. (2015) and an unpublished MIT field camp class map, courtesy of C. Burchfiel. This map shows the major detachment faults in this area and the expansion of the Kingston Peak Fm to the southwest. Red boxes outline the areas of the maps in Figs. 2.5 and 2.6.

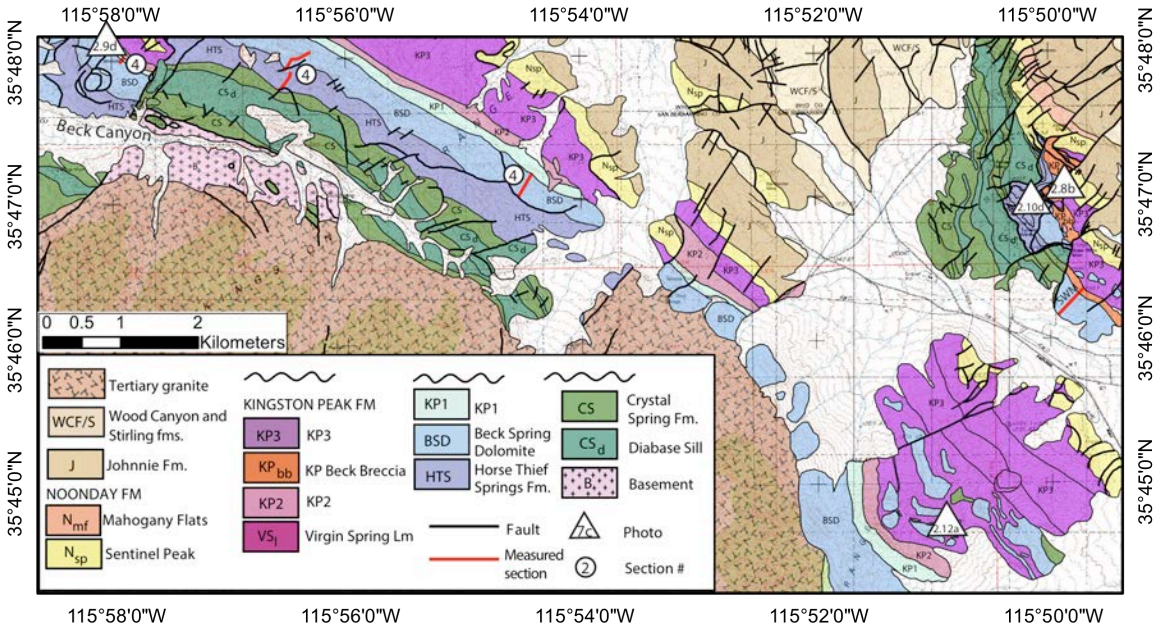

Figure 2.5. Geological map of the Northeast Kingston Range

Geological map of the NE Kingston Range, adapted from Calzia et al., (2000), Macdonald et al., (2013), and an unpublished MIT field camp class map, courtesy of C. Burchfiel. The Crystal Spring Formation through the Kingston Peak Formation was re-mapped by F. Macdonald and E. Smith on the Horse Thief Springs and East of Kingston Peak 1:24,000 topographic maps with UTM gridlines. Coordinates are marked with crosses. White circles mark locations of measured sections in Fig. 2.7. White triangles mark locations of photos in Figs. 2.8, 2.9, 2.10, and 2.12. Section SWM is the location of the measured section of Beck Spring Dolomite in Harwood and Sumner (2011).

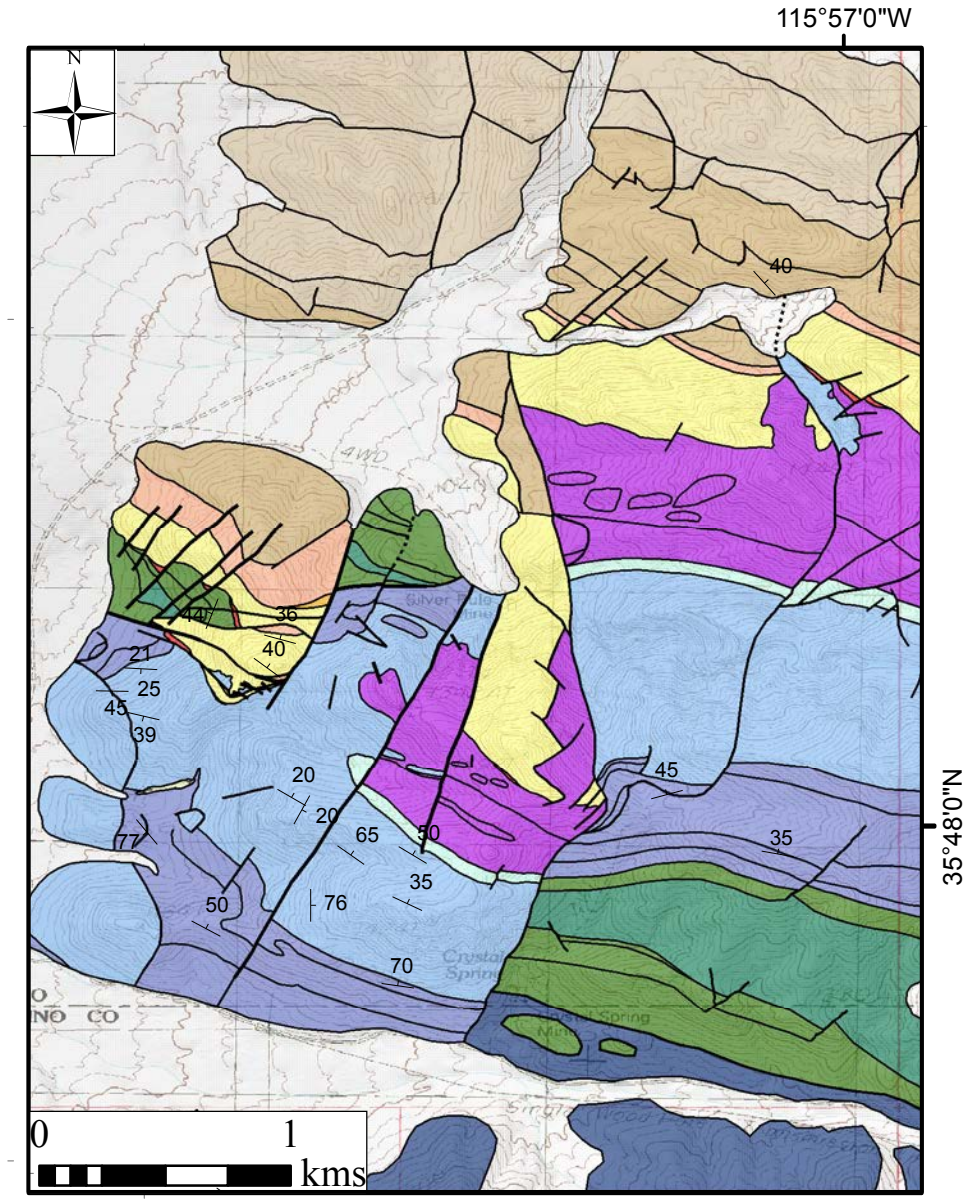

Figure 2.6. Detailed Geologic Map of West Beck Canyon.
Mapped by E. Smith and L. Nelson on a 1:10,000 scale. W. Beck Canyon was previously mapped by Calzia et al., 2000. Revised mapping here documents different generations of faulting and pre-KP2 folding. The oldest fault in this map area is the fault placing the Crystal Spring Fm against the Horse Thief Springs Fm (Fig. 2.10H). High angle strike slip faults that were active during KP2 and KP3 time are also present in this area. These faults are responsible for creating enough topography for the emplacement of olistoliths of TU2 (Fig. 2.12A). There are large facies changes in the KP Fm across these faults. White triangles mark locations of photos in Figs. 2.10, 2.11, and 2.12.

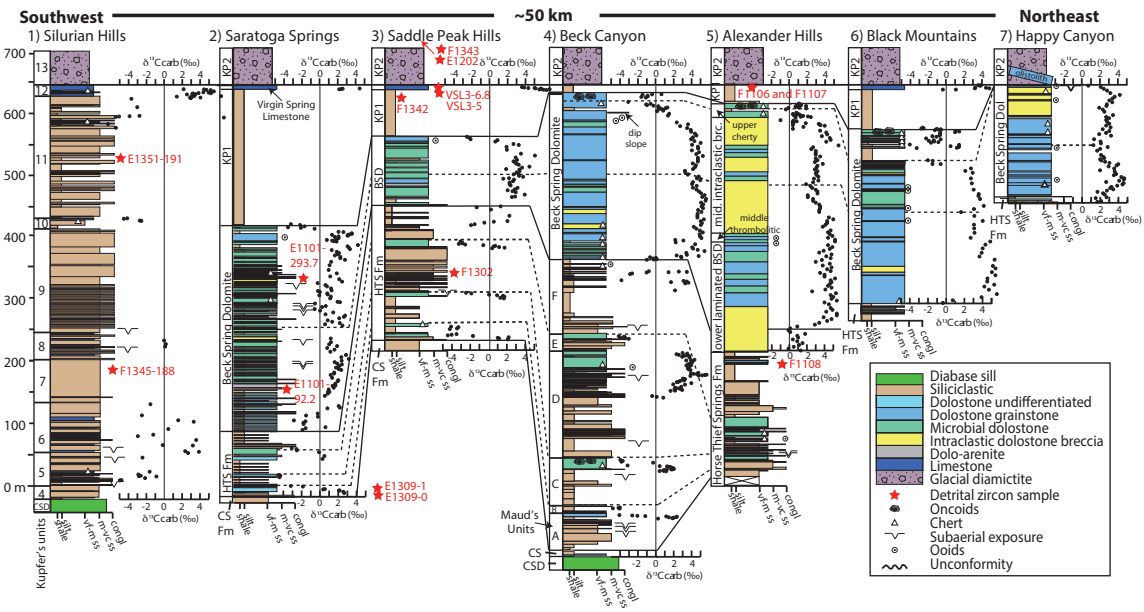

Figure 2.7. Chemo- and litho-stratigraphy of TU2 from seven measured sections in Southeast Death Valley and the Panamint Range.
See Figs. 2.1, 2.3 and 2.5 for location maps of sections. Kupfer's (1960) units for the Silurian Hills section are marked on the left side of the section. Similarly, the members described by Maud (1979; 1983) are marked on the left side of the Horse Thief Springs Formation section in Beck Canyon and lithofacies described by Harwood and Sumner (2011) are on the left side of the Beck Spring Dolomite section at Alexander Hills. The $\delta^{13}C$ values from the Virgin Spring Limestone and Beck Spring Dolomite sections in Beck Canyon, the Black Mountains, and Saddle Peak Hills were published in Macdonald et al. (2013a). In Alexander Hills, the sedimentology of the Beck Spring Dolomite is adapted from Harwood and Sumner (2011) and the $\delta^{13}C$ values are from Corsetti and Kaufman (2003). Correlation between the Silurian Hills sections and the other sections is uncertain so no tie lines are drawn. Detrital zircon samples are marked with red stars.

the top of the section is a very steep dip slope, preventing one from measuring a continuous section. The section in Fig. 2.7 is a composite from three localities in Beck Canyon (Fig. 2.5). The $\delta^{13}C$ data from the top 27 m of the section was sampled from a fault block in the far western part of the canyon that preserves the oncoids at the top of the Beck Spring Dolomite (Fig. 2.9D). The upper contact with KP1 was used as a tie point between the measured sections. Due to the dip slope and the uncertainty in

correlating between sections, the thickness of the section presented in Fig. 2.7 could be inaccurate by up to 30 m (see Fig. 2.7 break in section). The sedimentology of the Beck Spring Dolomite at the Alexander Hills section is modified from Harwood and Sumner (2011) and the carbon isotope values are from Corsetti and Kaufman (2003). All other data presented here are new.

2.4.2. Mass spectrometry

To test regional and global correlations, we sampled carbonate rocks spanning TU2 from all measured sections. Carbon ($\delta^{13}C$) and oxygen ($\delta^{18}O$) isotopic measurements were obtained on 466 samples. Samples were micro-drilled along individual laminations, where visible, to obtain 5 to 20 mg of carbonate powder; veins, fractures, and siliciclastic-rich areas were avoided. Carbonate $\delta^{13}C$ and $\delta^{18}O$ data were acquired simultaneously on a VG Optima dual inlet mass spectrometer in the Harvard University Laboratory for Geochemical Oceanography. Carbonate samples were reacted with orthophosphoric acid using a VG Isocarb preparation device, which includes a common acid bath with a magnetic stirrer. Approximately 1 mg of each sample was reacted in the bath at 90°C. Evolved CO_2 was collected cryogenically and analysed using an in-house reference gas. Potential memory effects resulting from partially unreacted samples in the common acid-bath system were minimised by increasing the reaction time for dolomite samples. Memory effect is estimated at <0.1‰ based on variability of standards run after dolomite samples. Standard deviation (1σ) from standards was better than ± 0.1‰ for both $\delta^{13}C$ and $\delta^{18}O$. Carbonate $\delta^{13}C$ and $\delta^{18}O$ isotopic results are reported in per mil notation relative to V-PDB (Vienna-Pee Dee Belemnite) by using an

in-house Cararra Marble standard that was calibrated against several NBS carbonate standards and cross-calibrated with other laboratories.

2.4.3. Detrital Zircon Geochronology

To better constrain sedimentary provenance, 17 samples through TU2 and TU3 (which includes KP2 and KP3) were collected and 1522 zircon grains were analysed from the Pahrump Group, targeting specifically the units in TU2. These studies complement those of MacLean et al. (2009) and Mahon et al. (2014a; 2014b). Detrital zircons were dated to assess the changes in provenance during basin development (Fig. 2.13B) and to find additional young (~780 Ma) grains (Mahon et al., 2014b). Samples E1309-0 and B1303 (both from the basal Horse Thief Springs Formation) were processed to search for young grains, and thus the data from these two samples are not plotted in Fig. 2.13B, but can be found in the supplementary material. The sections and stratigraphic positions of the samples are indicated in Fig. 2.7 with the exception of F1102 and B1303, which are from Sperry Wash and east Kingston Range, respectively.

Zircons from ~2-5 kg of rock were separated using standard methods and annealed at 900ºC for 60 hours. A random split of these grains (~100-200) was mounted in epoxy and polished until the centers of the grains were exposed. Cathodoluminescence (CL) images were obtained with a JEOL JSM-1300 scanning electron microscope and Gatan MiniCL. Zircons were analyzed by laser ablation inductively coupled plasma mass spectrometry (LA-ICPMS) using a ThermoElectron X-Series II quadrupole ICPMS and New Wave Research UP-213 Nd:YAG UV (213 nm) laser ablation system. In-house analytical protocols, standard materials, and data reduction software were used for acquisition and calibration of U-Pb dates and a suite of high field strength elements

(HFSE) and rare earth elements (REE). A detailed description of the methods and analyses can be found in the supplementary materials.

2.5. Results

2.5.1. Chemo- and litho-stratigraphy

2.5.1.1. Horse Thief Springs Formation

The Horse Thief Springs Formation is a 105-465 m thick, mixed siliciclastic-carbonate succession. For mapping purposes, we defined four regionally traceable siliciclastic-carbonate members in this formation, lumping Maud's (1979; 1983) A and B members and C and D members together (see Fig. 2.7); the basal three members are each capped by stromatolitic dolostone marker beds whereas the fourth member is capped by the orange and black dolostone interbedded with siltstone and fine-grained sandstone. The transition into the overlying Beck Spring Dolomite is gradational. The contact is placed at the base of the "bacon beds", two 0.1-0.5 m thick orange and black, microbial dolostone beds marking the onset of meter-scale mixed siliciclastic-carbonate parasequences that persist through the basal part of the Beck Spring Dolomite (see Fig. 2.8E for the contact at section in western Saddle Peak Hills).

The siliciclastic strata in the Horse Thief Springs Formation include purple and green argillite, texturally immature quartz arenite, locally arkosic, and poorly-sorted, quartzitic conglomerate. The thicknesses and grain size of these strata vary widely from section to section. There are multiple exposure surfaces throughout the succession marked by mudcracks and carbonate dissolution on upper surfaces of the dolomite beds.

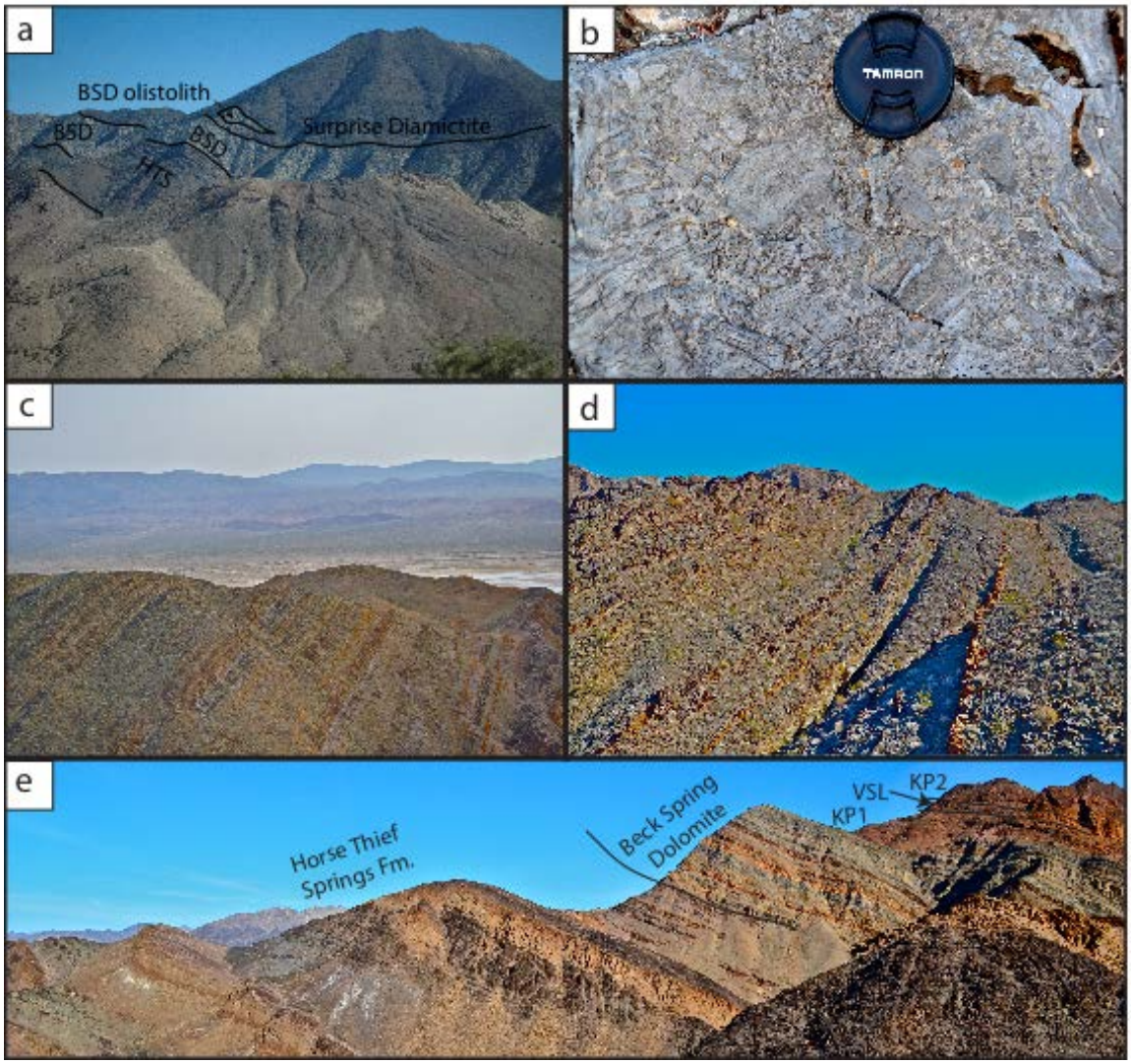

Figure 2.8. Pahrump Group photos.
Locations of photos in the Kingston Range, Saddle Peak Hills, and Saratoga Springs are marked with white triangles in Figs. 2.3 and 2.5. A) Measured section of Beck Spring Dolomite at Happy Canyon in the Panamint Mountains. Units outlined and labeled in black. B) Beck Spring Dolostone breccia in KP2 near Jupiter Mine in the Kingston Range. C) Mixed siliciclastic-carbonate parasequences at Saratoga Springs. D) Sandstone to conglomerate parasequences at Silurian Hills. Tan dolostones are at the top of Kupfer's unit 10 (see Fig. 2.7). E) Measured section of TU2 in west-central Saddle Peak Hills (see Fig. 2.3 for section location).

The carbonate rocks, often preserving *Baicalia* stromatolites, cap each of the clastic sequences across the basin (Cloud and Semikhatov, 1969; Maud, 1979; Maud, 1983).

Of the five new measured sections of the Horse Thief Springs Formation presented here, four were sampled for $\delta^{13}C$ analyses, providing the first high-resolution $\delta^{13}C$ data set for these strata. Carbonate carbon isotope trends are stratigraphically consistent across the basin (Fig. 2.7). At Beck Canyon, the thickest and most carbonate-rich section measured, the basal carbonate units trend from ~+2.5 to -4.5‰. In the middle of the section, an interval that is dominated by dolomite for ~80 m, there is a rise in $\delta^{13}C$ values from ~0 to +6‰ and then a decrease to ~-4.5‰. Similar trends are present in the relatively carbonate-poor Saddle Peak Hills and Saratoga Springs sections (Fig. 2.7).

A siliciclastic-dominated section in the Silurian Hills that is unconformably above the Crystal Spring Formation and Crystal Spring Diabase was also measured. Due to considerable facies changes and an upper greenschist facies overprint (Shafer, 1983) detailed lithological and chemostratigraphic correlations between this section and other TU2 sections remain unclear.

2.5.1.2. Beck Spring Dolomite

The Saratoga Springs section consists of 320 m of interbedded dolostone, siltstone, sandstone, and pebble conglomerate. The section is dominated by meter-scale carbonate-siliciclastic parasequences with pronounced cyclic appearance (Fig. 2.8C). Dolostone in the lower ~100 m preserves microbial textures interbedded with finely-laminated micrite, carbonate siltstone, sandstone, and minor quartz-arenite pebble conglomerate. The

quartz-pebble arkosic sandstone and conglomerate beds have rounded to subrounded clasts and preserve flat laminations and trough cross bedding. Microbial laminations commonly envelop trapped quartz and feldspar grains. Sandstone beds are lobate, pinching and swelling laterally, but often continuous for hundreds of meters along strike. Broken microbial mats and millimeter- to centimeter-scale carbonate clasts are common throughout the section. At ~120 m, exposure surfaces consisting of teepee structures and millimeter-scale karsting become common suggesting that there is a gradual shallowing-up in the section. Approximately 30 m from the top of the Beck Spring Dolomite, there is a gradual transgression in which interbedded pisoid (sometimes called 'giant ooids' in the literature) grainstone (Fig. 2.9E) and microbialite are succeeded by red fissile shale, high-relief, pseudo-branching stromatolites and bedded black chert. Stromatolitic morphologies such as these have been reported from subtidal, low to moderate energy environments (Awramik, 1971; Donaldson, 1976; Hoffman, 1976; Horodyski, 1977). Additionally, molar tooth structure (Fig. 2.9C) and black, oolitic limestone beds are present locally near the top of Beck Spring Dolomite. Sampling this section at higher resolution demonstrated that the "W-shape" profile exists. Data from this section has the most scatter and $\delta^{13}C$ values are on average 2 to 3‰ lighter throughout the section than

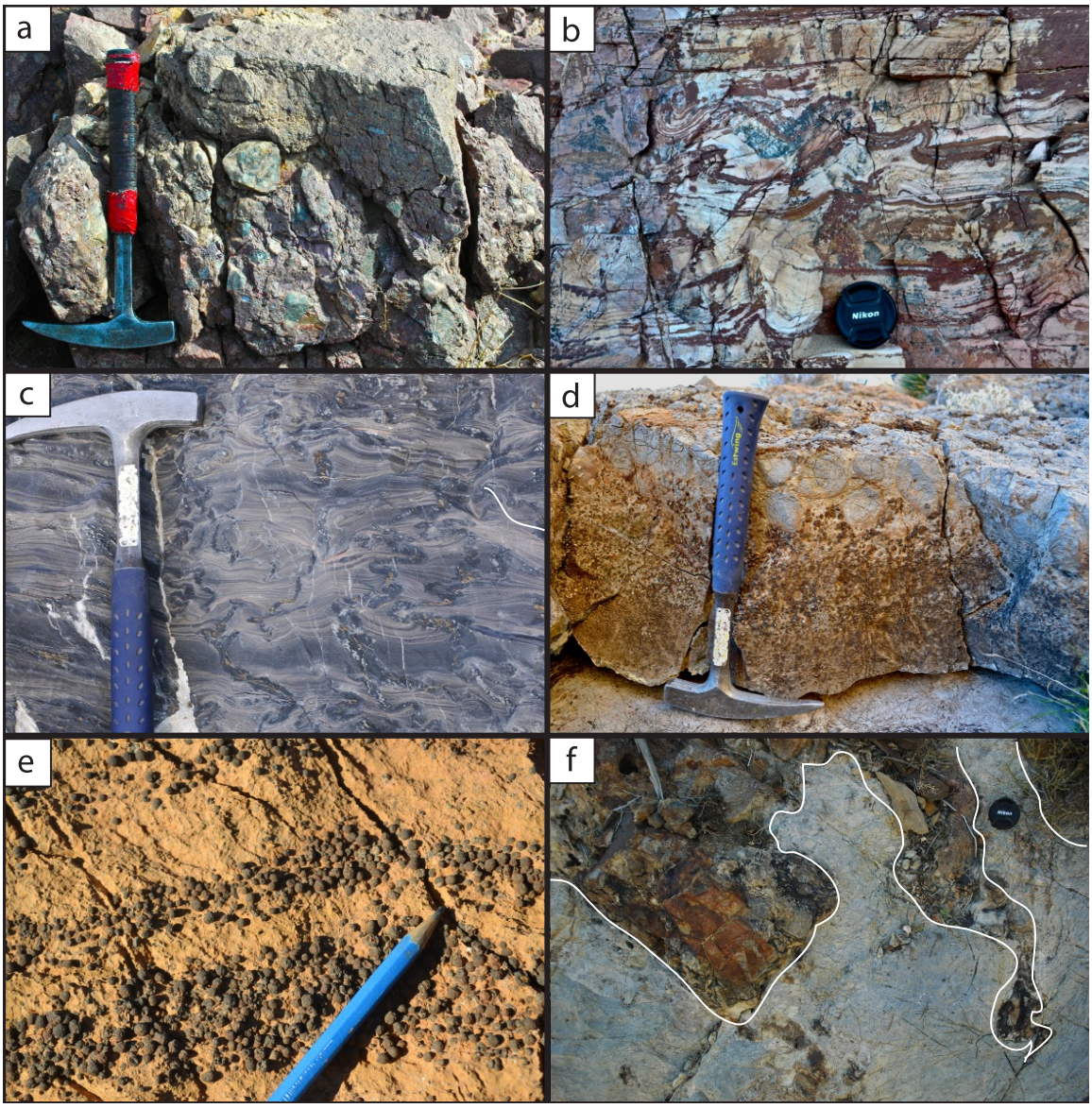

Figure 2.9. Sedimentary features of the Beck Spring Dolomite.
Locations of photos in the Kingston Range, Saddle Peak Hills, and Saratoga Springs are marked with white triangles in Figs. 2.3 and 2.5. A) Quartz pebble to cobble conglomerate in the upper part of the Beck Spring Dolomite in west-central Saddle Peak Hills. B) Soft sediment deformation in microbial facies of the Beck Spring Dolomite in western Saddle Peak Hills. C) Molar tooth structure in top of the Beck Spring Dolomite at Saratoga Springs. Photo taken north of measured section. D) Oncoids at the top of the Beck Spring Dolomite sampled from the fault block in western Beck Canyon. E) Giant, partially silicified ooids in the top of the Beck Spring Dolomite in western Saddle Peak Hills. Pencil for scale. F) White line outlines paleokarst along the contact between the Beck Spring Dolomite and overlying Surprise diamictite in Surprise Canyon, Panamint Mountains.

in other sampled sections (Fig. 2.7), perhaps due to the fact that it is the least carbonate buffered section sampled (Banner and Hanson, 1990). No evidence for exposure is present in the top ~30 m of this section.

The section on the western flank of the Saddle Peak Hills is 110 m thick, significantly thinner than the section measured in Saratoga Springs (Figs. 2.2 and 2.9E). This change in thickness could be in part due to the placement of the basal contact of the Beck Spring Dolomite in what is clearly a gradational contact. However, even by invoking facies change between the two sections, there still must be a significant change in thickness. Aside from the notable change in thickness between the two sections, the sedimentology is similar. Meter-scale mixed siliciclastic-carbonate parasequences with microbial fabrics comprise the base of the section. There is evidence for sub-aerial exposure in the middle of the section, and the top is composed of re-sedimented dolostone and pisolite. However due to small-scale faulting, diagenetic overprinting, and sandblasting from nearby sand dunes, the pisoids are variably preserved.

From north to south along the western flank of the Saddle Peak Hills, the Beck Spring Dolomite grades from a ~100 m blue-grey massive dolomite with few siliciclastic interbeds to interbedded dolomite and siliciclastics in well-developed ~1-10 m parasequences. The sandstone and conglomerate beds in this section preserve similar sedimentary features to those in Saratoga Springs. The coarse sandstone beds preserve flat laminations and with bed geometries that vary from quasi-tabular to lensatic. Approximately 3.5 km SE of the measured section in Saddle Peak Hills, just south of where the Virgin Spring Limestone rests unconformably on the Crystal Spring Formation (Fig. 2.3), the Beck Spring Dolomite is siliciclastic-poor with the exception of 2-3 very

poorly-sorted pebble to cobble quartz conglomerates with sub-rounded clasts of up to 10 cm in diameter near the top of the unit (Fig. 2.9A). The number of these conglomeratic beds is uncertain due to fault repetitions.

The section at Beck Canyon is ~290 m thick. We place the basal contact at the orange and black dolostone marker beds that are also present in other sections. Aside from the transition beds at the base and top of the unit, the Beck Spring Dolomite here is almost entirely dolostone that alternates between finely laminated grainstone, microbialaminite, stromatolite and stromatactis. The base has abundant bedded and nodular chert, occasionally with silicified pisoids. Sedimentary breccias are present in the lower-middle part of the section, but are not as abundant as they are in the Alexander Hills (Fig. 2.7). Like almost all the other sections, ooids and pisoids were found in the middle and top of the section here. Beautifully preserved ooids, pisoids, and oncoids are preserved in the upper 10 m of the section in the fault block in the west part of Beck Canyon (Fig. 2.9D). In this section and the Black Mountain section, more carbonate is preserved at the top of the Beck Spring Dolomite, recording a return to positive values of ~+2‰ after the negative $\delta^{13}C$ excursion. In these two sections, the oncolite bed correlates with the basal part of KP1 in other sections. This oncolite bed is the source of the fossiliferous oncolite olistoliths in the Kingston Peak Formation in the Kingston Range (Macdonald et al., 2013a).

Further to the east, revised mapping shows that the sedimentary Beck breccia, which was previously included in measured sections of the Beck Spring Dolomite near the Jupiter and Snow White mines (Harwood and Sumner, 2011), is actually re-deposited Beck Spring Dolomite at the base of KP2 (Fig. 2.5). Laterally the base of KP2 transitions

from Beck Spring Dolomite breccia into a massive diamictite with a mixture of clasts from many of the underlying units. Additionally, in a few gullies near Snow White Mine, there are small outcrops of mixed lithology KP2 glaciogenic facies that underlie the KP2 Beck breccia, confirming that the Beck breccia was deposited during Kingston Peak time rather than as debris infilling paleokarst caves during Beck Spring time. The heavily silicified horizon beneath the megabreccia is mapped as the basal Kingston Peak unconformity (Fig. 2.5).

Further north in the SW Black Mountains, the Beck Spring Dolomite is ~295 m of predominantly dolostone. The lower portion of this section is dominated by resedimented dolostone and intraclastic carbonate chip debris flows. There are a few meter-scale beds of intraclastic dolomite breccia composed of pebble- to cobble-sized angular, planar-laminated and stromatolite clasts. There are several beds of pisolites in the middle of the section, and the upper part of the section is dominated by microbialaminite, stromatolite and well-preserved stromatactis. One unusual feature of this section is that there is a 19 m thick fine-grained sandstone marker bed 30 m below the top contact with KP1. The top 30 m of the section is interbedded shale, silt, bedded chert, partially silicified microbialaminite, and conical stromatolites reminiscent of *Conophyton*. Similar to the section in Beck Canyon, oncolites are present in the top bed of the Beck Spring Dolomite here. The contact with KP1 is gradational, and the basal few meters of KP1 contain centimeter-scale silty dolostone beds. Just north of this measured section, the upper ~50 m of the Beck Spring Dolomite is absent, and instead, a thick sedimentary breccia of resedimented dolostone sits on the upper-middle portion of the Beck Spring Dolomite. The nature of the basal and top contacts was not clear due to fault complications. The

$\delta^{13}C$ values at the base of the section are +4 to +6‰, and these positive values persist for ~200 m. There is a negative excursion to -2‰ just below the sandstone marker bed. In the top 30 m of section, there is a return to positive values of +1 to +2‰. Thin tan dolostone beds in the basal ~5 m of KP1 show a steady decrease in $\delta^{13}C$ values.

The section at Happy Canyon in the Panamint Mountains (Fig. 2.8A) is ~180 m thick. The Beck Spring Dolomite here contains a strong foliation and is pervasively recrystallised. Here, the base of the section is defined as the base of the massive, light grey, resedimented dolostone. Below the Beck Spring Dolomite is a pink, quartz-rich, pebble conglomerate, and it is unclear if this contact is conformable or faulted. The lower to middle part of the section consists predominantly of light grey dolomite grainstone interbedded with local pisoid intervals, some of which are heavily silicified. The middle to upper part of the section is dominated by intraclastic dolostone debris flows and sedimentary breccias with angular clasts of black and white finely laminated dolostone that pinch out laterally over tens of meters. In places, there are microbialaminites and clasts of microbialaminites. Here, the top contact with the Surprise diamictite, which is thought to be correlative with KP3 in southern Death Valley (Macdonald et al., 2013a; Petterson et al., 2011; Prave, 1999), is erosive and a kilometer-sized olistolith of the Beck Spring Dolomite is present a few meters above that contact (Fig. 2.8A). North of this section in Surprise Canyon, the top contact of the Beck Spring Dolomite is marked by sand grykes that are in-filled with Surprise diamictite (Fig. 2.9F). This is the only locality at which we observed an unconformable karstic surface at the top of the Beck Spring Dolomite, and this karsting has a different age and intensity than the microkarst features that are present throughout the lower to middle Beck Spring Dolomite. Despite the

recrystallisation of the Happy Canyon section, the $\delta^{13}C$ values are remarkably similar to those in other sections. The $\delta^{13}C$ values at the base of the section rise from ~+1.5 to ~+4.5‰. In the middle of the section there is a decrease back to ~+1.5‰ followed by a gradual rise up to ~+4.5‰, similar to the "W-shape" profile that is seen in middle to upper parts of other sections. At the top of the section, there is a negative excursion to ~+0.5‰.

Due to large regional lateral facies changes, it is difficult to definitively identify the Beck Spring Dolomite at the Silurian Hills section. Kupfer's units 11 and 12 (Fig. 2.7), are comprised of siliciclastic-dominated, 1-10 m thick parasequences (Fig. 2.8D). This interval is 210 m thick and marked by alternating beds of siltstone, sandstone and pebble to cobble conglomerate, similar in thickness to the parasequences in the Beck Spring Dolomite at Saratoga Springs (Fig. 2.8C). Near the top of the section, the parasequences are mixed siliciclastic and limestone. The top is marked by a 5 m thick limestone unit containing molar tooth structure (top of Kupfer's unit 12). In Kupfer's units 10 and 11, the $\delta^{13}C$ values range between ~-6 and -2‰. At the top of the section, in Kupfer's unit 12, the $\delta^{13}C$ values are more positive, reaching values of ~+6.5‰. Kupfer's units 10-12 are correlative with either the Beck Spring Dolomite or the Virgin Spring Limestone. Carbon isotope values from unit 12 and its stratigraphic position directly below massive glacial deposits are very similar (between +1 and +6‰) to that of the Virgin Spring Limestone (Fig. 2.7).

2.5.1.3. KP1

KP1 is a fine-grained siliciclastic interval that gradationally overlies the Beck Spring Dolomite. It is 0-200 m thick and occasionally contains centimeter-thick

dolostone beds and nodules in the basal part of the unit. KP1 consists predominantly of 1-10 cm thick beds of siltstone to fine-grained sandstone with minor nodules of finely crystalline dolomite. Sandstone beds are characterized by millimeter-scale, planar parallel laminations, and locally display normal grading. Slump folding and soft sediment deformation in KP1 is pervasive in the SW exposures of the Saddle Peak Hills (Fig. 2.9B).

In the Panamint Mountains, KP1 is likely equivalent to part of the Limekiln Spring Member of the Kingston Peak Formation (Mrofka, 2010), however, in the Happy Canyon section, it is erosively cut out by the Surprise diamictite. In Alexander Hills and Beck Canyon, the top of KP1 is also truncated or absent; the variable thickness is a result of truncation along the unconformable base of TU3, or the base of the Virgin Spring Limestone, and active faulting at the time of deposition of KP1. In the SW Black Mountains, KP1 is ~65 m thick. However, just north of the section, KP1 and the top of the Beck Spring Dolomite are cut out and overlain by a sedimentary breccia composed entirely of clasts of the Beck Spring Dolomite. Further to the NE, at Rhoades Wash, the Virgin Spring Limestone sits unconformably on basement, with a thin sandstone at the basal contact.

2.5.2. Key sedimentological and structural relationships in TU2 and TU3

Saddle Peak Hills

In the western Saddle Peak Hills, sub-TU3 deformation occurs on the meter scale to kilometer scale. Both folds and faulting are sealed by the sub-Virgin Spring Limestone unconformity in this area. On map scale, in the central western Saddle Peak Hills, the Virgin Spring Limestone rests unconformably on broadly folded TU2 and TU0 strata (Fig.

2.3); in the northwestern and southwest parts of Saddle Peak Hills it sits unconformably above Unit KP1, while in between these area it sits on progressively older strata. The oldest strata that it rests above is the Crystal Spring Diabase. Meter to 100-meter scale folding in the Horse Thief Springs Fm and Beck Spring Dolomite is also present in many areas of the western Saddle Peak Hills (Figs. 2.10E and 2.10F). Additionally, in the southern Saddle Peak Hills, a fault between Unit KP1 and the Beck Spring Dolomite is sealed by the Virgin Spring Limestone (Fig. 2.3). All of the compressional structures are preserved in the sub-TU3 strata in Saddle Peak Hills.

Kingston Range

West Beck Canyon (Fig. 2.6) was previously mapped by Calzia et al. (2000). Revised mapping here documents different generations of faulting and pre-KP2 folding. Precambrian faults in this map area include a fault that places the Crystal Spring Fm against the Horse Thief Springs Fm (Fig. 2.10), with hundreds of meters of offset. This fault has been tilted to near vertical by Cenozoic deformation and was likely reactivated as a Cenozoic normal fault with minor displacement in the overlying Noonday Fm.

High angle Cenozoic tear faults that are oriented NE-SW have also reactivated Neoproterozoic structures (Fig. 2.6). There are only a few meters of displacement of Unit KP1 across these faults, but these same faults also place broadly folded TU2 strata against KP3 (Fig. 2.6). Additionally, syn-sedimentary faults are present in KP3 in this area. Significant discrepancies in the amount of stratigraphic offset along high-angle Tertiary faults, with major facies changes across these faults, are suggestive of the reactivation of Neoproterozoic faults.

Figure 2.10. Photos showing folding and faulting of pre-Virgin Spring Limestone units in the Saddle Peak Hills and Kingston Range.
The locations of photos are labeled in the geologic maps in Figs. 2.3, 2.5, and 2.6. A) Folding in Beck Spring Dolomite in W. Beck Canyon. B) Large scale (100s of m) folds of the Beck Spring Dolomite and Saratoga Spring Sandstone in an anticline-syncline pair. C) Isoclinal folds in Mb 3 of the Horse Thief Springs Fm in W. Beck Canyon. D) Isoclinal fold in the Horse Thief Springs Fm near Jupiter Mine in the Kingston Range. This is the same fold that was documented by Walker et al., 1986. E and F) Folding in the Horse Thief Springs Fm and Beck Spring Dolomite in W. Saddle Peak Hills. People for scale in F. G) Tight isoclinal folding of the Beck Spring Dolomite in W. Beck Canyon. Folding is capped by unfolded KPc (KP3). H) Faulted contact between the Crystal Spring Diabase and Mb 3 of the Horse Thief Springs Fm in W. Beck Canyon. We interpret this fault as a high-angle Precambrian thrust fault that has been subsequently reactivated during the Cenozoic.

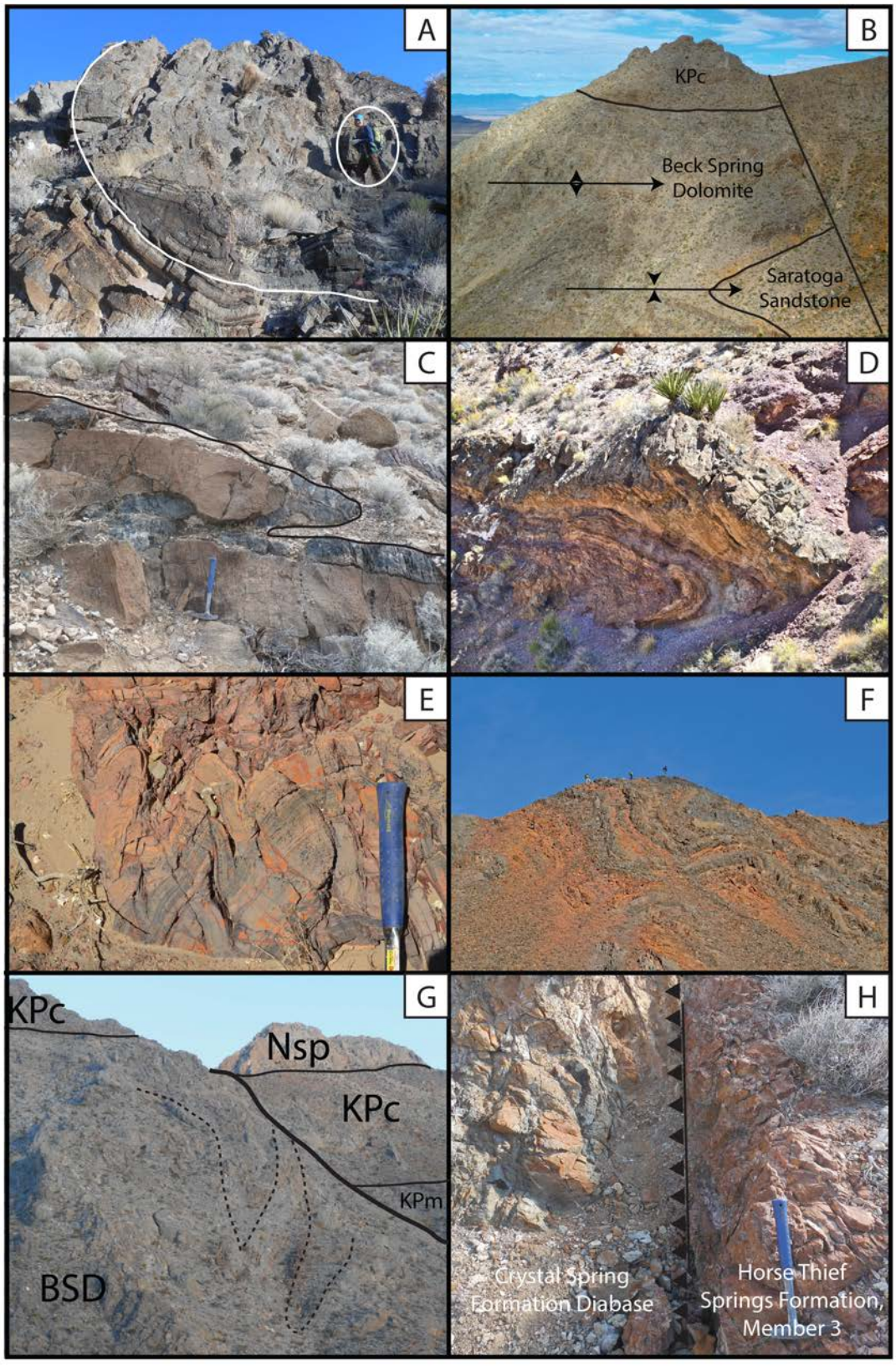

Figure 2.10 (continued).

In addition to Neoproterozoic faulting, there is also isoclinal folding that is sealed by undeformed strata of Unit KP3 (TU3). Map scale folding of TU2 is documented in Western Beck Canyon (Figs. 2.6 and 2.10B). There is also meter to 100-meter scale folding of TU2 units in this area and in Eastern Beck Canyon (Figs. 2.10A, 2.10C, 2.10D, and 2.10G). These meter to kilometer-scale folds are sealed by an unconformity between the Beck Spring Dolomite and Unit KP3 (Figs. 2.11A-C); there is no possibility that the contact between these two units is a fault contact.

In addition to there being evidence for Neoproterozoic faulting and folding in the Kingston Range, there is also evidence for the generation of topographic highs prior to and during the deposition of the Kingston Peak Fm. The presence of large olistoliths (<1 km) in West Beck Canyon and Southeast Kingston Range (Fi. 2.12A) requires that significant topography be generated prior to their deposition. Additionally, in western Beck Canyon, the Noonday Fm sits on a number of different units ranging from the Crystal Spring Fm to the Kingston Peak Fm over very short lateral distances (Fig. 2.6). In this same area, the Noonday rests non-uniformly above the Beck Spring Dolomite and Horse Thief Springs Fm (Fig. 2.12B and C).

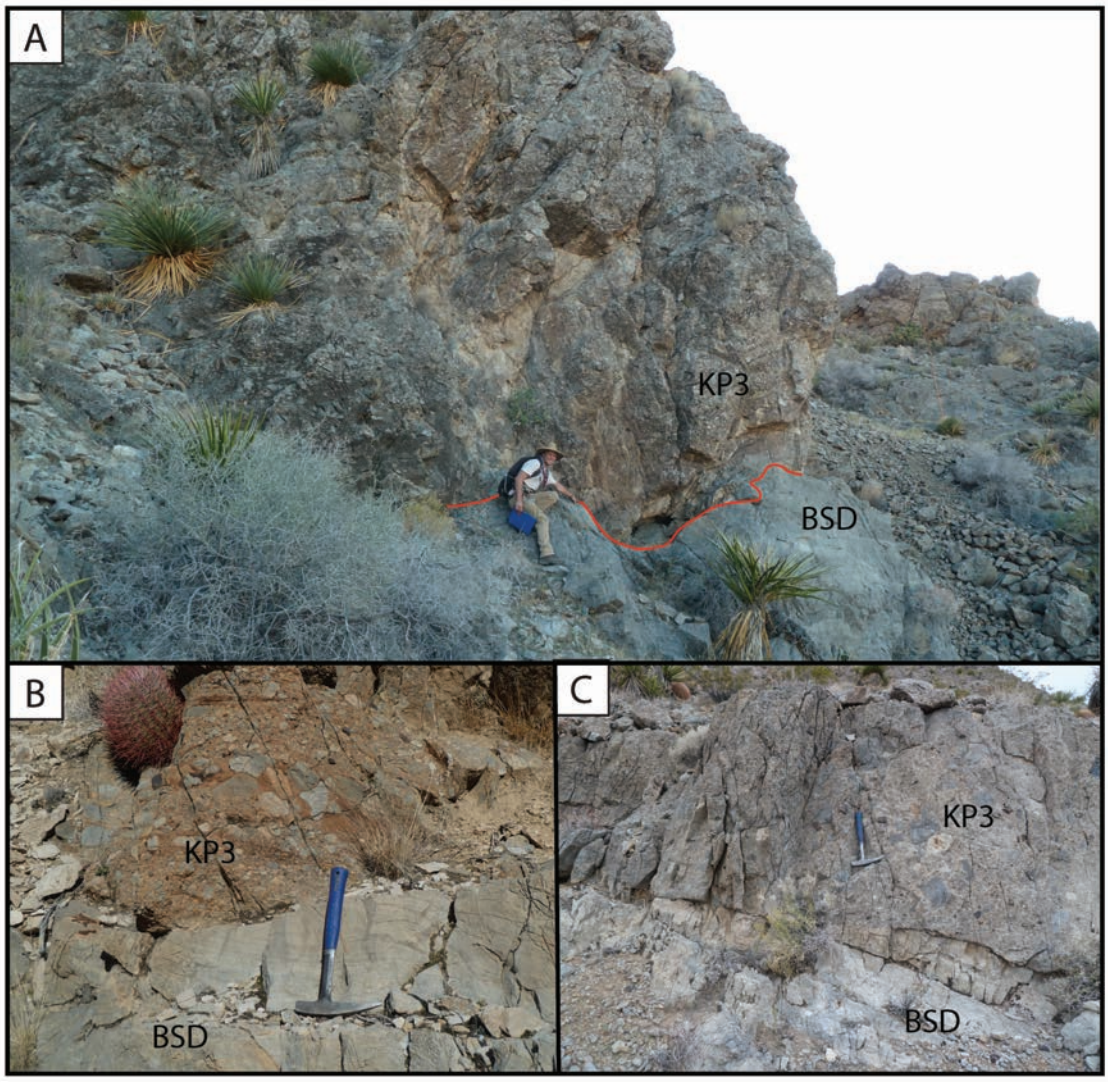

Figure 2.11. Photos showing angular unconformity between the Beck Spring Dolomite and KP3 (KPc) in West Beck Canyon.
Locations of the figures are indicated in Fig. 2.6. A) Red line shows angular and erosional unconformity between the Beck Spring Dolomite and the KPconglomerate facies of the KP3 Mb of the Kingston Peak Fm. B) and C) Angular unconformities between the Beck Spring Dolomite and KP3.

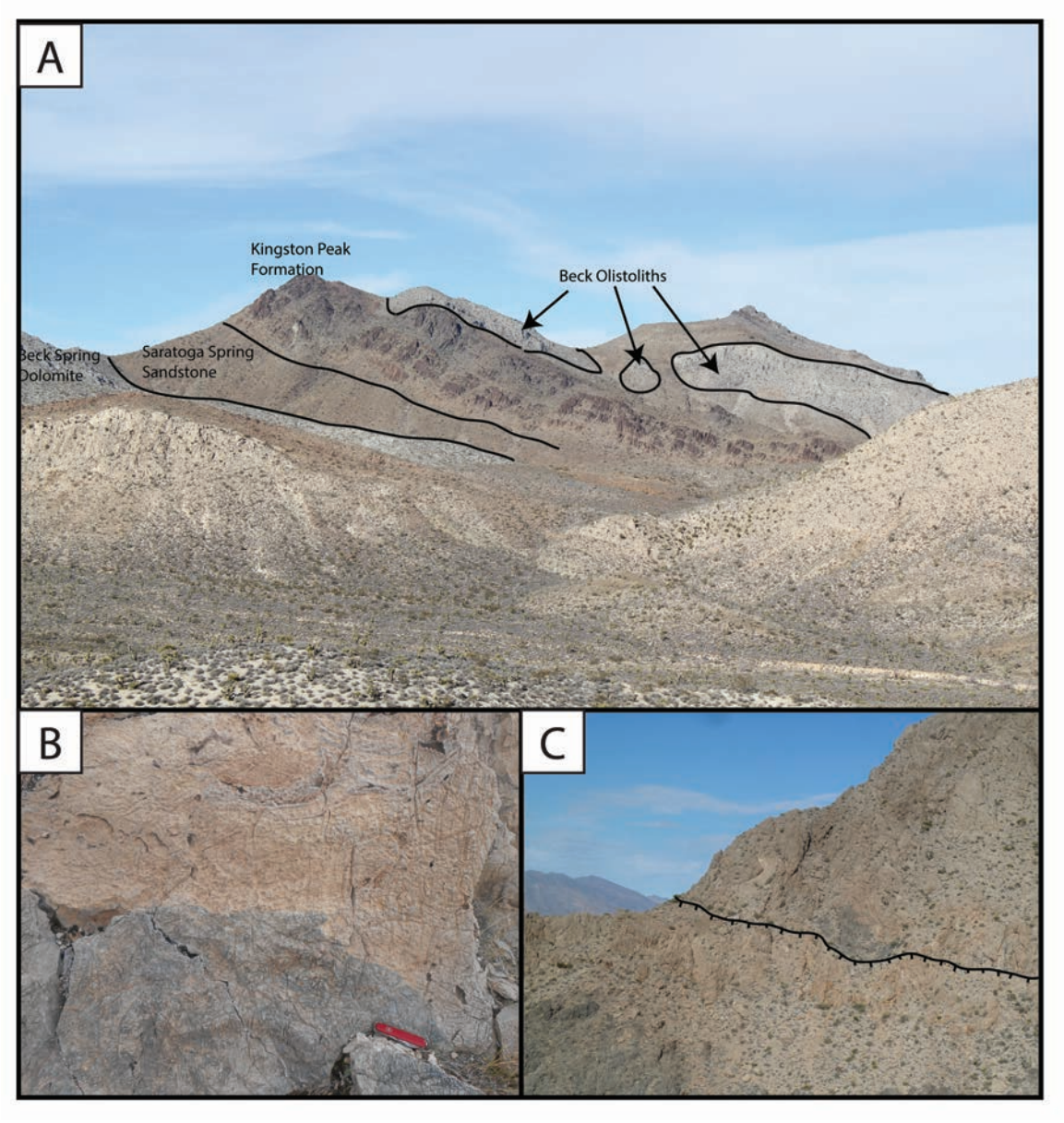

Figure 2.12. Photographic evidence for the generation of topography during TU2 time.

Locations of the photos are indicated in Figs. 2.5 and 2.6. A) Photo showing ~1 km Beck Spring Dolomite olistoliths in KP3. B) The Sentinel Peak Mb of the Noonday Fm on karsted Beck Spring Dolomite in W. Beck Canyon. Throughout the Kingston Range, the Noonday sits unconformably on different units that range from basement to the Kingston Peak Fm, progressively onlapping onto older units northward. This is a close-up photograph taken from the same locality as the photo in Fig 2.3C. C) Photo of a south-dipping normal fault with minor offset in W. Beck Canyon. On both sides of the fault, the Noonday Fm is sitting unconformably on the Beck Spring Dolomite. This is an important contact because a few 100 m further to the east, we document a south-vergent thrust fault that places the Crystal Spring Fm onto the upper Horse Thief Springs Fm (see geologic map of W. Beck Canyon to left).

2.5.3. Detrital Zircon Geochronology

Normal probability plots for 15 detrital zircon samples are plotted with a generalized geological map of the southern Mojave crustal province in Fig. 2.13. Samples from the Horse Thief Springs Formation yielded broad peaks at ~1780, 1550, 1450 and 1200 Ma with a minor Archaean peak. Of the 540 grains from the five samples from the Horse Thief Springs Formation that were analyzed, there were no grains from the ~780 Ma population that were found by Mahon et al. (2014b). The two samples from the measured section at Silurian Hills show very similar age distributions to other TU2 samples.

Horse Thief Springs, Beck Spring Dolomite, and KP1 samples show peaks at ~1780, 1450, and 1200 Ma, with a minor ~1650 Ma peak. Many of the separates from these samples contain abundant (~25%) faceted grains. Between the TU2 and Virgin Spring Limestone samples there is a change from spectra with local Mojave sediment sources to spectra with ~1300 and 1580 Ma age peaks (Fig. 2.13B) suggesting a change in sediment source. Spectra in the KP2 samples display prominent ~1780 peaks with minor ~1450 and 1200 Ma age peaks while the spectra in the KP3 sample just display broad peaks between 1450 and 1200 Ma.

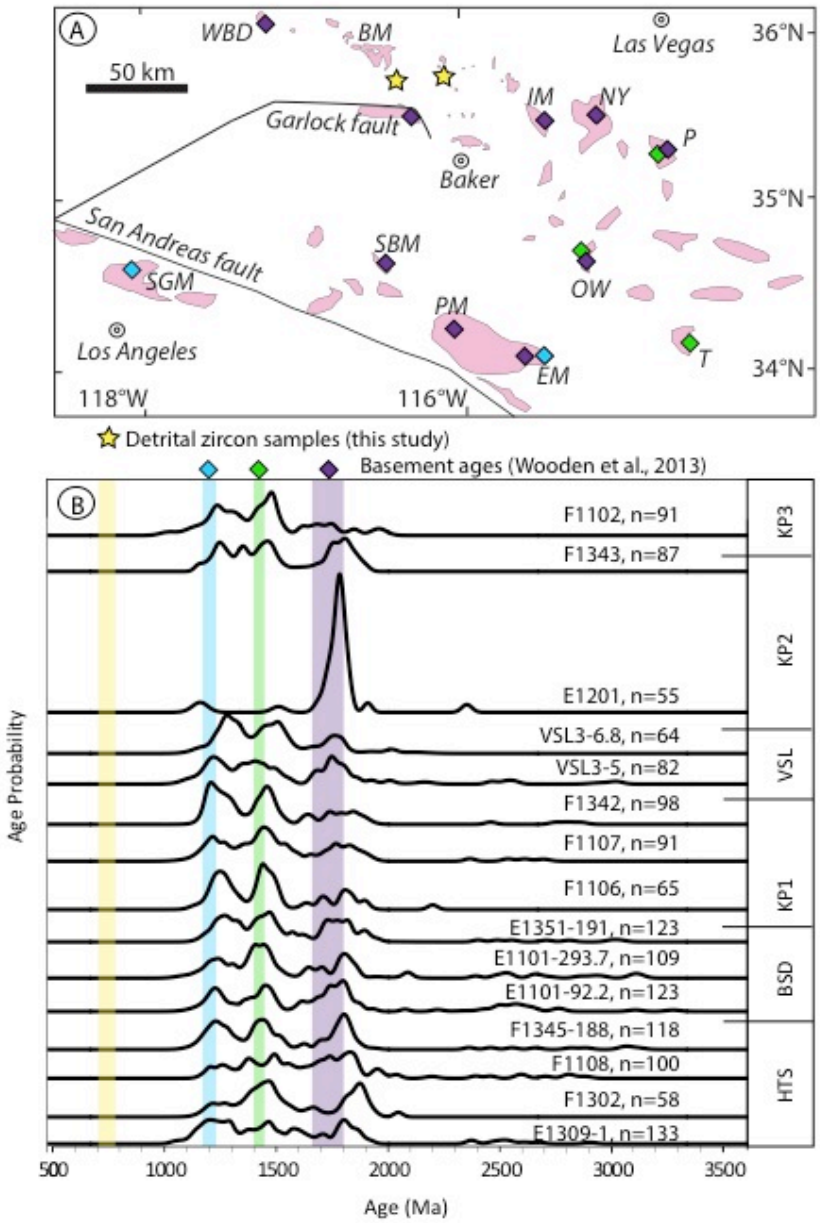

Figure 2.13. Detrital zircon geochronology of the Pahrump Group.
A) Generalized geological map of the southern Mojave crustal province (adapted from Wooden et al., 2013). Blue, green, and purple diamonds mark localities sampled by Wooden et al. (2013). Yellow stars mark localities of detrital zircon samples presented below. Abbreviations: EM – Eagle Mountains, IM – Ivanpah Mountains, NY – New York Mountains, OW – Old Woman Mountains, P – Piute Range, PM – Pinto Mountains, SBM – San Bernardino Mountains, SGM – San Gabriel Mountains, T – Turtle Mountains. B) Normal probability plots for 12 detrital zircon samples from SE Death Valley. The specific sections and stratigraphic horizons are indicated in Fig. 2.7. The lower nine samples are from TU2 and the upper three samples are from TU3. Blue, green, and purple shaded bars are basement ages from Wooden et al. (2013) and yellow shaded box is the age range for TU2 (Macdonald et al., 2013a; Mahon et al., 2014b).

2.6. Discussion

2.6.1. TU2 basin reconstructions

Reconstructing Neoproterozoic paleogeography in Death Valley is complicated by extensive Phanerozoic faulting. The region experienced Permian to Mesozoic orogenesis and magmatism (Burchfiel et al., 1992; Burchfiel et al., 1970; Snow et al., 1991; Snow and Wernicke, 2000; Wernicke et al., 1988; Wright et al., 1976) with associated felsic and mafic intrusions (Calzia et al., 2000; Fleck, 1970; Wright et al., 1991), followed by right-lateral transtension and the formation of pull-apart basins (Renik and Christie-Blick, 2013; Wright, 1976; Wright et al., 1991). In previous studies, the Mesozoic thrust sheets have been used as piercing points for palinspastic reconstructions (Bergmann et al., 2011; Petterson et al., 2011; Snow and Wernicke, 2000; Wernicke et al., 1988), however, much debate remains on the correlation of the thrust sheets (Renik and Christie-Blick, 2013). For the NW to SE ordering of the seven measured sections of TU2 (Fig. 2.7), we follow the reconstruction of Renik and Christie-Blick (2013) and Serpa and Pavlis (1996). For our reconstruction of the TU2 basin, the Panamint Mountains are on a different thrust sheet than the stratigraphy of SE Death Valley and do not restore south of the other measured sections in this study. Prave (1999) correlated Kupfner's units 5-12 with the Middle Park-Wildrose succession of the Kingston Peak Formation in the Panamint Range. The structural placement of the Panamint Mountains used in this study is more consistent with the interpretations of Maud (1983) in which the carbonate-dominated Beck Spring Dolomite section in Happy Canyon restores adjacent to the carbonate-dominated sections of the Black Mountains and Alexander Hills rather than in the southern siliciclastic belt in the Silurian Hills.

2.6.2. Facies Model

2.6.2.1. Horse Thief Springs Formation

The thickest section of the Horse Thief Springs Formation is at the type locality in Beck Canyon. Based on our reconstruction and the subsequent arrangement of measured sections from SW to NE (Fig. 2.7), maximum subsidence is occurring in the NE part of the basin. This arrangement of sections, with the siliciclastic-dominated sections in the SW and the carbonate-dominated sections in the NE, is consistent with paleoflow measurements that suggest that the sediment source was primarily from the south and the shoreline had a NW-SE orientation (Maud, 1979). Importantly, between basal TU0 (Macdonald et al. 2013a; TU1 is assigned to early Neoproterozoic strata from NW Laurentia, but is not present in Death Valley) and TU2, paleoflow measurements record a marked changed in being derived from the N and E to being derived from the S-SW (Maud, 1979; Maud, 1983; Roberts, 1982). These changes in sediment transport direction have been long recognized and were used as a line of evidence in support of the aulacogen model (Roberts, 1982). Considering that the duration of the unconformity between TU0 and TU2 is ca. 200-300 Myrs (Mahon et al., 2014b), an alternative model is that TU0 strata formed on a south- and west-facing open margin whereas deposition of TU2 strata marks the onset of a broadly N-NE facing basin bounded by an upland to the south of Death Valley.

2.6.2.2. Beck Spring Dolomite

Thicknesses and facies patterns of the Beck Spring Dolomite are similar to those of the Horse Thief Springs Formation; the shallower-water facies and more siliciclastic-dominated sections are in the SW and the carbonate-dominated sections are in the NE.

We interpret this facies architecture to reflect depositional environments in which a carbonate platform fringed an uplifted land surface to the SW (Fig. 2.14A).

The siliciclastic-rich facies of the Beck Spring Dolomite in Saratoga Springs and the Saddle Peak Hills contain sedimentary features that are characteristic of coarse braided fluvial deposits. We interpret the Silurian Hills section, the most southern section measured in this study, as being deposited closer to a southern upland, on the interface between an alluvial apron and coarse fluvial facies (Blair and McPherson, 1994; Bull, 1972). The base, top, and thickness of the Beck Spring Dolomite at this locality are difficult to identify due to the significant lateral facies change between here and Saratoga Springs. The recrystallised limestone at the top of our measured section (Kupfer's unit 12) looks similar sedimentologically to the Beck Spring Dolomite, but the $\delta^{13}C$ data is more similar to that of the Virgin Spring Limestone (Fig. 2.7). However, the details of this correlation do not compromise the depositional model.

Overall, our interpretation of the depositional environment of the Beck Springs differs from previous workers who suggested that this unit was deposited on a stable, shallow marine platform in a subtidal to intertidal environment. Instead, we suggest that accommodation space was created quickly in the basin, either by thinning or loading of the crust, while calcifying microbes competed against sediment influx to rapidly fill the space.

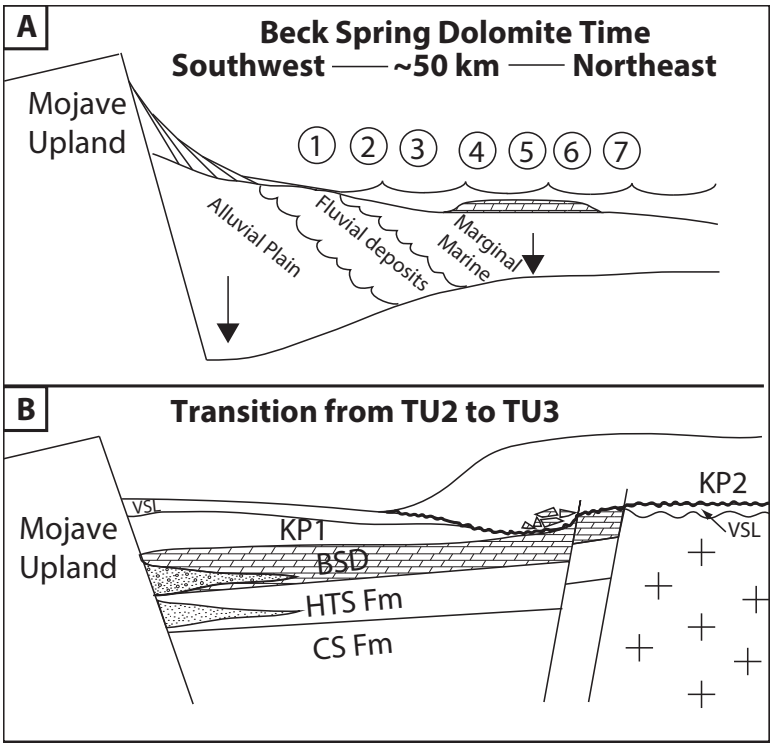

Figure 2.14. Schematic depositional and tectonic models for TU2.
A) Model for the Beck Spring Dolomite. The circled numbers refer to the general locations of the measured sections in Fig. 2.7 along a simplified north to south transect of the basin. Paleoflow is from the south. B) Tectonic model for the switch in basin polarity that occurs between TU2 and TU3. Unit KP1 and the Virgin Spring Limestone record this transition as a basin-bounding fault daylights. The basin switches from NE-facing to SW-facing across the TU2-TU3 boundary.

2.6.2.3. KP1

Based on our observations, we suggest that KP1 is part of the transgression that is recorded in the upper part of the Beck Spring Dolomite and was deposited on a more distal prodelta. The influx of siliciclastics that swamps the underlying carbonate platform during this transgression could be the result of either lateral migration of a delta front or the emergence of a basin-bounding fault. Given that there is evidence of syn-sedimentary faulting in TU2 (Macdonald et al., 2013a; Mahon, 2012), we suggest that the siltstone and fine-grained sandstone of KP1 were deposited very quickly with the development of a new basin-bounding fault.

The interpretation that KP1 was deposited during a period of major faulting is consistent with the pervasive slump folding in the Saddle Peak Hills (Fig. 2.9B) and the stratigraphic relationships of KP1, the Virgin Spring Limestone, and the Beck breccia in the Black Mountains. We suggest that the rapid influx of fine sediments during KP1 time marks the onset of basin reorganization (Fig. 2.14B).

2.6.3. The Beck Spring Mountains and the Saratoga Orogeny

Geologic mapping of Neoproterozoic structures in the Saddle Peak Hills and Kingston Range is complicated by large facies change in the Pahrump Group units, SE- and N-vergent Mesozoic folds and thrusts, and Cenozoic normal faults and detachments. Despite the structural complexity and tectonic overprinting in these areas, with integrated structural, stratigraphic, and sedimentological evidence, we demonstrate that: 1) Different scales (1-1000 m) of isoclinal folds (Figs. 2.10A-G) are sealed, at a knife-sharp contact, by undeformed strata of TU3 (Figs. 2.11A-C) in different areas around Death Valley. 2) Significant discrepancies in the amount of stratigraphic offset along high-angle Cenozoic faults, with major facies changes across these faults, are suggestive of the reactivation of Neoproterozoic faults. Specifically, in West Beck Canyon, a reverse fault juxtaposes the Crystal Spring Fm against the upper Horse Thief Springs Fm (Figs. 2.6 and 2.10H). This fault has been reactivated and tilted to near vertical during Cenozoic time. There are other high angle NE-SW oriented strike slip faults in West Beck Canyon that also have discrepancies in their offset (Fig. 2.6), that suggest that they were active during Kingston Peak time.

Together, these pieces of evidence demonstrate that there are at least two generations of Neoproterozoic faulting present in the Kingston Range. Reverse faults and

folds post-date the deposition of the Saratoga Spring Sandstone and pre-date the deposition of the Kingston Peak Fm. Later, high-angle normal or strike-slip faults were active during Kingston Peak time.

The folding in the TU2 units has been previously attributed to Mesozoic deformation that is localized along lithological boundaries or Cenozoic deformation beneath a roof detachment (Calzia et al., 2000). The orientation of the folds is similar to the orientation of the Cretaceous folds in the Nopahs (Pavlis et al., 2014), causing difficulty and confusion in distinguishing between different generations of compression. Here, with new mapping, particularly of the area in western Beck Canyon (Fig. 2.6), we provide strong sedimentological, stratigraphic, and structural evidence that suggests that the transpressional deformation in the TU2 units is Neoproterozoic in age. This transpressional tectonism, or the Saratoga Orogeny, generated topography, which we refer to as the "Beck Mountains", that is responsible for the subsequent emplacement of large olistoliths (<1 km long) in the overlying Sturtian-aged glacial deposits of the Kingston Peak Formation (Fig. 2.12A). We suggest that this Cryogenian tectonism is also at least in part responsible for the regional sub-Noonday unconformity (Figs. 2.13A-C). The geometry of the sub-Noonday unconformity is clearly seen in the eastern Kingston Range, where in the northeastern part of the Range the Noonday Fm is sitting unconformably on basement and ~8 km to the southwest it sits on kilometers of Kingston Peak strata (Fig. 2.4). By using the basal contact of the Noonday to restore the Cenozoic fault blocks, which have transported to the southwest, to the northeastern-most outcrop of the Noonday, it is clear that what is now the northern Kingston Range was a paleohigh during Kingston Peak time. The Cenozoic detachment faults are being reactivated along

the Neoproterozoic fault scarp. All of this deformation is sealed by KP4 and the Noonday Fm, or the Marinoan-aged glacial deposit and cap carbonate, respectively.

2.6.4. Basin Forming Mechanisms

The Meso- and Neoproterozoic Pahrump Group through the Ediacaran Johnnie Formation preserve four discrete basin-forming events that record the tectonic and sedimentological history of Death Valley, a promontory on SW Laurentia. Previous tectonic models have suggested that TU2 through TU5 formed in a long-lived rift basin prior to passive margin development in the Cambrian (Yonkee et al., 2014 and references cited therein). However, TU2 was deposited more than 200 Myrs before the rift to drift transition in lower Cambrian strata (Armin and Mayer, 1983; Bond et al., 1985). Thus, TU2 could not have been deposited by rifting of the proximal western margin. Instead, a model for formation of the ChUMP basin must account not only for local, syn-sedimentary faulting, but also low stretching factors necessary to delay thermal subsidence.

We are not the first to question the protracted rift model or transtension. In the eastern Kingston Range, Walker et al. (1986) documented Neoproterozoic folding and faulting in the Crystal Spring Formation, Beck Spring Dolomite, and lower part of the Kingston Peak Formation that is overlain by relatively un-deformed conglomerate and questioned tectonic models that invoked simple, protracted rifting. However, some of the thrust faults of Walker et al. (1986) are on the margins of olistolith blocks of the Beck Spring Dolomite that were emplaced during syn-Kingston Peak Formation normal faulting (Macdonald et al., 2013a).

Interestingly, deformation of a Neoproterozoic age has been described along a

narrow belt in NW Canada, referred to as the Corn Creek Orogeny (Eisbacher, 1981; Thorkelson, 2000). These structures include folding and thrusting of ca. 800 Ma strata of the Mackenzie Mountains Supergroup that are sealed by olistolith-bearing units of the ca. 650 Ma Mt. Profeit Dolostone (Macdonald et al., 2013b). To the east in the Mackenzie Mountains, the Coates Lake Group, which is in part coeval with the Beck Spring Dolomite (Macdonald et al., 2013a), was interpreted to have formed in a series of strike-slip basins (Eisbacher, 1981). These features suggest the Coates Lake Group, equivalent Callison Lake dolostone, and the Corn Creek structures formed during transtension and transpression.

Characteristic features of strike-slip basins include basin asymmetry, rapid, episodic subsidence, abrupt lateral facies changes, local unconformities, and large facies changes in coeval basins that formed in the same region (Christie-Blick, 1985). These basins also tend to preserve coarse-clastic units in fault-bounded basins (Ingersoll, 1988). Additionally, Reading (1980) predicts that strike-slip faults within continental crust often experience alternating periods of extension and compression as slip directions adjust along a fault. The opening and closing of basins along strike-slip faults is thus referred to as the 'Reading Cycle'. This model could help explain the multiple unconformity-bound, basin-forming events that occur in the Pahrump Group through Ediacaran strata in Death Valley, and localized deformation that continues up into the Argenta member of the Kingston Peak Formation (Petterson, 2009).

Break up of the supercontinent Rodinia started between 850 and 750 Ma and is associated with the emplacement of several Large Igneous Provinces (LIPs) (Li et al., 2008). Rifting of a more distal margin of Laurentia, or subsidence related to the

emplacement of the ca. 780 Ma Gunbarrel LIP in Laurentia and Australia and the coeval Kangding LIP in South China (Ernst et al., 2008; Li et al., 2003), may also account for local faulting and the narrow basin formation that accommodated deposition of TU2. However, importantly, these deposits do not record rifting of the proximal western margin of Laurentia that culminated in the Ediacaran to Cambrian passive margin, but instead reflect a distinct and separate tectonothermal event.

2.6.5. Carbon Isotope Chemostratigraphy and Laurentian Correlations

Our data include the first high-resolution $\delta^{13}C$ curve for the Horse Thief Springs Formation. If the $\delta^{13}C$ values presented here reflect the carbon isotopic composition of dissolved inorganic carbon in seawater, then our data show multiple previously undocumented negative carbon isotope excursions between ca. 780 and 730 Ma. To test the possibility that these values reflect a global signature, they should be reproducible in other correlative Laurentian basins. Alternatively, if the base of TU2 is slightly older than LA-ICPMS detrital zircon ages suggest (Mahon et al., 2014b), the Horse Thief Springs Formation could be correlative with the Bitter Springs Stage, which has been constrained to between ca. 811 and 780 Ma (Macdonald et al., 2010). This correlation could be tested with additional geochemical analyses that would provide greater age precision on detrital zircons from the base of the Horse Thief Springs Formation.

The $\delta^{13}C$ values of the Beck Spring Dolomite refine correlations within the TU2 basin. The slight downturn in negative $\delta^{13}C$ values in the middle of the "W-shape" profile is a marker of synchronicity that is documented across the basin. Similarly, the negative excursion at the top of the Beck Springs Dolomite is another synchronous marker. Values from the top 5-20 m of the Beck Canyon, Alexander Hills, and Black Mountains sections

return to positive $\delta^{13}C$ values, demonstrating diachronous deposition of carbonate across the basin. Coupled with remarkable similarity to data from the Callison Lake dolostone (Fig. 2.15), we suggest that the anomaly at the top of the Beck Spring Dolomite is global and correlative with the ca. 735 Ma Islay anomaly (Hoffman et al., 2012; Strauss et al., 2014).

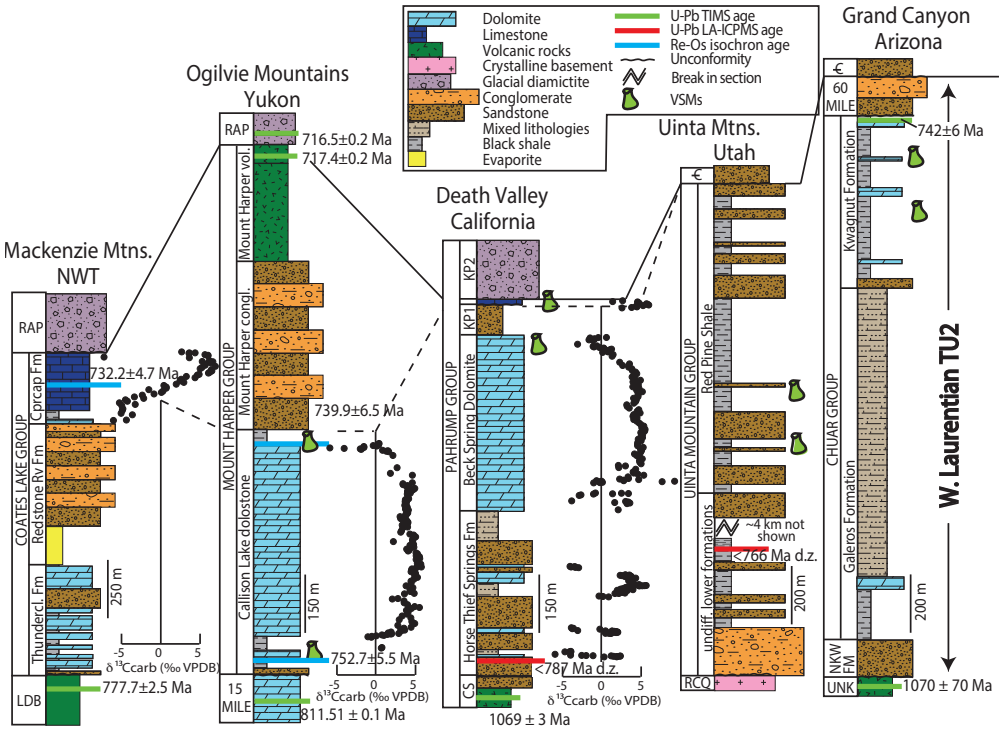

Figure 2.15. Refined regional correlations for successions from western US and NW Canada that are generally coeval with TU2 strata in Death Valley.
Detrital zircons at the base of the Horse Thief Springs Formation have been dated using LA-ICPMS at c. 780 Ma (Mahon et al., 2014b), providing a maximum age constraint for TU2. Ages at the base of KP2 are from correlation to NW Canada (Macdonald et al., 2013a; Macdonald et al., 2010). Age constraints on the Chuar Group include a 742 ± 6 Ma U-Pb zircon age from an ash (Karlstrom et al., 2000) at the top of the Kwagnut Formation. The shale at the top of the Callison Lake Dolostone has a Re-Os age of 739.9 ± 6.5, providing a date for the Islay excursion (Strauss et al., submitted). Additionally, the basal Callison Lake dolostone has a Re-Os age of 752.7 ± 5.5 Ma (Rooney et al., 2015). A Re-Os age of 732.2 ± 4.7 is from the organic-rich limestone of the Coppercap Formation of the Coates Lake Group (Rooney et al., 2014). VSMs have been identified in the upper Beck Spring Dolomite and Virgin Spring Limestone (Licari, 1978; Macdonald et al., 2013a), the Red Pine Shale (Vidal and Ford, 1985), the Kwagnut Formation (Dehler et al., 2007), and the Callison Lake Dolostone (Strauss et al., submitted). Carbonate $\delta^{13}C$ values are plotted for carbonate-rich successions (Macdonald et al., 2013a; Macdonald et al., 2010; Rooney et al., 2014). Given the proposed tectonic setting of a strike-slip margin for TU2, we emphasize the broader correlation of coeval basins along western Laurentia rather than formation-specific ones.

It is also possible that the $\delta^{13}C$ values from TU2 may not represent ancient seawater composition, but rather some local sedimentary processes including authigenic precipitation or post-depositional alteration. However, the isotope excursions appear to be inconsistent with an explanation that invokes surface exposure and alteration through interaction with terrestrial soils (Knauth and Kennedy, 2009). There is abundant evidence for exposure in the Horse Thief Springs Formation, but there is no systematic way in which the exposure surfaces correlate with the negative $\delta^{13}C$ values. In fact, some of the carbonates that show evidence for exposure have positive $\delta^{13}C$ values of up to +5‰. In addition, the $\delta^{13}C$ excursions in the Horse Thief Springs Formation are continuous and do not display much variability, a feature that would be expected if the negative excursion was a result of penetration of depleted fluids from terrestrial soils into the underlying carbonate.

Our evidence that the negative isotope excursion at the top of the Beck Spring Dolomite is not related to surface exposure and alteration through terrestrial soils is geological and sedimentological in nature. Our geological mapping of the Beck Spring Dolomite shows that the "paleokarst caves" that have been reported from the top of the Beck Spring Dolomite in the Kingston Range were formed during Kingston Peak time, not Beck Spring Dolomite time. Additionally, in several of our measured sections, we demonstrate that the $\delta^{13}C$ excursion at the top of the unit is not associated with karsting or exposure but rather a transgression. These are significant results because they demonstrate that this anomaly can no longer be used as evidence for Neoproterozoic greening of land (Knauth and Kennedy, 2009).

TU2 has been correlated with the Chuar Group in Arizona, the Uinta Mountain Group in Utah, and the Coates Lake Group and Callison Lake dolostone of NW Canada (Dehler et al., 2010; Macdonald et al., 2013a; Macdonald et al., 2010; Strauss et al., 2014). All five of these basins share similar features and age constrains, however, given that we do not yet understand how to interpret the $\delta^{13}C$ values for the units in TU2, we do not advocate for member- and formation-specific correlations between TU2 and these other basins. We instead emphasize broader correlations between tectonostratigraphic units (Fig. 2.15). Additionally, if these basins are being accommodated by strike-slip motion along the margin of Laurentia, it is possible that subsidence is localized and these basins are not completely synchronous with one another. Nonetheless, researchers working on these five basins should continue to look for $\delta^{13}C$ curves similar to those from the Horse Thief Springs Formation and to use geochronology to refine the ages of different members and formations that are part of these basins to better constrain these correlations.

2.6.6. Detrital Zircon Provenance

Grenville-aged detrital zircons in the Neoproterozoic basins of northern and western Laurentia are commonly interpreted to be sourced from eastern Laurentia via transcontinental rivers (Dehler et al., 2010; Rainbird et al., 1992; Rainbird et al., 1997). However, an alternative interpretation is that grains from at least some of these basins were sourced from the more proximal southern extension of the Grenville Province (Anderson and Morrison, 1992; Bickford and Anderson, 1993). Granites dated at ~1220 Ma are present in the San Gabriel Mountains in SE California (Barth et al., 1995; Barth et al., 2001; Ekstrom et al., 1994), and New Mexico, Arizona, and Chihuahua host granites

that are ~1070 Ma (Iriondo et al., 2004; Rämö et al., 2003; Stewart et al., 2001). Neoproterozoic detrital zircon samples from Death Valley offer evidence for a southern, more local sedimentary source.

Sandstone in the Horse Thief Springs Formation contain zircons derived locally from the Mojave province (1780-1660, 1430-1400, and 1210-1180 Ma; Wooden et al., 2013), but also contain grains with ages between ~1950-1800 and 1650-1450 Ma (Figs. 2.13A and B) that do not have a local basement source. One possibility is that these grains are sourced from reworked Crystal Spring Formation, although the limited detrital zircon data from the Crystal Spring Formation do not yield these ages (Mahon et al., 2014b). Another possibility is that these grains are sourced from the Yavapai and Mazatzal crustal provinces (Amato et al., 2008; Cox et al., 2002; Duebendorfer et al., 2001; Iriondo et al., 2004; Karlstrom and Humphreys, 1998; Rämö et al., 2003). A third possibility is that an unknown source lay south or west of Laurentia during the Neoproterozoic. Many sandstone beds in the Horse Thief Springs Formation are texturally and compositionally mature, and paleoflow measurements indicate provenance from the SW (Maud, 1979; Maud, 1983; Roberts, 1982). A source that is consistent with these sedimentological observations is the Gawler Craton of Australia, which includes the ~1850 Ma Donington Suite and the ~1590-1570 Ma Gawler Range Volcanics (Blissett et al., 1993; Fanning et al., 1988; Peucat et al., 2002; Reid and Hand, 2012).

In the Beck Spring Dolomite, peaks become sharper and more dominated by the local, Mojave province peaks (Fig. 2.13B). This is consistent with the interpretation that as this basin was forming, coeval uplift to the south was occurring and limiting more regional sediment influx to the basin; siliciclastic input into the basin during Beck Spring

Dolomite time was tectonically-derived from local sources. Stratigraphically higher, in KP1 and the Virgin Spring Limestone, the 1780-1660 Ma peak becomes less dominant. The Virgin Spring Limestone samples contain different age peaks than those in the TU2 samples, suggesting sediment input from an additional source (Fig. 2.13B). This change in detrital zircon age spectra is consistent with basin reorganization occurring between TU2 and TU3 (Fig. 2.14B).

Again, during Kingston Peak time, syn-sedimentary normal faults were active and local depocentres developed with paleoflow generally to the south (Mrofka, 2010; Petterson et al., 2011). This can be seen in the Saddle Peak Hills area (Fig. 2.3) and in the Kingston Range (Figs. 2.4 and 2.5) where the stratigraphy expands southward below a sub-Noonday unconformity (Macdonald et al., 2013a). KP2 sample displays a sharp peak at 1780 Ma implies derivation from local basement, an inference supported by the observation that a large proportion of these grains have severe radiation damage, similar to grains described in the vicinity of World Beater Dome (Lanphere, 1962). The other KP2 sample, F1342, has three age peaks between 1500 and 1250 Ma in addition to the 1780 Ma peak. The sample from KP3, a medium-grained sandstone within graded beds, lacks the local 1780 Ma peak, but again displays two broad peaks between 1500 and 1250 Ma, similar to samples from the Virgin Spring Limestone (Fig. 2.13B).

The detrital zircon data of TU2 in Death Valley show important similarities as well as differences with coeval strata of the Chuar Group in Arizona and the Uinta Mountain Group in Utah (Fig. 2.16). The ten samples from TU2 in Death Valley are dominated by the Mojave province peaks while the Chuar and Uinta Mountain Groups have additional sedimentary sources from other Laurentian basement. The samples from

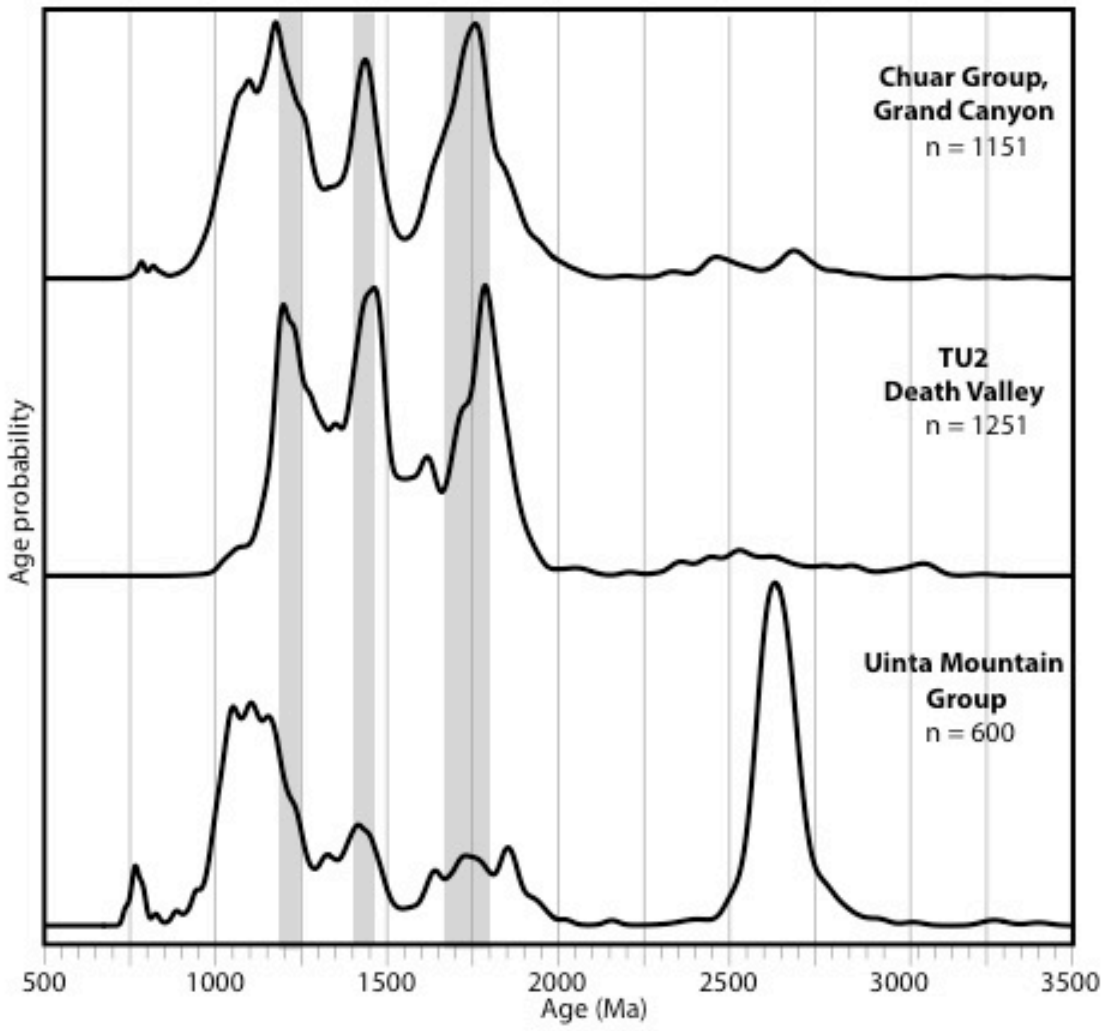

Figure 2.16. Detrital zircon age profiles from Neoproterozoic strata in Death Valley, the Grand Canyon, and the Uinta Mountains.

Detrital zircon age profiles TU2 in Death Valley, the Chuar Group in Arizona (Timmons et al., 2005) and the Uinta Mountain Group in Utah (Dehler et al., 2010). The ages from Death Valley are from the lower nine samples in Fig. 2.13. Probability density plots for the Chuar Group and Uinta Mountain Group show ages that are from a mix of local and continental sources, while the TU2 samples are dominated by ages from very local sources. Shaded bars represent Mojave basement ages from Wooden et al. (2013).

the Chuar Group also have a significant 1700-1600 Ma peak from the Mazatzal Province and a 1200-1000 Ma peak from the Grenville Province (Gehrels et al., 2011). The age profile of samples from the Uinta Mountain Group is very different from the age distributions of TU2 and the Chuar Group. In addition to minor Mojave-aged peaks, it has a significant Archaean peak from the Wyoming and Superior Cratons, an 1800-1700 Ma peak from the Yavapai and Central Plains provinces, and a 1200-1000 Ma peak from the Grenville Province (Dehler et al., 2010; Rybczynski, 2009). With the exception of rare ca. 780 Ma grains, all of the detrital grains in TU2 of Death Valley can be accounted for with local sources to the south in the Mojave block, whereas the Chuar and Uinta Mountains groups show a more cosmopolitan Laurentian signature. These data demonstrate that TU2 detritus was sourced locally from the western margin of Laurentia and not from transcontinental rivers.

2.6.7. Implications for Rodinia Reconstructions

Different Rodinia reconstructions have placed Australia, Antarctica, Congo, Kalahari, Siberia, South China and Tasmania along the south and west margins of Laurentia during the early Neoproterozoic (Burrett and Berry, 2000; Dalziel, 1991; Hoffman, 1991; Karlstrom et al., 1999; Li et al., 1996; Li et al., 2008; Li et al., 1995; McMenamin and McMenamin, 1990; Sears and Price, 2000). Detrital zircon geochronology is one tool that can be used to test these proposed ties. However, detrital zircon age profiles from TU2 of Death Valley, the Uinta Mountain Group, and the Chuar Group (Fig. 2.16), three Laurentian basins that are known to be roughly coeval, show how local sedimentary sources can dominate age populations, potentially limiting the usefulness of this tool. Stratigraphic progression of changing sedimentary sources just

within TU2 (Fig. 2.13B) further demonstrates how active tectonism can mute or eliminate some sedimentary sources within a single basin. Nonetheless, detrital zircon spectra from Neoproterozoic sequences on the Congo, Tasmania, Australia, and the Cathaysia block of South China are generally more similar to the TU2 samples derived primarily from the Mojave block (Fig. 2.13A and B), whereas those from Neoproterozoic sequences on the Yangtze block of South China, Kalahari and Siberia are distinctly different (Belousova et al., 2009; Berry et al., 2001; Black et al., 2004; Blissett et al., 1993; Fanning et al., 1988; Goodge et al., 2010; Hofmann et al., 2014; Jacobs et al., 2008; Konopásek et al., 2013; Li et al., 1995; Li et al., 2002; Li et al., 2007; MacLean et al., 2009; Peucat et al., 2002; Reid and Hand, 2012; Sears and Price, 2000; Sears et al., 2004; Wang et al., 2007; Zhao et al., 2011).

Additionally, there is no known source for the rare ~790-760 Ma detrital zircons that have been reported from the ChUMP basins (Dehler et al., 2010; Mahon et al., 2014b) and the 742 ± 6 Ma ash from the top of the Chuar Group (Karlstrom et al., 2000). Our study demonstrates that these grains are exceedingly rare, representing less than .01% of grains. Unless grains of this age came from Moine pegmatites in the Dalradian block of eastern Laurentia (Rogers et al., 1998; Van Breemen et al., 1974) or the Mt. Rogers Formation in the southern Appalachians (Aleinikoff et al., 1995), and travelled across Laurentia, we should be looking for a source of these young grains to use as a Rodinia piercing point. And as discussed above, there is no evidence for transcontinental rivers providing detritus to TU2. Pb-Pb SHRIMP zircon ages from granite on King Island and NW Tasmania yielded ages of 760 ± 12 Ma and 770 ± 7 Ma, respectively (Turner et al., 1998). It is unclear whether these granites are related to a

Neoproterozoic orogenic event (Turner et al., 1998) or Neoproterozoic rifting (Berry et al., 2008). While speculative, these granites are one possible source for the ca. 770 Ma grains. Further work is necessary to document the distribution of these grains throughout Laurentia and to refine their age with TIMS. Additionally, 800-720 Ma magmatic ages are common in South China (e.g. Zhou et al., 2002). Potential candidates as a source for the 742 ± 6 Ma Chuar Group ash include the 752-741 Ma Rosh Pinah Formation in the Gariep Belt of the Kalahari Craton of SW Namibia (Frimmel et al., 1996) and the 746 ± 2 Ma Naauwpoort Formation on the Congo Craton of north-central Namibia (Hoffman et al., 1996). Basement ages of the Namaqua-Natal Belt of the Kalahari Craton (Eglington, 2006) also share similarities with SW Laurentia.

2.7. Conclusions

Here we demonstrate that there are large facies changes in the Beck Spring Dolomite and its bounding units over short lateral distances. The new depositional model and detrital zircon analyses presented here extend others' work on the Horse Thief Springs Formation (Mahon et al., 2014b; Maud, 1979; Maud, 1983) to suggest that the Beck Spring Dolomite and KP1 also fringed a coeval paleo-high to the south. During TU2 time, accommodation space was being created quickly in a tectonically active basin, while calcifying microbes competed against sediment influx from the SW to fill the space.

We present new high-resolution carbon isotope chemostratigraphy of the Horse Thief Springs Formation and Beck Spring Dolomite, refining basinal correlations. We demonstrate that the carbon isotope excursion at the top of the Beck Spring Dolomite is a reproducible feature across the basin and is not associated with karsting or exposure but rather a transgression. Without better age constraints or understanding of the local

sedimentary processes affecting carbon isotopes in this basin, we emphasize broader tectonostratigraphic correlations rather than member- and formation-specific chemostratigraphic ones between TU2 and the equivalent strata in the western US (i.e. the ChUMP basins) and NW Canada.

We refine the timing of these three discrete basin-forming events in the Pahrump Group, all of which predate the NW-facing margin during Ediacaran time. Particularly, we suggest that TU2 was deposited rapidly around ca. 735 Ma and did not form during protracted rift-related extensional tectonism of the western margin of Laurentia. We suggest instead that the Horse Thief Spring Fm, the Beck Spring Dolomite, and the Saratoga Spring Sandstone were accommodated by strike-slip motion and subsequently folded in a transpressional orogenic event that we refer to as the "Saratoga Orogeny". A second phase of Neoproterozoic tectonism, one in which emplaces large (<1 km) olistoliths and accommodates extensional basins, is recorded in units KP2 and KP3. These two phases of tectonism may have been occurring at approximately the same time as ca. 780-635 Ma transpressional structures related to the Neoproterozoic Corn Creek Orogeny in NW Canada, representing a margin-wide transpressional event.

2.8. Acknowledgements

We thank NAI MIT Astrobiology node for support. We thank T. Prave and C. Burchfiel for freely sharing their data and thoughts. We thank G. Eischeid and S. Manley for assistance of laboratories at Harvard University. We thank S. Lawson, E. Sperling, J. Strauss, and R. Petterson for help in the field. We thank the National Park Service at Death Valley for permitting us to sample within the Park. We thank C. Dehler for thoughtful reviews on a version of this manuscript.

2.9. References

Aleinikoff, J.N., Zartman, R.E., Walter, M., Rankin, D.W., Lyttle, P.T. and Burton, W.C., 1995. U-Pb ages of metarhyolites of the Catoctin and Mount Rogers formations, Central and Southern Appalachians; evidence for two pulses of Iapetan rifting. American Journal of Science, 295(4): 428-454.

Amato, J.M., Boullion, A.O., Serna, A.M., Sanders, A.E., Farmer, G.L., Gehrels, G.E. and Wooden, J.L., 2008. Evolution of the Mazatzal province and the timing of the Mazatzal orogeny: Insights from U-Pb geochronology and geochemistry of igneous and metasedimentary rocks in southern New Mexico. Geological Society of America Bulletin, 120(3-4): 328-346.

Anderson, J. and Morrison, J., 1992. The role of anorogenic granites in the Proterozoic crustal development of North America. Developments in Precambrian Geology, 10: 263-299.

Armin, R.A. and Mayer, L., 1983. Subsidence analysis of the Cordilleran miogeocline: Implications for timing of Late Proterozoic rifting and amount of extension. Geology, 11: 702-705.

Awramik, S.M., 1971. Precambrian columnar stromatolite diversity: reflection of metazoan appearance. Science, 174(4011): 825-827.

Banner, J.L. and Hanson, G.N., 1990. Calculation of simultaneous isotopic and trace element variations during water-rock interaction with applications to carbonate diagenesis. Geochimica et Cosmochimica Acta, 54(11): 3123-3137.

Barth, A.P., Wooden, J., Tosda, R., Morrison, J., Dawson, D. and Hernly, B., 1995. Origin of gneisses in the aureole of the San Gabriel anorthosite complex and implications for the Proterozoic crustal evolution of southern California. Tectonics, 14(3): 736-752.

Barth, A.P., Wooden, J.L. and Coleman, D.S., 2001. SHRIMP-RG U-Pb Zircon Geochronology of Mesoproterozoic Metamorphism and Plutonism in the Southwesternmost United States. The Journal of Geology, 109(3): 319-327.

Barth, A.P., Wooden, J.L., Coleman, D.S. and Fanning, C.M., 2000. Geochronology of the Proterozoic basement of southwesternmost North America, and the origin and evolution of the Mojave crustal province. Tectonics, 19(4): 616-629.

Belousova, E., Reid, A., Griffin, W.L. and O'Reilly, S.Y., 2009. Rejuvenation vs. recycling of Archean crust in the Gawler Craton, South Australia: evidence from U–Pb and Hf isotopes in detrital zircon. Lithos, 113(3): 570-582.

Bergmann, K.D., Zentmyer, R.A. and Fischer, W.W., 2011. The stratigraphic expression of a large negative carbon isotope excursion from the Ediacaran Johnnie Formation, Death Valley. Precambrian Research, 188: 45-56.

Berry, R., Jenner, G., Meffre, S. and Tubrett, M., 2001. A North American provenance for Neoproterozoic to Cambrian sandstones in Tasmania? Earth and Planetary Science Letters, 192(2): 207-222.

Berry, R.F., Steele, D.A. and Meffre, S., 2008. Proterozoic metamorphism in Tasmania: implications for tectonic reconstructions. Precambrian Research, 166(1): 387-396.

Bickford, M. and Anderson, J., 1993. Middle Proterozoic magmatism. Geology of North America, 2: 281-292.

Black, L.P., Kamo, S.L., Allen, C.M., Davis, D.W., Aleinikoff, J.N., Valley, J.W., Mundil, R., Campbell, I.H., Korsch, R.J., Williams, I.S. and Foudoulis, C., 2004. Improved (206)Pb/(238)U microprobe geochronology by the monitoring of a trace-element-related matrix effect; SHRIMP, ID-TIMS, ELA-ICP-MS and oxygen isotope documentation for a series of zircon standards. Chemical Geology, 205(1-2): 115-140.

Blair, T.C. and McPherson, J.G., 1994. Alluvial fans and their natural distinction from rivers based on morphology, hydraulic processes, sedimentary processes, and facies assemblages. Journal of sedimentary research, 64(3): 450-489.

Blissett, A., Creaser, R., Daly, S., Flint, R. and Parker, A., 1993. Gawler range volcanics. The Geology of South Australia, 1: 107-124.

Bloeser, B., 1985. Melanocyrillium, a new genus of structurally complex late Proterozoic microfossils from the Kwagunt Formation (Chuar Group), Grand Canyon, Arizona. Journal of Paleontology, 59: 741-765.

Bond, G.C., Christie-Blick, N., Kominz, M.A. and Devlin, W.J., 1985. An early Cambrian rift to post-rift transition in the Cordillera of western North-America. Nature, 315: 742-746.

Bond, G.C. and Kominz, M.A., 1984. Construction of tectonic subsidence curves for the early Paleozoic miogeocline, southern Canadian Rocky Mountains: Implications for subsidence mechanisms, age of breakup, and crustal thinning. Geological Society of America Bulletin, 95(2): 155-173.

Brehm, C., 2008. Sedimentology, stratigraphy, and organic geochemistry of the Red Pine Shale, Uinta Mountains, Utah: A prograding deltaic system in a "Western Neoproterozoic Seaway", Utah State University, Logan, 232 pp.

Bull, W.B., 1972. Recognition of Ancient Sedimentary Environments. In: J.K. Rigby and W.K. Hamblin (Editors), Special Publication 16. Society of Economic Paleontologists and Mineralogists, pp. 63-83.

Burchfiel, B.C., Cowan, D.S. and Davis, G.A., 1992. Tectonic overview of the Cordilleran orogen in the western United States. In: B.C. Burchfiel, P.W. Lipman and M.L. Zoback (Editors), The Geology of North America. Geological Society of America, Boulder, pp. 407-479.

Burchfiel, B.C., Pelton, P.J. and Sutter, J., 1970. An early Mesozoic deformation belt in south-central Nevada-southeasterrn California. Geological Society of America Bulletin, 81: 211-215.

Burrett, C. and Berry, R., 2000. Proterozoic Australia–Western United States (AUSWUS) fit between Laurentia and Australia. Geology, 28(2): 103-106.

Calver, C., Crowley, J., Wingate, M., Evans, D., Raub, T. and Schmitz, M., 2013. Globally synchronous Marinoan deglaciation indicated by U-Pb geochronology of the Cottons Breccia, Tasmania, Australia. Geology, 41(10): 1127-1130.

Calzia, J.P., Troxel, B.W., Wright, L.A., Burchfiel, B.C., Davis, G.A. and McMackin, M.R., 2000. Geologic map of the Kingston Range, southern Death Valley, California, Open-File Report, U.S. Geological Survey, pp. 2 sheets.

Christie-Blick, N., 1985. Deformation and basin formation along strike-slip faults.

Clapham, M.E. and Corsetti, F.A., 2005. Deep valley incision in the terminal Neoproterozoic (Ediacaran) Johnnie Formation, eastern California, USA: tectonically or glacially driven? Precambrian Research, 141: 154-164.

Cloud, P. and Semikhatov, M., 1969. Proterozoic stromatolite zonation. American Journal of Science, 267(9): 1017-1061.

Cloud, P.E., Licari, G.R., Wright, L.A. and Troxel, B.W., 1969. Proterozoic eucaryotes from Eastern California. Proceedings of the National Academy of Sciences of the United States of America, 62(3): 623-631.

Condon, D., Zhu, M.Y., Bowring, S., Wang, W., Yang, A.H. and Jin, Y.G., 2005. U-Pb ages from the Neoproterozoic Doushantuo Formation, China. Science, 308(5718): 95-98.

Corsetti, F.A. and Kaufman, A.J., 2003. Stratigraphic investigations of carbon isotope anomalies and Neoproterozoic ice ages in Death Valley, California. Geological Society of America Bulletin, 115(8): 916-932.

Cox, R., Martin, M.W., Comstock, J.C., Dickerson, L.S., Ekstrom, I.L. and Sammons, J.H., 2002. Sedimentology, stratigraphy, and geochronology of the Proterozoic Mazatzal Group, central Arizona. Geological Society of America Bulletin, 114(12): 1535-1549.

Dalziel, I.W.D., 1991. Pacific margins of Laurentia and east Antarctica Australia as a conjugate rift pair - evidence and implications for an Eocambrian supercontinent. Geology, 19(6): 598-601.

Dehler, C.M., Elrick, M., Bloch, J.D., Crossey, L.J., Karlstrom, K.E. and Des Marais, D.J., 2005. High-resolution delta C-13 stratigraphy of the Chuar Group (ca. 770-742 Ma), Grand Canyon: Implications for mid-Neoproterozoic climate change. Geological Society of America Bulletin, 117(1-2): 32-45.

Dehler, C.M., Elrick, M., Karlstrom, K.E., Smith, G.A., Crossey, L.J. and Timmons, J.M., 2001. Neoproterozoic Chuar Group (similar to 800-742 Ma), Grand Canyon: a record of cyclic marine deposition during global cooling and supercontinent rifting. Sedimentary Geology, 141: 465-499.

Dehler, C.M., Fanning, C.M., Link, P.K., Kingsbury, E.M. and Rybczynski, D., 2010. Maximum depositional age and provenance of the Uinta Mountain Group and Big Cottonwood Formation, northern Utah: Paleogeography of rifting western Laurentia. Geological Society of America Bulletin, 122(9-10): 1686-1699.

Dehler, C.M., Porter, S.M., De Grey, L.D., Sprinkel, D.A. and Brehm, A., 2007. The Neoproterozoic Uinta Mountain Group revisited: a synthesis of recent work on the Red Pine Shale and undivided clastic strata, northeastern Utah. Proterozoic Geology of Western North America and Siberia. Society of Sedimentary Geology, Special Publication, 86: 151-166.

Donaldson, J., 1976. .2 Paleoecology of Conophyton and Associated Stromatolites in the Precambrian Dismal Lakes and Rae Groups, Canada. Developments in Sedimentology, 20: 523-534.

Duebendorfer, E.M., Chamberlain, K.R. and Jones, C.S., 2001. Paleoproterozoic tectonic history of the Cerbat Mountains, northwestern Arizona: Implications for crustal assembly in the southwestern United States. Geological Society of America Bulletin, 113(5): 575-590.

Eglington, B., 2006. Evolution of the Namaqua-Natal Belt, southern Africa–A geochronological and isotope geochemical review. Journal of African Earth Sciences, 46(1): 93-111.

Eisbacher, G.H., 1981. Sedimentary tectonics and glacial record in the Windermere Supergroup, Mackenzie Mountains, northwestern Canada. Geological Survey of Canada.

Ekstrom, H., Morrison, J. and Anderson, J.L., 1994. Petrogenetic modeling and stable isotopic evaluation of anorthositic and jotunitic to syenitic magma series in the San Gabriel anorthosite complex, southern California. Precambrian Research, 70(1): 1-24.

Ernst, R., Wingate, M., Buchan, K. and Li, Z., 2008. Global record of 1600–700Ma Large Igneous Provinces (LIPs): implications for the reconstruction of the proposed Nuna (Columbia) and Rodinia supercontinents. Precambrian Research, 160(1): 159-178.

Fanning, C., Flint, R., Parker, A., Ludwig, K. and Blissett, A., 1988. Refined Proterozoic evolution of the Gawler craton, South Australia, through U-Pb zircon geochronology. Precambrian Research, 40: 363-386.

Fedo, C.M. and Cooper, J.D., 2001. Sedimentology and sequence stratigraphy of Neoproterozoic and Cambrian units across a craton-margin hinge zone,

southeastern California, and implications for the early evolution of the Cordilleran margin. Sedimentary Geology, 141: 501-522.

Fleck, R.J., 1970. Age and tectonic significance of volcanic rocks, Death Valley area, California. Geological Society of America Bulletin, 81: 2807-2816.

Frimmel, H.E., Klötzli, U.S. and Siegfried, P.R., 1996. New Pb-Pb single zircon age constraints on the timing of Neoproterozoic glaciation and continental break-up in Namibia. The Journal of Geology, 104: 459-469.

Gehrels, G.E., Blakey, R., Karlstrom, K.E., Timmons, J.M., Dickinson, B. and Pecha, M., 2011. Detrital zircon U-Pb geochronology of Paleozoic strata in the Grand Canyon, Arizona. Lithosphere, 3(3): 183-200.

Goodge, J.W., Fanning, C.M., Brecke, D.M., Licht, K.J. and Palmer, E.F., 2010. Continuation of the Laurentian Grenville province across the Ross Sea margin of East Antarctica. The Journal of Geology, 118(6): 601-619.

Gutstadt, A.M., 1968. Petrology and depositional environments of the Beck Spring Dolomite (Precambrian), Kingston Range, California. Journal of Sedimentary Research, 38(4): 1280-1289.

Harwood, C.L. and Sumner, D.Y., 2011. Microbialites of the Neoproterozoic Beck Spring Dolomite, Southern California. Sedimentology, 58(6): 1648-1673.

Harwood, C.L. and Sumner, D.Y., 2012. Origins of microbial microstructures in the Neoproterozoic Beck Spring Dolomite: variations in microbial community and timing of lithification Journal of Sedimentary Research, 82(9-10): 709-722.

Heaman, L.M. and Grotzinger, J.P., 1992. 1.08 Ga diabase sills in the Pahrump Group, California; implications for development of the Cordilleran Miogeocline. Geology, 20(7): 637-640.

Hewett, D., 1940. New formation names to be used in the Kingston Range. Ivanpah Quadrangle, California: Washington Academy of Sciences Journal, 30: 239-240.

Hoffman, P.F., 1976. Environmental Diversity of Middle Precambrian Stromatolites. Developments in Sedimentology, 20: 599-611.

Hoffman, P.F., 1991. Did the breakout of Laurentia turn Gondwanaland inside-out? Science, 252(5011): 1409-1412.

Hoffman, P.F., Halverson, G.P., Domack, E.W., Maloof, A.C., Swanson-Hysell, N.L. and Cox, G.M., 2012. Cryogenian glaciations on the southern tropical paleomargin of Laurentia (NE Svalbard and East Greenland), and a primary origin for the upper Russoya (Islay) carbon isotope excursion. Precambrian Research, 206: 137-158.

Hoffman, P.F., Hawkins, D.P., Isachsen, C.E. and Bowring, S.A., 1996. Precise U–Pb zircon ages for early Damaran magmatism in the Summas Mountains and

Welwitschia Inlier, northern Damara belt, Namibia. Communications of the geological survey of Namibia, 11: 47-52.

Hoffmann, K.H., Condon, D.J., Bowring, S.A. and Crowley, J.L., 2004. U-Pb zircon date from the Neoproterozoic Ghaub Formation, Namibia: Constraints on Marinoan glaciation. Geology, 32(9): 817-820.

Hofmann, M., Linnemann, U., Hoffmann, K.-H., Gerdes, A., Eckelmann, K. and Gärtner, A., 2014. The Namuskluft and Dreigratberg sections in southern Namibia (Kalahari Craton, Gariep Belt): a geological history of Neoproterozoic rifting and recycling of cratonic crust during the dispersal of Rodinia until the amalgamation of Gondwana. International Journal of Earth Sciences, 103(5): 1187-1202.

Horodyski, R., 1987. A new occurrence of the vase-shaped fossil Melanocyrillium and new data on this relatively complex late Precambrian fossil. Melanocyrillium, Geol. Soc. Am.

Horodyski, R.J., 1977. Lyngbya mats at Laguna Mormona, Baja California, Mexico; comparison with Proterozoic stromatolites. Journal of Sedimentary Research, 47(3): 1305-1320.

Horodyski, R.J. and Knauth, L.P., 1994. Life on land in the Precambrian. Science, 263(5146): 494-498.

Hurtgen, M.T., Arthur, M.A. and Prave, A.R., 2004. The sulfur isotope composition of carbonate-associated sulfate in Mesoproterozoic to Neoproterozoic carbonates from Death Valley, California. Special papers - Geological Society of America, 379: 177-194.

Ingersoll, R.V., 1988. Tectonics of sedimentary basins. Geological Society of America Bulletin, 100(11): 1704-1719.

Iriondo, A., Premo, W.R., Martínez-Torres, L.M., Budahn, J.R., Atkinson, W.W., Siems, D.F. and Guarás-González, B., 2004. Isotopic, geochemical, and temporal characterization of Proterozoic basement rocks in the Quitovac region, northwestern Sonora, Mexico: Implications for the reconstruction of the southwestern margin of Laurentia. Geological Society of America Bulletin, 116(1-2): 154-170.

Jacobs, J., Pisarevsky, S., Thomas, R.J. and Becker, T., 2008. The Kalahari Craton during the assembly and dispersal of Rodinia. Precambrian Research, 160(1): 142-158.

Jefferson, C. and Parrish, R., 1989. Late Proterozoic stratigraphy, U-Pb zircon ages, and rift tectonics, Mackenzie Mountains, northwestern Canada. Canadian Journal of Earth Sciences, 26(9): 1784-1801.

Karlstrom, K.E., Bowring, S.A., Dehler, C.M., Knoll, A.H., Porter, S.M., Des Marais, D.J., Weil, A.B., Sharp, Z.D., Geissman, J.W., Elrick, M.B., Timmons, J.M., Crossey, L.J. and Davidek, K.L., 2000. Chuar Group of the Grand Canyon:

Record of breakup of Rodinia, associated change in the global carbon cycle, and ecosystem expansion by 740 Ma. Geology, 28(7): 619-622.

Karlstrom, K.E., Harlan, S.S., Williams, M.L., McLelland, J., Geissman, J.W. and Ahall, K.-I., 1999. Refining Rodinia: Geologic evidence for the Australia–western US connection in the Proterozoic. GSA Today, 9(10): 1-7.

Karlstrom, K.E. and Humphreys, E.D., 1998. Persistent influence of Proterozoic accretionary boundaries in the tectonic evolution of southwestern North America Interaction of cratonic grain and mantle modification events. Rocky Mountain Geology, 33(2): 161-179.

Kenny, R. and Knauth, L.P., 2001. Stable isotope variations in the Neoproterozoic Beck Spring Dolomite and Mesoproterozoic Mescal Limestone paleokarst: Implications for life on land in the Precambrian. Geological Society of America Bulletin, 113(5): 650-658.

Knauth, L.P. and Kennedy, M.J., 2009. The late Precambrian greening of the Earth. Nature, 460(7256): 728-732.

Konopásek, J., Košler, J., Sláma, J. and Janoušek, V., 2013. Timing and sources of pre-collisional Neoproterozoic sedimentation along the SW margin of the Congo Craton (Kaoko Belt, NW Namibia). Gondwana Research.

Kupfer, D.H., 1960. Thrust faulting and chaos structure, Silurian Hills, San Bernardino County, California. Geological Society of America Bulletin, 71(2): 181-214.

Labotka, T.C., Albee, A.L., Lanphere, M.A. and McDowell, S.D., 1980. Stratigraphy, structure, and metamorphism in the central Panamint Mountains (Telescope-Peak Quandrangle), Death-Valley Area, California - Summary. Geological Society of America Bulletin, 91(3): 125-129.

Lanphere, M.A., 1962. I. Geology of the Wildrose area, Panamint Range, California. II. Geochronologic studies in the Death Valley-Mojave Region, California, California Institute of Technology, Pasadena.

Li, Z., Zhang, L. and Powell, C.M., 1996. Positions of the East Asian cratons in the Neoproterozoic supercontinent Rodinia. Australian Journal of Earth Sciences, 43(6): 593-604.

Li, Z.-X., Bogdanova, S., Collins, A.S., Davidson, A., De Waele, B., Ernst, R., Fitzsimons, I.C., Fuck, R., Gladkochub, D. and Jacobs, J., 2008. Assembly, configuration, and break-up history of Rodinia: a synthesis. Precambrian research, 160(1): 179-210.

Li, Z., Evans, D.A. and Halverson, G.P., 2013. Neoproterozoic glaciations in a revised global paleogeography from the breakup of Rodinia to the assembly of Gondwanaland. Sedimentary Geology, 294: 219-232.

Li, Z., Li, X., Kinny, P., Wang, J., Zhang, S. and Zhou, H., 2003. Geochronology of Neoproterozoic syn-rift magmatism in the Yangtze Craton, South China and correlations with other continents: evidence for a mantle superplume that broke up Rodinia. Precambrian Research, 122(1): 85-109.

Li, Z., Zhang, L. and Powell, C.M., 1995. South China in Rodinia: part of the missing link between Australia–East Antarctica and Laurentia? Geology, 23(5): 407-410.

Li, Z., Li, X., Zhou, H. and Kinny, P.D., 2002. Grenvillian continental collision in south China: New SHRIMP U-Pb zircon results and implications for the configuration of Rodinia. Geology, 30: 163-166.

Li, Z., Wartho, J., Occhipinti, S., Zhang, C., Li, X., Wang, J. and Bao, C., 2007. Early history of the eastern Sibao Orogen (South China) during the assembly of Rodinia: New mica 40Ar-39Ar dating and SHRIMP U-Pb detrital zircon provenance constraints. Precambrian Research, 159: 79-94.

Licari, G.R., 1978. Biogeology of late Pre-Phanerozoic Beck Spring Dolomite of Eastern California. Journal of Paleontology, 52(4): 767-792.

Link, P.K., Christie-Blick, N., Devlin, W.J., Elston, D.P., Horodyski, R., Levy, M., Miller, J.M.G., Pearson, R.C., Prave, A.R., Stewart, J.H., Winston, D., Wright, L.A. and Wrucke, C.T., 1993. Middle and Late Proterozoic stratigried rocks of the western Cordillera, Colorado Plateau, and Basin and Range province. Precambrian: Conterminous US, The Geology of North America, 2. United States Geological Society of America, Boulder.

Loyd, S.J. and Corsetti, F.A., 2010. The origin of the millimeter-scale lamination in the Neoproterozoic lower Beck Spring Dolomite: Implications for widespread, fine-scale, layer-parallel diagenesis in Precambrian carbonates. Journal of Sedimentary Research, 80(7): 678-687.

Ludwig, K., 2008. Manual for Isoplot 3.7: Berkeley Geochronology Center. Special Publication(4): 77.

Macdonald, F.A., Prave, A.R., Petterson, R., Smith, E.F., Pruss, S.B., Oates, K., Waechter, F., Trotzuk, D. and Fallick, A.E., 2013a. The Laurentian record of Neoproterozoic glaciation, tectonism, and eukaryotic evolution in Death Valley, California. Geological Society of America Bulletin, 125(7-8): 1203-1223.

Macdonald, F.A., Schmitz, M.D., Crowley, J.L., Roots, C.F., Jones, D.S., Maloof, A.C., Strauss, J.V., Cohen, P.A., Johnston, D.T. and Schrag, D.P., 2010. Calibrating the cryogenian. Science, 327(5970): 1241-1243.

Macdonald, F.A., Strauss, J.V., Sperling, E.A., Halverson, G.P., Narbonne, G.M., Johnston, D.T., Kunzmann, M., Schrag, D.P. and Higgins, J.A., 2013b. The stratigraphic relationship between the Shuram carbon isotope excursion, the oxygenation of Neoproterozoic oceans, and the first appearance of the Ediacara

biota and bilaterian trace fossils in northwestern Canada. Chemical Geology, 362: 250-272.

MacLean, J., Sears, J., Chamberlain, K., Khudoley, A., Prokopiev, A., Kropachev, A. and Serkina, G., 2009. Detrital zircon geochronologic tests of the SE Siberia-SW Laurentia paleocontinental connection. Stephan Mueller Special Publication Series, 4(4): 111-116.

Mahon, R.C., 2012. Detrital zircon provenance, geochronology and revised stratigraphy of the Mesoproterozoic and Neoproterozoic Pahrump (Super)Group, Death Valley Region, California and Geology of the Saddle Peak Hills 7.5' Quadrangle, San Bernardino County, California, Idaho State University, 181 pp.

Mahon, R.C., Dehler, C.M., Link, P.K., Karlstrom, K.E. and Gehrels, G.E., 2014a. Detrital zircon provenance and paleogeography of the Pahrump Group and overlying strata, Death Valley, California. Precambrian Research.

Mahon, R.C., Dehler, C.M., Link, P.K., Karlstrom, K.E. and Gehrels, G.E., 2014b. Geochronologic and stratigraphic constraints on the Mesoproterozoic and Neoproterozoic Pahrump Group, Death Valley, California: A record of the assembly, stability, and breakup of Rodinia. Geological Society of America Bulletin, 126: 652-664.

Marian, M.L., 1979. Sedimentology of the Beck Spring Dolomite, eastern Mojave Desert, University of Southern California, Los Angeles.

Marian, M.L. and Osborne, R.H., 1992. Petrology, petrochemistry, and stromatolites of the middle to late Proterozoic Beck Spring Dolomite, eastern Mojave Desert, California. Canadian Journal of Earth Sciences, 29(12): 2595-2609.

Maud, R.L., 1979. Stratigraphy and depositional environments of the carbonate-terrigenous member of the Crystal Spring Formation, Pennsylvania State University, University Park, Pennsylvania, 177 pp.

Maud, R.L., 1983. Stratigraphy, petrography and depositional environments of the carbonate-terrigenous member of the Crystal Spring Formation, Pennsylvania State University, University Park, Pennsylvania, 221 pp.

Mbuyi, K. and Prave, A.R., 1993. Unconformities in the mid-late Proterozoic Pahrump Group: Stratigraphic evidence from the upper member Crystal Spring Formation, Geological Society of America, Abstracts with Programs, pp. 98.

McMenamin, M.A. and McMenamin, D.L.S., 1990. The emergence of animals: the Cambrian breakthrough. Columbia University Press.

Miller, J.M.G., 1985. Glacial and syntectonic sedimentation: the upper Proterozoic Kinston Peak Formation, southern Panamint Range, eastern California. Geological Society of America Bulletin, 96: 75-85.

Moores, E.M., 1991. Southwest United-States-East Antarctic (SWEAT) connection - a hypothesis. Geology, 19(5): 425-428.

Mrofka, D.D., 2010. Competing models for the timing of Cryogenian Glaciation: evidence from the Kingston Peak Formation, southeastern California University of California, Riverside, 284 pp.

Nelson, C., 1978. Late Precambrian-Early Cambrian stratigraphic and faunal succession of eastern California and the Precambrian-Cambrian boundary. Geological Magazine, 115(2): 121-126.

Noble, L.F., 1934. Rock formations of Death Valley, California. Science, 80(2069): 173-178.

Petterson, R., 2009. The basal Ediacaran Noonday Formation, Eastern California, and implications for Laurentian equivalents, California Institute of Technology, 225 pp.

Petterson, R., Prave, A.R., Wernicke, B.P. and Fallick, A.E., 2011. The Neoproterozoic Noonday Formation, Death Valley region, California. Geological Society of America Bulletin, 123(7-8): 1317-1336.

Peucat, J., Capdevila, R., Fanning, C., Ménot, R., Pécora, L. and Testut, L., 2002. 1.60 Ga felsic volcanic blocks in the moraines of the Terre Adélie Craton, Antarctica: comparisons with the Gawler Range Volcanics, South Australia. Australian Journal of Earth Sciences, 49(5): 831-845.

Pierce, D. and Cloud, P., 1979. New microbial fossils from 1.2 billion-year-old rocks of eastern California. Geomicrobiology Journal, 1(3): 295-309.

Porter, S.M. and Knoll, A.H., 2000. Testate amoebae in the Neoproterozoic Era: evidence from vase-shaped microfossils in the Chuar Group, Grand Canyon. Paleobiology, 26(3): 360-385.

Prave, A.R., 1999. Two diamictites, two cap carbonates, two delta C-13 excursions, two rifts: The Neoproterozoic Kingston Peak Formation, Death Valley, California. Geology, 27(4): 339-342.

Rainbird, R.H., Hearnan, L.M. and Young, G., 1992. Sampling Laurentia: Detrital zircon geochronology offers evidence for an extensive Neoproterozoic river system originating from the Grenville orogen. Geology, 20(4): 351-354.

Rainbird, R.H., McNicoll, V., Theriault, R., Heaman, L., Abbott, J., Long, D. and Thorkelson, D., 1997. Pan-continental river system draining Grenville Orogen recorded by U-Pb and Sm-Nd geochronology of Neoproterozoic quartzarenites and mudrocks, northwestern Canada. The Journal of Geology, 105: 1-17.

Rämö, O.T., McLemore, V.T., Hamilton, M.A., Kosunen, P.J., Heizler, M. and Haapala, I., 2003. Intermittent 1630–1220 Ma magmatism in central Mazatzal province:

New geochronologic piercing points and some tectonic implications. Geology, 31(4): 335-338.

Reading, H.G., 1980. Characteristics and recognition of strike-slip fault systems. Sedimentation in oblique-slip mobile zones, 4: 7-26.

Reid, A.J. and Hand, M., 2012. Mesoarchean to Mesoproterozoic evolution of the southern Gawler Craton, South Australia. Episodes-Newsmagazine of the InternationalUnion of Geological Sciences, 35(1): 216.

Renik, B. and Christie-Blick, N., 2013. A new hypothesis for the amount and distribution of dextral displacement aliong the Fish Lake Valley-northern Death Valley-Furnace Creek fault zone, California-Nevada. Tectonics, 32: 123-145.

Roberts, M.T., 1982. Depositional environments and tectonic setting of the Crystal Spring Formation, Death Valley region, California. In: J.P. Cooper, B.W. Troxel and L.A. Wright (Editors), Western Mojave Desert and Southern Great Basin, California: Geological Society of America Cordilleran Section Meeting Guidebook, Field Trip 9: Shoshone, California. Death Valley Publishing Company, pp. 143-154.

Rogers, G., Hyslop, E., Strachan, R., Paterson, B. and Holdsworth, R., 1998. The structural setting and U–Pb geochronology of Knoydartian pegmatites in W Inverness-shire: evidence for Neoproterozoic tectonothermal events in the Moineof NW Scotland. Journal of the Geological Society, 155(4): 685-696.

Rooney, A.D., Macdonald, F.A., Strauss, J.V., Dudás, F.Ö., Hallmann, C. and Selby, D., 2014. Re-Os geochronology and coupled Os-Sr isotope constraints on the Sturtian snowball Earth. Proceedings of the National Academy of Sciences, 111: 51-56.

Rooney, A.D., Strauss, J.V., Brandon, A.D. and Macdonald, F.A., 2015. A Cryogenian chronology: Two long-lasting synchronous Neoproterozoic glaciations. Geology, 43(5): 459-462.

Rybczynski, D., 2009. Correlation, paleogeography, and provenance of the eastern Uinta Mountain Group, Goslin Mountain area, Daggett County, northeastern Utah, Utah State University, Logan, UT, 224 pp.

Sears, J.W. and Price, R.A., 2000. New look at the Siberian connection: no SWEAT. Geology, 28(5): 423-426.

Sears, J.W., Price, R.A. and Khudoley, A.K., 2004. Linking the Mesoproterozoic Belt-Purcell and Udzha basins across the west Laurentia–Siberia connection. Precambrian Research, 129(3): 291-308.

Shafer, D.C., 1983. Petrology and depositional environments of the Beck Spring Dolomite, southern Death Valley region, University of California at Davis, 195 pp.

Sláma, J., Košler, J., Condon, D.J., Crowley, J.L., Gerdes, A., Hanchar, J.M., Horstwood, M.S., Morris, G.A., Nasdala, L. and Norberg, N., 2008. Plešovice zircon—a new natural reference material for U–Pb and Hf isotopic microanalysis. Chemical Geology, 249(1): 1-35.

Smith, E.F., Macdonald, F.A., Crowley, J.L., Hodgin, E.B. and Schrag, D.P., 2015. Tectonostratigraphic evolution of the c. 780–730 Ma Beck Spring Dolomite: Basin Formation in the core of Rodinia. Geological Society, London, Special Publications, 424: SP424. 6.

Snow, J.K., Asmerom, Y. and Lux, D.R., 1991. Permian-Triassic plutonism and tectonics, Death Valley region, California and Nevada. Geology, 19(6): 629-632.

Snow, J.K. and Wernicke, B.P., 2000. Cenozoic tectonism in the central Basin and Range: Magnitude, rate, and distribution of upper crustal strain. American Journal of Science, 300: 659-719.

Stewart, J.H., 1970. Upper Precambrian and Lower Cambrian strata in the southern Great Basin, California and Nevada. U.S. Geological Survey Professional Paper, 260, 206 pp.

Stewart, J.H., 1975. Initial deposits in the Cordilleran geosyncline: Evidence of a late Precambrian (<850 m.y.) continental separation. Geological Society of America Bulletin, 83(5): 1345-1360.

Stewart, J.H., Gehrels, G.E., Barth, A.P., Link, P.K., Christie-Blick, N. and Wrucke, C.T., 2001. Detrital zircon provenance of Mesoproterozoic to Cambrian arenites in the western United States and northwestern Mexico. Geological Society of America Bulletin, 113(10): 1343-1356.

Strauss, J.V., Rooney, A.D., Macdonald, F.A., Brandon, A.D. and Knoll, A.H., 2014. 740 Ma vase-shaped microfossils from Yukon, Canada: Implications for Neoproterozoic chronology and biostratigraphy. Geology, 42(8): 659-662.

Strickland, B.A., Wooden, J.L., Mattinson, C.G., Ushikubo, T., Miller, D.M. and Valley, J.W., 2013. Proterozoic evolution of the Mojave crustal province as preserved in the Ivanpah Mountains, southeastern California. Precambrian Research, 224: 222-241.

Summa, C.L., 1993. Sedimentologic, stratigraphic, and tectonic controls of a mixed carbonate-siliciclastic succession; Neoproterozoic Johnnie Formation, Southeast California, Massachusetts Institute of Technology, Cambridge, MA, 615 pp.

Thorkelson, D.J., 2000. Geology and mineral occurrences of the Slats Creek, Fairchild Lake and “Dolores Creek” areas, Wernecke Mountains (106D/16, 106C/13, 106C/14), Yukon Territory. Exploration and Geological Services Division, Yukon, Indian and Northern Affairs Canada. Bulletin, 10: 73.

Timmons, J.M., Karlstrom, K.E., Dehler, C.M., Geissman, J.W. and Heizler, M.T., 2001. Proterozoic multistage (ca. 1.1 and 0.8 Ga) extension recorded in the Grand Canyon Supergroup and establishment of northwest-and north-trending tectonic grains in the southwestern United States. Geological Society of America Bulletin, 113(2): 163-181.

Timmons, J.M., Karlstrom, K.E., Heizler, M.T., Bowring, S.A., Gehrels, G.E. and Crossey, L.J., 2005. Tectonic inferences from the ca. 1255–1100 Ma Unkar Group and Nankoweap Formation, Grand Canyon: Intracratonic deformation and basin formation during protracted Grenville orogenesis. Geological Society of America Bulletin, 117(11-12): 1573-1595.

Tucker, M.E., 1982. Precambrian dolomite - petrographic and isotopic evidence that they differ from Phanerozoic dolomites. Geology, 10(1): 7-12.

Tucker, M.E., 1983. Diagenesis, geochemistry, and origin of a Precambrian dolomite - the Beck Spring Dolomite of eastern California. Journal of Sedimentary Petrology, 53(4): 1097-1119.

Turner, N., Black, L. and Kamperman, M., 1998. Dating of Neoproterozoic and Cambrian orogenies in Tasmania. Australian Journal of Earth Sciences, 45(5): 789-806.

Van Breemen, O., Pidgeon, R. and Johnson, M., 1974. Precambrian and Paleozoic pegmatites in the Moines of northern Scotland. Journal of the Geological Society, 130(6): 493-504.

Vidal, G. and Ford, T.D., 1985. Microbiotas from the late Proterozoic Chuar Group (northern Arizona) and Uinta Mountain Group (Utah) and their chronostratigraphic implications. Precambrian Research, 28(3): 349-389.

Walker, J.D., Klepacki, D.W. and Burchfiel, B., 1986. Late Precambrian tectonism in the Kingston Range, southern California. Geology, 14(1): 15-18.

Wang, X., Zhou, J., Griffin, W., Wang, R.-C., Qiu, J., O'Reilly, S., Xu, X., Liu, X. and Zhang, G.-L., 2007. Detrital zircon geochronology of Precambrian basement sequences in the Jiangnan orogen: dating the assembly of the Yangtze and Cathaysia Blocks. Precambrian Research, 159(1): 117-131.

Wasserburg, G.J., Wetherill, G.W. and Wright, L.A., 1959. Ages in the Precambrian terrane of Death Valley, California. Journal of Geology, 67(6): 702-708.

Watson, E., Wark, D. and Thomas, J., 2006. Crystallization thermometers for zircon and rutile. Contributions to Mineralogy and Petrology, 151(4): 413-433.

Wernicke, B.P., Axen, G.J. and Snow, J.K., 1988. Basin and Range extensional tectonics at the latitude of Las Vegas, Nevada. Geological Society of America Bulletin, 100: 1738-1757.

Wooden, J.L., Barth, A.P. and Mueller, P.A., 2013. Crustal growth and tectonic evolution of the Mojave crustal province: Insights from hafnium isotope systematics in zircons. Lithosphere, 5(1): 17-28.

Wright, L.A., 1954. Geology of the Alexander Hills area, Inyo and San Bernardino Counties, California. California Division of Mines and Geology, pp. Map Sheet 17.

Wright, L.A., 1976. Late Cenozoic fault patterns and stress fields in the Great Basin and westward displacement of the Sierra Nevada block. Geology, 4: 489-494.

Wright, L.A., Thompson, R.A., Troxel, B.W., Pavlis, T.L., DeWitt, E.H., Otton, K., Ellis, M.A., Miller, M.G. and Serpa, L.F., 1991. Cenozoic magmatic and tectonic evolution of the east-central Death Valley region, California. In: M.J. Walawender and B.B. Hanan (Editors), Geological Excursions in Southern California and Mexico, Field Trip Guidebook. Geological Society of America, Boulder, CO, pp. 93-127.

Wright, L.A., Troxel, B.W. and Prave, A.R., 1992. Field traverse of Proterozoic rock units, Alexander Hills and southern Nopah Range, Death Valley region, CA, Late Phanerozoic Penrose Conference, Geological Society of America pp. 1-11.

Wright, L.A., Troxel, B.W., Williams, E.G., Roberts, M.T. and Diehl, P.E. (Editors), 1976. Precambrian sedimentary environments of the Death Valley region, eastern California. Geologic features, Death Valley, California. California Division of Mines and Geology, Sacramento, CA., 7-15 pp.

Yonkee, W., Dehler, C., Link, P., Balgord, E., Keeley, J., Hayes, D., Wells, M., Fanning, C. and Johnston, S., 2014. Tectono-stratigraphic framework of Neoproterozoic to Cambrian strata, west-central US: Protracted rifting, glaciation, and evolution of the North American Cordilleran margin. Earth-Science Reviews, 136: 59-95.

Zempolich, W.G., Wilkinson, B.H. and Lohmann, K.C., 1988. Diagenesis of late Proterozoic carbonates - the Beck Spring Dolomite of eastern California. Journal of Sedimentary Petrology, 58(4): 656-672.

Zhao, J., Zhou, M.-F., Yan, D., Zheng, J. and Li, J., 2011. Reappraisal of the ages of Neoproterozoic strata in South China: no connection with the Grenvillian orogeny. Geology, 39(4): 299-302.

Zhou, M., Yan, D., Kennedy, A.K., Li, Y. and Ding, J., 2002. SHRIMP U–Pb zircon geochronological and geochemical evidence for Neoproterozoic arc-magmatism along the western margin of the Yangtze Block, South China. Earth and Planetary Science Letters, 196(1): 51-67.

CHAPTER 3. DISCOVERY OF THE YOUNGEST EDIACARAN FOSSILS IN THE GREAT BASIN OF CALIFORNIA AND NEVADA: IMPLICATIONS FOR BIOLOGICAL AND ENVIRONMENTAL CHANGE THROUGH THE EDIACARAN-CAMBRIAN TRANSITION

Abstract

Precise global correlations of integrated, high-resolution datasets that span the latest Ediacaran and earliest Cambrian are necessary to understand rates and mechanisms of biological and environmental change across this critical transition. Here, we report exceptionally preserved late Ediacaran to early Cambrian fossil horizons from the Deep Spring Formation in Nevada. The older of the two horizons preserves *Gaojiashania* in siltstone and sandstone in between *Cloudina*-rich wackestone and packstone of the Dunfee Member of the Deep Spring Formation. This fossil horizon is the first report of *Gaojiashania* outside of China, extending its biogeographic range and suggesting its use as a latest Ediacaran index fossil. The younger of the two fossil horizons preserves pyritized *Conotubus* in siltstone and shale of the Esmeralda Member of the Deep Spring Formation. The *Conotubus* horizon occurs just below the most negative $\delta^{13}C$ values in the basal Cambrian $\delta^{13}C$ excursion, establishing it as the youngest Ediacaran fossil to date.

The fossil horizons are placed into a high-resolution $\delta^{13}C$ chemostratigraphic framework, allowing for regional and global correlation to other Ediacaran-Cambrian Boundary sections. In addition to chemostratigraphic data from the Deep Spring Formation, we present high-resolution $\delta^{13}C$ data from two sections of the lower Member of the Wood Canyon Formation in Death Valley, CA and five sections of the Zuun-Arts

Formation in Western Mongolia. Using sequence and chemostratigraphy, composite $\delta^{13}C$ curves are constructed for the Great Basin and Western Mongolia. Together, these chemostratigraphic curves show that instead of a single, rapid $\delta^{13}C$ excursion at the Ediacaran-Cambrian Boundary, there is one broad excursion with reproducible secondary structure. Additionally, we suggest that the 541 Ma age from Oman dates the onset rather than the nadir of the negative $\delta^{13}C$ excursion, leaving the interval between the onset of this excursion and the Fortunian-Stage 2 Boundary largely unconstrained by absolute ages. We use our new fossil finds and refined chemostratigraphy to construct a composite datum of last appearances of Ediacaran fauna and Cloudinids and first appearances of trace fossils and small shelly fossils relative to the existing geochronological constraints.

3.1. Introduction

The Ediacaran-Cambrian (E-C) transition witnessed a number of global changes: The advent of a burrowing behavior marked by the first appearance of *Treptichnus pedum,* the extinction of Ediacaran macroscopic soft-body fauna and the biomineralizing *Cloudina* and *Namacalathus*, the first appearance of small shelly fossils (SSFs), and a large negative carbon isotope ($\delta^{13}C$) excursion. Calibrating rates of paleontological and geochemical change across the E-C Boundary has been problematic, in large part because the global record of this critical transition has been pieced together from a number of different localities, none of which preserves all of these changes. The ability to resolve the relative and absolute timing of different biological and environmental records – and thus provide an accurate framework to interpret the mechanistic links for these changes – has been hindered by imprecise and inconsistent ways of identifying and correlating the

E-C Boundary and by a lack of fossiliferous, carbonate-dominated sections that span this time interval. Mongolia is one of the few places globally that preserves the latest Ediacaran in expanded, continuous limestone strata. In addition, the Great Basin of Nevada and California, USA offers a rare window into fossiliferous sections that preserve the late Ediacaran ~4-6‰ plateau into the high frequency $\delta^{13}C$ fluctuations in the earliest Cambrian in expanded, nearly continuous, carbonate-rich strata. Moreover, the section at Mt. Dunfee, Nevada is the only section globally to preserve *Cloudina*, the first appearance datum (FAD) of *T. pedum*, crucial $\delta^{13}C$ chemostratigraphic markers, and now two horizons of exceptionally preserved Ediacaran body fossils. Together, datasets from these two localities provide a new chemostratigraphic framework to for Ediacaran-Cambrian datasets globally.

3.2. Ediacaran-Cambrian Transition in the Great Basin, USA

The late Ediacaran through Cambrian strata in the southern Great Basin were deposited during the rift to drift transition along western Laurentia (Armin and Mayer, 1983; Bond and Kominz, 1984; Christie-Blick et al., 1989; Fedo and Cooper, 2001; Stewart, 1972). The classic view of the Ediacaran-Cambrian basin architecture in the Great Basin is that it thickens from southeast to northwest, with siliciclastic-dominated successions in Death Valley deposited in a proximal shelf environment and carbonate-dominated successions in the White-Inyo Mountains and Esmeralda County deposited in an outer shelf environment (Corsetti and Hagadorn, 2000; Fedo and Cooper, 1990; Mount et al., 1991; Nelson, 1978; Nelson, 1976; Stewart, 1970). The isopach maps that are used for this paleogeographic model assume a displacement of ~80 km on the Death Valley-

Furnace Creek Fault system. Others have disputed this proposed amount of strike-slip offset along this fault system and have placed much lower limits on the amount of offset on this fault using Precambrian facies belts and the northern extent of Mesozoic volcanics (Pavlis et al., 2014; Wright and Troxel, 1966; Wright and Troxel, 1967). Combining these lower estimates of strike-slip offset with thickness and facies trends, others have suggested that during Ediacaran to Cambrian time, a north-northwest oriented trough was present in the Amaragosa Desert area, with a topographic high to the southwest (Wright and Troxel, 1966).

While exact Ediacaran to Cambrian paleogeographic reconstructions and geometries remain uncertain, chemostratigraphic correlations between the Death Valley and White-Inyo Mountains strata are becoming increasingly more precise. Of these more off-shore successions north of Death Valley, the strata in Esmeralda County (Fig. 3.1A) are better preserved and are of lower metamorphic grade than the strata in the White-Inyo Mountains to the west. Despite their better preservation, superimposed Cretaceous contractional (Burchfiel et al., 1992; DeCelles, 2004; Dickinson, 2004) and Cenozoic extensional faulting (Snow and Wernicke, 2000; Wernicke et al., 1988; Wright et al., 1976), lateral facies change, and variable dolomitization of the upper Member (Mb) of the Reed Formation (Fm) and the lowermost part of the Deep Spring Fm have previously hindered researchers from systematic stratigraphic study at this locality. Here we reconcile these complications by presenting the first detailed geological map of the Mt. Dunfee area, which provides the base for our stratigraphic, geochemical, and paleontological data.

Figure 3.1. Carbon isotope chemostratigraphy of the Ediacaran-Cambrian transition in the Great Basin, USA.

A) Locality map for the three sections from the Great Basin in California and Nevada. B) Three composite measured sections with biostratigraphy and $\delta^{13}C$ chemostratigraphic profiles of Precambrian-Cambrian Boundary sections from Echo Canyon and Boundary Canyon in Death Valley, CA, and Mt. Dunfee, in Esmeralda County, NV. Stratigraphic horizons of the two new Ediacaran lagerstätten from the Deep Spring Fm are marked with stars. The younger of the two fossil horizons is the same horizon that contains the multicellular algal fossil, *Elainabella* (Rowland and Rodriguez, 2014). The extended range of *Cloudina* is also shown on the right-hand side of the measured section of the Deep Spring Fm. The locations of the measured sections of the Deep Spring Fm are indicated in Fig. 3.3. Dashed lines show sequence and chemostratigraphic correlation between the three sections. A photo of the Echo Canyon section is shown Fig. 3.2 and photos of some of the Deep Spring Fm sections are included in Fig. 3.4.

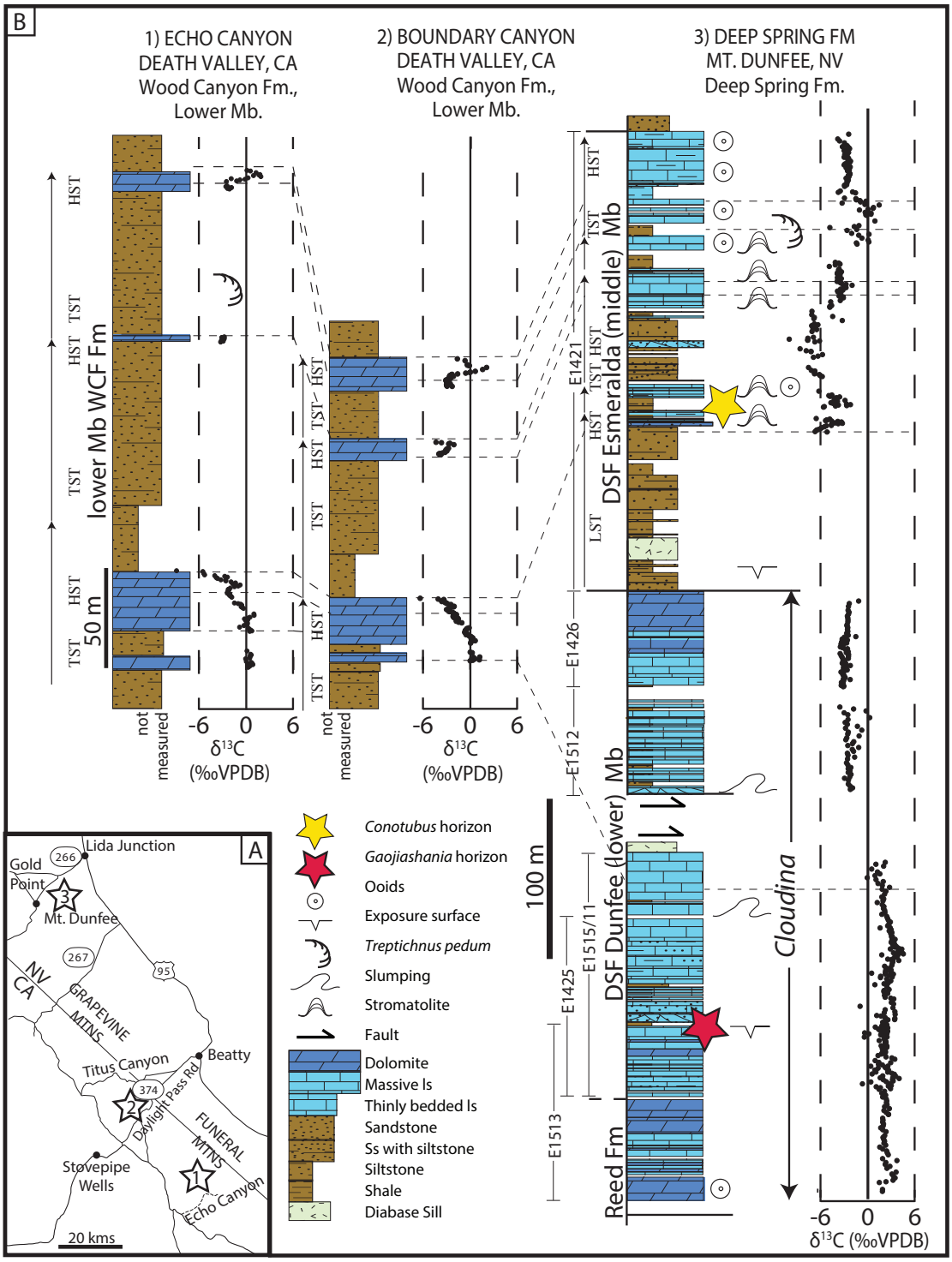

Figure 3.1 (continued).

3.2.1. Death Valley Stratigraphy

Efforts to characterize the Precambrian-Cambrian Boundary in Death Valley have focused on the upper Stirling Quartzite and lower Wood Canyon Formation (Fm) (Corsetti and Hagadorn, 2000). The upper Stirling Quartzite consists of white to grey cross-bedded mature quartz arenite. The contact between the Wood Canyon Fm and the underlying Stirling Quartzite is sharp and disconformable in most sections, particularly in southern Death Valley (Stewart, 1970). The lower member of the Wood Canyon Fm, in contrast, is predominantly a purple to brown arkosic subtidal sandstone of the lower member of the Wood Canyon Fm. There are three parasequences in the lower member of the Wood Canyon Fm, each of which is capped by a tan to buff dolomite marker bed; these three resistant, dolomite beds are easily traceable across northern Death Valley (Diehl, 1974; Stewart, 1970). The middle Wood Canyon Fm is a pebble conglomerate that, in southern Death Valley, incises the lower member, creating a prominent sequence boundary (Fedo and Cooper, 1990).

In Death Valley, *Cloudina* has been reported from member D of the Stirling Quartzite (Langille, 1974). Other possible Ediacaran tubular fossils and simple bed-parallel trace fossils have been reported from the siltstone and sandstone at the base of the Wood Canyon Fm (Hagadorn and Waggoner, 2000). The FAD of *T. pedum* is reported from the sandstone beds above the second dolomite marker bed in the lower member of the Wood Canyon Fm, occurring also just above the nadir of a broad negative $\delta^{13}C$ excursion marking the E-C Boundary (Corsetti and Hagadorn, 2000). This locality and a low-resolution section through the upper Windermere Group in the Mackenzie Mountains (Kaufman et al., 1997; Narbonne et al., 1994) are the only two sections

globally that are cited as preserving a relationship between the FAD of *T. pedum* and the large negative $\delta^{13}C$ excursion.

3.2.2. White-Inyo Mountains and Esmeralda County Stratigraphy

In the White-Inyo Mountains, the E-C Boundary is in the Deep Spring Fm, which consists of the Dunfee, Esmeralda, and Gold Point members (Ahn et al., 2012; Corsetti and Kaufman, 1994; Rowland and Corsetti, 2002). The Dunfee Member (Mb) is 300-350 m thick, composed primarily of grey to pale orange dolomitic limestone with minor greenish-grey siltstone, calcareous sandstone, and quartzite (Albers and Stewart, 1972). There are slump and load structures in the upper part of the member. Pink to blue recrystallized dolostone of the Dunfee Mb is sharply overlain by tan to green shoreface sandstone with mud cracks and abundant trace fossils of the Esmeralda Mb. The Esmeralda Mb is ~250 m thick and composed of quartzite and calcareous sandstone, stromatolitic and ooilitic limestone, and minor siltstone and shale (Albers and Stewart, 1972).

The end-Ediacaran fossil, *Cloudina*, has been reported from the Reed Fm and the Dunfee Mb of the Deep Spring Fm (Gevirtzman and Mount, 1986; Grant, 1990; Mount et al., 1983; Signor et al., 1987; Taylor, 1966) and the algal fossil, *Elainabella*, has been reported from the middle Dunfee Mb (Rowland and Rodriguez, 2014). The FAD of *T. pedum*, and thus the E-C Boundary (Brasier et al., 1994; Landing, 1994), was identified above a large negative basal Cambrian $\delta^{13}C$ excursion (Corsetti and Kaufman, 1994; Oliver and Rowland, 2002). Until now, no additional chemostratigraphy had been conducted on the strata at Mt. Dunfee, largely because of structural complications and the lack of a detailed geological map of the area.

Although the White-Inyo Mountains are geographically very close to the Death Valley area and the two regions contain units of similar age, precise regional correlations have been hindered by a lack of absolute ages, sparse biostratigraphic control, and structural complexity. Stewart (1970) proposed a lithostratigraphic correlation framework for the southern Great Basin. In this framework, he proposed that the Deep Spring Fm was an offshore equivalent of the lower member of the Wood Canyon Fm, the Hines Tongue through the upper Reed Dolomite were equivalent to the upper siliciclastic Stirling Quartzite, and the lower Reed Dolomite was equivalent to the dolomitic "member D" of the Stirling Quartzite. The underlying Wyman Fm was tentatively correlated with the Johnnie Fm through the middle Stirling Quartzite. More recently, using chemostratigraphy and biostratigraphy, others have suggested instead that the upper Reed Dolomite and Dunfee Mb of the Deep Spring Fm correlate with the upper Stirling, and that the Wyman-Reed unconformity correlates with the upper Johnnie Fm unconformity (Corsetti et al., 2000). In this framework, the Hines Tongue of the Reed Dolomite, correlates with the lower to middle Stirling Quartzite (Corsetti et al., 2000).

3.3. Ediacaran-Cambrian Transition in Western Mongolia

The Zuun-Arts Fm of the Zavkhan Terrane in Western Mongolia preserves a thick, latest Ediacaran to early Cambrian succession that is composed almost entirely of thin-bedded limestone and ooilitic limestone grainstone. The Zuun-Arts Fm overlies a ~40 Ma unconformity above the Shuurgat Fm, marking the onset of basin formation as the Zavkhan Terrane subducted to the southwest beneath the Khantaishir-Dariv Arc (Bold et al., 2013; Macdonald et al., 2009; Smith et al., 2015). The Zuun-Arts Fm is overlain by the fossiliferous, mixed carbonate-siliciclastic Bayangol Fm. Because these strata were

deposited in a foreland basin (Macdonald et al., 2009; Smith et al., 2015), accommodation and sedimentation rates were very high, making this locality one of the few places globally to preserve the latest Ediacaran in expanded, continuous, carbonate-dominated strata.

The base and top contacts of the Zuun-Arts Fm are marked by phosphatic shale with nodular limestone intervals that record major transgressions across the Zavkhan Terrane (Smith et al., 2015). The strata in between these phosphatic shale intervals are almost entirely limestone, recording slope to shelf deposition in a broad shallowing-up sequence. Within the Zuun-Arts Fm there is extreme diachroneity of deposition across the basin (Smith et al., 2015), but, because of the two sharp, synchronous sequence boundaries that bookend the formation, the correlations between Zuun-Arts sections are restricted to being between the condensed phosphatic horizons. More details about the Zuun-Arts Fm and the specific localities of the measured sections can be found in Chapter 4.

The Zuun-Arts Fm preserves simple bed planar trace fossils, vertical burrows, possible hold fast impressions (Jones, 2009), and a negative $\delta^{13}C$ excursion that has been used to identify the E-C Boundary on the Zavkhan Terrane (Brasier et al., 1996). To date, no confirmed body fossils have been found within the formation (Smith et al., 2015). More recently, additional higher-resolution sections of the Zuun-Arts Fm were published, demonstrating that there is diachronous deposition across the Zavkhan Terrane and that there is more structure to the Zuun-Arts Fm $\delta^{13}C$ chemostratigraphic curves than had been previously documented (Smith et al., 2015).

3.4. Methods

3.4.1. Geologic mapping, sedimentology, $\delta^{13}C$ chemostratigraphy, and biostratigraphy

3.4.1.1. Death Valley

Two sections of the lower member of the Wood Canyon Fm were measured and sampled for $\delta^{13}C$ at a 0.3-0.5 m resolution (Fig. 3.1A, B)[1]. Because these sections have been measured by others (Corsetti and Hagadorn, 2000; Stewart, 1970), the focus for this study was only on the three dolomite marker beds. Sections at Echo Canyon (Fig. 3.2) and Boundary Canyon were targeted because they are among the northernmost sections, and thus the most carbonate-dominated sections, of the lower member of the Wood Canyon Fm in Death Valley. The section at Boundary Canyon, along the Daylight Pass Road, is the same section that was measured and sampled at lower resolution by Corsetti and Hagadorn (2000).

3.4.1.2. Mt. Dunfee

Geologic mapping of the Mt. Dunfee area was done on the Gold Point Quadrangle 1:24,000 topographic map, southeast of Gold Point, NV (Figs. 3.1A and 3.3). A composite section of the upper Reed Fm through the Esmeralda Mb was constructed from four individual measured sections (Figs. 3.1B and 3.3). Section E1421 (locality is marked on geologic map in Fig. 3.3 and shown in Fig. 3.4A, B) of the Esmeralda Mb of the Deep Spring Fm is the same section as the one described by Rowland et al. (2008) and sampled

[1] Carbon and oxygen isotope methods and data tables for the Death Valley sections can be found in Appendix A4

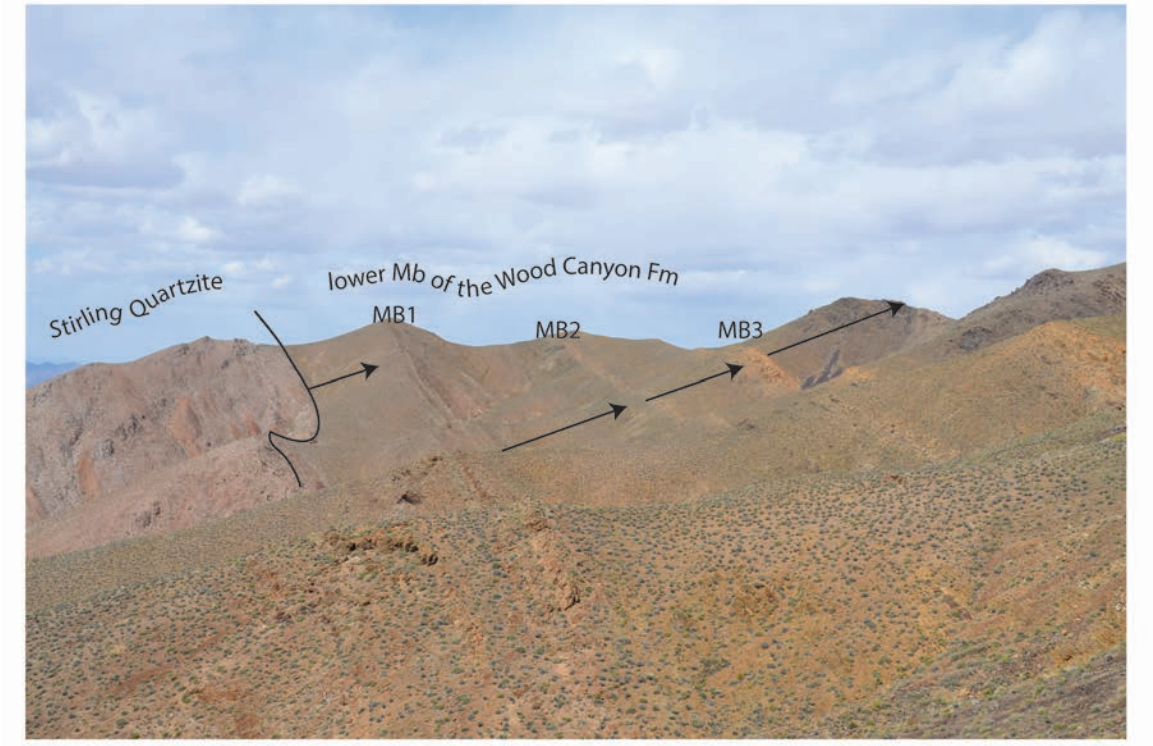

Figure 3.2. Photo of the lower member of the Wood Canyon Formation in Echo Canyon, Death Valley

Photo of the lower member of the Wood Canyon Fm in Echo Canyon (see Fig. 3.1A for locality and 3.1B for stratigraphic column). The three white to tan marker beds (MB1-3) are marked in the photo. The contact between the lower and middle members of the Wood Canyon Fm is not visible. The arrows mark the shallowing up sequences.

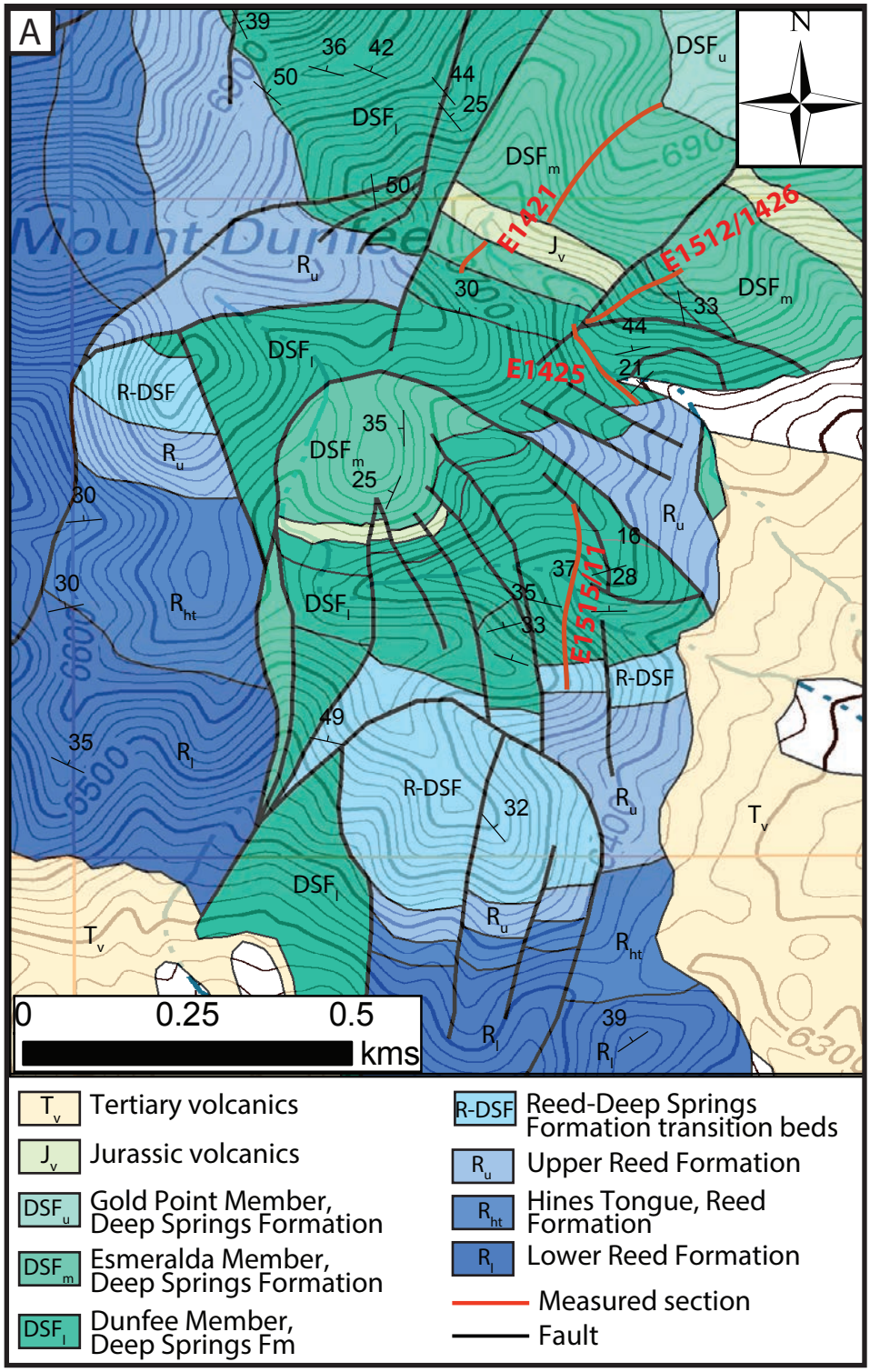

Figure 3.3. Geologic map of Mt. Dunfee.
Geologic map of Mt. Dunfee area, southeast of Gold Point, NV. The map area is location 3 in Figure 3.1A. Measured sections in red are plotted in Fig. 3.1B.

Figure 3.4. Field photos from Mt. Dunfee area.
Field photos from the Mt. Dunfee area. A) Outcrop scale photo of the Esmeralda Mb of the Deep Spring Fm. This photo was taken looking east and is the same locality of section E1421 (see Fig. 3.3 for exact location). The yellow star marks the *Conotubus* horizon and the black symbol marks the FAD of *T. pedum;* these are the same symbols used in Fig. 3.1B. B) A photo looking northwest of the creek bed in which section E1425 was measured. Section E1421 is in the background. C) A lag deposit of *Cloudina* debris (in between the two white lines). This photo is from the middle of section E1425. D) A bedding surface of *Cloudina*. This specimen was found close to section E1425.

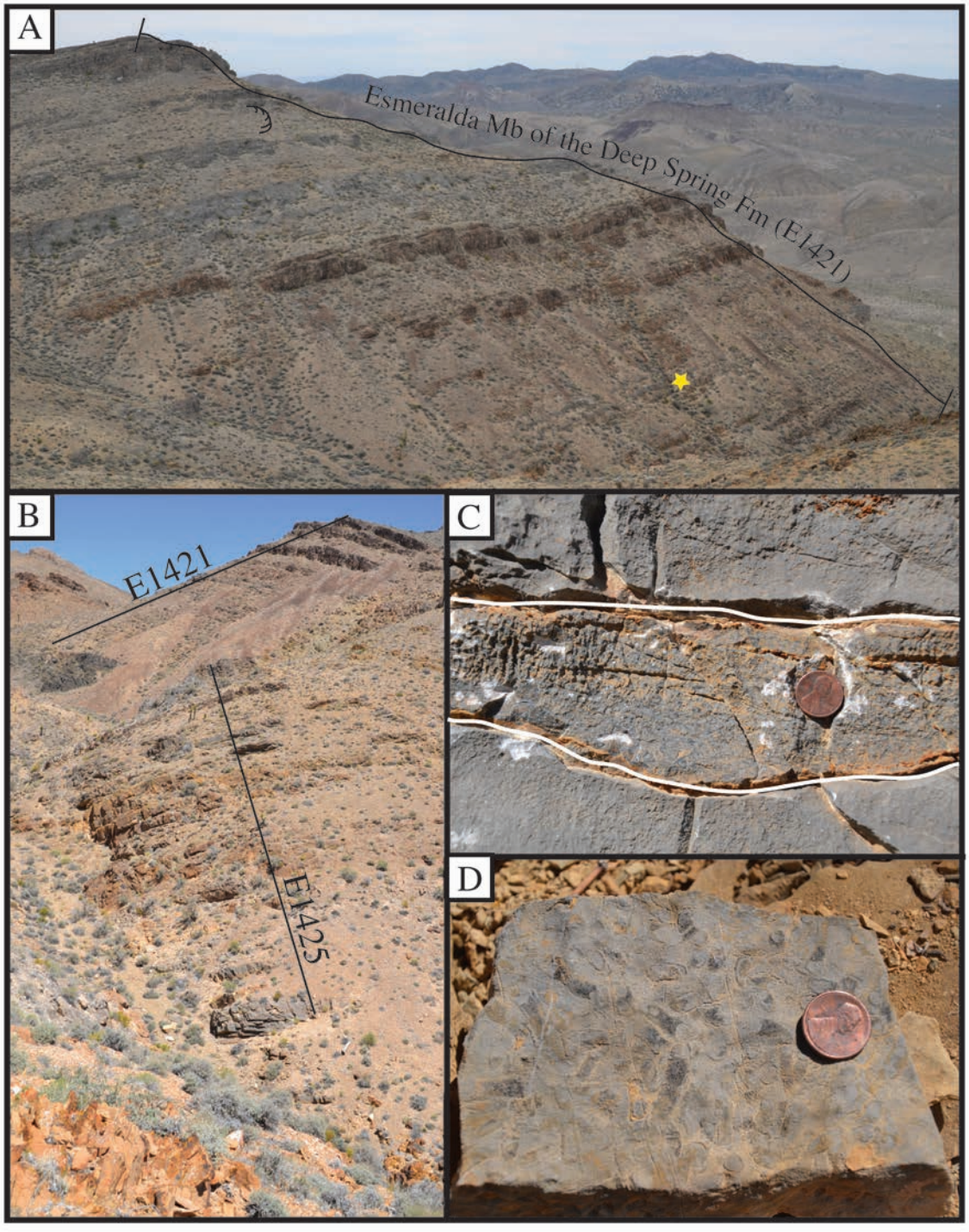

Figure 3.4 (continued).

at low resolution for $\delta^{13}C$ chemostratigraphy by Corsetti and Kaufman (1994). For the other three sections presented here from the upper Reed Dolomite through Dunfee Mb of the Deep Spring Fm, marker beds were used to construct a composite section. While measuring stratigraphic sections, carbonate samples were collected at a 0.3-2 m resolution[2]. Paleontological data presented here were collected while mapping and measuring section, and placed into a stratigraphic context.

3.4.1.3. Zavkhan Terrane, Western Mongolia

Three of the five sections presented here were published in Smith et al. (2015), and more information on the sedimentology of the individual sections can be found on them in Chapter 4. Data from two additional sections, from Khongor and Zuun-Arts Ridge, were excluded from Chapter 4 because at these localities, the overlying Bayangol Fm, which was the focus of Chapter 4, is not well-exposed. The sections at Khongor and Zuun-Arts Ridge were measured and simultaneously sampled for $\delta^{13}C$ chemostratigraphy at the ~1 m resolution[3].

3.4.1.4. Constructing composite carbon isotope curves

The composite carbon isotope curves for the Great Basin, USA and the Zavkhan Terrane in SW Mongolia were constructed first by generating a five point running average to eliminate some of the local variability and scatter, and then by matching the chemostratigraphic curves point by point. The sections were correlated under the assumption that the $\delta^{13}C$ values reflected the isotopic composition of global seawater at

[2] Carbon and oxygen isotope methods and data tables for the Mt. Dunfee sections can be found in Appendix A5

[3] Carbon and oxygen isotope methods and data tables for the two sections of the Zuun-Arts Fm at Zuun-Arts Ridge and Khongor can be found in Appendix A6. Data from the other Zuun-Arts sections can be found in Appendix A7.

the time of deposition, and that there was not an isotopic gradient of more than 1-2‰ in the oceans at the time of deposition or diagenetic alteration of more than 1-2‰.

3.5. Results

3.5.1. Geologic mapping, $\delta^{13}C$ chemostratigraphy, and biostratigraphy for the Wood Canyon and Deep Spring formations

3.5.1.1. Death Valley

At Boundary Canyon, the measured thickness of the portion of the strata between the uppermost and lowermost dolomite marker beds is 155 m. At Echo Canyon, the measured thickness of this same interval is 230 m (Figs. 3.1B and 3.2). Each of the three parasequences in the lower member of the Wood Canyon Fm records subtidal siliciclastic rocks that are gradationally overlain by shallow marine dolostone. The $\delta^{13}C$ values generally reproduce the curve that was previously published (Corsetti and Hagadorn, 2000); however, the higher-resolution data show that there is reproducible secondary structure that is superimposed upon the broad negative $\delta^{13}C$ excursion (Fig. 3.1B).

3.5.1.2. Mt. Dunfee

Here, the first detailed geologic map of Mt. Dunfee is presented (Fig. 3.3), allowing for the construction of a higher resolution composite carbon isotope curve, not only of the previously sampled Esmeralda Mb of the Deep Spring Fm, but also the upper Reed Fm and Dunfee Mb of the Deep Spring Fm (Fig. 3.1B). The dominant structural features at Mt. Dunfee are detachment, normal, and tear faults with tectonic transport to the south. Distinctive marker beds were used for mapping purposes and facilitated the construction of the composite stratigraphic section.

At Mt. Dunfee, the upper Reed and lower Deep Spring formations preserve a 3-4‰ $\delta^{13}C$ plateau (Fig. 3.1B). Above this interval, there is a downturn in $\delta^{13}C$ values to -2-0‰ in the dolomitized and recrystallized upper ~50 m of the Dunfee Mb. Above siliciclastic rocks of the basal Esmeralda Mb, the previously documented broad negative $\delta^{13}C$ excursion was reproduced (Corsetti and Kaufman, 1994), but, similar to the new chemostratigraphic data from Death Valley, there is additional, previously undocumented secondary structure superimposed on it (Fig. 3.1B). The lowermost limestone beds in the Esmeralda Mb contain $\delta^{13}C$ values as low as -6.2‰. Above this, the $\delta^{13}C$ values increase up to -3 to -2‰ before they again decrease to -9.5‰. The Esmeralda Mb fossil horizon occurs above the -6.2‰ values and below the -9.5‰ values. Stratigraphically above this, there is a gradual return to $\delta^{13}C$ values of ~0‰ over ~130 m.

Complementing the chemostratigraphy and sequence stratigraphy, here we report new Ediacaran biostratigraphy. *Cloudina* had previously been reported from the lower to middle part of the Dunfee Mb of the Deep Spring Fm at Mt. Dunfee (Parsons, 1996; Signor et al., 1987). In this study, *Cloudina* was discovered in the uppermost bed of the Dunfee Mb (Fig. 3.1B, 3.4C-D), extending the last appearance datum (LAD) of this Ediacaran index fossil in a chemostratigraphic context at Mt. Dunfee. Additionally, two new fossil horizons are described in detail below.

3.5.2. New Late Ediacaran Fossil Horizons in the Deep Spring Formation at Mt. Dunfee

3.4.2.1. Fossil horizon in the Esmeralda Mb of the Deep Spring Fm

The older of the two fossil horizons reported here is from the lower part of the Dunfee Mb of the Deep Spring Fm (Fig. 3.1B). Mold and cast impressions of *Gaojiashania* (Fig. 3.5A-H) were discovered from different bedding surfaces within ~3 m of strata of interbedded micaceous green shale, micaceous brown to green siltstone, and micaceous fine- to medium-grained sandstone. Some of the fossiliferous horizons contain <1 cm-sized mud chips. Mud-cracks were found just below the fossiliferous interval. The same stratigraphic horizon was identified in three different fault blocks in the Mt. Dunfee area, but all of the *Gaojiashania* specimens were discovered in a talus slope from one section that can be directly traced to a horizon in section.

3.5.2.2. Fossil horizon in the Esmeralda Mb of the Deep Spring Fm

The younger of the two fossil horizons (Fig. 3.6A-O) at Mt. Dunfee is from the middle part of the Esmeralda Mb of the Deep Spring Fm. Rowland and Rodriguez (2014) reported *Elainabella*, a multicellular alga, from the same stratigraphic interval. The most abundant fossil in this interval is a narrow conical tube with transverse annulations. The diameter of this fossil is ~1 mm and the length of articulated fossil specimens ranges from 0.5-3 cm. The narrow ends of these fossils are pointed and closed (Fig. 3.6A, D, J). The cross-section and the operculum of the fossil are circular. Non-uniform curvature is present in some of these fossils. These fossils are often stained orange or red, in contrast to the black to brown to green matrix of the host siltstone and shale, most likely the result of a pyrite pseudomorph remnant of the original wall. The fossils were found in different

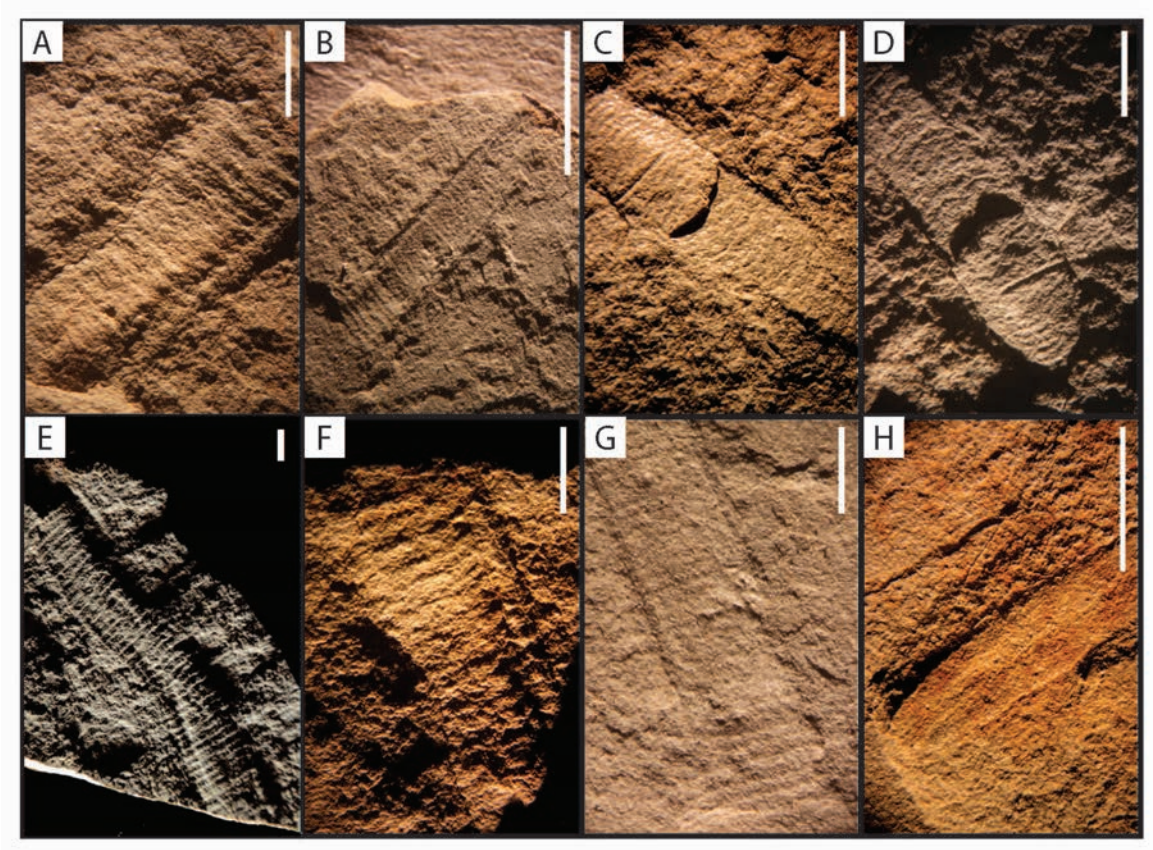

Figure 3.5. Photographs of the Ediacaran macrofossil *Gaojiashania* from the Dunfee Member of the Deep Spring Formation.
Photographs of Ediacaran macrofossils from the Dunfee Mb of the Deep Spring Fm lagerstätte. All of these fossils were found in a talus slope near section E1511. A-H) Bedding plane cast and mold impressions of the problematic Ediacaran macrofossil *Gaojiashania* from the Dunfee Mb of the Deep Spring Fm. Scale bar in all photographs is 0.5 cm.

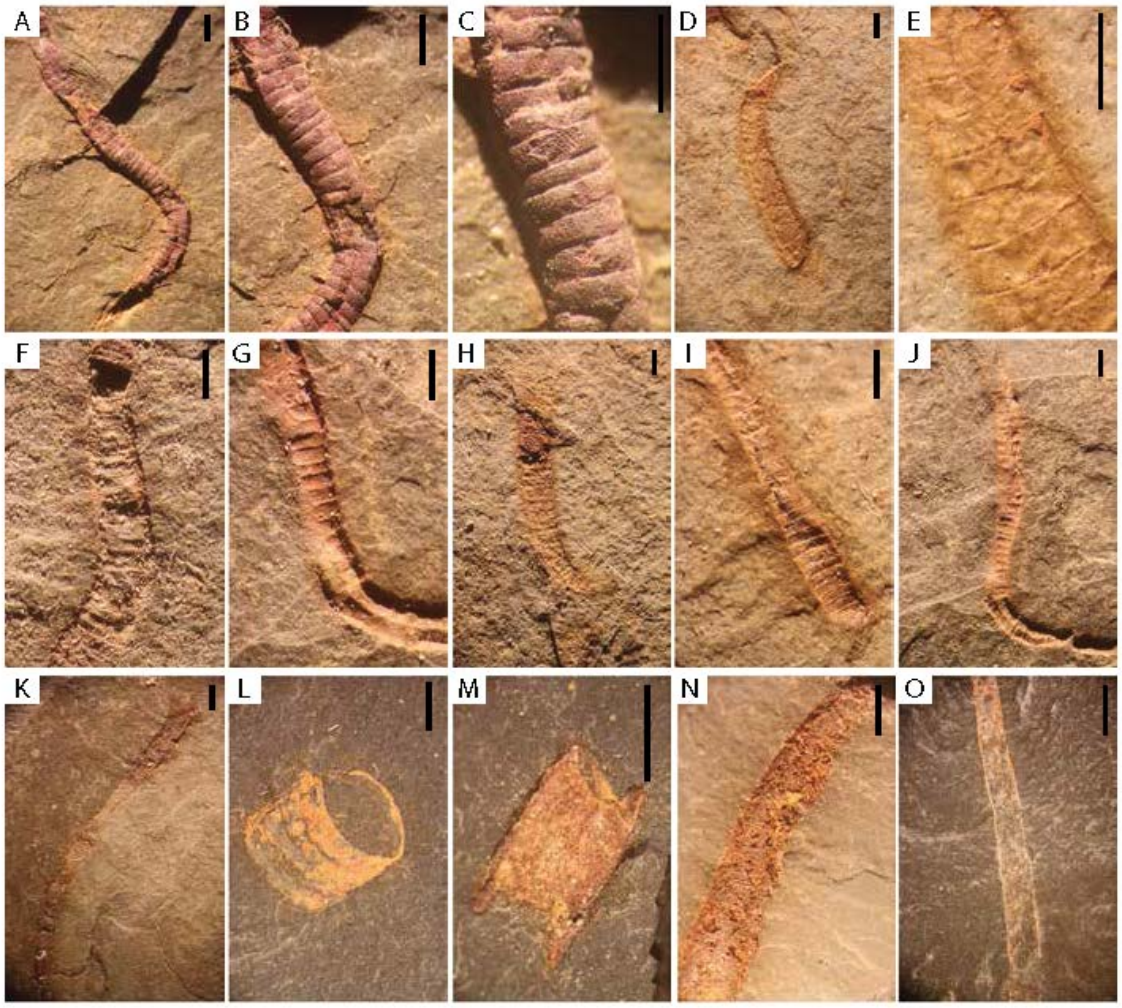

Figure 3.6. Photographs of the Ediacaran macrofossil *Conotubus* from the Esmeralda Member of the Deep Spring Formation.
This is the same horizon from which Rowland and Rodriguez (2014) report exceptional preservation of the alga *Elainabella*. These fossils were found in section E1421 and in a scree slope above E1426. Scale bar in all photographs is 0.1 cm. A-C) Different scales of one specimen of *Conotubus* that has been replaced by iron oxides. This specimen shows the stacked funnels and the high relief of the animal. D-E) Two different scales of a lightly pyritized mold of *Conotubus*. F-K) *Conotubus* specimens showing the range in size and preservation of these fossils. L-M) broken pieces *Conotubus*. N-O) Two unidentified smooth tubular fossils that do not preserve annulations.

horizons within distinctive ~2 m of shale and siltstone that occur in between the columnar stromatolites in "microbial horizons A and B" described by Oliver and Rowland (2002) and Rowland et al. (2008). Over 100 fossil specimens, many of which are broken or disarticulated, were collected from four nearby fault blocks in the Mt. Dunfee area.

3.5.3. Sedimentology, biostratigraphy, and chemostratigraphy of the Zuun-Arts Formation in Western Mongolia

The Zuun-Arts Fm is almost entirely low-grade limestone that records a gradually shallowing-up sequence over ~200-400 m of stratigraphy. Simple, bed planar trace fossils were documented in several sections of the Zuun-Arts Fm (Fig. 3.7A) and bed-penetrating burrows were documented in the top of the Zuun-Arts Fm at Orolgo Gorge (Fig. 3.7C) and in the upper part of the Bayan Gorge section. Jones (2009) recognized annuli along bedding planes in the lower to middle part of the Zuun-Arts Fm (Fig. 3.7B) and interpreted them as possible holdfast impressions. The presence of vertical burrows in other horizons of the Zuun-Arts Fm suggests that the annuli could instead be diagenetic rings around vertical burrows. Digitate stromatolites were documented in the lower to middle part of two of the Zuun-Arts Fm sections (Figs. 3.7E-F). In between many of these mounds, micritic cement fill the void space, which in places resembles and could be mistaken for bed-penetrating burrows (Fig. 3.7D).

Figure 3.7. Photographs of the Zuun-Arts Formation
Photographs of the sedimentology and biostratigraphy of the Zuun-Arts Fm in Western Mongolia. A) Simple bed planar trace fossils in the lower Zuun-Arts Fm from Bayan Gorge. B) Annuli preserved along a bedding surface. These have been interpreted as possible hold fast impressions (Jones, 2009), but they could also be diagenetic rims around vertical burrows. C) Bed-penetrating bioturbation in the upper part of the Zuun-Arts Fm at Orolgo Gorge. D) Micritic cements infilling space around irregular digitate stromatolite mounds at Zuun-Arts Ridge. E and F) Digitate stromatolites in the lower middle part of the Zuun-Arts Fm at Zuun-Arts Ridge.

Carbon isotope chemostratigraphic curves from five sections of the Zuun-Arts Fm are plotted next to schematic measured sections (more detailed measured sections from the Bayan Gorge, KTN, and Southeast Khukh-Davaa can be found in Chapter 4; Fig. 3.8). These sections document negative $\delta^{13}C$ values as low as -9.5‰ near the top of all of the sections and positive $\delta^{13}C$ values of up to 6.5‰ in the lower to middle part of the sections at Zuun-Arts Ridge and in Southeast Khukh-Davaa (Fig. 3.8). The highly variable $\delta^{13}C$ values occur between two phosphatic shale units that bookend the formation, marking two transgressions that represent synchronous sequence boundaries across the Zavkhan Terrane.

3.6. Discussion and Conclusion

3.6.1. Carbon isotope ($\delta^{13}C$) chemostratigraphy

3.6.1.1. Carbon isotope chemostratigraphy in the Great Basin

One interesting result of the new chemostratigraphic data from the Great Basin is that the broad negative $\delta^{13}C$ excursion at the base of the Cambrian preserves secondary, regionally reproducible structure that is superimposed on the single broad negative $\delta^{13}C$ excursion. The second order $\delta^{13}C$ structure on the broad negative excursion allows for higher precision correlations between the Ediacaran to Cambrian strata in Death Valley and the White Inyo Mountains. Using a combination of sequence stratigraphy and chemostratigraphy, we correlate between the two regions (Figs. 3.1B and 3.9). Using the 0‰ crossing point and the -6.5‰ values in the basal limestone units of the Esmeralda Mb, we suggest that the upper part of the Dunfee Mb through the shoreface sandstone in the

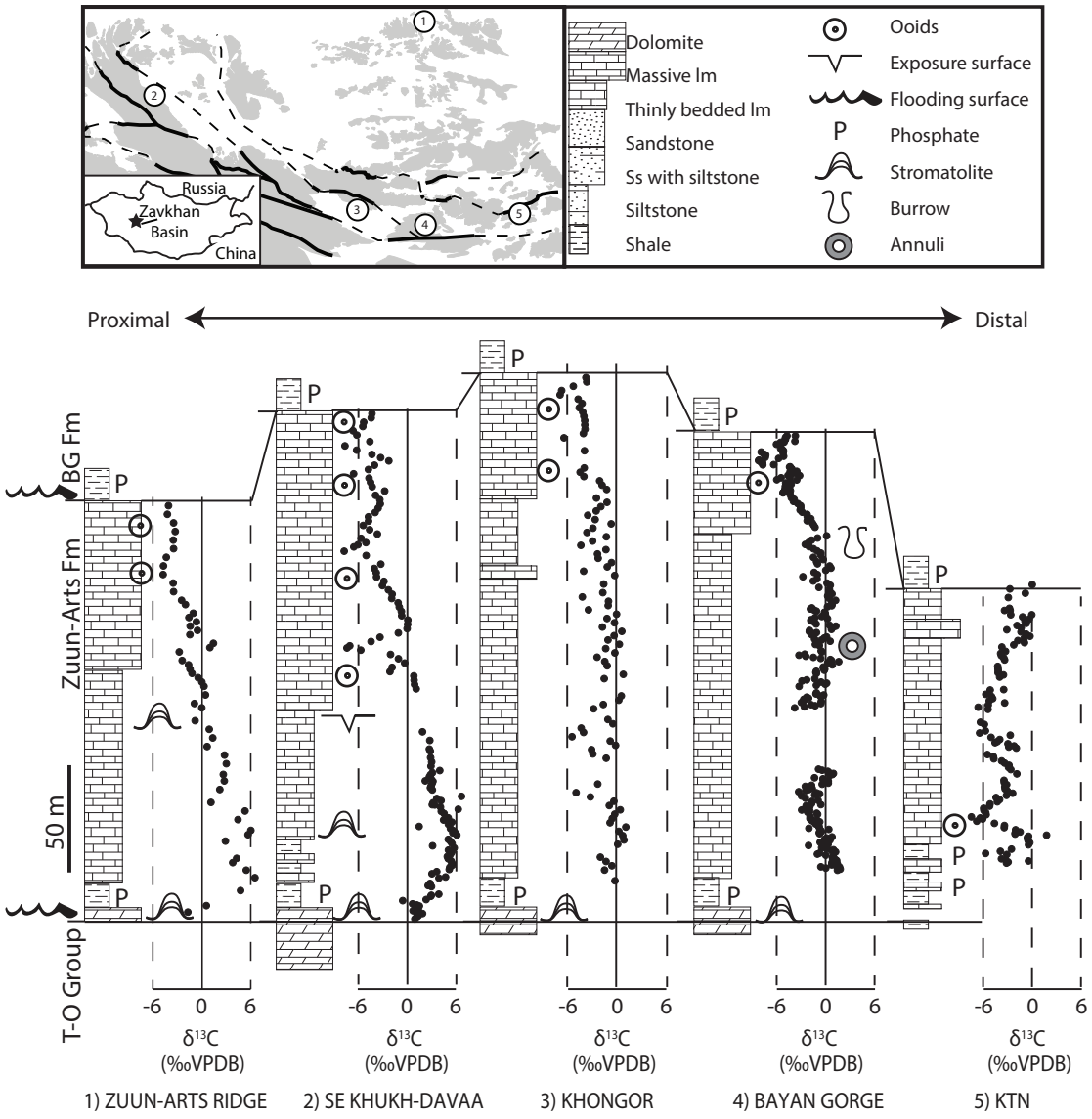

Figure 3.8. Carbon isotope chemostratigraphy and biostratigraphy from five sections of the Zuun-Arts Formation

Five measured sections and $\delta^{13}C$ chemostratigraphy of the late Ediacaran Zuun-Arts Fm from Western Mongolia. The map in the upper left-hand corner shows where in the Zavkhan Terrane the sections are located. Refer to figures 4.1 and 4.6 for more detailed maps. The chemostratigraphy from three of the five sections is presented in figure 4.8. More detailed descriptions of the Zuun-Arts Fm and additional Zuun-Art Fm localities are described in Chapter 4.

Figure 3.9. Composite Ediacaran carbon isotope curve from the Great Basin
Composite chemostratigraphic curve for the Great Basin. The red and blue lines are used to show the five-point running average of the $\delta^{13}C$ data for the Wood Canyon Fm and Deep Spring Fm sections, respectively. These lines are used to construct the composite curve for the southern Great Basin on the right-hand side of the figure. The biostratigraphy is show on the right-hand side of the curve.

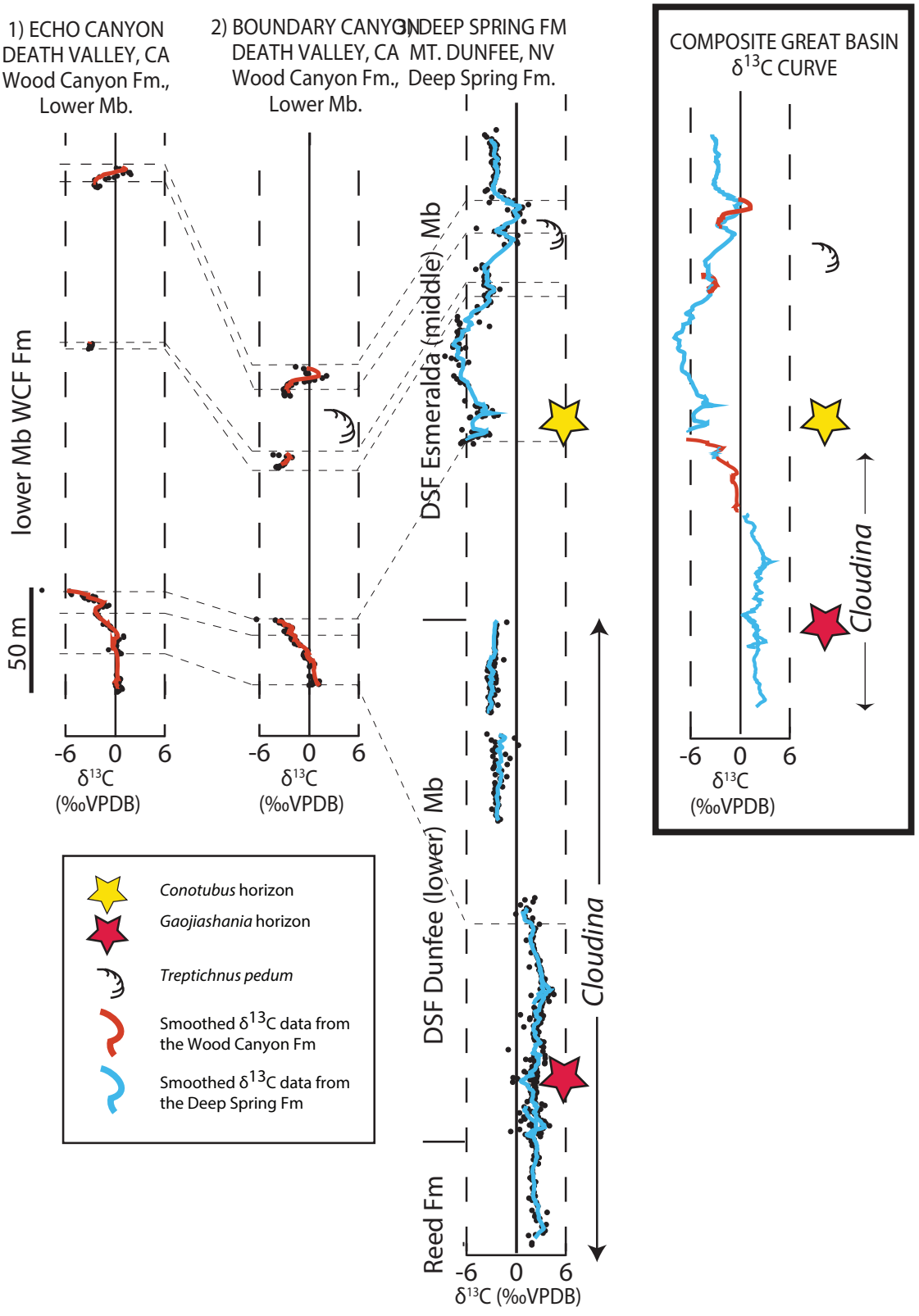

Figure 3.9 (continued).

lower Dunfee Mb are correlative with the lowermost dolomite marker bed of the lower member of the Wood Canyon Fm (Fig. 3.9). Using the 0‰ crossing point above the negative $\delta^{13}C$ excursion, the upper dolomite marker bed of the lower member of the Wood Canyon Fm is correlated to the upper part of the Esmeralda Mb (Figs. 3.1 and 3.9). This correlation scheme is similar to previous ones (Corsetti et al., 2000), but here we correlate the lower member of the Wood Canyon Fm with the Dunfee and Esmeralda members instead of just the Esmeralda Mb. In light of these new correlations, the stratigraphic ranges of *Cloudina* and *Conotubus* extend into the lower dolomite marker bed of the Wood Canyon Fm and the siltstone just above it, respectively. This revised correlation scheme is more consistent with the paleogeographic interpretation that the Death Valley to White-Inyo Mountain transition represents a thickening wedge of carbonate production to the northwest during the HSTs.

3.6.1.2. Carbon isotope chemostratigraphy in Western Mongolia

The Zuun-Arts Fm in Western Mongolia is one of the few places globally that preserves the latest Ediacaran in expanded, low-grade, limestone strata that lack unconformities. The limestone of Zuun-Arts Fm preserves small-scale sedimentological detail exquisitely (Fig. 3.7A-F), and none of the $\delta^{13}C$ values of the Cambrian limestone strata above the Zuun-Arts Fm has been systematically diagenetically altered. Thus, the significant lateral $\delta^{13}C$ variability within the Zuun-Arts Fm has been argued to be the result of diachronous deposition across the Zavkhan Terrane (Smith et al., 2015).

The base and top of the sections are correlated using sequence stratigraphy, and there is a broad shallowing-up sequence in the formation. Due to the lack of obvious smaller-scale parasequences, internal Zuun-Arts Fm correlations are done using primarily

$\delta^{13}C$ chemostratigraphy (Fig. 3.10). Using the 0‰ crossing points in the sections and secondary $\delta^{13}C$ structure, tie lines are drawn between the five point running averages of the Zuun-Arts Fm sections (Fig. 3.10). These tie lines record a TST to HST transition across the basin, and the corresponding migration of carbonate production across the basin (Figs. 3.8 and 3.10). The more distal, or basinal, sections record the TST in the condensed phosphatic shale at the base of the Zuun-Arts Fm; these sections are carbonate starved until the HST, when the belt of carbonate production progrades out toward the trench of the basin. The top of the Zuun-Arts Fm at the more proximal localities is truncated during the HST, and thus, does not record the 0‰ $\delta^{13}C$ crossing point following the nadir of the basal Cambrian $\delta^{13}C$ excursion (Fig. 3.10).

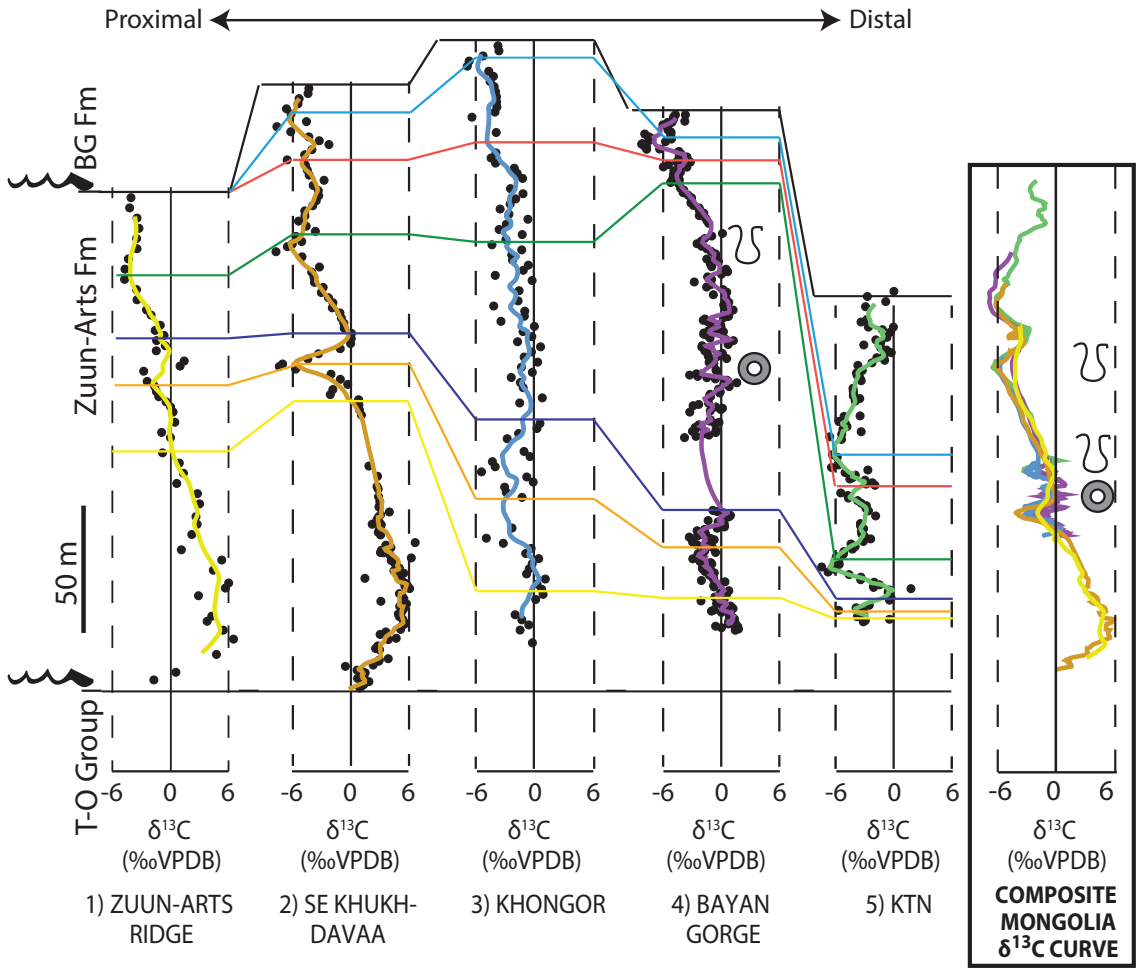

Figure 3.10. Composite Ediacaran carbon isotope curve from the Zuun-Arts Formation in Western Mongolia

Chemostratigraphic tie lines in the Zuun-Arts Fm are used to construct a composite chemostratigraphic curve for the Zavkhan Basin. The bold colored lines show the five-point running average of the $\delta^{13}C$ data for each section. The horizontal colored lines show chemostratigraphic correlations between the five sections. These correlations highlight the degree of diachronous deposition that there was in this basin and how carbonate production progrades away from the margin during the transition from the TST to HST sequence stratigraphic stages. The legend for the symbols can be found in Fig. 3.8. The lines showing the five-point running averages are used to construct the composite curve for the Zavkhan Terrane on the right-hand side of the figure.

3.6.1.3. Late Ediacaran carbon isotope chemostratigraphy globally

The new composite $\delta^{13}C$ curves from the Great Basin, USA and Western Mongolia (Figs. 3.9 and 3.10) are used to construct a new $\delta^{13}C$ chemostratigraphic curve for the latest Ediacaran (Fig. 3.11). The construction of the new $\delta^{13}C$ chemostratigraphic curve assumes that, due to rapid air-sea gas exchange and ocean mixing times, the $\delta^{13}C$ composition of the oceans globally is the same with 1-2‰ of local variability. We also assume that there are no diagenetic effects that are greater than 1-2‰ that have post-depositionally altered the $\delta^{13}C$ composition. Integrating these $\delta^{13}C$ datasets with those that have U/Pb chemical abrasion-ion dilution-thermal ionization mass spectrometry (CA-ID-TIMS) zircon ages on ashes from Namibia (Bowring et al., 2007; Grotzinger et al., 1995; Ries et al., 2009), South China (Condon et al., 2005; Gamper et al., 2015; Sawaki et al., 2010), and Oman (Amthor et al., 2003; Bowring et al., 2007) highlight some of the uncertainties in how the composite $\delta^{13}C$ Ediacaran curve has been constructed since the last ratification of the GSSP for the basal Cambrian. There is a subsequent steady decline in $\delta^{13}C$ values until the 0‰ $\delta^{13}C$ crossing point that is constrained to be between ~542.5 and 541 Ma by six ashes from Namibia and Oman. Previously, it was assumed that the negative $\delta^{13}C$ values of -4 to -2‰ stratigraphically above the youngest of these ashes represented the singular negative excursion at the E-C Boundary; however, in light of the new data presented here, these values likely represent just the onset of the negative $\delta^{13}C$ excursion (Fig. 3.11). We suggest that the true nadir of the excursion is not recorded in carbonate strata in Namibia or Oman due to being cut out by sequence boundaries or being preserved in siliciclastic deposition. Thus, the nadir of the excursion globally remains unconstrained by absolute ages and is likely more than a

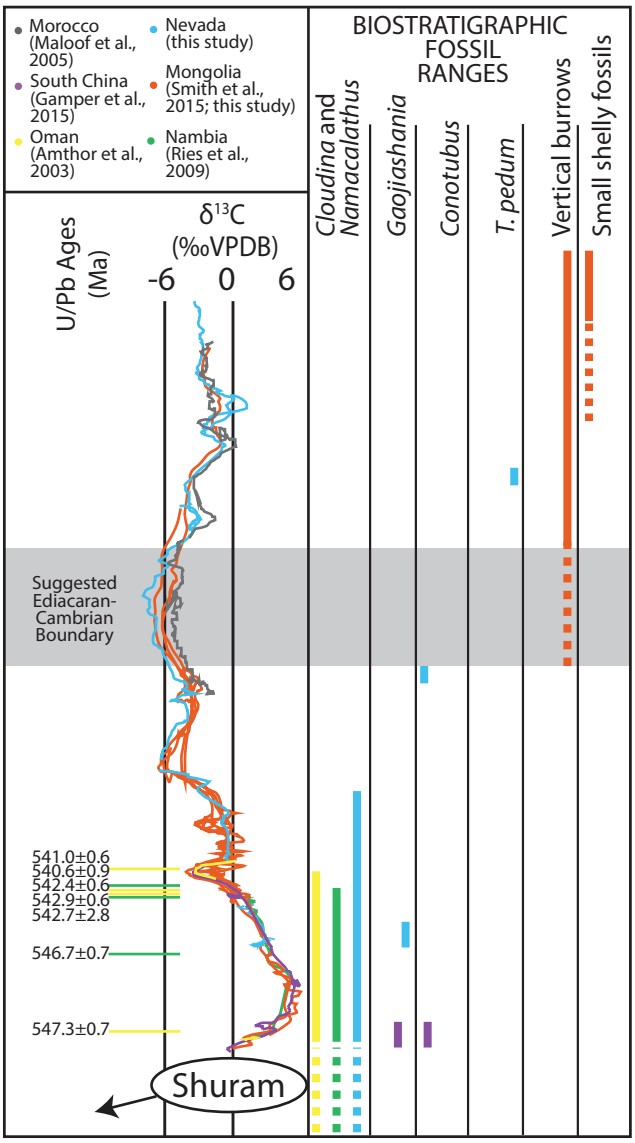

Figure 3.11. Diagram showing composite carbon isotope chemostratigraphy, biostratigraphy, U/Pb ash ages from the late Ediacaran to early Cambrian.
Global composite chemostratigraphy, biostratigraphy, and geochronology for the latest Ediacaran. The composite chemostratigraphic curves are constructed using the five-point running averages from individual sections. Combined, these data show that there is more secondary structure to the single broad negative $\delta^{13}C$ basal Cambrian excursion, and that the Oman and Namibia U/Pb ash ages likely date just the onset of the broad negative excursion. These expanded, high-resolution datasets suggest that the duration of this excursion could have been longer than was previously thought, creating a new chemostratigraphic framework for which to interpret late-Ediacaran to early Cambrian biostratigraphic ranges and absolute ages. The Namibia U/Pb ash ages of 541.0+0.6 (Bowring et al., 2007) and 542.7±2.8 (Grotzinger et al., 1995) constrain the basal Cambrian and extinction of Ediacaran megafauna and *Cloudina*. The 542.4±0.6 Ma and 542.9±0.6 Ma ages from Oman further constrain the extinction of Ediacaran macrofossils and *Cloudina*, respectively (Bowring et al., 2007). The Oman age of 546.7±0.7 Ma and the Namibia age of 547.3±0.7 Ma provide age constraints on the positive carbon isotope excursions following the Shuram excursions (Bowring et al., 2007).

million years younger than was previously thought. The next youngest U/Pb ash age is ~533 Ma from South China (Brooks et al., 2006; Jenkins et al., 2002). This age, however, is bookended by unconformities, and thus lacks robust chemostratigraphic context. Above that, the next youngest robust absolute age is the U/Pb age of 525.34±0.09 Ma from Morocco (Maloof et al., 2010b; Maloof et al., 2005) that marks the FAD of archaeocyaths (or the Fortunian-Cambrian Stage 2 Boundary). There are no absolute ages tied to the 0‰ $\delta^{13}C$ crossing point above the multiple large negative excursions in the latest Ediacaran and there are no absolute ages tied precisely to any of the high frequency $\delta^{13}C$ excursions in the earliest Cambrian. Thus, the time interval between ~541 and 525 Ma is still largely unconstrained.

The positive Ediacaran $\delta^{13}C$ values of 3 to 5.5‰ that are recorded in both the Zuun-Arts Fm and Deep Spring Fm are thought to be characteristic of latest Ediacaran $\delta^{13}C$ values globally and have been documented in South China, Namibia, and Oman (Amthor et al., 2003; Gamper et al., 2015; Grotzinger et al., 1995; Ries et al., 2009; Zhou and Xiao, 2007; Zhu et al., 2007). In Oman and Namibia, the positive $\delta^{13}C$ plateau is constrained by a 546.7±0.7 Ma U/Pb ash age just below the most positive values of the younger excursion in Oman and a 547.3±0.7 Ma U/Pb ash age just above the most positive values of the older excursion in Namibia (Bowring et al., 2007; Schmitz, 2012). We suggest that the basal Zuun-Arts Fm was deposited just after the Shuram anomaly, recording this positive $\delta^{13}C$ plateau and that the +3‰ values in the Deep Spring Fm record the end of the positive $\delta^{13}C$ plateau (Fig. 3.11).

3.6.2. Sequence stratigraphy and its relationship to the carbon cycle

The paired sequence and chemostratigraphic data from the Great Basin and Western Mongolia offer ways to test the hypothesis that some of the $\delta^{13}C$ variability in the Ediacaran and early Cambrian is linked to sequence stratigraphic boundaries, and thus driven, in part by changes in sea level (Brasier and Lindsay, 2001; Smith et al., 2015). The mixed carbonate-siliciclastic passive margin succession in the Great Basin is an ideal locality to test this hypothesis because relative changes in sea level are not as affected by regional tectonism as they are in tectonically active basins. In a mixed carbonate-siliciclastic sequence stratigraphic framework, the dolostone marker beds in the lower member of the Wood Canyon Fm represent the early highstand systems tract (HST), with the maximum flooding surface at the base of the dolostone unit (Mullins et al., 1987; Spence and Tucker, 1997; Vail et al., 1977). The siliciclastic units were deposited during the falling stage systems tracts (FSST), lowstand systems tracts (LST), and early transgressive systems tracts (TSTs), but we suggest that in these shelf deposits the LST is largely not preserved.

In the Esmeralda Mb of the Deep Spring Fm, we suggest that the shoreface sandstone and siltstone with mudcracks and abundant trace fossils at the base of this member were deposited during the FSST and LST (Fig. 3.1B). The first maximum flooding surface is in the lowermost shale and siltstone, just below the first stromatolite marker bed in the middle part of the Esmeralda Mb. Just above the first parasequences is another much thicker one. The maximum flooding surface is a thicker unit of shale and siltstone (the same interval that is marked by a yellow star in Fig. 3.1B). The overlying stromatolites were deposited during the early stages of the HST. Above this, the

interbedded sandstone, siltstone, and limestone were deposited during the HST to FSST. Near the top of the Esmeralda Mb, there are two much thinner parasequences, each composed of shale and siltstone that are capped by ooid grainstone. Again, here the base of the limestone grainstone marks the MFS and the limestone records the early HST.

The rapid, smaller-scale 1-4‰ $\delta^{13}C$ fluctuations in the Great Basin strata are occurring in the transitions from TST to the early stages of the HST. Assuming that by latest Ediacaran time the margin was tectonically inactive and thermally subsiding, there remains the question of what was driving the sequence stratigraphic architecture, and possibly the some of the secondary structure on the $\delta^{13}C$ chemostratigraphic curve in the Wood Canyon and Deep Spring formations. These three major parasequences appear to be correlative throughout the region over hundreds of kilometers, suggesting they are not the product of autocyclic processes like the lateral movement of bypass channels. Using an average sediment accumulation rate on a passive margin of 30 cm/kyr, the major sequence boundaries occur on timescales of less than 1 Myr. This timescale is too short to be driven by changes in eustatic sea-level in the absence of high-latitude glaciers and thus, we suggest that the sequences were driven by glacial eustasy modulated by >100 Kyr Milankovich cycles. Although several authors have suggested high-latitude late Ediacaran to early Cambrian glaciation (Baode et al., 1986; Chumakov and Elston, 1989; Chumakov, 2011a; Chumakov, 2011b; Etemad-Saeed et al., 2015; Hebert et al., 2010; Meert and Van der Voo, 1994; Rice et al., 2011; Stodt et al., 2011; Torsvik et al., 1996; Zhu and Wang, 2011) the timing and extent of this putative glaciation are still poorly constrained.

The Zuun-Arts Fm, however, preserves the secondary $\delta^{13}C$ fluctuations in a single TST-HST transition; at this locality, there is no evidence that the secondary $\delta^{13}C$ fluctuations are linked to sequence boundaries. We suggest that this is because the relative changes in sea level in the Zuun-Arts Basin were being driven almost entirely by tectonic loading rather than changes in eustatic sea level. The second major transgression in the E-C foreland basin occurs above the Zuun-Arts Fm and marks an influx of siliciclastic sediment to the basin, which could mark the daylighting of a thrust fault in the basin. With the preservation of mixed-carbonate siliciclastic strata, the large and small scale stratigraphic sequences are well-preserved in the formations overlying the Zuun-Arts Fm. Here, we still suggest that the <1 Ma smaller-scale 1-4‰ $\delta^{13}C$ fluctuations in the early Cambrian are being modulated by sea level, but this idea needs to be further tested at additional localities where it is possible to separate tectonically-driven changes in sea level from eustatic ones.

3.6.3. Paleontology at Mt. Dunfee

3.6.3.1. Fossil Horizon in the Dunfee Mb of the Deep Spring Fm

The genus *Gaojiashania* was first established and described by Lin et al. (1986) and Zhang (1986), and its preservation, life mode, morphology, and paleoecology were later described by Cai et al. (2011; 2012; 2013), Chen et al. (2001), and Weber et al. (2007). To date, all reports of *Gaojiashania* are from the late Ediacaran (~551-541 Ma) Gaojiashan Lagerstätte in the Dengying Fm (Cai et al., 2010; Cai et al., 2013; Hua et al., 2000; Li et al., 1992; Lin et al., 1986; Weber et al., 2007; Zhang, 1986) and the Taozichong Fm (Hua et al., 2004), both in China (see Zhuravlev et al., 2009; Cai and Hua, 2011). There are several proposed taxa for similarly annulated tubular fossils, with the

distinctions being based on size, shape (cylindrical, conical, tapering), annulation regularity, and annulation density.

We identify the specimens from the lower horizon as *Gaojiashania* because of the morphological similarities to those described from China; particularly, these fossils are cylindrical body fossils with densely spaced, sharply articulated transverse body rings, with no evidence of tapering at either end. The body rings of the Mt. Dunfee fossils appear to be thickened and articulated by a very thin membrane or wall, which can be seen in Fig. 3.5A-H. A similar feature was identified in the specimens from China and referred to as "annuli-bearing tube walls situated between the rings", or "buckets" (Cai et al., 2013). In another description, the body of this fossil is compared to an "accordion-like tube" (Cai and Hua, 2011). Cai and Hua (2011) point to this feature as a way of distinguishing *Gaojiahsania* from the enigmatic ribbon-shaped, annulated fossil *Shaanxilithes ningqingensis* (Xing et al., 1984). However, more recently, Tarhan et al. (2014) interpreted the transverse ridges of *Shaanxilithes* specimens from India as representing anatomical wall thickenings of a tubular organism, which challenges Cai and Hua's distinction.

Cai and Hua (2011) also use the range of sizes for *Gaojiashania* and *Shaanxilithes* to distinguish between the fossils (Cai and Hua, 2011). The specimens of *Gaojiashania* found at Mt. Dunfee are 1.5-10 cm in length, although most specimens are incompletely preserved, and 3-10 mm in diameter. The diameter of *Shaanxilithes* ranges from 0.8 to 7.8 mm, while that of *Gaojiashania* specimens is typically larger, ranging from 7-12 mm (Cai et al., 2013; Meyer et al., 2012). New data on *Shaanxilithes*, however, demonstrate that the size ranges of the two fossils overlap much more than was

previously thought, and differentiating between *Shaanxilithes* and *Gaojiashania* simply based on size is potentially problematic (Tarhan et al., 2014). Perceived morphological differences between the two fossils may reflect different taphonomic pathways rather than anatomical differences (Tarhan et al., 2014).

Whether or not the morphological differences are true anatomical differences or not, we use them to classify the fossils from Mt. Dunfee as *Gaojiashania,* but remain open to the possibility that these two genera could be synonymous. The Dunfee Mb fossils are also similar in size and morphology to *Wutubus annularis* specimens from the Shibantan Mb (correlative with the Gaojiashan Mb) of the Dengying Fm (Chen et al., 2014). Despite some similarities, however, none of the specimens collected has the conical apex that is diagnostic of *Wutubus annularis*. The Mt. Dunfee *Gaojiashania* is an important discovery for changing its known biostratigraphic range within the latest Ediacaran; here we show that *Gaojiashania* overlaps with the biostratigraphic range of *Cloudina* instead of occurring only below it as it does in South China (Cai et al., 2010). Additionally, the *Gaojiashania* from Mt. Dunfee expand the geographic range of this fossil, suggesting that it has potential to be used as a late Ediacaran index fossil.

3.6.3.2. Fossil horizon in the Esmeralda Mb of the Deep Spring Fm

Fossils in the upper horizon are assigned to *Conotubus*, again, based on the morphological similarity with these fossils in China. The family Cloudinidae is characterized by its tubular form with nested cylindrical or cup-shaped units (Grant, 1990). This family includes *Cloudina*, *Conotubus*, and their synonyms, which include *Sinotubulites*, *Nevadatubulus*, and *Wyattia* (Chen and Sun, 2001; Conway Morris et al., 1990; Grant, 1990). Both *Cloudina* and *Conotubus* are characterized by nested funnels,

however, *Cloudina* tubes are thought to be biomineralized (Grant, 1990) and *Conotubus* tubes are either weakly or non-biomineralized (Hua et al., 2007). Moreover, some *Cloudina* species show evidence of branching while this has not been documented in any specimens of *Conotubus* (Cai et al., 2011).

The presence of non-uniform bends and curves in some of the fossil specimens described herein suggests that these fossils were not biomineralizing, but the relatively high relief of the fossil suggests that the original wall could have been lightly calcified or composed of chitin. No branching was observed in any of the specimens collected from this horizon. As a result, we classify these annulated tubular fossils as *Conotubus*, which, until now, has only been found in the Gaojiashan Lagerstätte in the Dengying Fm in South China (Cai et al., 2011; Hua et al., 2007). Not only are the morphological features similar to those described from China, but the preservational mode is also very similar to the pyritized *Conotubus* in the Chinese sections (Cai et al., 2011; Schiffbauer et al., 2014). The *Conotubus* from Mt. Dunfee appear ~100 m above the LAD of *Cloudina*. With its morphological and epibenthic life-mode similarities, *Conotubus* has been interpreted as a possible evolutionary precursor of *Cloudina* (Cai et al., 2011; Hua et al., 2007). The data presented here, however, establish an inverse biostratigraphic relationship between *Conotubus* and *Cloudina*. We suggest instead that the differences between these genera are possibly only taphonomic and that the two could be synonymous with each other.

The two new exceptionally preserved fossil horizons in the Deep Spring Fm are among the very few Ediacaran to early Cambrian lagerstätten in the SW USA, expanding the geographic distribution of *Gaojiashania* and *Conotubus* and adding a new taphonomic and biological window into this critical evolutionary transition. Particularly,

the Mt. Dunfee *Gaojiashania* overlaps with the biostratigraphic range of *Cloudina* instead of occurring only below it as it does in South China (Cai et al., 2010), and the *Conotubus* occurs within the broad negative $\delta^{13}C$ excursion at the base of the Cambrian, just below the nadir. Using this chemostratigraphic framework, it appears to be the youngest Ediacaran fossil discovered to date. The expansion and better calibration of their biostratigraphic ranges in the latest Ediacaran provide evidence that both *Gaojiashania* and *Conotubus* have temporally narrow but spatially broad ranges and have potential to be used as Ediacaran index fossils.

3.6.4. Defining the Ediacaran-Cambrian Boundary

The Global Stratotype Section and Point (GSSP) was chosen to coincide with the FAD of the trace fossil *T. pedum,* but is now known to lie above the FAD of *T. pedum* (Gehling et al., 2001); however, defining and identifying the E-C Boundary in this way has proved to be problematic because 1) the presence of this trace fossil is strongly controlled by lithofacies (Gehling et al., 2001; Geyer, 2005; Geyer and Uchman, 1995; Wilson et al., 2012), 2) *T. pedum* is often not preserved near the E-C Boundary on other paleocontinents, especially in carbonate-dominated sections in China, Siberia, Kazakhstan, and Mongolia (Babcock et al., 2014; Goldring and Jensen, 1996; Landing et al., 2013; Smith et al., 2015), and 3) there is no evidence to support that the evolutionary appearance of the behavior marked by this trace fossil was synchronous on a global scale (Babcock et al., 2014; Landing et al., 2013). Ideally, the horizon coinciding with the GSSP would have a combination of absolute ages, biostratigraphic markers, and non-biostratigraphic markers; however, currently it is only constrained by trace fossils.

As a result of the impossibility of identifying the E-C Boundary globally by strictly adhering to the FAD of *T. pedum*, it has become common practice to use what was previously considered a single, rapid negative $\delta^{13}C$ excursion as a secondary chronostratigraphic marker (Brasier et al., 1996; Grotzinger et al., 1995; Maloof et al., 2010; Maloof et al., 2005; Peng et al., 2012; Smith et al., 2015; Zhu et al., 2006). This chemostratigraphic marker is additionally problematic because it is uncertain if the negative excursion actually coincides with the first evolutionary appearance of the behavior represented by *T. pedum*. Here, we demonstrate with data from the Great Basin, USA and Western Mongolia that there is more reproducible structure to the negative $\delta^{13}C$ excursion than has been previously documented. Additionally, because this excursion occurs over hundreds of meters of strata that were thought to be deposited on a passive margin, we suggest that this excursion is documented over at least a million years, and more likely a few million years.

To complicate global compilations, many of the negative excursions that have been used to identify the E-C Boundary are in carbonate-poor and/or unconformity-bound strata. The nadirs of the excursions that have been used globally range from -9.5 to -2.6‰ (Amthor et al., 2003; Condon et al., 2005; Knoll et al., 1995; Kouchinsky et al., 2007; Maloof et al., 2005; Ries et al., 2009; Smith et al., 2015). The documentation of the additional $\delta^{13}C$ structural complexity presented here, on the one hand, demonstrates the imprecise way in which the E-C Boundary has been identified or correlated globally, but, on the other hand, provides a higher-resolution chemostratigraphic framework for reconstructing the Ediacaran-Cambrian transition (Fig. 3.11). Here, we suggest that the true E-C Boundary is younger than 541 Ma, coincides with the nadir of the basal $\delta^{13}C$

excursion, and marks a sharp biological turnover. This integrated framework promises a new direction forward for integrating E-C datasets globally.

3.6.5. Global Implications

It was previously assumed that because a singular large negative excursion generally coincides with a mass extinction of the Ediacaran biota and a radiation of life, it represents a single large environmental disturbance (Knoll and Carroll, 1999; Amthor et al., 2003). With the data presented here, it now appears that the latest Ediacaran is characterized by high frequency, secondary $\delta^{13}C$ fluctuations that are superimposed upon one large broad negative $\delta^{13}C$ excursion that likely lasted for a few million years. These data provide an expanded, continuous, higher-resolution chemostratigraphic framework that spans the E-C Boundary. The secondary structure within the larger Cambrian excursion is reproducible in three sections across the Great Basin.

Although the exact driver of the broad, negative $\delta^{13}C$ excursion and the secondary, superimposed structure to the curve are beyond the scope of this chapter, in the canonical framework (e.g. Kump and Arthur, 1999), these isotopic variations represent the addition of large amounts of isotopically light carbon to the ocean and concomitant changes in redox state over a prolonged period. We suggest that this multimillion year $\delta^{13}C$ excursion, with $\delta^{13}C$ values as low as -9.5‰ that are well below mantle values, cannot be explained just by outgassing models. Additional levers, such as the loss of an authigenic carbonate sink, are needed to explain such a large $\delta^{13}C$ excursion. These emerging integrated bio-, chrono-, chemo- and sequence stratigraphic datasets suggest that, unlike the iridium-enriched layer at Cretaceous-Paleogene (K-Pg) Boundary, across the E-C Boundary there is no single global horizon that marks a sharp environmental change that

resulted in an extinction and subsequent radiation; no evidence exists to suggest that there was one sharp perturbation to the carbon cycle that resulted in perhaps the most drastic biological change in Earth's history. Rather, with the data presented here, it appears that there was a pulsed, cumulative stressor on the environment that culminated in one final end Ediacaran extinction.

3.7. Acknowledgements

We thank the National Science Foundation Graduate Student Fellowship to E. Smith and the NASA Astrobiology Institute for financial support. We thank Harvard University for supporting some of the fieldwork in California and Nevada. We thank E. Hodgin, and F. Liu for assistance in the field, and E. Sperling, A. Knoll, P. Myrow, L. Tarhan, J. Hagadorn, S. Rowland, M. Strange, G. Zhang, H. Cui and S. Xiao for advice and stimulating discussions. We thank S. Manley and G. Eischeid for the use of and assistance in the stable isotope laboratory at Harvard University.

3.8. References

Ahn, S.Y., Babcock, L.E. and Hollingsworth, J., 2012. Revised stratigraphic nomenclature for parts of the Ediacaran-Cambrian Series 2 succession in the southern Great Basin, USA. Memoirs of the Association of Australasian Paleontologists(42): 105.

Albers, J.P. and Stewart, J.H., 1972. Geology and mineral deposits of Esmeralda County, Nevada, 78. Mackay School of Mines, University of Nevada.

Amthor, J.E., Grotzinger, J.P., Schröder, S., Bowring, S.A., Ramezani, J., Martin, M.W. and Matter, A., 2003. Extinction of Cloudina and Namacalathus at the Precambrian-Cambrian boundary in Oman. Geology, 31(5): 431-434.

Armin, R.A. and Mayer, L., 1983. Subsidence analysis of the Cordilleran miogeocline: Implications for timing of late Proterozoic rifting and amount of extension. Geology, 11(12): 702-705.

Babcock, L.E., Peng, S., Zhu, M., Xiao, S. and Ahlberg, P., 2014. Proposed reassessment of the Cambrian GSSP. Journal of African Earth Sciences, 98: 3-10.

Baode, G., Ruitang, W., Hambrey, M. and Wuchen, G., 1986. Glacial sediments and erosional pavements near the Cambrian—Precambrian boundary in western Henan Province, China. Journal of the Geological Society, 143(2): 311-323.

Bold, U., Macdonald, F.A., Smith, E.F., Crowley, J.L. and Minjin, C., 2013. Elevating the Neoproterozoic Tsagaan-Olom Formation to a Group. Mongolian Geoscientist, 39(5).

Bond, G.C. and Kominz, M.A., 1984. Construction of tectonic subsidence curves for the early Paleozoic miogeocline, southern Canadian Rocky Mountains: Implications for subsidence mechanisms, age of breakup, and crustal thinning. Geological Society of America Bulletin, 95(2): 155-173.

Bowring, S.A., Grotzinger, J.P., Condon, D.J., Ramezani, J., Newall, M.J. and Allen, P.A., 2007. Geochronologic constraints on the chronostratigraphic framework of the Neoproterozoic Huqf Supergroup, Sultanate of Oman. American Journal of Science, 307(10): 1097-1145.

Brasier, M., Cowie, J. and Taylor, M., 1994. Decision on the Precambrian-Cambrian boundary stratotype. Episodes-Newsmagazine of the International Union of Geological Sciences, 17(1): 3-8.

Brasier, M., Shields, G., Kuleshov, V. and Zhegallo, E., 1996. Integrated chemo-and biostratigraphic calibration of early animal evolution: Neoproterozoic–early Cambrian of southwest Mongolia. Geological Magazine, 133(04): 445-485.

Brasier, M.D. and Lindsay, J.F., 2001. Did supercontinental amalgamation trigger the "Cambrian Explosion". The ecology of the Cambrian radiation: 69-89.

Burchfiel, B.C., Cowan, D.S. and Davis, G.A., 1992. Tectonic overview of the Cordilleran orogen in the western United States. In: B.C. Burchfiel, P.W. Lipman and M.L. Zoback (Editors), The Geology of North America. Geological Society of America, Boulder, pp. 407-479.

Cai, Y. and Hua, H., 2011. Discussion of 'First finds of problematic Ediacaran fossil Gaojiashania in Siberia and its origin'. Geological Magazine, 148(02): 329-333.

Cai, Y., Hua, H., Xiao, S., Schiffbauer, J.D. and Li, P., 2010. Biostratinomy of the late Ediacaran pyritized Gaojiashan Lagerstätte from southern Shaanxi, South China: importance of event deposits. Palaios, 25(8): 487-506.

Cai, Y., Hua, H. and Zhang, X., 2013. Tube construction and life mode of the late Ediacaran tubular fossil Gaojiashania cyclus from the Gaojiashan Lagerstätte. Precambrian Research, 224: 255-267.

Cai, Y., Schiffbauer, J.D., Hua, H. and Xiao, S., 2011. Morphology and paleoecology of the late Ediacaran tubular fossil Conotubus hemiannulatus from the Gaojiashan Lagerstätte of southern Shaanxi Province, South China. Precambrian Research, 191(1): 46-57.

Cai, Y., Schiffbauer, J.D., Hua, H. and Xiao, S., 2012. Preservational modes in the Ediacaran Gaojiashan Lagerstätte: Pyritization, aluminosilicification, and carbonaceous compression. Paleogeography, Paleoclimatology, Paleoecology, 326: 109-117.

Chen, Z. and Sun, W., 2001. Late Sinian (tubular) metazoan fossils: Cloudina and Sinotubulites from southern Shaanxi. Acta Micropaleontologica Sinica, 18(2): 180-2002.

Chen, Z., Sun, W. and Hua, H., 2001. Preservation and morphologic interpretation of late Sinian Gaojiashania from southern Shaanxi. Acta Paleontologica Sinica, 41(3): 448-454.

Chen, Z., Zhou, C., Xiao, S., Wang, W., Guan, C., Hua, H. and Yuan, X., 2014. New Ediacara fossils preserved in marine limestone and their ecological implications. Scientific reports, 4.

Christie-Blick, N., Levy, M., Mount, J.F., Signor, P.W. and Link, P.K., 1989. Stratigraphic and tectonic framework of upper Proterozoic and Cambrian rocks in the western United States. Late Proterozoic and Cambrian Tectonics, Sedimentation, and Record of Metazoan Radiation in the Western United States: Pocatello, Idaho, to Reno, Nevada 20-29 July, 1989: 7-21.

Chumakov, N. and Elston, D., 1989. The paradox of Late Proterozoic glaciations at low latitudes. Episodes, 12(2): 115-&.

Chumakov, N.M., 2011a. Glacial deposits of the Baykonur Formation, Kazakhstan and Kyrgyzstan. Geological Society, London, Memoirs, 36(1): 303-307.

Chumakov, N.M., 2011b. Glacial deposits of the Bokson Group, East Sayan Mountains, Buryatian Republic, Russian Federation. Geological Society, London, Memoirs, 36(1): 285-288.

Condon, D., Zhu, M., Bowring, S., Wang, W., Yang, A. and Jin, Y., 2005. U-Pb ages from the neoproterozoic Doushantuo Formation, China. Science, 308(5718): 95-98.

Conway Morris, S., Mattes, B. and Chen, M., 1990. The early skeletal organism Cloudina: new occurrences from Oman and possibly China. American Journal of Science, 290: 245-260.

Corsetti, F.A., Awramik, S.M., Pierce, D. and Kaufman, A.J., 2000. Using chemostratigraphy to correlate and calibrate unconformities in Neoproterozoic strata from the southern Great Basin of the United States. International Geology Review, 42(6): 516-533.

Corsetti, F.A. and Hagadorn, J.W., 2000. Precambrian-Cambrian transition: Death Valley, United States. Geology, 28(4): 299-302.

Corsetti, F.A. and Kaufman, A.J., 1994. Chemostratigraphy of Neoproterozoic-Cambrian units, White-Inyo Region, eastern California and western Nevada: implications for global correlation and faunal distribution. Palaios: 211-219.

DeCelles, P.G., 2004. Late Jurassic to Eocene evolution of the Cordilleran thrust belt and foreland basin system, western USA. American Journal of Science, 304(2): 105-168.

Dickinson, W.R., 2004. Evolution of the North American cordillera. Annu. Rev. Earth Planet. Sci., 32: 13-45.

Diehl, P., 1974. Stratigraphy and sedimentology of the Wood Canyon Formation, Death Valley area, California. Death Valley Region, California and Nevada, Geol Soc Am, Cordilleran Section Guidebook, In: 38-48.

Etemad-Saeed, N., Hosseini-Barzi, M., Adabi, M.H., Miller, N.R., Sadeghi, A., Houshmandzadeh, A. and Stockli, D.F., 2015. Evidence for ca. 560Ma Ediacaran glaciation in the Kahar Formation, central Alborz Mountains, northern Iran. Gondwana Research.

Fedo, C.M. and Cooper, J.D., 1990. Braided fluvial to marine transition: the basal Lower Cambrian Wood Canyon Formation, southern Marble Mountains, Mojave Desert, California. Journal of Sedimentary Research, 60(2).

Fedo, C.M. and Cooper, J.D., 2001. Sedimentology and sequence stratigraphy of Neoproterozoic and Cambrian units across a craton-margin hinge zone, southeastern California, and implications for the early evolution of the Cordilleran margin. Sedimentary Geology, 141: 501-522.

Gamper, A., Struck, U., Ohnemueller, F., Heubeck, C. and Hohl, S., 2015. Chemo-and biostratigraphy of the Gaojiashan section (northern Yangtze platform, South China): a new Pc-C boundary section.

Gehling, J.G., Jensen, S., Droser, M.L., Myrow, P.M. and Narbonne, G.M., 2001. Burrowing below the basal Cambrian GSSP, Fortune Head, Newfoundland. Geological Magazine, 138(02): 213-218.

Gevirtzman, D.A. and Mount, J.F., 1986. Paleoenvironments of an earliest Cambrian (Tommotian) shelly fauna in the southwestern Great Basin, USA. Journal of Sedimentary Research, 56(3).

Geyer, G., 2005. The Fish River Subgroup in Namibia: stratigraphy, depositional environments and the Proterozoic–Cambrian boundary problem revisited. Geological Magazine, 142(05): 465-498.

Geyer, G. and Uchman, A., 1995. Ichnofossil assemblages from the Nama Group (Neoproterozoic-Lower Cambrian) in Namibia and the Proterozoic-Cambrian boundary problem revisited. Beringeria Special Issue, 2: 175-202.

Goldring, R. and Jensen, S., 1996. Trace fossils and biofabrics at the Precambrian–Cambrian boundary interval in western Mongolia. Geological Magazine, 133(04): 403-415.

Grant, S., 1990. Shell structure and distribution of Cloudina, a potential index fossil for the terminal Proterozoic. American Journal of Science, 290: 261-294.

Grotzinger, J.P., Bowring, S.A., Saylor, B.Z. and Kaufman, A.J., 1995. Biostratigraphic and geochronologic constraints on early animal evolution. Science: 598-598.

Hagadorn, J.W. and Waggoner, B., 2000. Ediacaran fossils from the southwestern Great Basin, United States. Journal Information, 74(2).

Hebert, C.L., Kaufman, A.J., Penniston-Dorland, S.C. and Martin, A.J., 2010. Radiometric and stratigraphic constraints on terminal Ediacaran (post-Gaskiers) glaciation and metazoan evolution. Precambrian Research, 182(4): 402-412.

Hua, H., Chen, Z. and Yuan, X., 2007. The advent of mineralized skeletons in Neoproterozoic Metazoa—new fossil evidence from the Gaojiashan Fauna. Geological Journal, 42(3-4): 263-279.

Hua, H., Chen, Z. and Zhang, L., 2004. Shaanxilithes from lower Taozichong Formation, Guizhou Province and its geological and paleobiological significance. Journal of Stratigraphy, 28: 265-269.

Hua, H., Zhang, L., Zhang, Z. and Wang, J., 2000. Fossil evidence of latest Neoproterozoic Gaojiashan biota and their characteristics. Acta Paleontologica Sinica, 39: 507-515.

Jones, D.S., 2009. Stable isotopes in Neoproterozoic and early Paleozoic earth history: Correlation and climate. Harvard University.

Kaufman, A.J., Knoll, A.H. and Narbonne, G.M., 1997. Isotopes, ice ages, and terminal Proterozoic earth history. Proceedings of the National Academy of Sciences, 94(13): 6600-6605.

Knoll, A.H., Grotzinger, J.P., Kaufman, A.J. and Kolosov, P., 1995. Integrated approaches to terminal Proterozoic stratigraphy: an example from the Olenek Uplift, northeastern Siberia. Precambrian Research, 73(1): 251-270.

Kouchinsky, A., Bengtson, S., Pavlov, V., Runnegar, B., Torssander, P., Young, E. and Ziegler, K., 2007. Carbon isotope stratigraphy of the Precambrian–Cambrian Sukharikha River section, northwestern Siberian platform. Geological Magazine, 144(04): 609-618.

Kump, L.R. and Arthur, M.A., 1999. Interpreting carbon-isotope excursions: carbonates and organic matter. Chemical Geology, 161(1): 181-198.

Landing, E., 1994. Precambrian-Cambrian boundary global stratotype ratified and a new perspective of Cambrian time. Geology, 22(2): 179-182.

Landing, E., Geyer, G., Brasier, M.D. and Bowring, S.A., 2013. Cambrian evolutionary radiation: context, correlation, and chronostratigraphy—overcoming deficiencies of the first appearance datum (FAD) concept. Earth-Science Reviews, 123: 133-172.

Langille, G.B., 1974. Earliest Cambrain-Latest Proterozoic Ichnofossils and Problematic Fossils from Inyo County, California, State University of New York at Binghamton, Department of Geological Sciences.

Li, Y., Ding, L., Zhang, L., Dong, J. and Chen, H., 1992. Descriptions of the fossils. In: L. Ding, L. Zhang, Y. Li and J. Dong (Editors), The Study of the Late Sinian–Early Cambrian Biotas from the Northern Margin of the Yangtze Platform. Scientific and Technical Documents Publishing House, Beijing, Beijing, pp. 80-112.

Lin, S., Zhang, Y., Zhang, L., Tao, X. and Wang, M., 1986. Body and trace fossils of metazoa and algal macrofossils from the upper Sinian Gaojiashan Formation in southern Shaanxi. Geology of Shaanxi, 4(1): 9-17.

Macdonald, F.A., Jones, D.S. and Schrag, D.P., 2009. Stratigraphic and tectonic implications of a new glacial diamictite-cap carbonate couplet in southwestern Mongolia. Geology, 37: 123-126.

Maloof, A.C., Porter, S.M., Moore, J.L., Dudás, F.Ö., Bowring, S.A., Higgins, J.A., Fike, D.A. and Eddy, M.P., 2010. The earliest Cambrian record of animals and ocean geochemical change. Geological Society of America Bulletin, 122(11-12): 1731-1774.

Maloof, A.C., Schrag, D.P., Crowley, J.L. and Bowring, S.A., 2005. An expanded record of Early Cambrian carbon cycling from the Anti-Atlas Margin, Morocco. Canadian Journal of Earth Sciences, 42(12): 2195-2216.

Meert, J.G. and Van der Voo, R., 1994. The Neoproterozoic (1000–540 Ma) glacial intervals: no more snowball earth? Earth and Planetary Science Letters, 123(1): 1-13.

Meyer, M., Schiffbauer, J., Xiao, S., Cai, Y. and Hua, H., 2012. Taphonomy of the upper Ediacaran enigmatic ribbonlike fossil Shaanxilithes. Palaios, 27(5): 354-372.

Mount, J.F., Gevirtzman, D.A. and Signer, P.W., 1983. Precambrian-Cambrian transition problem in western North America: Part I. Tommotian fauna in the southwestern Great Basin and its implications for the base of the Cambrian System. Geology, 11(4): 224-226.

Mount, J.F., Hunt, D.L., Greene, L.R. and Dienger, J., 1991. Depositional systems, biostratigraphy and sequence stratigraphy of Lower Cambrian grand cycles, southwestern Great Basin.

Mullins, H.T., Gardulski, A.F., Wise, S.W. and Applegate, J., 1987. Middle Miocene oceanographic event in the eastern Gulf of Mexico: implications for seismic stratigraphic succession and Loop Current/Gulf Stream circulation. Geological Society of America Bulletin, 98(6): 702-713.

Narbonne, G.M., Kaufman, A.J. and Knoll, A.H., 1994. Integrated chemostratigraphy and biostratigraphy of the Windermere Supergroup, northwestern Canada: Implications for Neoproterozoic correlations and the early evolution of animals. Geological Society of America Bulletin, 106(10): 1281-1292.

Nelson, C., 1978. Late Precambrian-Early Cambrian stratigraphic and faunal succession of eastern California and the Precambrian-Cambrian boundary. Geological Magazine, 115(2): 121-126.

Nelson, C.A., 1976. Late Precambrian-Early Cambrian stratigraphic and faunal succession of eastern California and the Precambrian-Cambrian boundary.

Oliver, L.K. and Rowland, S.M., 2002. Microbialite reefs at the close of the Proterozoic Eon: The Middle Member Deep Spring Formation at Mt. Dunfee, Nevada.

Parsons, S.M., 1996. Sequence stratigraphy and biostratigraphy of the lower member of the Deep Spring Formation: implications for the Neoproterozoic-Cambrian boundary in the Basin and Range Province, western United States.

Pavlis, T.L., Rutkofske, J., Guerrero, F. and Serpa, L.F., 2014. Structural overprinting of Mesozoic thrust systems in eastern California and its importance to reconstruction of Neogene extension in the southern Basin and Range. Geosphere, 10(4): 732-756.

Peng, S., Babcock, L. and Cooper, R., 2012. The Cambrian Period. The geologic time scale, 2: 437-488.

Rice, A.H.N., Edwards, M.B., Hansen, T.A., Arnaud, E. and Halverson, G.P., 2011. Glaciogenic rocks of the Neoproterozoic Smalfjord and Mortensnes formations, Vestertana Group, E. Finnmark, Norway. Geological Society, London, Memoirs, 36(1): 593-602.

Ries, J.B., Fike, D.A., Pratt, L.M., Lyons, T.W. and Grotzinger, J.P., 2009. Superheavy pyrite (δ^{34}Spyr>δ^{34}SCAS) in the terminal Proterozoic Nama Group, southern Namibia: a consequence of low seawater sulfate at the dawn of animal life. Geology, 37(8): 743-746.

Rowland, S.M. and Corsetti, F.A., 2002. A brief history of research on the Precambrian-Cambrian boundary in the southern Great Basin.

Rowland, S.M., Oliver, L.K. and Hicks, M., 2008. Ediacaran and early Cambrian reefs of Esmeralda County, Nevada: non-congruent communities within congruent ecosystems across the Neoproterozoic–Paleozoic boundary. Field Guides, 11: 83-100.

Rowland, S.M. and Rodriguez, M.G., 2014. A multicellular alga with exceptional preservation from the Ediacaran of Nevada. Journal of Paleontology, 88(2): 263-268.

Sawaki, Y., Ohno, T., Tahata, M., Komiya, T., Hirata, T., Maruyama, S., Windley, B.F., Han, J., Shu, D. and Li, Y., 2010. The Ediacaran radiogenic Sr isotope excursion in the Doushantuo Formation in the three Gorges area, South China. Precambrian Research, 176(1): 46-64.

Schiffbauer, J.D., Xiao, S., Cai, Y., Wallace, A.F., Hua, H., Hunter, J., Xu, H., Peng, Y. and Kaufman, A.J., 2014. A unifying model for Neoproterozoic–Paleozoic exceptional fossil preservation through pyritization and carbonaceous compression. Nature communications, 5.

Schmitz, M.D., 2012. Appendix 2: Radiometric ages used in GTS 2012. In: F.M. Gradstein, et al. (Editor), The geological time scale 2012. Elsevier, Amsterdam, pp. 1045–1083.

Signor, P.W., Mount, J.F. and Onken, B.R., 1987. A pre-trilobite shelly fauna from the White-Inyo region of eastern California and western Nevada. Journal of Paleontology: 425-438.

Smith, E.F., Macdonald, F.A., Petach, T.A., Bold, U. and Schrag, D.P., 2015. Integrated stratigraphic, geochemical, and paleontological late Ediacaran to early Cambrian records from southwestern Mongolia. Geological Society of America Bulletin.

Snow, J.K. and Wernicke, B.P., 2000. Cenozoic tectonism, in the central Basin and Range: magnitude, rate, and distribution of upper crustal strain. American Journal of Science, 300(9): 659.

Spence, G.H. and Tucker, M.E., 1997. Genesis of limestone megabreccias and their significance in carbonate sequence stratigraphic models: a review. Sedimentary Geology, 112(3): 163-193.

Stewart, J.H., 1970. Upper Precambrian and Lower Cambrian strata in the southern Great Basin California and Nevada. US Geol Surv Prof Pap.

Stewart, J.H., 1972. Initial deposits in the Cordilleran geosyncline: Evidence of a late Precambrian (<850 my) continental separation. Geological Society of America Bulletin, 83(5): 1345-1360.

Stodt, F., Rice, A.H.N., Björklund, L., Bax, G., Halverson, G.P. and Pharaoh, T., 2011. Evidence of late Neoproterozoic glaciation in the Caledonides of NW Scandinavia. Geological Society, London, Memoirs, 36(1): 603-612.

Tarhan, L.G., Hughes, N.C., Myrow, P.M., Bhargava, O.N., Ahluwalia, A.D. and Kudryavtsev, A.B., 2014. Precambrian–Cambrian boundary interval occurrence and form of the enigmatic tubular body fossil Shaanxilithes ningqiangensis from the Lesser Himalaya of India. Paleontology, 57(2): 283-298.

Taylor, M.E., 1966. Precambrian mollusc-like fossils from Inyo County, California. Science, 153(3732): 198-201.

Torsvik, T., Smethurst, M., Meert, J.G., Van der Voo, R., McKerrow, W., Brasier, M., Sturt, B. and Walderhaug, H., 1996. Continental break-up and collision in the Neoproterozoic and Paleozoic—a tale of Baltica and Laurentia. Earth-Science Reviews, 40(3): 229-258.

Vail, P.R., Mitchum Jr, R. and Thompson III, S., 1977. Seismic Stratigraphy and Global Changes of Sea Level: Part 4. Global Cycles of Relative Changes of Sea Level.: Section 2. Application of Seismic Reflection Configuration to Stratigraphic Interpretation.

Weber, B., Steiner, M. and Zhu, M.-Y., 2007. Precambrian–Cambrian trace fossils from the Yangtze Platform (South China) and the early evolution of bilaterian lifestyles. Paleogeography, Paleoclimatology, Paleoecology, 254(1): 328-349.

Wernicke, B.P., Axen, G.J. and Snow, J.K., 1988. Basin and Range extensional tectonics at the latitude of Las Vegas, Nevada. Geological Society of America Bulletin, 100: 1738-1757.

Wilson, J.P., Grotzinger, J.P., Fischer, W.W., Hand, K.P., Jensen, S., Knoll, A.H., Abelson, J., Metz, J.M., McLoughlin, N. and Cohen, P.A., 2012. Deep-water incised valley deposits at the Ediacaran-Cambrian boundary in southern Namibia contain abundant Treptichnus pedum. Palaios, 27(4): 252-273.

Wright, L.A. and Troxel, B.W., 1966. Strata of late Precambrian-Cambrian age, Death Valley region, California-Nevada. AAPG Bulletin, 50(5): 846-857.

Wright, L.A. and Troxel, B.W., 1967. Limitations on right-lateral, strike-slip displacement, Death Valley and Furnace Creek fault zones, California. Geological Society of America Bulletin, 78(8): 933-950.

Wright, L.A., Troxel, B.W., Williams, E.G., Roberts, M.T. and Diehl, P.E. (Editors), 1976. Precambrian sedimentary environments of the Death Valley region, eastern California. Geologic features, Death Valley, California. California Division of Mines and Geology, Sacramento, CA., 7-15 pp.

Xing, Y., Ding, Q., Luo, H., He, T. and Wang, Y., 1984. The Sinian-Cambrian Boundary of China and its related problems Geological Magazine, 121(3): 155-170.

Zhang, L., 1986. A discovery and preliminary study of the late stage of late Gaojiashan biota from Sinian in Ningqiang county, Shaanxi Northwest Geoscience, 2: 006.

Zhou, C. and Xiao, S., 2007. Ediacaran $\delta^{13}C$ chemostratigraphy of South China. Chemical Geology, 237(1): 89-108.

Zhu, M., Babcock, L.E. and Peng, S., 2006. Advances in Cambrian stratigraphy and paleontology: integrating correlation techniques, paleobiology, taphonomy and paleoenvironmental reconstruction. Paleoworld, 15(3): 217-222.

Zhu, M. and Wang, H., 2011. Neoproterozoic glaciogenic diamictites of the Tarim Block, NW China. Geological Society, London, Memoirs, 36(1): 367-378.

Zhu, M., Zhang, J. and Yang, A., 2007. Integrated Ediacaran (Sinian) chronostratigraphy of South China. Paleogeography, Paleoclimatology, Paleoecology, 254(1): 7-61.

Zhuravlev, A.Y., Vintaned, J.A.G. and Ivantsov, A.Y., 2009. First finds of problematic Ediacaran fossil Gaojiashania in Siberia and its origin. Geological Magazine, 146(05): 775-780.

CHAPTER 4. INTEGRATED STRATIGRAPHIC, GEOCHEMICAL, AND PALEONTOLOGICAL LATE EDIACARAN TO EARLY CAMBRIAN RECORDS FROM SOUTHWESTERN MONGOLIA.

A version of this chapter was published in:

[Smith, E. F., Macdonald, F. A., Petach, T. P., Bold, U. & Schrag, D. P. (2015). Integrated stratigraphic, geochemical, and paleontological late Ediacaran to early Cambrian records from southwestern Mongolia. *GSA Bulletin*.]

Abstract

The Zavkhan Terrane in western Mongolia preserves thick, fossiliferous, carbonate-rich strata that span the Ediacaran-Cambrian transition. Measured stratigraphic sections and geological mapping of these strata, which include the Zuun-Arts, Bayangol, Salaagol, and Khairkhan formations, reveal large lateral facies changes over short distances that necessitate revisions to previous lithostratigraphic correlations and biostratigraphic range charts. Here, we integrate new geological mapping and measured stratigraphic sections across the Zavkhan Terrane with high-resolution carbon isotope ($\delta^{13}C$) chemostratigraphy, sequence stratigraphy, and biostratigraphy. Using these data we revise correlations within the Zavkhan Terrane and place small shelly fossil and ichnofossil horizons in a refined temporal and spatial framework. Finally, we integrate these data from Mongolia with absolute ages and chemostratigraphy from sections in Morocco and Oman. Our revised age model suggests that deposition of the Bayangol

Formation and the lower part of the Salaagol Formation was limited to the Nemakit-Daldynian and Tommotian stages.

With the new correlations and age model, we place the small shelly fossil first appearance datum in the basal Bayangol Formation instead of the basal Zuun-Arts Formation, which moves this horizon hundreds of meters higher in the stratigraphy, above the large negative excursion in the Zuun-Arts Formation. The first appearance datum of *Treptichnus pedum* is ~275 m above the large negative excursion in the Zuun-Arts Fm and ~250 m above the first appearance datum of small shelly fossils, highlighting the rarity of and facies dependence for its preservation.

We shift the first appearance datums of tommotiids, orthothecimorphs, hyolithelminths, cap-shaped fossils, protoconodonts, and *Salanacus* to just below the positive peak 3p. This interpretation differs from previous chronostratigraphic placements of first appearance data of genera between positive excursions 1p and 2p. Using this level as the first appearance datum in Mongolia for these genera, we replot global fossil first appearances. With this new compilation, there are still three distinct pulses of fossil first appearances, as was suggested in previous compilations; however, we suggest that this pattern is controlled largely by regional sedimentation and taphonomy rather than the rate of taxonomic origination.

4.1. Introduction

Since Charles Darwin's observation of the apparently rapid appearance of fossils in what is now known as Cambrian strata (1859), the Precambrian-Cambrian boundary has been widely regarded as one of the evolutionary pivoting points in the history of life.

Despite the persisting interest on this topic, the causes, triggers, and tempo of change remain controversial. Following the extinction of Ediacaran biota and the calcifying metazoan *Cloudina*, the early Cambrian (or Terreneuvian Series) encompasses an evolutionary interval characterized by increases in diversity and disparity (Marshall, 2006) that coincides with multiple carbon isotope excursions with amplitudes of <8‰ (e.g. Zhu et al., 2006; Porter, 2007; Maloof et al., 2010a; Erwin et al., 2011) over a geologically brief interval in Earth history (Valentine, 2002). Most recently, Maloof et al. (2010a) suggested that the Cambrian fossil first appearances occurred in three discrete pulses associated with rapid reorganizations in the carbon cycle. To test this hypothesis and others about mechanistic links between environmental change and evolutionary milestones across the Ediacaran-Cambrian (E-C) transition, it is necessary to integrate records around the globe. However, previous global syntheses (e.g. Maloof et al., 2010a) have been limited to a small number of localities with large uncertainties in both local and global stratigraphic correlations and the lack of absolute ages directly linked to biostratigraphic and chemostratigraphic data, particularly with respect to critical data from Asia. Because the global dataset is biased by just a few localities, refining local correlations and grounding them in regional geology is necessary before an accurate global synthesis of fossil occurrence data can be constructed and interpreted.

The E-C boundary is defined at the GSSP as the first appearance datum (FAD) of the bilaterian trace fossil *Treptichnus pedum* (Landing, 1994), but the boundary has also been associated with the FAD of small shelly fossils (SSFs) and a large negative carbon isotope excursion (Corsetti and Hagadorn, 2000; Narbonne et al., 1994). These occurrences in the rock record are generally assumed to be broadly coincident, but both

the precise and relative timing of these evolutionary milestones and perturbations to the carbon cycle are not directly constrained. The subsequent earliest Cambrian period is marked by FADs of SSFs in many clades and high frequency oscillations in the carbon cycle (Maloof et al., 2010a), but again, there are few absolute ages tied to these FADs or excursions. Because there is no one section globally in which it is possible to integrate the ichnofossil record, body fossil record, carbon isotope chemostratigraphy, and absolute ages, the calibration of this evolutionarily important transition remains piecemeal resulting in much uncertainty in determining rates of origination and geochemical change. With a dearth of absolute ages tied to the fossil record, carbon isotope ($\delta^{13}C$) chemostratigraphy has proven to be a powerful tool for global correlation of E-C successions (Brasier et al., 1993; Brasier et al., 1990; Kirschvink et al., 1991; Knoll et al., 1995a; Maloof et al., 2010a; Zhu et al., 2007; Zhu et al., 2006).

The Zavkhan (Dzabkhan) Terrane in western Mongolia hosts thick, well-exposed, low-grade, carbonate-rich, fossiliferous successions of late Ediacaran through early Cambrian strata, providing an opportunity to more precisely calibrate evolutionary changes in a chemo- and sequence-stratigraphic context. This succession hosts dozens of well-exposed sections with several horizons of SSFs, archaeocyathid reefs, and ichnofossils (Goldring and Jensen, 1996; Khomentovsky and Gibsher, 1996; Kruse et al., 1996), many of which are being reported and documented here for the first time. However, because Ediacaran to early Cambrian strata on the Zavkhan Terrane was deposited in a foreland basin (Macdonald et al., 2009), topography generated during tectonism resulted in large lateral facies changes, which confounded previous lithostratigraphic correlations and biostratigraphic compilations (Brasier et al., 1996b;

Khomentovsky and Gibsher, 1996). In this study we present new geological mapping and SSF biostratigraphy for the Nemakit-Daldynian through Tommotian strata in the necessary context of a high-resolution $\delta^{13}C$ chemostratigraphic age model and basin-wide sequence stratigraphy.

Because there are only a handful of carbonate-rich fossiliferous sections globally that span the E-C transition, namely sections in Sibera, China, Kazakhstan, SW United States, NW Canada, and Mongolia, calibrating the timing and tempo of the radiation is heavily influenced by each record. This contribution of an age model, geological mapping, and revised biostratigraphy change known global rates of early Cambrian evolution and provide the necessary geological and stratigraphic framework for integrating geochemical, paleontological, and geochronological data from southwest Mongolia into the global record of the E-C transition.

4.2. Geologic Background and Tectonostratigraphic Framework

4.2.1. Previous studies

The Zavkhan Terrane is a Precambrian crustal fragment embedded in the core of the Central Asian Orogenic Belt (CAOB) (Fig. 4.1). After late Ediacaran to Ordovician accretion of arc terranes to the south, the late Ordovician to Silurian record of Mongolia is marked by extensional magmatism and basin formation (Gibson et al., 2013; Kröner et al., 2010). During this time, the Zavkhan Terrane was part of a composite ribbon continent that was adjacent to Siberia (Wilhem et al., 2012). From the Devonian to early Permian, the Zavkhan Terrane was oroclinally buckled during the arrival of North China and Tarim (Edel et al., 2014; Lehmann et al., 2010). Locally, on the Zavkhan Terrane,

this late Paleozoic collision is manifested in dextral strike-slip wrench structures (Fig. 4.1A and C) and widespread Permian plutonism (Jahn et al., 2009).

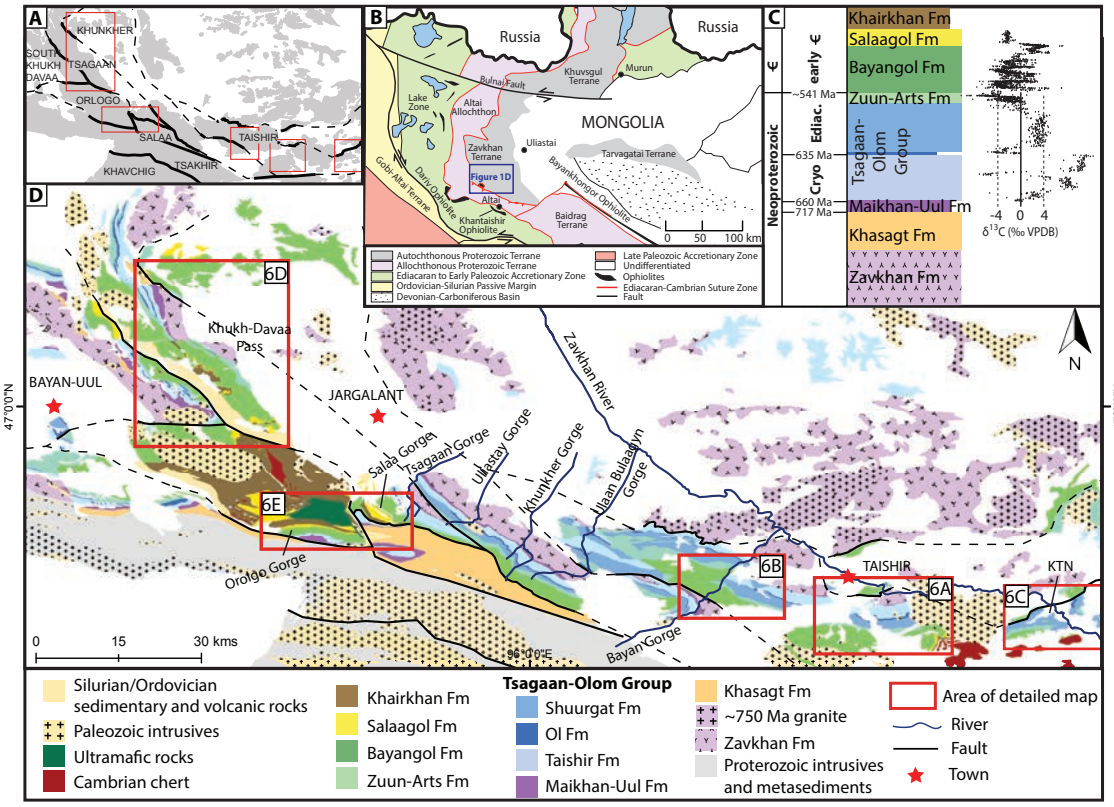

Figure 4.1. Geologic map of the Zavkhan Basin in Southwest Mongolia

A) Shaded outcrop of Zavkhan Terrane showing major fault blocks. B) Terrane map of Mongolia. Area of Fig. 4.1D is boxed in dark blue. Adapted from Bucholz et al. (2014). C) $\delta^{13}C$ profile from Macdonald et al. (2009) and this study plotted against generalized early Cambrian through Neoproterozoic stratigraphy in the Zavkhan Terrane. The age constraints are dated by correlation. The basal Maikhan-Uul Fm has been correlated with the basal Sturtian glacial deposit in NW Canada at 717.4 ± 0.2 Ma (Macdonald et al., 2010) and 662.4 ± 4.9 Ma (Rooney et al., 2014). The Ol cap carbonate has been correlated with the Marinoan cap, which has been dated globally at ca. 635 Ma (Calver et al., 2013; Calver et al., 2004; Condon et al., 2005). D) Geologic map of the Zavkhan Terrane. Red boxes mark areal extent of detailed maps in Fig. 4.3.6.

The Neoproterozoic through Cambrian stratigraphy of the Zavkhan Terrane was first described by Bezzubtsev (1963) in the Bayan Gorge. Before the early 1990s, research in Mongolia was largely restricted to Mongolian and Russian researchers who worked primarily on the Ediacaran through early Cambrian strata in the Zavkhan Terrane (Zhegallo and Zhuravlev, 1991). Shortly after Mongolia opened back up to Western researchers, an international research team participated in the IGCP Project 303, "Precambrian-Cambrian Event Stratigraphy," in 1993, representing the first effort to bring together specialists from different sub-disciplines of Earth sciences for an integrated approach to addressing the Precambrian-Cambrian transition in western Mongolia. During this international excursion, they visited five previously documented sections to study in more detail. The Geological Magazine publications that resulted from this project were the first time these key sections were described in English and placed into a regional and global context (Brasier et al., 1996a; Brasier et al., 1996b; Goldring and Jensen, 1996; Khomentovsky and Gibsher, 1996; Kruse et al., 1996; Lindsay et al., 1996a; Lindsay et al., 1996b).

Voronin et al. (1982), Gibsher and Khomentovsky (1990), Gibsher et al. (1991), and Khomentovsky and Gibsher (1996) described the stratigraphy and published preliminary, schematic, hand-drawn maps of the southern and northern blocks of the Bayan Gorge, Tsagaan Gorge, Salaa Gorge, and Taishir. In addition, biostratigraphy is documented from Orolgo (Orolchayan) Gorge (Endonzhamts and Lkhasuren, 1988) and Kvetee Tsakhir Nuruu (KTN) (Dorjnamjaa et al., 1993; Esakova and Zhegallo, 1996; Zhegallo and Zhuravlev, 1991). Detailed paleontological work was conducted primarily by Russian paleontologists; however, much of this work lacked a stratigraphic context.

The series of 1996 publications was the first attempt at placing the SSF first appearances in a litho- and chemostratigraphic framework (Brasier et al., 1996b; Khomentovsky and Gibsher, 1996). Brasier et al. (1996b) presented the first carbon, oxygen, and strontium chemostratigraphy for the Neoproterozoic through Cambrian carbonates in the Zavkhan Terrane. More recently, the age and depositional environment of the Cryogenian strata have been more tightly constrained by Macdonald et al. (2009), Macdonald (2011), and Bold et al. (2013).

4.2.2. Cryogenian to early Ediacaran stratigraphy

Along the Zavkhan River, the oldest exposed rocks are felsic volcanic rocks of the Zavkhan Formation (Fm) (Figs. 4.1B and C; Bold et al., 2013), that have been dated using LA-ICPMS U/Pb on zircon to between 770 and 805 Ma (Levashova et al., 2010) and using SHRIMP U/Pb on zircon at 777 ± 6 Ma (Zhao et al., 2006). Granites that intrude the Zavkhan Fm have been dated using TIMS bulk multigrain U/Pb on zircon at 755 ± 3 Ma (Yarmolyuk et al., 2008). The Zavkhan Fm is overlain by the syn-rift siliciclastic deposits informally referred to as the Khasagt Suite (Ruzhentsev and Burashnikov, 1996) and passive margin deposits of the Tsagaan-Olom Group (Bold et al., 2013; Macdonald et al., 2009).

The Tsagaan-Olom Group (note recent changes in spelling and formalization of stratigraphy, Bold et al., 2013) contains two Cryogenian glacial diamictites and cap carbonates (Macdonald et al., 2009). The oldest formation in this Group is the Maikhan-Uul Fm, a Sturtian-aged diamictite (Lindsay et al., 1996b; Macdonald, 2011; Macdonald et al., 2009), which has been constrained globally by correlation to between ~717 and 660 Ma (Macdonald et al., 2010; Rooney et al., 2014). Overlying the Maikhan-Uul Fm is

the carbonate-dominated Taishir Fm, comprised of the Sturtian cap carbonate and interglacial strata (Johnston et al., 2012; Macdonald, 2011; Macdonald et al., 2009; Shields et al., 2002; Shields-Zhou et al., 2012). The overlying Khongor and Ol fms have been correlated to Marinoan glacial deposits and the ca. 635 Ma basal Ediacaran cap carbonate, respectively (Calver et al., 2013; Condon et al., 2005; Macdonald et al., 2009). The Ol Fm is overlain by the early Ediacaran Shuurgat Fm (previously referred to informally as the Ulaan Bulaagyn member of the Tsagaan-Olom Fm), which consists of 100-500 m of carbonate and is unconformably overlain by the latest Ediacaran Zuun-Arts Fm (Bold et al., 2013; Macdonald et al., 2009).

4.2.3. Latest Ediacaran to early Cambrian stratigraphy, biostratigraphy, and chemostratigraphy

During the latest Ediacaran, the Zavkhan Terrane began to subduct to the southwest beneath the Khantaishir-Dariv Arc, creating the foreland basin which accommodated the thick sequence of latest Ediacaran to earliest Cambrian strata (Macdonald et al., 2009). These strata, along with kilometers of Neoproterozoic strata, are exposed in northeast-vergent thrust sheets in the Zavkhan Terrane.

From oldest to youngest, the late Ediacaran and early Cambrian strata on the Zavkhan Terrane is comprised of the carbonate-dominated Zuun-Arts Fm, the mixed carbonate-siliciclastic Bayangol Fm, the carbonate-dominated Salaagol Fm, and the siliciclastic Khairkhan Fm (Fig. 4.2). Together, these strata range from ~800-2700 m in thickness. The Khairkhan Fm comprises allochthonous mélange, flysch and molasse, marking the closure of the foredeep and the end of deposition in this basin (Macdonald et al., 2009).

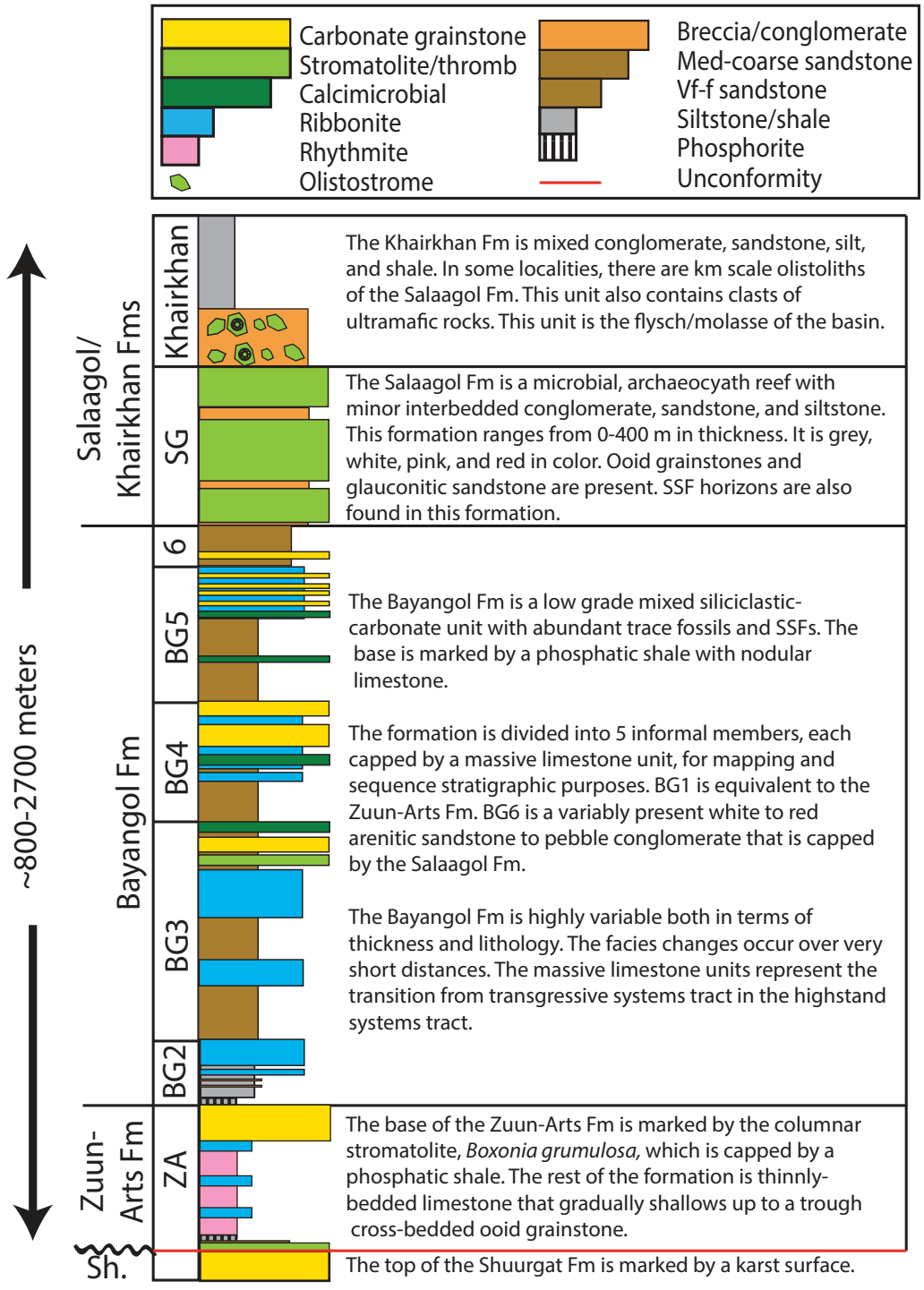

Figure 4.2. Generalized late Ediacaran to early Cambrian stratigraphy of the Zavkhan Terrane.

A schematic stratigraphic column alongside descriptions of the late Ediacaran through early Cambrian strata in the Zavkhan Basin. Note the recent changes in spelling and formalization of stratigraphy in the Zavkhan Terrane by Bold et al. (2013).

4.2.3.1. Zuun-Arts Fm

Strata above the uppermost karst surface in the underlying Shuurgat Fm are marked by buff- to pink-colored microbial dolostone that preserves the columnar stromatolite *Boxonia grumulosa* (Fig. 4.3A; Markova et al., 1972). The distinct stromatolitic horizon is overlain by variably phosphatized green shale with nodular carbonate, marking an abrupt flooding surface. In some localities, a lag deposit of coarse, immature sandstone is present between the stromatolite and phosphatic shale. Overlying the phosphatic shale is ~150-400 m of thinly-bedded, medium grey limestone (Fig. 4.3B) with occasional intraclast breccia. The top 5-200 m of the Zuun-Arts Fm consists of several 5-20 m-scale parasequences culminating with a distinctive white and black cross-bedded ooid grainstone (Fig. 4.3C). The top contact of the Zuun-Arts Fm is defined at a sharp contact between the ooid grainstone and a second horizon of microcrystalline phosphatic shale (Fig. 4.3D; Lindsay et al., 1996a).

The FAD of anabaritids, the earliest SSF, has been reported near the base of the Zuun-Arts Fm (Brasier et al., 1996b; Dorjnamjaa et al., 1993; Endonzhamts and Lkhasuren, 1988; Khomentovsky and Gibsher, 1996); however, we refine the position of this FAD horizon herein. Simple bed planar trace fossils are also present in this formation (Brasier et al., 1996b). Neither cloudinid nor the Shuram carbon isotope excursion has been documented in the Zuun-Arts or Shuurgat fms. Carbon isotope ($\delta^{13}C$) values of the Shuurgat Fm range between -0.5 and +8.5‰, values that more closely resemble the carbon isotopic profile of the lower Ediacaran than the upper Ediacaran (Macdonald et al., 2009), which would imply a substantial hiatus at the karst surface between the Shuurgat and Zuun-Arts fms (Bold et al., 2013; Macdonald et al., 2009).

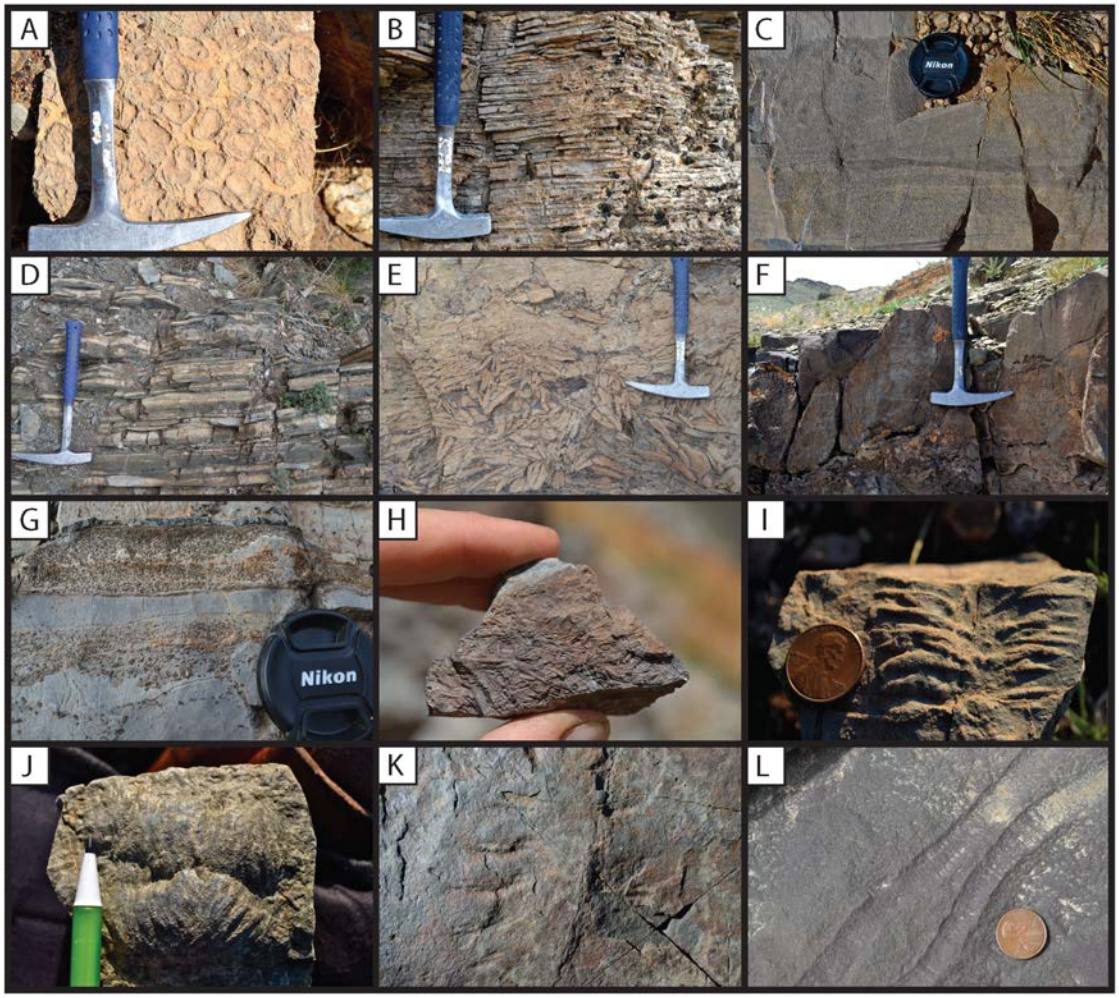

Figure 4.3. Photomontage of the Zuun-Arts and Bayangol formations.
A) Stromatolite *Boxonia grumulosa* from the base of the Zuun-Arts Fm. B) Thinly-bedded, medium grey limestone of lower to middle Zuun-Arts Fm. C) Cross bedded ooid grainstone of upper Zuun-Arts Fm. D) Phosphatic shale with nodular limestone of lower Bayangol Fm. E) Intraclast conglomerate in lower Bayangol Fm. F) Thrombolites in upper part of Bayangol Fm in Bayan Gorge. G) Phosphatized SSFs, grains, and ooids in lag deposit in basal part of Bayangol Fm (137 m above basal contact) in Orolgo Gorge. H) Anabaritids from basal Bayangol Fm in Orolgo Gorge. I-K) early arthropod trace fossils from the middle and upper Bayangol Fm (BG3-BG5) in Khunkher Gorge. L) bed-planar trace fossil from the upper Bayangol Fm (BG5) in S. Bayan Gorge.

4.2.3.2. Bayangol Fm

The Bayangol Fm, along with the underlying Zuun-Arts and Shuurgat fms was previously included in the Tsagaan-Olom Fm and has been characterized and subdivided as numbered units by Voronin et al. (1982), Gibsher and Khomentovsky (1990) and Gibsher et al. (1991). The base of the Bayangol Fm is marked by phosphatic shale with nodular carbonate. The Bayangol Fm consists of mixed carbonate and siliciclastic strata, and ranges from ~500-1250 m in thickness. In most sections in the basin, in the lower to middle part of the formation there are at least three thick limestone units capping interbedded siliciclastic and limestone units. Fig. 4.4 shows examples a few of these massive limestone units and how they mark some of the large-scale sequence boundaries in the strata. In most sections in the basin, above the massive third limestone marker bed is hundreds of meters of predominantly fine to coarse sandstone.

The Bayangol Fm hosts diverse and well-preserved stromatolites, thrombolites, and other bioconstructions with a wide range in size and morphology (Kruse et al., 1996). Importantly for this study, there is also a rich assemblage of SSF and abundant trace fossils that have been previously documented in the Bayan, Salaa, and Tsagaan gorges, Taishir, and KTN (Fig. 4.1; Korobov and Missarzhevsky, 1977; Voronin et al., 1982; Endonzhamts and Lkhasuren, 1988; Goldring and Jensen, 1996; Khomentovsky and Gibsher, 1996). To create a composite biostratigraphic range chart for the Bayangol Fm, these sections were previously correlated primarily using lithostratigraphic correlations. However, as discussed below, these lithostratigraphic correlations were compromised by large lateral facies changes. These lithostratigraphic correlations utilized the numbered units of Voronin et al. (1982) and were followed by the authors in the series of 1996

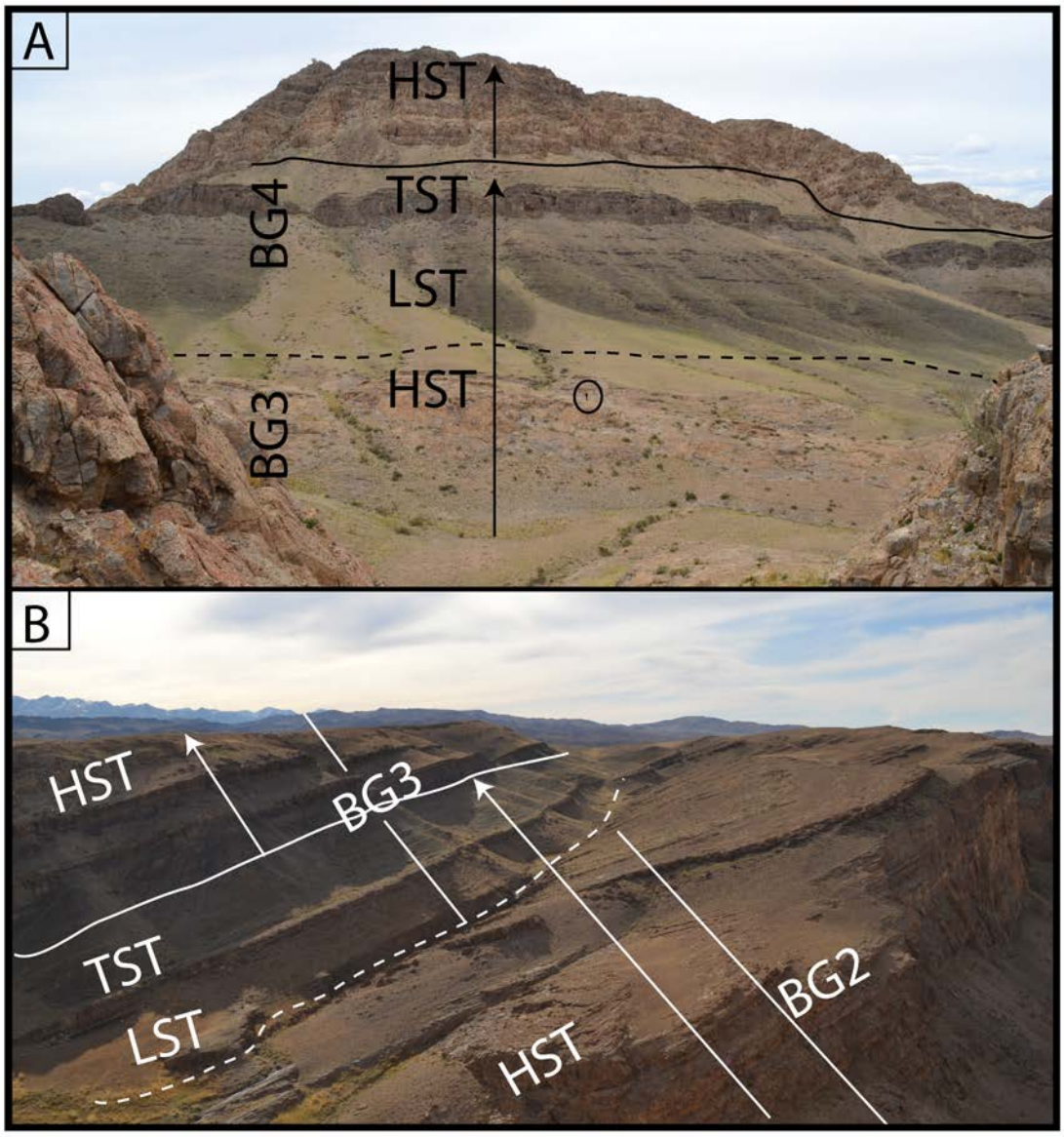

Figure 4.4. Photograph showing major sequences in the Bayangol Formation
A) Annotated photo looking to the NW in section E1211, NE of Khukh-Davaa Pass. The major sequence stratigraphic systems tracts of members BG3 and BG4 of the Bayangol Fm that are shown in Fig. 4.8 are depicted here (the solid black line marks the maximum flooding surface and the dashed line marks the boundary between BG3 and BG4). The dominant facies associations are also shown; however, it is not possible to mark all the facies associations at this scale. Human circled for scale. B) Annotated photo looking to the west in the southern block of the Bayan Gorge is depicted here. Major sequence stratigraphic systems tracts and facies associations of the lower two members of the Bayangol Fm are depicted here (the solid white line marks the maximum flooding surface while the dashed line marks the top of BG2). Minor facies associations are not shown.

Geological Magazine publications. Although these numbered units are useful in identifying specific beds within a single gorge, they cannot be used to construct an accurate framework for basin-wide correlations.

4.2.3.3. Salaagol Fm

The Salaagol Fm is a <400 m-thick white, grey, pink, and red microbial and archaeocyathan reef (Figs. 4.5A and B) that has only been described in detail from Salaa Gorge and Zuun-Arts Ridge (Kruse et al., 1996; Voronin et al., 1982; Wood et al., 1993). It has variably thick red silts and conglomerate interbeds. The formation also contains other bioclastic debris that includes chancellorid sclerites, sponge spicules, coralomorphs, and hyoliths (Kruse et al, 1996). The archaeocyathan assemblage at Salaa Gorge is typified by *Archaeolynthus*, *Dokidocyathus*, *Nochoroicyathus*, and *Rotundocyathus*, and based on archaeocyathan biostratigraphy, Kruse et al. (1996) assigned it a Tommotian to Botomian age.

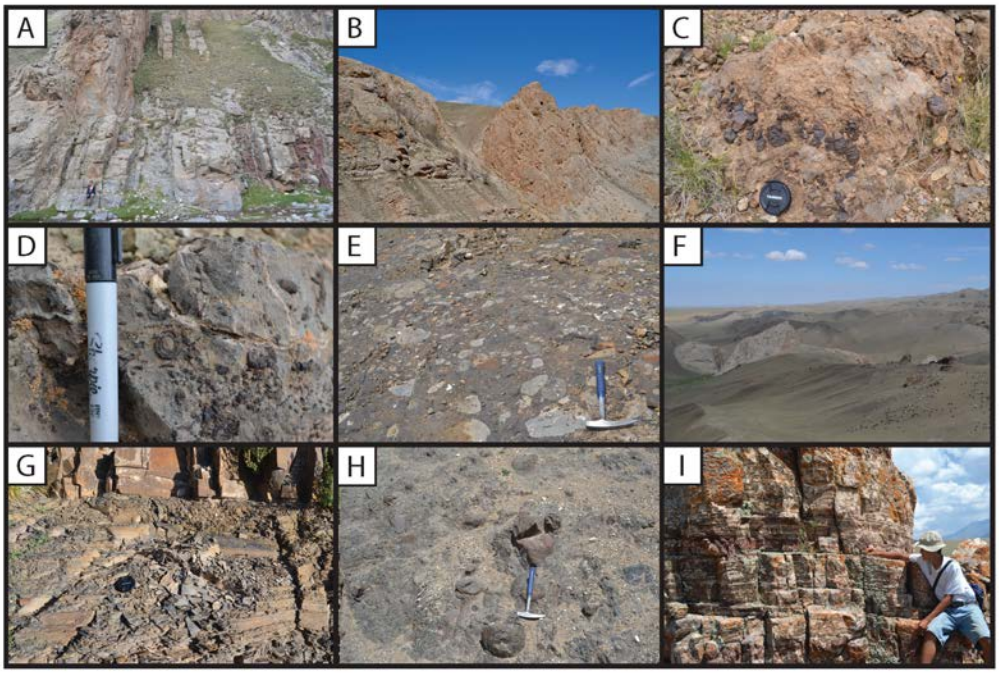

Figure 4.5. Photomontage of the Salaagol and Khairkhan formations.
A) Interbedded microbial limestone and red silt near the base of the Salaagol Fm in Orolgo Gorge. B) The upper Salaagol Fm (E1109) in Salaa Gorge with a goat herd for scale. C) Rounded quartzite cobbles on top bedding surface of archaeocyath reef south of Khukh-Davaa Pass. Camera lens cap for scale. D) Phosphatized grains, SSFs, and archaeocyaths at top of Salaagol Fm south of Khukh-Davaa Pass. E) Very poorly-sorted, matrix-supported Khairkhan Formation conglomerate in Orolgo Gorge. Limestone clasts contain archaeocyaths. F) Building-size olistolith of Salaagol Fm in Khairkhan Fm west of Orolgo Gorge. Goat herd for scale. G) Black to brown silt of upper Khairkhan Fm south of Khukh-Davaa Pass. H) Very poorly-sorted, matrix-supported Khairkhan Formation conglomerate NW of Orolgo Gorge. I) Partially silicified red to buff colored microbial dolostone of unknown age.

4.2.3.4. Khairkhan Fm

The Khairkhan Fm has only been described in Salaa Gorge as a >200 m siliciclastic succession that unconformably overlies older units (Dorjnamjaa and Bat-Ireedui, 1991; Kruse et al., 1996; Voronin et al., 1982). Our mapping and measured sections across the terrane demonstrate that the Khairkhan Fm is locally much thicker and consists of mixed siltstone, sandstone, and conglomerate, often containing large boulders of carbonate of the Salaagol Fm and chert and basalts clasts of unknown provenance. The Khairkhan Fm is the youngest Cambrian unit in the Zavkhan Terrane, and has been interpreted as the mélange, flysch and molasse of the foredeep (Macdonald et al., 2009). This interpretation is further supported by the structural position of the Khairkhan Fm at Orolgo Gorge (Figs. 4.1 and 4.6E), where it is overthrust by a klippe of ultramafic cumulates and serpentinite.

Figure 4.6. Detailed geological maps from across the Zavkhan Terrane.
Locations of maps are indicated in Fig. 4.1.A) Geological map of area SE of Taishir. B) Geological maps of the southern and northern fault blocks in Bayan Gorge. C) Geological maps of KTN. D) Geological map of Khukh-Davaa Pass (NW of town of Jargalant). E) Geological maps of Orolgo, Salaa, and Tsagaan gorges.

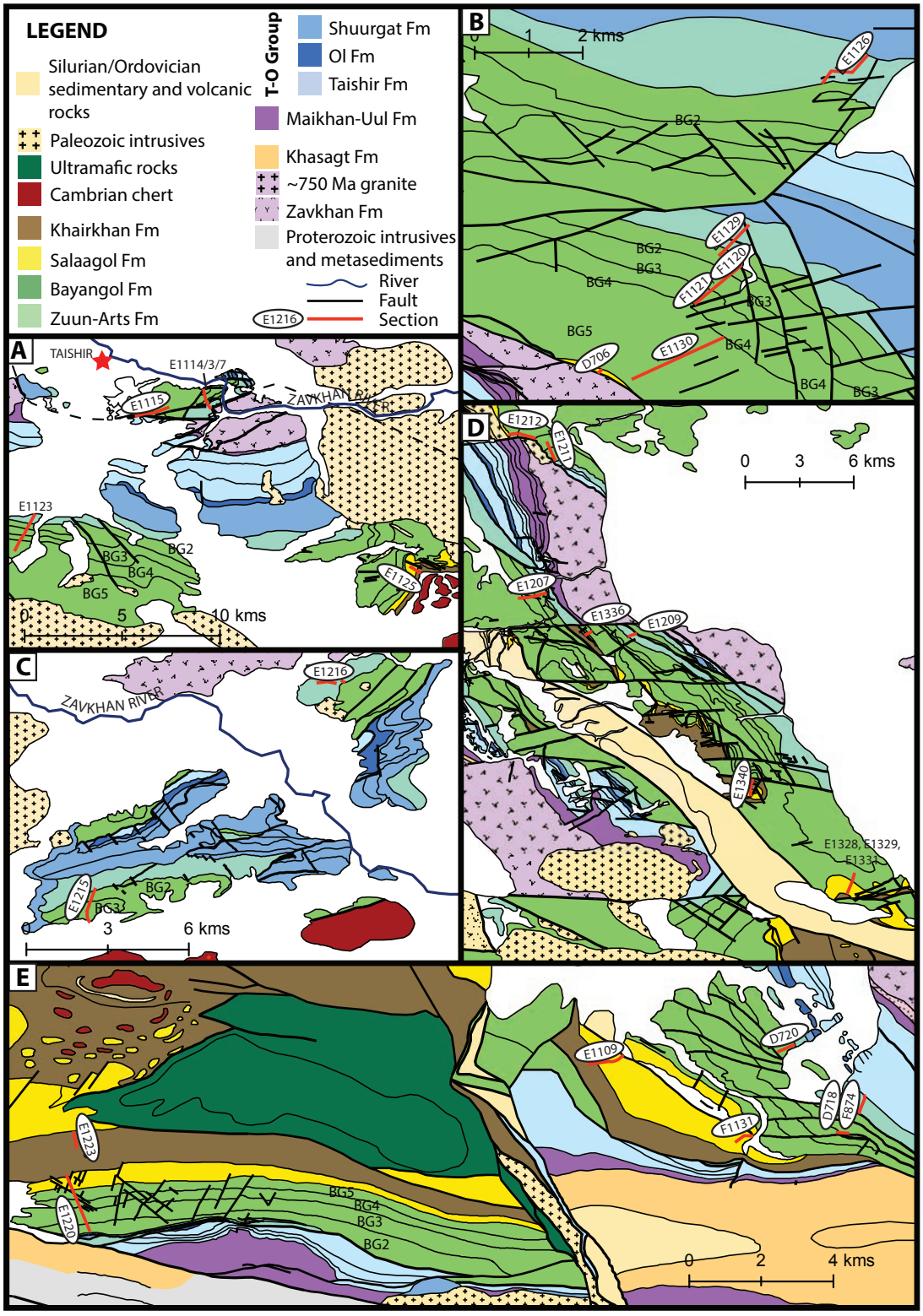

Figure 4.6 (continued).

4.3. Methods

4.3.1. Geological Mapping

Geological mapping was conducted over the course of three summers between 2011 and 2013. The detailed geologic mapping presented here provides the necessary context for lithostratigraphy, chemostratigraphy, and biostratigraphy presented in this study. Higher resolution stratigraphic studies of previously described and undescribed sections would not have been possible without new geological mapping. We returned to the five key areas that were described in the 1996 Geological Magazine publications, Bayan Gorge, KTN, Orolgo Gorge, Salaa and Tsagaan gorges, and Taishir to remap those areas in greater detail (Figs. 4.6A, B, C, and E). Additionally, we mapped many other parts of the Zavkhan Terrane, targeting areas with good exposure and continuous sections of the Zuun-Arts, Bayangol, and Salaagol Fms (Figs. 4.6A, C, D, and E). Geological mapping enabled measuring stratigraphic sections in the new, previously undescribed areas with the goal of putting together a more complete basin-wide facies model and to construct a chemostratigraphic age model. Geologic mapping was conducted using LANDSAT satellite imagery, which offered the highest resolution imagery available at the time.

For mapping purposes and sequence stratigraphic correlation, we informally divide the Bayangol Fm into five different members (BG2-BG6), of which, the lower three members are capped by massive carbonate units that are clearly visible in satellite imagery (Fig. 4.4). When we initially divided units in the late Ediacaran to early Cambrian strata, we used BG1 interchangeably with Zuun-Arts because the Zuun-Arts Fm marks the onset of basin formation and is genetically related to the Bayangol Fm

(Bold et al., 2013). Here, we use Zuun-Arts Fm in place of BG1. As the result of our detailed stratigraphic and mapping work, we have defined eight structural blocks (Taishir, Salaa, Tsakhir, Khavchig, Tsagaan, Orlogo, Khunkher, and South Khukh Davaa) that are characterized by distinct stratigraphy and are bound by major faults (Fig. 4.1A).

4.3.2. Facies associations and sequence stratigraphy

Nine facies associations were identified in this succession (Table 4.1), and for ease of discussion, they are grouped into five broad categories: (1) carbonate-dominated facies associations that were deposited on an outer shelf to slope environment below storm wave base, (2) siliciclastic-dominated associations that were deposited on an outer shelf to slope environment below storm wave base, (3) carbonate-dominated facies associations that were deposited in shelf to shoreface environments, (4) siliciclastic-dominated facies associations that were deposited in shelf to shoreface environments, and (5) flysch and mélange facies associations that were deposited during the terminal closure of early Cambrian orogenesis. These facies associations were used to identify the major stratigraphic sequences boundaries in Zuun-Arts through Salaagol Fm succession.

The late-Ediacaran to early Cambrian succession on the Zavkhan Terrane contains multiple sequences that are appropriate for high-resolution sequence stratigraphy. In our analysis, we use the four commonly recognized system tracts that include lowstand systems tract (LST), transgressive systems tract (TST), highstand systems tract (HST), and falling-stage systems tracts (FSST) following Van Wagoner et al. (1990). We interpret carbonate deposition to represent transgressive systems tracts and highstand systems tracts of relative sea level in the basin (Vail et al., 1977). For the carbonate-dominated slope facies in the lower to middle Zuun-Arts and lowermost Bayangol fms,

Table 4.1. Facies Associations of the late Ediacaran to early Cambrian strata in Southwest Mongolia

Association	General character	Grain size	Bed thickness	Sedimentary structures	Origin and depositional environment
FA1: Thinly- and well-bedded limestone	Clean, well-bedded medium to dark grey limestone; sometimes interbedded with very minor shale	Lime mudstone to wackestone	Very thin to thin; 1-5 cm thick	Rare slump folding; rare possible hold fast imprints and bed-planar trace fossils; rare stromatolites	Pelagic settling; deposited by turbidity currents on outer shelf to lower continental slope; deposited below storm wave base
FA2: Parted to ribbon-bedded limestone	Interbedded medium grey limestone and mudstone	Lime mudstone to wackestone; partings are of shale to siltstone	Very thin to thin; 1-10 cm thick	Rare slump folding; rare possible Ediacaran fossils and bed-planar trace fossils; rare stromatolites	Pelagic to hemipelagic settling; deposited by turbidity currents on outer shelf to lower continental slope; deposited below storm wave base
FA3: Slope-derived carbonate breccia	Intraformational limestone tabular breccia; clasts derived from FAs 1 and 2; laterally discontinuous	Packstone; limestone clasts with lime matrix	0.1-5 m thick; laterally discontinuous	Clast to matrix supported	Deposited on a continental slope by debris flow
FA4: Phosphatic shale to siltstone	Phosphatic shale to siltstone with minor nodular limestone; minor amounts of phosphate	Microcrystalline shale with minor amounts of phosphate	1-20 m thick	Limestone nodulates; rare phosphatic hardgrounds with phosphatic grains, ooids, and SSFs	Deposited in continental slope environments during marine transgressions

Table 4.1 (continued)

FA5: Turbididtic siltstone and sandstone	Interbedded siltstone and sandstone with isolated limestone beds	Siltstone to medium grained sandstone	Thin to medium	Normally graded beds; load structures	Deposited on continental slope via dilute turbidity currents
FA6: Oolitic to oncolitic limestone	Limestone containing ooids and oncoids; thickly bedded	Packstone to grainstone	Thin to very thickly bedded	Trough cross bedding	High-energy carbonate shoal
FA7: Platformal limestone	Massive microbialaminite, stromatolite, thrombolite, and archaeocyath reef. Light grey limestone occasionally with minor sandstone to siltstone beds	Boundstone to bindstone	Thin to very thickly bedded	Bioturbation, stromatolites, thrombolites, archaeocyaths, non-phosphatized SSFs rarely preserved; rare vugs	Deposited on carbonate shelf
FA8: Cross-bedded to swaley-bedded sandstone	Bedded sandstone	V.f. to v.c. sand, dominantly f. to m; locally contains dolomitic matrix	Thin to medium	High angle trough cross-bedding; parallel laminations; ripple cross lamination; bioturbation common;	High energy shoreface
FA9: Massive to graded conglomerate	Very poorly sorted, thickly bedded conglomerate;	Poorly sorted sand matrix with pebble to boulder size clasts; olistoliths present locally	Medium to very thickly bedded	High-angle cross bedding; unit bases erosional; laterally discontinuous; building size olistoliths	Deposited by high-density turbidity currents in submarine channels; molasse and flysch desposits

we utilize the TST and HST for correlation across the basin. The rest of the sequence contains abundant parasequences and bypass channels, so to pick out the major sequence boundaries, we use the LST which are marked by an influx of medium to coarse sandstone and conglomerate across the basin (Mullins et al., 1987; Spence and Tucker, 1997; Vail et al., 1977).

4.3.3. $\delta^{13}C$ Chemostratigraphy

To test regional and global correlations, we sampled limestone spanning the Zuun-Arts Fm through the Salaagol Fm from across the Zavkhan Terrane. Limestone rocks were sampled at 0.5-4 m resolution from 14 composite stratigraphic sections, many of which are composite sections (exact locations of measured sections are indicated in Fig. 4.6). Clean limestone samples without siliciclastic components, secondary veining or cleavage were targeted while sampling. Carbon ($\delta^{13}C$) and oxygen ($\delta^{18}O$) isotopic measurements were obtained on 2763 samples. Samples were micro-drilled along individual laminations, where visible, to obtain 5 to 20 mg of powder. Veins, fractures, and siliciclastic-rich areas were avoided. Carbonate $\delta^{13}C$ and $\delta^{18}O$ data were acquired simultaneously on a VG Optima dual inlet mass spectrometer at the Harvard University Laboratory for Geochemical Oceanography. Carbonate samples were reacted with orthophosphoric acid using a VG Isocarb preparation device, which includes a common acid bath with a magnetic stirrer. Approximately 1 mg of micro-drilled samples was reacted in the bath at 90°C. Evolved CO_2 was collected cryogenically and analyzed using an in-house reference gas. Potential memory effect resulting from the common acid-bath system was minimized by increasing the reaction time for dolomite samples. Memory effect is estimated at <0.1‰ based on variability of standards run after dolomite samples.

Standard deviation (1σ) from standards was better than ± 0.1‰ for both $\delta^{13}C$ and $\delta^{18}O$. Carbonate $\delta^{13}C$ and $\delta^{18}O$ isotopic results are reported in per mil (‰) notation relative to V-PDB (Vienna-Pee Dee Belemnite) by using an in-house Cararra Marble standard that was calibrated against several NBS carbonate standards and cross-calibrated with other laboratories.

4.3.4. Constructing an age model

Because global stages 2-4 of the early Cambrian have not been defined yet and previous global correlation of early Cambrian data use stratigraphic terminology from Siberia and Kazakhstan, for the sake of consistency, we also use the stage system for the Lower Cambrian on the Siberian Platform in this study. The Lower Cambrian on the Siberian Platform in which it is divided into the Nemakit-Daldynian, Tommotian, Atdabanian, Botomian, and Toyonian (Repina and Rozanov, 1992; Rozanov et al., 2008). Generally, the Nemakit-Daldynian and Tommotian are thought to be correlative with the Terreneuvian Series. The Atdabanian and Botomian are thought to be correlative with the undefined Series 2 of the early Cambrian.

Similar to the way in which previous workers created composite $\delta^{13}C$ curves and correlated sections globally, a combination of positive and negative excursions are used as tie points in this study. These $\delta^{13}C$ excursions were first labeled in Siberia (e.g. Kouchinsky et al., 2007) and have been used in several global compilations since. With these data, 1n, the most negative $\delta^{13}C$ value at the E-C boundary, and five positive $\delta^{13}C$ excursions (2p-6p) were identified in each section. A composite $\delta^{13}C$ chemostratigraphic curve was constructed by stretching the $\delta^{13}C$ values between each of these tie points assuming constant sedimentation rates in each section. Calibration points for positive

excursions are the same as those used in Maloof et al. (2010a). Details of the correlation between measured sections of the Zuun-Arts Fm are discussed in Appendix A6.

4.3.5. Paleontology

Body and trace fossils were sampled and photographed while measuring stratigraphic sections. This study places previously described SSF horizons into the necessary stratigraphic context and a refined age model. Revised mapping and correlation among sections has resulted in different interpretations of the stratigraphic position of the SSF horizons.

SSF taxon names from previous SSF horizons were taken from the compilation done by Brasier et al. (1996b) and Khomentovsky and Gibsher (1996) and the publication by Esakova and Zhegallo (1996). For generic and higher group assignments for individual taxa, we followed the supplementary material of Maloof et al. (2010a) and references therein.

4.4. Results

4.4.1. Palinspastic Reconstructions of the Zavkhan Terrane

Based on geological mapping, we have identified major faults in the Zavkhan Terrane (Fig. 4.1A) and have grouped measured sections that are on the same fault block together. The southern thrust sheets preserve more distal sections and the northern ones are more proximal. The measured sections presented here are ordered according to depositional paleo-depth (Fig. 4.8). Below, we organize the results from more proximal to more distal.

4.4.2. Facies Associations

The facies associations (FAs) described below grouped according to paleo-water depth and the descriptions and environmental interpretations are summarized in Table 4.1.

4.4.2.1. Slope to outer shelf-deposited carbonate facies associations

Three carbonate-dominated FAs show evidence of deposition in deeper-water slope to outer shelf settings. These facies are characteristic of the lower to middle Zuun-Arts Fm.

Facies association 1: FA 1 is characterized by thinly-bedded, normally graded packstone, wackestone, or lime mudstone with very minor amounts of siliciclastic material. Typically these beds are dark to light grey in color. The limestone beds have sharp bases and tops and are normally graded. Occasionally soft sedimentary slumping is present. FA 1 is the dominant facies in the lower to middle part of the Zuun-Arts Fm, and is interpreted to represent outer shelf to upper slope deposition that is below storm wave base.

Facies association 2: FA 2 is a ribbon-bedded limestone, similar to FA 1 in that is a thinly-bedded, carbonate-dominated facies. Typically these beds are medium to light gray in color. FA 2 differs from FA 1 in that it contains shale or siltstone partings. This facies association is common in the middle part of Zuun-Arts Fm as well as portions of the Bayangol Fm, and we interpret it to represent outer shelf to lower slope deposition that is below storm wave base.

Facies association 3: FA 3 is a slope-derived carbonate breccia that consists of clast- to matrix-supported intraformational limestone conglomerate. Clasts are tabular with composition similar to the underlying and overlying units and indicative of

derivation from surrounding slope deposits. This type of sedimentary breccia is present in some sections of the lower Zuun-Arts Fm and lower Bayangol Fm. Some of the sedimentary breccias in the Zuun-Arts Fm are found in association with slump folding suggesting that these breccias are deposited during slope failure. Other breccias could represent storm-dominated facies.

4.4.2.2. Slope-deposited siliciclastic facies associations

Facies association 4: FA 4 is present at the base of the Zuun-Arts and Bayangol fms and is characterized by laminated phosphatic shale to siltstone. Locally, this FA is present at the contact between the Salaagol and Khairkhan fms. Tan carbonate nodules in the shale and siltstone are locally present. Volumetrically, FA 4 is not a major component of the succession; however, it is a distinct and important stratigraphic marker.

Facies association 5: FA 5 is characterized by thinly-bedded, finely laminated siltstone, turbiditic sandstones, and pebble conglomerates. Fining upward sequences are common. Bouma units A-C (and D-E in some sections) are commonly preserved. FA 5 is present in the middle to upper part of the Khairkhan Formation.

Shelf to shoreface carbonate facies associations

Facies association 6: FA 6 is cross- to swaley-bedded oolitic to oncolitic limestone. Occasionally the oolitic limestone contains quartz grains. This facies is found in the uppermost Zuun-Arts Fm, throughout the Bayangol Fm, and in parts of the Salaagol Fm.

Facies association 7: FA 7 is anything ranging from microbialaminites, stromatolites, and thrombolites to an archaeocyath reef. Different microbial and thrombolitic textures are common throughout the Bayangol Fm and parts of the Salaagol

Fm. The Salaagol Fm also contains beautifully preserved archaeocyath and hyolith reefs that range in size from laterally discontinuous patch reefs to hundreds of meters thick and for more than a kilometer along strike.

4.4.2.3. Shelf to shoreface siliciclastic facies associations

Facies association 8: FA 8 is a cross-bedded to swaley-bedded sandstone. It is characterized by finely- to thickly-bedded, very fine to very coarse-grained quartz-arenite to calc-arenite. Sedimentary structures include high-angle cross-stratification, parallel bedding, current ripples, and normally graded beds. Bioturbation is common is this FA. FA 8 is found throughout the Bayangol Fm.

Facies association 9: FA 9 is an immature, poorly-sorted pebble to boulder conglomerate. Conglomerates are found in the Bayangol through Khairkhan Fm but differ in texture, composition, and thickness. The Bayangol Fm contains cm-thick lenticular pebble conglomerates. Often these conglomerates are red-colored and feldspathic, and they can contain phosphatized grains and SSFs. In the Salaagol Fm, there is a wide range of conglomerates that include cm-thick pebble conglomerates with angular clasts to cobble conglomerates that are tens of meters thick with rounded clasts of underlying strata. These conglomerates occur between archaeocyath reefs. Additionally, this facies is found in the shallow-water facies of the Khairkhan Fm, and is interpreted as the molasse of the foreland.

4.4.3. Key Locations: Geologic mapping, sedimentology, and stratigraphy

Below, we present the results of geological mapping (Figs. 4.1 and 4.6), sedimentology and stratigraphy that have enabled the refinement of the SSF biostratigraphy in the Zavkhan Basin. These results are synthesized for each locality. In

some cases the geological mapping has greatly changed the interpretation of the stratigraphy, including the SSF biostratigraphy and the chemostratigraphy. The deformation in the Zavkhan Terrane is almost entirely brittle deformation and, generally, is dominated by a conjugate set of right lateral strike slip faults and oblique en echelon thrust faults.

4.4.3.1. Taishir (E1114, E1113, E1115, E1117, E1325)

Most previous studies at this locality focused on the underlying Tsagaan-Olom Group (Goldring and Jensen, 1996; Khomentovsky and Gibsher, 1996; Macdonald, 2011; Macdonald et al., 2009) and the fossils, bioherms and patch reefs of the Bayangol Fm (Dorjnamjaa and Bat-Ireedui, 1991; Goldring and Jensen, 1996; Kruse et al., 1996). Detailed mapping of the Zuun-Arts and Bayangol fms just to the southeast of the town of Taishir, allowed us to measure a composite section of the two formations at this locality and to place previously poorly contextualized fossil horizons into a coherent stratigraphic framework. Additional geologic mapping to the south-southwest and southeast of the town of Taishir led to the discovery of more previously unreported, well-exposed sections. A section of the Zuun-Arts and Bayangol fms are well-exposed to the south-southwest in a low creek bed (Fig. 4.6A). Additionally, just south of the large Permian intrusion, sections of the upper Bayangol through Khairkhan fms are well exposed. All of these sections described here are on the same fault block as the Bayan Gorge sections.

One of the measured sections of the Zuun-Arts Fm, E1114, was measured near the town of Taishir. Section E1114 was measured just south of the Zavkhan River and east of the town of Taishir. The total measured thickness of E1114 is 176 m. Only the top surface of *Boxonia grumulosa* is exposed in a gully. Brown and black, cherty, phosphatic

shale overlies the buff- to pink-colored *Boxonia grumulosa*. Similar to the Bayan Gorge sections, the basal portion of this section is dominated by very thinly-bedded limestone with nodular and bedded chert and abundant interclast breccia beds that pinch out laterally. The top 24 m of the Zuun-Arts Fm is light grey cross-bedded ooid grainstone.

For the Bayangol Fm, Kruse et al. (1996) presented a 30 m section which they referred to as 'Tayshir I' (not to be confused with the Tayshir I and II sections of the Maikhan Uul and Taishir fms in Khomentovsky and Gibsher (1996)), which we mapped as members BG2 and BG3. They also describe two 7 m section that they called 'Discovery site' and 'Ovoo site' and which we interpret as being a portion of BG4 in our section E1115. However, without much context, it is difficult to know exactly where these previously measured sections are. The fossil horizons from Taishir are not included in previous SSF biostratigraphic compilations (i.e. Khomentovsky and Gibsher, 1996 & Maloof et al., 2010). Here, we present a composite measured section of the Bayangol Fm (E1113, E1115, and E1117) that enables us to put new and previous fossil finds into the correct stratigraphic context.

Members BG2 through lower BG4 sit conformably above the Zuun-Arts Fm in a well-exposed section to the south and west of a bend in the Zavkhan River. The rest of the Bayangol section (very upper BG3 through BG5) is exposed in a broad syncline to the west of a left lateral strike-slip fault. There is a poorly sorted red conglomerate overlain by elongate stromatolites at the BG3-BG4 contact that were used to tie the sections together. Member BG5 is very shallowly-dipping near the top of the section, and the upper contact of the formation is not exposed.

Members BG4 and BG5 of this section (E1115) have a few exceptional features including abundant and diverse trace fossils and SSF assemblages. The elongation of the stromatolites at the base of BG4 is oriented at 210 degrees, an indicator that the paleoshoreline was oriented perpendicular to the direction of elongation along a NW-SE transect in modern coordinates (Hoffman, 1967). The upper part of BG5 is notable because of its >100 m of siltstone to sandstone beds that contain few sedimentary features. Some of the beds are slightly graded but many are structure-less medium to coarse sandstone units that lack bedding surfaces.

Just SE of Taishir, there is an excellent section of the Salaagol Fm called E1325. The basal contact of the Salaagol Fm is not exposed at this section, but laterally, it rests conformably on a white to pink quartz pebble conglomerate. The Salaagol Fm is 177 m thick at this locality. The basal ~38 m of the formation consists of microbialaminite and massive recrystallized limestone. The recrystallization is patchy and is most likely the result of the contact metamorphism from nearby intrusion. At 38 m above the base of the formation, well-preserved archaeocyaths appear, and at 84 m, they are the dominant reef former.

The Khairkhan Fm rests conformably on top of the Salaagol Fm at this locality. Just to the south of E1325, this formation is better exposed as a poorly sorted, very coarse sandstone to pebble conglomerate. The top contact of the Khairkhan Fm is not exposed anywhere in this area. There is ~10-20 m of non-exposure between the top contact of the Khairkhan Fm and a red to black chert of unknown age.

4.4.3.2. Kvetee Tsakhir Nuruu (KTN; E1216, E1215, E1217, E1219)

This ridge is located ~30 km southeast of the town of Taishir on the south side of the river (Fig. 4.6C). The Zuun-Arts Fm and the basal Bayangol Fm are exposed on the southwestern side of the ridge. Additional mapping northeast of the river resulted in the discovery of a well-exposed section of the Zuun-Arts Fm (E1216) and a well-exposed but faulted and folded section of the lower Bayangol Fm (E1215, E1217, E1219).

Phosphatic shale and subcrop of thinly-bedded limestone mark the base of the Zuun-Arts Fm at this locality. *Boxonia grumulosa* is present in other sections at KTN but is not exposed at the exact place this section was measured. The basal 50 m of this measured section is thinly-bedded limestone with black, phosphatic shale and minor intraclastic breccia. The black shale here was thicker and more abundant than in any other section. The middle part of the section is dominated by thinly-bedded limestone with more intraclastic breccia and slump folding with vergence to the southeast (n=41). The top of the section contains more thinly-bedded limestone and debris flows but also abundant sandstone and siltstone interbeds. This is the only section in which sandstone, siltstone, and shale were observed at the top of the section instead of cross-bedded ooid grainstone.

The measured section of the Bayangol Fm (E1215) is the same section as the previously described section at KTN, south of the Zavkhan River (Brasier et al., 1996b; Dorjnamjaa et al., 1993; Zhegallo and Zhuravlev, 1991). At this locality, the Bayangol Fm is relatively thin and only the basal part is exposed. The base of the section is marked by thinly-bedded limestone that grades up into massively weathering, partially recrystallized limestone that looks similar to the upper part of the Zuun-Arts Fm. This

limestone is capped by shale, an obvious lenticular pebble conglomerate that contains phosphatized ooids and SSFs, and bioturbated limestone.

More strata of the Bayangol Fm are exposed north of the Zavkhan River, where the basal contact with the Zuun-Arts Fm is clearly exposed. However, there, much of the Bayangol Fm strata are faulted, folded, relatively flat-lying, and massively weathering, preventing us from measuring a complete section of the formation. Sections E1217 and E1219 (not plotted in Fig. 4.8) comprise a composite section of BG2 and BG3 strata. E1217 sits conformably on E1216, the measured section of the Zuun-Arts Fm described above, and E1219 is a measured section of member BG3, exposed in the limb of a syncline.

4.4.3.3. SE of Bayan Gorge (E1123)

South of the town of Taishir and SE of Bayan Gorge is a previously undescribed, well-exposed section of the Bayangol Fm (E1123). Because this section is on the same fault block as the southern Bayan Gorge section, it is similar in facies and thickness to the composite section there.

The basal portion of the Zuun-Arts Fm is not well exposed at this locality, so only the upper 106 m were measured. The beds in this section are shallowly dipping and the exposure of this section is not as good as the exposures in Bayan Gorge or Taishir. Nonetheless, the section offers another opportunity to measure and sample the middle to upper part of the Zuun-Arts Fm. The measured thickness of BG2-BG4 here is 357 m, and sedimentologically it is very similar to the measured section in Bayan Gorge. The upper part of the formation (BG5) was not measured in detail at this locality because, due to a major fault, there is no top contact with the Salaagol Fm.

4.4.3.4. Bayan Gorge (E1126, E1129, F1120, F1121, E1130, D706)

The Bayan Gorge is on the south side of the Zavkhan River, ~15 km west of Taishir (Fig. 4.6B). It hosts a northern and southern fault block of very well-exposed sections of the Zuun-Arts and Bayangol fms. Despite abundant, but minor, conjugate fault sets in the Gorge, the mapping is tractable. We present revised maps of Bayan Gorge and use this new mapping to construct a composite section of the Zuun-Arts (E1129 from the southern block) through Bayangol fms (F1120, F1121, E1130, and D706 from the northern block). Previous workers suggested that in the southern fault block, there was repetition of the lower Bayangol Fm (their units 17 and 18, our BG2) due to thrust faults (Gibsher et al., 1991; Khomentovsky and Gibsher, 1996); however, we observed only small offsets due to the conjugate sets of faults. Importantly, this revised mapping changed the stratigraphy and placement of SSF horizons into the composite SSF range chart. Instead of repeating strata (units 17 and 18, our BG2), on the west side of the Gorge, we observed continuous stratigraphy that is much thicker than previously reported.

Two sections of the Zuun-Arts Fm, one on the southern fault block (E1129) and the other on the northern fault block (E1126) were measured in Bayan Gorge; however, the data in Fig. 4.8 are from E1129. The two sections are both very well-exposed with similar thickness and stratigraphy.

Beginning at the top contact of the stromatolite *Boxonia grumulosa*, the measured section on the southern block (E1129) is 221 m thick. The base of the section is marked by green phosphatic shale with bedded chert and nodular limestone that is overlain by thinly-bedded limestone with bedded and nodular chert. The lower part of the Zuun-Arts

Fm is predominantly thinly-bedded (1-2 cm) dark grey limestone (Fig. 4.3B) with 0.5-1.5 m beds of limestone interclastic breccia. In the middle to upper part of the Zuun-Arts Fm, there are several 5-15 m parasequences. The bases of the parasequence are marked by planar, thinly-bedded limestone interbedded with pink calcisiltite. Up-section, the beds become thicker, and the tops of some of the parasequences are capped by cross-bedded ooid grainstone.

Beginning at the top contact of the stromatolite *Boxonia grumulosa*, the measured section in the north block (E1126) is 203 m thick. This section is very similar sedimentologically to the section E1129. Well-preserved simple bed-planar trace fossils were found at 169 m. The upper contact with the Bayangol Fm is a sharp transgression between massive ooid grainstone of the Zuun-Arts Fm and green phosphatic shale interbedded with limestone of the basal Bayangol Fm.

The section of the Bayangol Fm on the southern block of Bayan Gorge is the most-studied section and the type locality of the Bayangol Fm. Two sets of unit numbering, painted onto the cliff faces, have been used by Zhegallo and Zhuravlev (1991) and Gibsher et al. (1991), which was subsequently used by Khomentovsky and Gibsher (1996). However, due to the mismapping of the Gorge, we do not use either of the numbering schemes. The three thick carbonates that cap members BG2-BG4 are clearly visible in satellite imagery and are present in many other localities. This is an important distinction because previous writers have interpreted what we refer to as BG3 (units 18 and 19 in Gibsher et al. (1991)) as being a thrust repetition of BG2. As a result, our measured section is thicker and contains additional strata that are missing in the middle of previous measured sections.

4.4.3.5. Khukh-Davaa

'Khukh-Davaa' is the name of the pass along a left lateral, east-west oriented, strike-slip fault in the northwestern Khevtee Tsakhir Range (Fig. 4.6D). New mapping in this area resulted in the discovery of many new sections of the late Ediacaran through early Cambrian stratigraphy both north and south of the Khukh-Davaa Pass. Geologic mapping was focused on the eastern side of the NW-SE Late Ordovician to Silurian graben. There is a major fault separating the NE section from the SE one so the results from these two sections are discussed separately below. The SE section is interpreted to have been deposited on the same fault block as the section from Salaa and Tsagaan gorges (Figs. 4.1A and D), whereas the NE Khukh-Davaa section is interpreted to be on the same fault block as the section from Khunkher Gorge. Based on mapping, of these two fault blocks, we interpret the thrust sheet with the sections from SE Khuhkh-Davaa and Salaa and Tsagaan gorges to be the more proximal of the two.

4.4.3.6. SE Khukh-Davaa (E1209, E1207, E1336, E1328, E1329, E1331, E1339, E1340)

The section of the Zuun-Arts Fm at this locality (E1209) is exceptional in several regards, including unusual sedimentary features and expanded portions of different parts of the formation. The total thickness of this measured section is 263 m. The base of the section is marked by a silicified karst surface followed by thinly-bedded, graded dolosiltite and a 10 m horizon of *Boxonia grumulosa*. Capping the stromatolites are phosphatic shales interbedded with mechanically bedded light grey dolostone. Overlying the basal interbedded phosphatic shale and dolostone is dark grey to black, sulfidic limestone and dolostone with rare domal stromatolites. The top 134 m is dominated by cross-bedded limestone ooid and mudchip grainstone. Paleoflow of the cross-beds is to

the southeast. The cross-bedded ooid grainstone shoal at the top of this section is much thicker here than it is in any other section measured.

The section of the Bayangol Fm is a composite section in which BG2-BG4 of the Bayangol Fm (E1207) was measured just north of Khukh-Davaa Pass and the upper part (BG5) of the formation (E1336) was measured just south of the pass in a broad anticline. The two sections are separated by a left-lateral strike slip fault; however, the offset of the fault is not major.

The base of the E1207 is marked by an unusually thick section of red and green shale sharply overlying cross-bedded ooid grainstone of the upper Zuun-Arts Fm. There are many small, insidious faults and few distinct marker beds in the lowermost part of the Bayangol Fm in this section, and it is possible that the thickness in Fig. 4.8 is exaggerated due to structural repetition of the shale beds. The top of BG2 is marked by a few SSF horizons interbedded with black shale and a phosphatic hard ground. Similar to other sections, member BG3 at this locality is carbonate dominated in the middle part of the member as well as the upper part. It has thick, bioturbated limestone beds, oncolites, and ooilites that are interbedded with siltstone and fine to coarse sandstones in the lower to middle part of the member.

The base of section E1336 is marked by the resistant thick limestone unit that is just south of the left-lateral fault marking Khukh-Davaa Pass. This section is composed of predominantly green-colored, fine to medium grained sandstone. 1-3 m microbial patch reefs and small cm-scale microbial balls with diffuse edges are present throughout the section. Additionally, coarse white quartz arenites become increasingly more dominant and coarser up section. The 20 m below the first archaeocyath reef, the

sandstone is white, medium to very coarse, and quartz dominated. We call this upper 20 of the Bayangol Fm 'member BG6'; however, the contact between BG5 and BG6 is gradational.

The Salaagol and Khairkhan fms are well exposed in several localities south of the Khukh-Davaa Pass (Fig. 4.6D). Both formations are highly variable along strike, and two sections that capture that variability are presented here (Fig. 4.9). The Salaagol Fm ranges in thickness from 0-175 m. In many sections in this area the limestone of the Salaagol Fm interfingers with siltstone, sandstone, and conglomerate that are lithologically similar to the overlying Khairkhan Fm. We define the top of the Salaagol Fm as the uppermost limestone unit. In some sections, the Salaagol Fm is composed of m-scale patch reefs that pinch out laterally. In other sections, it is composed of ~10 m-scale archaeocyath reefs with ~50 m cobble conglomerates between (Fig. 4.5C). And in other sections, the Salaagol Fm is entirely absent, with a cobble conglomerate resting unconformably on very coarse quartz-rich sands of the upper Bayangol Fm.

In the thickest measured section of the Salaagol Fm (E1328 and E1329), the base of the Salaagol Fm is composed of thinly-bedded, medium grey limestone grainstone with ooids. At ~50 m, there is a gradational contact with ooid grainstone and thrombolites with occasional quartz pebble conglomerates. Further up section, thrombolitic and hyolith reefs dominate, with occasional sandstones and conglomerates. Dispersed archaeocyaths first appear at 111 m on the edges of stromatolites and become the dominant reef builders at 124 m. The upper 8 m of the section is thinly-bedded limestone with glauconitic sandstone and phosphatic hard grounds. Phosphatized and partially phosphatized hyoliths, chancelorids, and archaeocyaths are present in the sandy limestone at the contact with the

Khairkhan Fm (Fig. 4.5D). Phosphatic hard grounds and lag deposits with coated phosphate grains, SSFs, and archaeocyaths are also present in other sections nearby in this area. The top of the section is marked by a transgression into hundreds of meters of thinly-bedded sandstone and brown siltstone (Figs. 4.5G and H).

In the other measured section in this area (E1340), archaeocyath reefs are interbedded with tens of meters of cobble to boulder conglomerate. The conglomerate beds are well-sorted with rounded clasts of sandstone and granite to very poorly sorted with angular carbonate and sandstone clasts. Clasts of almost all of the underlying Neoproterozoic to Cambrian units were found, and we suggest these conglomerate beds mark a regional unconformity. The archaeocyath reefs in the section are 1-3 m in scale and pinch out to the east. This section does not have a top contact because the section is exposed in a shallowly dipping syncline.

In the area south of the Khukh-Davaa Pass, many facies of the Khairkhan Fm are present ranging from siltstone to sandstone to conglomerate. In some conglomeratic facies, limestone archaeocyath-rich clasts of the Salaagol Fm are dominant, but in other facies, they are absent. In the most southern part of Fig. 4.6D, the Khairkhan Fm contains building-size limestone olistoliths that are visible in satellite imagery. The upper part of the Khairkhan Fm consists of light green, grey, brown, and black finely-laminated siltstone (Figs. 4.5G and 4.7C). The thickness of the formation is difficult to determine due to faulting, folding, lateral facies change, and poor exposure of the upper Khairkhan Fm, but in this area, it is hundreds of meters thick.

Overlying the Khairkhan Fm in the area just south of the Khukh-Davaa Pass (Figs. 4.1D and 4.6D) is a buff to red-colored, variably silicified microbial dolostone of

unknown age (Fig. 4.5I). This unit is also present in the section southeast of Taishir and near KTN. The contact between the Khairkhan Fm and this chert unit was not exposed in any of the localities included in this study.

4.4.3.7. Salaa Gorge and Tsagaan Gorge (F874, D718, D720, F1131, E1109)

These two gorges are ~4 km away from each other on the northern flank of the Khevtee Tsakhir Range, with Tsagaan Gorge being the eastern of the two (Fig. 4.6E). They are ~20 km southwest of the village of Jargalant. Khomentovsky and Gibsher (1996) mapped a thrust repetition in the lower part of the Bayangol Fm; however, we saw no evidence for a major thrust repetition and instead mapped this area as having a number of right-lateral faults. Unfortunately there is non-exposure between Tsagaan Gorge and the exposure to the NW, close to where section D720 was measured, that obscures some of the fault traces in the lower Bayangol Fm. Because this area was more structurally complex than was previously suggested (Khomentovsky and Gibsher, 1996) and there was uncertainty in the nature and offset of some of the faults, we did not measure or sample the middle Bayangol at high-resolution.

The Tsagaan Gorge section of the Zuun-Arts Fm was previously measured, described and sampled by Voronin et al. (1982), Gibsher and Khomentovsky (1990), Brasier et al. (1996b), and Khomentovsky and Gibsher (1996). These studies failed to note that the upper-middle part of the section is faulted and recrystallized, obscuring bedding and sedimentary features. This portion of the strata was not measured or sampled, and as a result, the thickness of the Zuun-Arts Fm at this locality is uncertain. The unmeasured portion is marked by a fault in Fig. 4.8. The basal Bayangol Fm was measured between Tsagaan and Salaa gorges.

The sedimentology, paleontology, and paleoenvironment of the Salaagol Fm at Salaa Gorge have been described in detail by Kruse et al. (1996). We re-measured this section to use the detailed sedimentology and paleontology of previous workers as a reference point, and also to sample the entire formation at a higher resolution (~4 m) for $\delta^{13}C$ chemostratigraphy. The total measured thickness of the composite section at this locality is 380 m. A red to yellow carbonaceous silt was used to tie sections F1131 and E1109 together. Fig. 4.5B shows the upper half of the measured section (E1109) overlain by the Khairkhan Fm.

4.4.3.7. NE Khukh-Davaa (E1211, E1212)

A nearly complete, well-exposed section of the Bayangol Fm was found north of Khukh-Davaa Pass and northeast of a major NW-SE trending fault, which faults the E-C strata against the Zavkhan Fm (Fig. 4.6D). The total thickness of the Bayangol Fm at this locality is 765 m but lacks a top contact with the Salaagol Fm. The base of the section is marked by the contact between a cross-bedded ooid grainstone of the Zuun-Arts Fm and red to green phosphatic shale of the basal Bayangol Fm.

In present-day coordinates, this section is closest to E1207, a section just north of Khukh-Davaa Pass; however, these sections are separated by a major fault, and as a result, have different facies. The overall thicknesses for the different members of the Bayangol Fm are relatively similar, but the carbonate content and rock type within each of the members differs. For example, BG3 is expanded in both of these sections; however, it is more carbonate-dominated in section E1207 than it is in this one. At this locality, on the other hand, BG4 is more carbonate-dominated and thicker. The limestone capping this member was difficult to measure and sample because the terrain is very steep and

massive weathering, making it difficult to see bedding and sedimentary textures. Member BG5, consisting of poorly-sorted fine to very coarse sandstone, is only 87 m thick here, relatively thin compared to other localities. The top of the section is marked by what appear to be massively recrystallized white to pink limestone stromatolites that are likely still part of the upper Bayangol Fm. The top of this measured section is faulted against a Paleozoic intrusion.

4.4.3.8. Khunkher Gorge (E1138)

This previously undescribed section of the Zuun-Arts Fm through Bayangol Fm was measured in Khunkher Gorge and on the ridge to the west of the Gorge. There are no major structural complications of the Zuun-Arts and Bayangol fms at Khunkher Gorge, so no detailed map is presented herein, but the location is shown in Fig. 4.1D.

The Zuun-Arts Fm was thickest at this locality. Sedimentologically, it resembles the Zuun-Arts sections in SE Khukh-Davaa. The Bayangol Fm has a basal contact with the Zuun-Arts Fm ooid grainstone and an upper contact with the Salaagol Fm. The upper contact is not shown in Fig. 4.8 because there could be minor faulting at the base of the Salaagol Fm. Similar to other sections, members BG2 and BG3 are siliciclastic successions capped by thick limestone units. However, member BG4 is either much thicker or is much more siliciclastic-dominated in this section. The upper part of the section has abundant beds with ooids, coated grains, and oncoids. The thick oncolite bed near the top of the section looks very similar to the oncolite bed in Salaa Gorge.

4.4.3.9. Orolgo Gorge (E1220, E1223)

Insidious minor faulting is present throughout this section; however, the predictability of the conjugate fault sets, the excellent exposure, and the numerous distinct marker beds allow for tractable geological mapping, a detailed measured section, and high-resolution sampling. Our mapping in Orolgo Gorge shows that the uppermost Zuun-Arts Fm is faulted against the Taishir Fm (Fig. 4.6E); nowhere in this Gorge is the lower to middle Zuun-Arts Fm exposed. This finding is important for SSF biostratigraphy because the FAD of *Anabarites trisulcatus* and *Cambrotubulus decurvatus* is reported from the base of the Zuun-Arts Fm at this locality, most likely because the phosphatic shale at the base of the Bayangol Fm was mistaken as the phosphatic shale at the base of the Zuun-Arts Fm (Endonzhamts and Lkhasuren, 1988). As a result of our revised geologic map, we place this SSF horizon 200-300 m stratigraphically higher, in the base of the Bayangol Fm.

SSF horizons had been previously described at Orolgo Gorge, but no measured section or chemostratigraphy has been reported from this locality. The Bayangol, Salaagol and Khairkhan fms are particularly well-exposed, expanded, and carbonate-dominated in this section, and geologic mapping allowed for detailed litho- and chemo-stratigraphic studies in this gorge.

The measured section in Orolgo Gorge is the thickest, most carbonate-dominated section that was measured of the Bayangol Fm. In modern coordinates, it is close to Salaa Gorge; however, the two are separate be a major fault and this section restores to the east. The exposure in the creek is excellent, but abundant minor conjugate fault sets had to be

mapped in detail before measuring this section (Fig. 4.6E). The section has both a basal contact with the Zuun-Arts Fm and a top contact with the Salaagol Fm.

Similar to other sections, the base of the Bayangol Fm at this locality is marked by cross-bedded ooid grainstone sharply overlain by phosphatic green shale with nodular limestone. The basal ~155 m of this section are sedimentologically different from other measured sections. It is characterized by very thinly-bedded (0.5-5 cm) grey to tan limestone that are often interbedded with black shale. Horizons containing SSFs are abundant. At 137.5 m above the basal contact, there is a lenticular phosphatic hard ground overlain by 10 cm of phosphatized ooids (Fig. 4.3G). Above this distinct marker bed, the limestone beds are thicker and no additional SSF horizons were found for hundreds of meters. Above the thick, resistant limestone unit in the middle of BG2, is ~70 m of non-exposure in the creek. Above this covered interval is a green bioturbated siltstone and fine-grained sandstone that contains slump folds and some fault repetitions.

Although BG2 is expanded at this locality, BG3 is condensed. However, it is similar to other sections in that there are thick limestone units in the lower-middle part of the member. One distinctive feature of BG4 is the basal portion that is characterized by red and green shale interbedded with pink thrombolites and limestone microbialaminites. A thick microbial limestone ridge-former caps member BG4. Member BG5 is perhaps the most unusual part of this measured section because it has far more limestone beds than any other measured section in the basin. The base of BG5 is characterized by fine to very coarse, planar to cross-bedded sandstone. There is a distinct microbialaminite and microbial balls in the middle of the siliciclastics. The top of BG5 is characterized by abundant, channelized cross-bedded calc-arenites, ooilites, oncolites interbedded with

cross-bedded sandstone. Above the carbonate-dominated portion of BG5 are more coarse to very coarse cross-bedded quartz and calc-arenites. The top contact with the Salaagol Fm is marked by red to grey silty limestone microbial reefs with dispersed archaeocyaths.

The section of the Salaagol Fm measured here (top of E1220) is a continuation of the section of the Bayangol Fm from this locality. The upper part of the Bayangol Fm has thick limestone units that are not present in other sections. As a result, the boundary between the Bayangol and Salaagol fms was difficult to determine. Here we define the base of the Salaagol Fm as the base of the last major carbonate unit that is stratigraphically below the Khairkhan Fm. The base of this section is marked by a distinct red siltstone and silty microbial limestone (Fig. 4.5A).

The Salaagol Fm in this Gorge is over 343 m thick. The top of the Formation is a talus slope and is not exposed on either side of the Gorge. The basal to middle part of the formation is predominantly grey to pink to green limestone microbialites with siltstone interbeds. The first archaeocyaths appear 70 m above the basal contact. The middle to upper portion of the section continues to be dominated by microbialites, but thinly-bedded nodular limestone beds and oncolites become increasingly more common in the upper part of the section.

The overlying Khairkhan Fm is folded in a syncline at this locality. The formation was not measured in detail but was instead just generally characterized on an overturned limb on the north side of the fold (Fig. 4.6E). The estimated thickness of the formation here is ~550 m. The basal part of the formation contains limestone boulders and olistoliths that are concordant to the surrounding matrix of shale and silt, and slumping. The rest of the formation is dominated by sequences of very poorly-sorted, matrix-

supported conglomerate with angular clasts of black chert, quartz, ultramafics, and limestone (Fig. 4.5E and 4.5H) that fine up to sandstone and siltstone. Many of conglomerates and coarse sandstone are channelized. Some of the conglomerates contain larger boulders and olistoliths of archaeocyath-rich limestone. To the north and west of this section are building-size olistoliths of the Salaagol Fm in the Khairkhan Fm (Fig. 4.5F). The contact between the Salaagol and Khairkhan fms is not well exposed in this Gorge; however, samples with phosphatized archaeocyaths and SSFs (similar to those in Fig. 4.5A) were discovered in a talus slope near the contact.

The Khairkhan and Salaagol fms are in fault contact with ultramafic cumulates and serpentinite (Fig. 4.7B), and in the area to the north and west of Orolgo Gorge, the Khairkhan Fm contains clasts of the ultramafic rocks (Fig. 4.6E). Northwest of the ultramafic rocks in Orolgo Gorge and on the northeastern edge of the large Paleozoic intrusion, there are hundreds of meters of very finely laminated green to white to brown siltstone of the Khairkhan Fm (Figs. 4.5G, 4.7A, 4.7C). Due to the poor exposure and the nearby intrusion, the nature of the underlying contact is not clear; however, the map relation with the underlying olistolith facies of the Khairkhan Fm suggests that it is a fault contact (Fig. 4.7A).

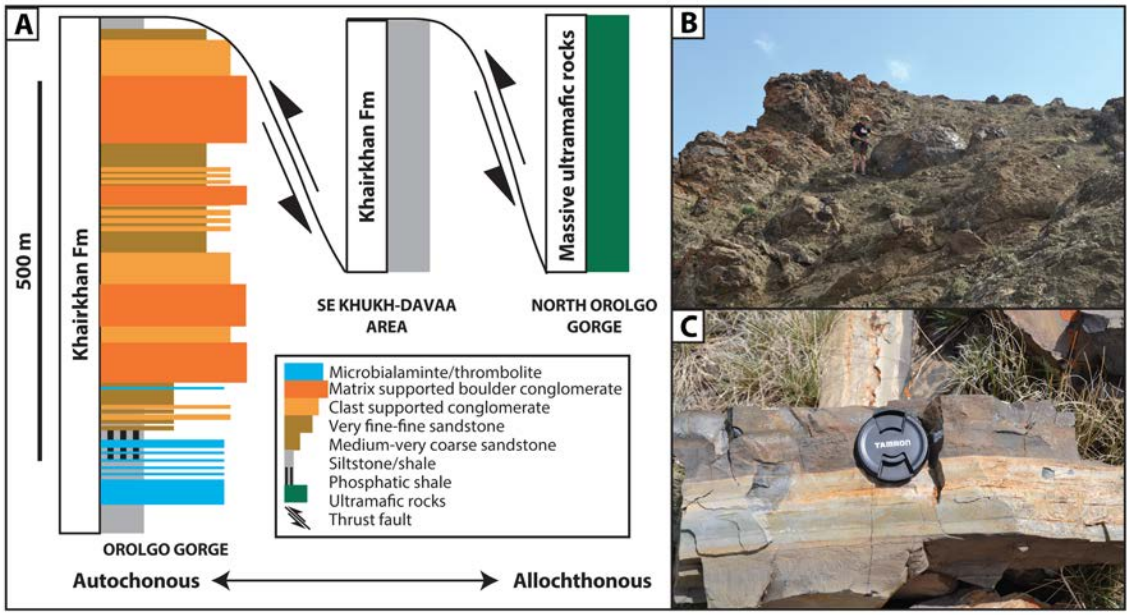

Figure 4.7. Different facies of the Khairkhan Formation
A) Autochthonous to allochthonous thrust sheets of different facies of the Khairkhan Fm and cumulate ultramafics and serpentinite. Clasts of ultramafic rock have been found in Khairkhan Fm. Together, these stratigraphic and sedimentological results support the claim that the Zavkhan Basin was a foreland basin (Macdonald et al., 2009). B) Photo of the cumulative ultramafics in thrust contact with the Salaagol Fm in northern Orolgo Gorge. C) Photo of the parautochthonous facies of the Khairkhan Fm from SE Khukh-Davaa area.

4.4.4. Small shelly fossil biostratigraphy

We place previously reported SSF horizons (Endonzhamts and Lkhasuren, 1988; Goldring and Jensen, 1996; Khomentovsky and Gibsher, 1996; Korobov and Missarzhevsky, 1977; Voronin et al., 1982; Zhegallo and Zhuravlev, 1991) into the new stratigraphic and $\delta^{13}C$ chemostratigraphic context as well as document new SSF horizons in multiple sections from across the Zavkhan Terrane. Here we present results of how stratigraphic placement of previously described SSF horizons and the resulting revised FADs have changed as a result of geologic mapping and refined correlations.

The lowermost SSF finds on the Zavkhan Terrane are reported from the Zuun-Arts Fm in three localities: KTN (Dorjnamjaa et al., 1993), Orolgo Gorge, and Salaa Gorge (Endonzhamts and Lkhasuren, 1988). Dorjnamjaa et al. (1993) reported *Anabarites trisulcatus* from siliceous phosphorite at the base of the Zuun-Arts Fm; however, other workers were not able to confirm this finding (Brasier et al., 1996b). After extensive searching near the base of the Zuun-Arts Fm at this locality, we were not able to find any SSF horizons, and we suspect that the siliceous phosphatic horizon at the base of the Bayangol Fm was confused for the one at the base of the Zuun-Arts Fm.

Similarly, the FADs of *Anabarites trisulcatus* and *Cambrotubulus decurvatus* from the base of the Zuun-Arts Fm in Orolgo and Salaa gorges could not be confirmed (Endonzhamts and Lkhasuren, 1988). In fact, in Orolgo Gorge, the Zuun-Arts Fm is faulted against the Taishir Fm and only the uppermost part of the former is present (Fig. 4.6E). Again, we suspect that confusion between the two phosphatic horizons resulted in the misplacement of this important FAD. These revisions are shown in Fig. 4.8.

Using the locations of previously published SSF horizons from Bayan Gorge (Khomentovsky and Gibsher, 1996) and our revised mapping, some of the SSF horizons (R-IV through R-X; see Fig. 4.8) have been moved stratigraphically up into member BG3. The previous interpretation was the result of incorrect mapping of BG3 as a thrust repetition of BG2 (Khomentovsky and Gibsher, 1996).

The SSF horizons from the Taishir section had not been put into stratigraphic context because the area had neither a detailed map nor a composite measured section. With our revised mapping and composite measured section, we place the previously reported SSF horizon in the upper part of member BG3 (see Fig. 4.8).

Figure 4.8. Integrated lithostratigraphy, sequence stratigraphy, and carbon isotope chemostratigraphy of the Zuun-Arts and Bayangol formations.
Measured sections are numbered according to proximity to the paleo-shoreline, with more distal sections on the right and more proximal sections on the left. Locations of the individual measured sections are shown on the map in the lower left side of the figure. Small shelly fossils horizons from this study are marked with red stars and those from previous studies are marked with green stars. Purple circles mark ichnofossil horizons. Previous paleontological data from Orolgo (Orolchayn) Gorge is revised from Endonzhamts and Lkhasuren (1988). Paleontological data from Salaa and Tsagaan gorges are from Voronin et al. (1982), Esakova and Zhegallo (1996), and Khomentovsky and Gibsher (1996). The paleontological data from Bayan Gorge is from Khomentovsky and Gibsher (1996). Each of the previous SSF horizons is labeled according to the labeling schemes of the different collections. Shaded colored boxes show correlation between sections.

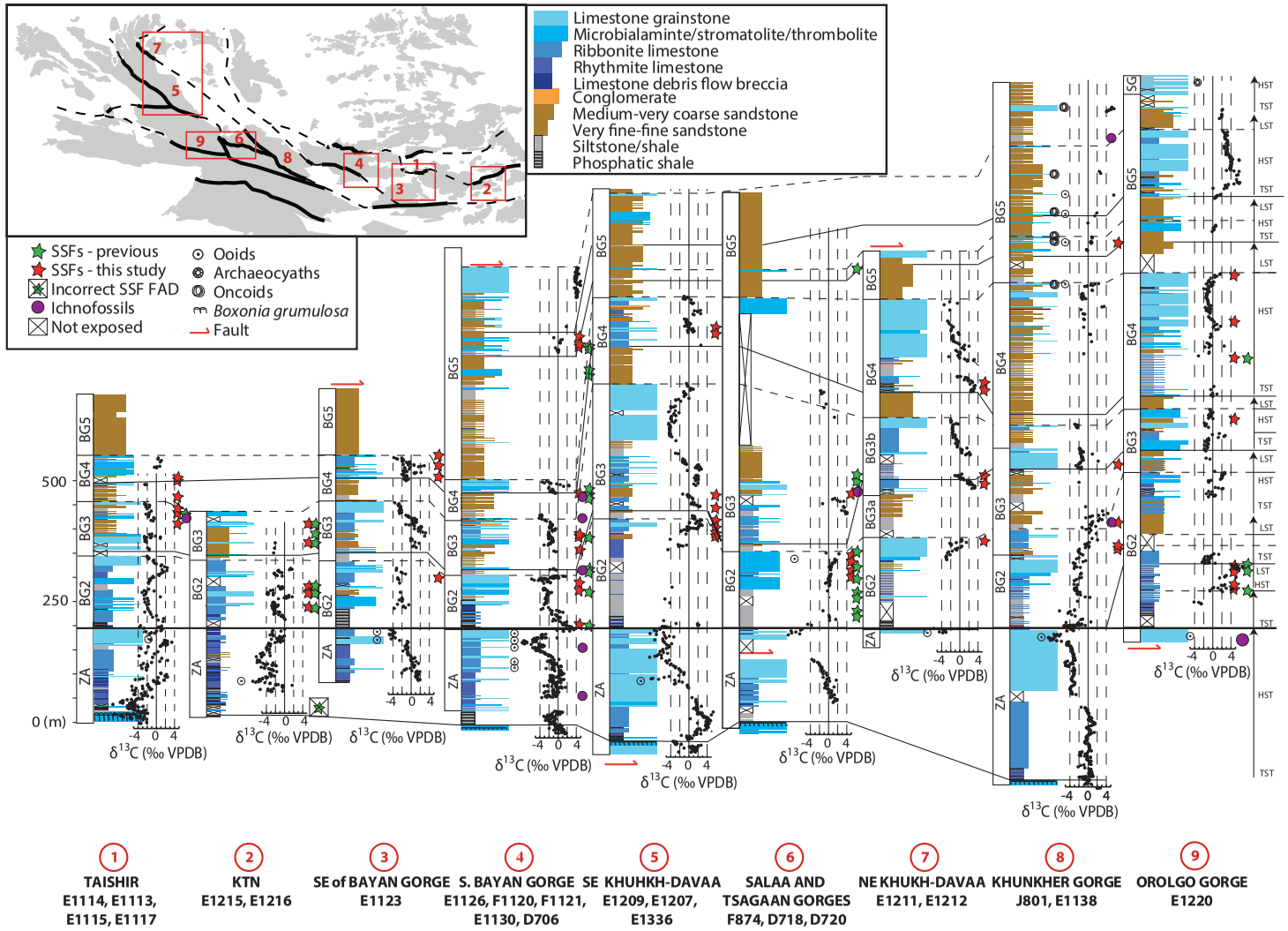

Figure 4.8 (continued).

New SSF horizons are reported here, but the phosphatized SSFs within them have not yet been dissolved, identified, or imaged. The SSF horizons are almost always preserved as lenticular lag deposits that pinch in and out laterally (Fig. 4.3G). They are often found in association with phosphatized coated grains and ooids. One exception to this is the type of preservation seen in the SSF horizons in the basal part of Orolgo Gorge where the SSFs are large, unbroken, and not found in association with other grains (Fig. 4.3H). Additionally, they are found on dozens of bedding planes in the basal ~200 m of measured section E1220. More generally, the SSF horizons are not discrete beds that are continuous markers across the basin, but they rather occur at different stratigraphic horizons in different sections, consistent with the rapid lateral facies changes across the basin.

4.4.5. Ichnofossil biostratigraphy

Abundant and diverse trace fossils are present throughout the Bayangol Fm, and as Goldring and Jensen (1996) point out, western Mongolia is one of the few places globally in which they are interbedded with skeletal fossil assemblages providing the opportunity to calibrate the relative timing of these two types of fossil records. Here, we present a few more notable finds to add to the well-documented ichnotaxa that have been previously described and adjust their stratigraphic placement.

Given that the Precambrian-Cambrian boundary is defined as occurring at the FAD of the trace fossil *T. pedum* at the Fortune Head section (Landing, 1994), ichnologists working in the Zavkhan Terrane devoted much time and energy trying to document the FAD of this trace fossil. The FAD of this fossil, according to Goldring and

Jensen (1996), is in unit 20 of the Bayangol Fm. With our revised geological mapping and stratigraphy (see previous results sections 'Geological mapping' and 'Description of key sections'), we place this unit at the contact between members BG3 and BG4 (see Fig. 4.8). Other ichnogenera from unit 20 include *Monomorphichnus* isp, *Hormosiroidea*, isp. and *Rusophycus* cf. *avalonensis* (Goldring and Jensen, 1996). Just below, in unit 18, or what we interpret as the lower part of member BG3, *Helminthoida*, *Spatangopsis*, and *Nemiana* were found. The trace fossil assemblage from member BG4 at Taishir includes *Oldhamia, Plagiogmus,* and possible *Zoophycus* (Fig. 4.8; Goldring and Jensen, 1996).

We emphasize that the preservation of *T. pedum* and the other trace fossils is highly facies dependent in the Zavkhan Terrane. Although we were not extensively searching for *T. pedum*, we did not find it at any other stratigraphic horizon or in any other measured section. We agree with previous workers that placing the Precambrian-Cambrian boundary at the FAD of *T. pedum* on the Zavkhan Terrane contradicts other lines of evidence that suggest that the Precambrian-Cambrian boundary is actually much lower in the stratigraphy. Although some workers have shown that there is a wide environmental tolerance for *T. pedum* and have used this to argue for further support of the GSSP type section of the Precambrian-Cambrian boundary (Buatois et al., 2013), many other workers have shown trace fossil production and preservation of *T. pedum* to be strongly lithofacies controlled (Gehling et al., 2001; Geyer, 2005; Geyer and Uchman, 1995; MacNaughton and Narbonne, 1999). As a result, using *T. pedum* as a global chronostratigraphic marker has been problematic on most Cambrian paleocontinents, notably in Siberia, China, Mongolia, and Kazakhstan (Babcock et al., 2011, 2012; Landing et al., 2013).

Although *T. pedum* was extremely difficult to find in the Zavkhan Terrane, there were many sandstone horizons that yielded abundant and diverse trace fossils. Figs. 4.3I, J, K, and L display a few of the exceptional ichnofossils that were found in the Khunkher and Bayan gorges. The early arthropod trace fossils in Figs. 4.3I and J are from middle BG3 and Fig. 4.3K is from BG5 in the Khunkher section (see Fig. 4.8 for exact horizons). The trace fossil in Fig. 4.3L is from BG5 in Bayan Gorge.

4.4.6. Carbon isotope chemostratigraphy

Carbon isotope ($\delta^{13}C$) chemostratigraphy for individual sections of the Zuun-Arts and Bayangol fms and of the Salaagol Fm for each locality are presented in Figs. 4.8 and 9, respectively. The $\delta^{13}C$ values from seven measured sections of the Zuun-Arts Fm are presented here. The top of the Zuun-Arts Fm is marked by at least one large negative excursion that has a minimum of ~-7‰. This excursion was recognized by previous workers (referred to as anomaly "W"), and has been correlated globally with the negative $\delta^{13}C$ excursion that, despite some uncertainty in precise correlations (see Babcock et al., 2014 for summary), has been found in association with the FAD of *T. pedum* (Brasier et al., 1996b; Corsetti and Hagadorn, 2000; Narbonne et al., 1994).

The $\delta^{13}C$ values from nine measured sections of the Bayangol Fm are presented here. Brasier et al. (1996b) identified positive excursions B-F in the Bayangol Fm, and data presented here confirm the existence of at least 5 positive excursions. All measured sections presented here show high frequency oscillations in $\delta^{13}C$ values that range between ~-6 and +6‰. Interestingly, the positive excursions are sharp and pronounced whereas the negative excursions have less-pronounced minimum values. The limestone beds in BG5 from Orolgo, Bayan, and Khunkher gorges, the three gorges that have

exposure of carbonates in the upper Bayangol Fm, have unusually high $\delta^{13}C$ values of <+6‰.

The $\delta^{13}C$ profiles for the Salaagol Fm were surprisingly different from the previously reported $\delta^{13}C$ values from Salaa Gorge and Zuun-Arts Ridge (Brasier et al., 1996b). In Orolgo Gorge, the $\delta^{13}C$ values are as high as 7‰. In Salaa Gorge and in SE Taishir, the $\delta^{13}C$ values in the lower-middle part of the section reach ~+4.5‰. The $\delta^{13}C$ values in the upper part of the measured sections at Salaa Gorge, Khukh-Davaa, and SE Taishir drop to ~-2 to -1‰. Brasier et al. (1996b) report 23 $\delta^{13}C$ values that range between -0.6 and -1.6‰ from 44 m of strata of the Salaagol Fm at Zuun-Arts locality and $\delta^{13}C$ values that range between -0.2 and -1.2‰ from 22 samples from the upper 117 m of the Salaagol Fm at Salaa Gorge. The discrepancy between the range of $\delta^{13}C$ values reported here and previously reported values is the result of earlier workers only sampling the upper portions of the Salaagol Fm.

4.5. Discussion

4.5.1. Facies model and sequence stratigraphy

Within the Zuun-Arts through Khairkhan succession, there are several major sequence boundaries that can be used as stratigraphic tie lines across the basin. The phosphatic shale units at the bases of the Zuun-Arts and Bayangol fms vary in thickness and color but are easily recognizable stratigraphic markers of transgressions in the sequence. The phosphatic shale at the base of the Bayangol Fm is a distinct stratigraphic marker that we use as the datum upon which to align the sections in Fig. 4.8. The sequence boundaries with the Bayangol Fm are discussed in detail below. The top contact of the Salaagol Fm with the Khairkhan Fm is marked by a LST overlain by a sharp

transgression that, in some sections, is marked by a phosphatic hardground overlain by phosphatized SSFs, archaeocyaths, and coated grains. In many sections, this contact is faulted, perhaps because the contact represents a sharp rheologic boundary between a massive limestone reef and more fissile mixed siliciclastic units. Nonetheless, there are many sections that are well-preserved and not compromised by faulting for which the transgression can be used as the datum for the sections in Fig. 4.9.

The tie lines in Figs. 4.8 and 4.9 show how the measured sections in the Zavkhan Terrane correlate to one another using major sequence boundaries within the Bayangol and Salaagol fms. Portions of the major sequences within the Bayangol Fm are also shown and annotated in photographs from portions of the sections in N Khukh-Davaa Pass and S Bayan Gorge in Fig. 4.4. Generally, the massive carbonate reefs that cap each informal member of the Bayangol Fm represent the HST of the sequences, with the MFS near the base of each of these. These are in turn overlain by medium to coarse sands that represent the LST of the sequences. The thicknesses of the LSTs and TSTs varies between sections, depending on a section's proximity to the shoreline. The more distal sections tend to preserve thinner LSTs and thicker TSTs than the more proximal ones.

Complicating the identification of major sequence system tracts are minor shallowing-up sequences within the large sequences as well as bypass channel sands. Obvious examples of bypass channel sands are in members BG4 and BG5 of the Khunkher Gorge section (Fig. 4.10). The nearby sections contain ~150 m thick limestone reefs capping BG4 and BG5, whereas the section in Khunkher Gorge instead has relatively thin limestone units with abundant oncolite, ooid, and calcarenite beds at the same stratigraphic horizon. The $\delta^{13}C$ chemostratigraphic curves provide independent

confirmation that the lithologically different units of BG4 and BG5 units of Orolgo and Khunkher gorges were being deposited synchronously.

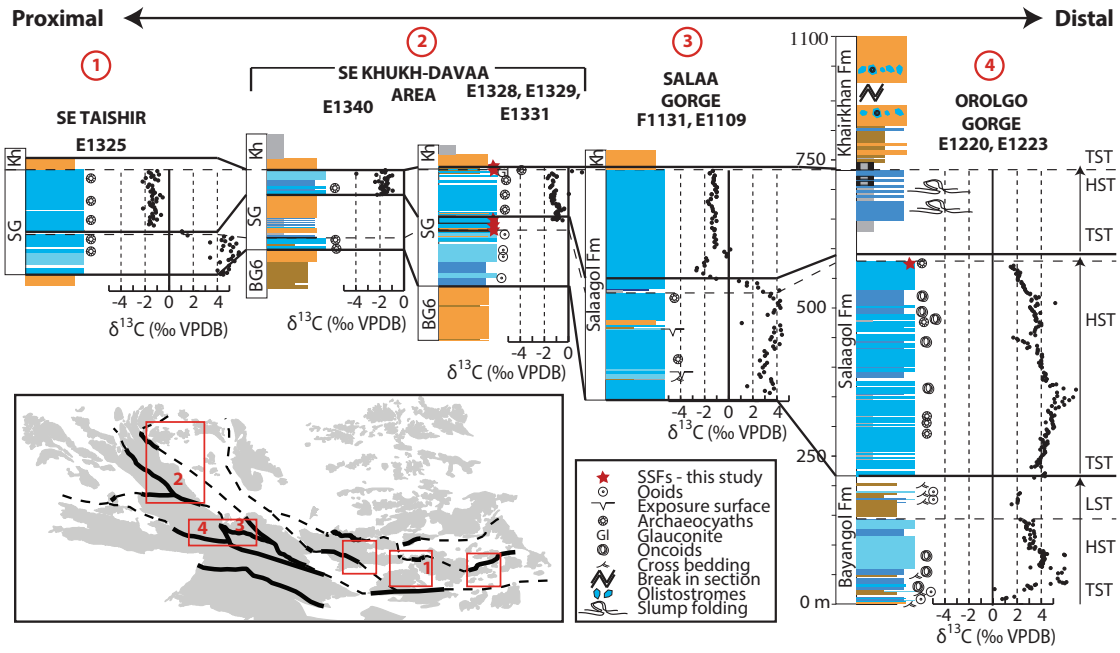

Figure 4.9. Integrated lithostratigraphy, sequence stratigraphy, and carbon isotope chemostratigraphy of the uppermost Bayangol, Salaagol, and Khairkhan formations.

The five measured sections are numbered according to proximity to the paleo-shoreline, with more distal sections on the right and more proximal sections on the left. Locations of the individual measured sections are shown on the map in the lower left side of the figure. (precise locations of measured sections are indicated on Fig. 4.6. The sections are correlated using the LST of the sequence. Lithologies are the same as those used in Fig. 4.8

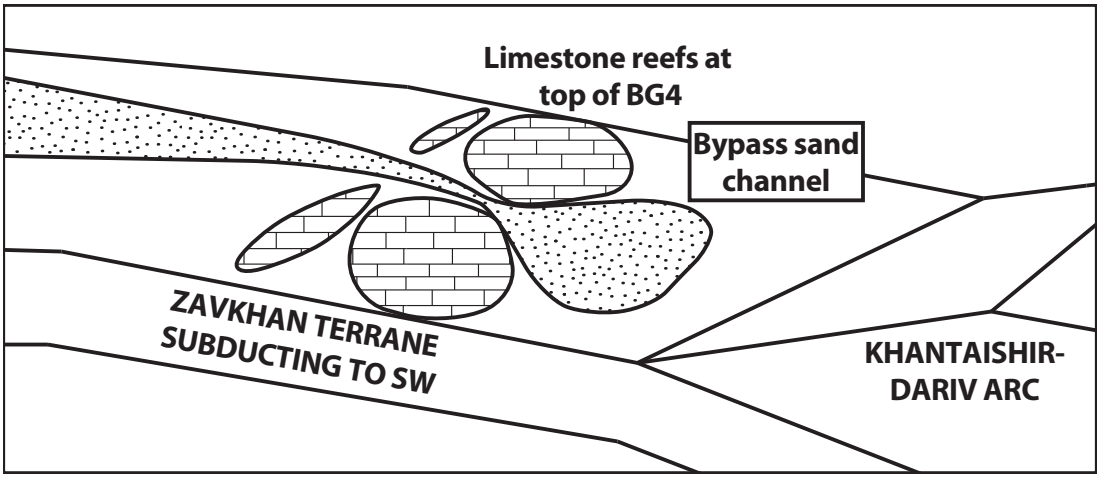

Figure 4.10. Schematic depositional model for member BG4 of the Bayangol Formation.
Evidence for bypass channel sands exist in the measured section of the upper Bayangol Fm in Khunkher Gorge (Fig. 4.8).

One interesting feature of the integrated chemostratigraphy and sequence stratigraphy is that the large $\delta^{13}C$ excursions of the Bayangol Fm generally seem to occur at the same frequency as the major sequence boundaries. With sedimentological, stratigraphic, and chemostratigraphic data from across the basin, mechanistic hypotheses about the relationships between feedbacks in sea level, associated nutrient input, and the carbon cycle can begin to be tested with data from the rock record. The negative $\delta^{13}C$ excursions rarely coincide with major sequence boundaries, but the pronounced positive $\delta^{13}C$ excursions are often found preserved between the TST and the HST of the sequences. Using the age model presented herein and the resulting estimates for sedimentation rates, below we calculate the lag time between transgressions and positive $\delta^{13}C$ excursions.

An important tectonic result of the new facies model for the Zavkhan Terrane is the documentation of the deep-water, allochthonous facies of the Khairkhan Fm in northern Orolgo Gorge (Fig. 4.7A). These include poorly-sorted conglomeratic facies of the Khairkhan Fm that contain ultramafic clasts. Nearby, the Khairkhan and Salaagol fms are in thrust contact with the large ultramafic body (Figs. 4.6E and 4.7B). The second deep-water facies of the Khairkhan Fm is hundreds of meters of very finely laminated siltstone in the area just to the north of Orolgo Gorge (Figs. 4.7A and C). We suggest that the deeper water facies of the Khairkhan Fm are allochthonous to the Zavkhan Terrane, bolstering the stratigraphic argument that the late Ediacaran to early Cambrian strata were deposited in a foreland basin (Macdonald et al., 2009). Thus, although small-scale transgressions associated with positive $\delta^{13}C$ excursions may be global and eustatic, the larger-scale sequences and basin architecture are undoubtedly the product of local tectonism.

4.5.2. Constructing a composite carbon isotope curve for the Zavkhan Terrane

The $\delta^{13}C$ chemostratigraphic data are generally consistent with the sequence stratigraphic correlations used in Figs. 4.8 and 4.9. In Fig. 4.11 the composite curve is presented next to the $\delta^{13}C$ curve from Orolgo Gorge, the most expanded, carbonate-dominated section in the Zavkhan Terrane in which 2p-6p are preserved. Details regarding the specific tie points used in each of the late Ediacaran to early Cambrian Mongolian formations are discussed below in stratigraphic order. The specific $\delta^{13}C$ values that were used as tie points between sections in the Zavkhan Terrane are in the supplementary material.

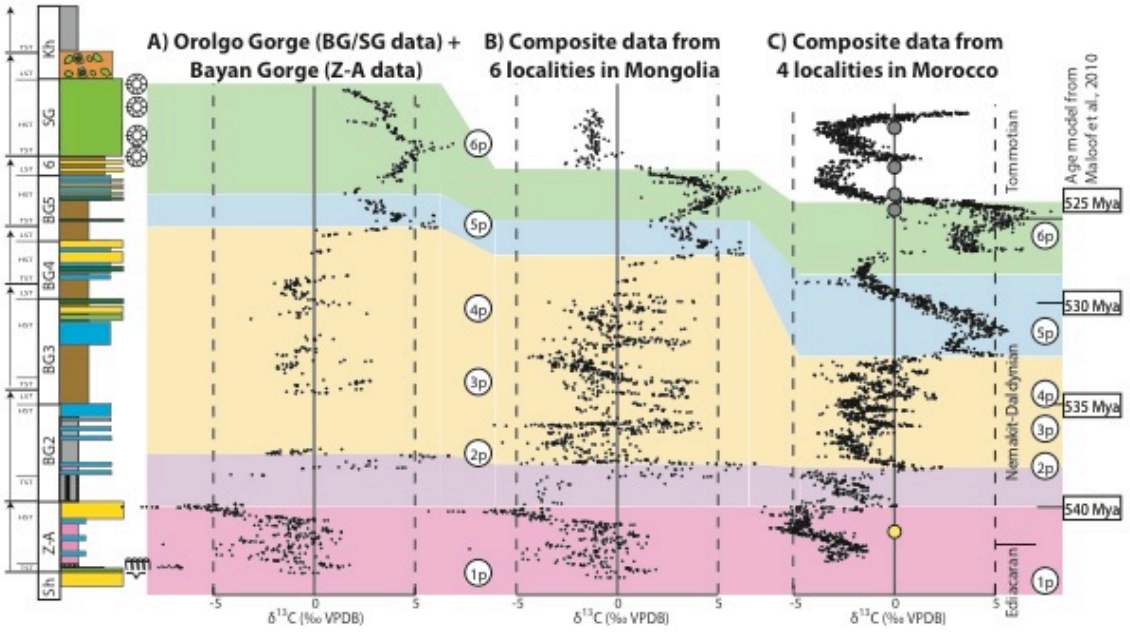

Figure 4.11. Revised carbon isotope chemostratigraphic age model for the Zuun-Arts through Salaagol formations in the Zavkhan Terrane.
A) $\delta^{13}C$ isotopes plotted next to a generalized stratigraphic column for the Zuun-Arts Fm at Bayan Gorge and the Bayangol through Khairkhan fms at Orolgo Gorge. Here, $\delta^{13}C$ values are plotted against measured thickness. These data are plotted because Orolgo Gorge has the thickest, most carbonate-dominated section of the Bayangol and Salaagol fms. B) A composite $\delta^{13}C$ curve of six sections from the Zavkhan Terrane. Generally, sections are correlated using sequence stratigraphy, and here, the composite curve is constructed by using positive $\delta^{13}C$ excursions for tie points and stretching the $\delta^{13}C$ curves between. The uppermost Salaagol and Khairkhan fms are Tommotian in age. C) A composite $\delta^{13}C$ curve from 4 localities in Morocco, a locality where there are absolute age constraints (Maloof et al., 2010a; Maloof et al., 2010b). Here, $\delta^{13}C$ values are plotted against age. U/Pb tie points are marked by yellow (Oman: Bowring et al., 2007) and gray (Maloof et al., 2005; 2010a) circles. The age model on the right side of the figure is from Maloof et al., 2010a. The transparent colored boxes show how these three $\delta^{13}C$ chemostratigraphic curves correlate to each other. Following Maloof et al. (2010a), positive excursions in the late Ediacaran through Nemakit-Daldynian are numbered and labeled with white circles.

Although high-resolution $\delta^{13}C$ chemostratigraphic correlation within the Zuun-Arts Fm is complicated by high-frequency variability in the lower half of the Formation, there is one large negative excursion that is <9.5‰ in magnitude preserved near at the top of all measured sections of the Zuun-Arts Fm. The more proximal sections (Taishir and

KTN) preserve a negative $\delta^{13}C$ excursion in the middle of the Formation. The lateral variability within the Zuun-Arts Fm is the result of diachronous deposition. The two phosphatic shales the bookend the Formation mark two transgressions that represent two synchronous sequence boundaries across the Zavkhan Terrane. Using this sedimentological and sequence stratigraphic argument, the upper part of the Zuun-Arts Fm in the proximal sections cannot be correlative with the lower Bayangol Fm in the more distal sections.

Correlations between the nine measured sections of the Bayangol Fm are not as straightforward as those in the Zuun-Arts and Salaagol fms for three reasons: 1) unlike the other two formations, there is not continuous carbonate deposition in the Bayangol Fm, 2) there are large lateral changes in facies and bed thickness across the basin that are further complicated by sandstone-filled bypass channels, and 3) the carbon cycle is rapidly oscillating during the earliest Cambrian with several excursions that, taken alone, are non-distinct. To further complicate correlations, compared to the very smooth $\delta^{13}C$ profile with five clear positive excursions from Sukharikha, Siberia (Kouchinsky et al., 2007), the sections of the Bayangol Fm preserve additional minor excursions (Fig. 4.8).

The magnitude of the positive excursions as well as the thicknesses over which they occur varies between the sections. It is also clear from comparing both the lithostratigraphy and chemostratigraphy between measured sections that the facies transitions are diachronous across the basin. This interpretation is supported by comparing the sections from Khunkher and Orolgo gorges (Fig. 4.8); the chemostratigraphic profiles for the upper parts of the Bayangol Fm are almost identical, but the lithostratigraphy is very different. There is also obvious diachroneity between the

two measured sections near Khukh-Davaa Pass, with the chemostratigraphic profiles closely matching each other but with noticeable differences in the lithostratigraphy. These are just two of many obvious examples of how lithologically variable the sections of the Bayangol Fm are, highlighting the importance of the integrated approach used here.

One interesting chemostratigraphic feature is the positive excursion (~7‰) at the base of the measured section at Orolgo Gorge. Sedimentologically, the basal part of this section looks very different from any other section because it contains a much thicker section of phosphatic shale, black shale, and interbedded limestone. We have interpreted this portion of the stratigraphy as an expanded basal part of the Bayangol Fm. It is important to note; however, that the sharp drop from positive to negative $\delta^{13}C$ values occurs across a sharp sedimentological contact that contains a phosphatic hardground, phosphatized ooids, and pyrite pseudomorphs (Fig. 4.3G). We have interpreted this as a small unconformity in the succession.

Compared to the correlations within the lower formations, sequence and chemostratigraphic correlations between sections of the Salaagol Fm (Fig. 4.9) are relatively straightforward. Comparison of the sedimentology and chemostratigraphy between sections demonstrates that there is diachronous deposition of this formation and large facies changes across the basin. This interpretation is supported by comparing parts of the formation between the sections at Orolgo (E1220) and Salaa Gorge (F1131 and E1109). The section at Orolgo Gorge is much more expanded with abundant oncolite beds. Also of note is that across a sequence boundary in the Salaagol Fm, $\delta^{13}C$ values jump from positive to negative. The details and age model implications of this change in $\delta^{13}C$ values are discussed below.

4.5.3. Refined age model

Carbon isotope chemostratigraphy is useful as both a correlation tool and, with the absence of absolute ages, for constructing a more precise age model that can be used to correlate between the composite $\delta^{13}C$ curve from the Zavkhan Terrane and other sections globally that do contain absolute ages. Additionally, under the assumption that changes in $\delta^{13}C$ values mark synchronous, global markers, chemostratigraphic correlation avoids circular arguments that result from correlating poorly-established, facies dependent, and highly regional paleontological biozones.

We correlate the largest negative $\delta^{13}C$ excursion at the top of the Zuun-Arts Fm with other negative $\delta^{13}C$ excursions that have been documented globally near the E-C boundary in localities that include Morocco, China, Siberia, Oman, the Western United States, and Northwestern Canada (Corsetti and Hagadorn, 2000; Kouchinsky et al., 2007; Li et al., 2009; Maloof et al., 2005; Narbonne et al., 1994). This negative excursion at the E-C boundary, the high frequency oscillations during the Nemakit-Daldynian, and the two very high excursions at the end of the Nemakit-Daldynian and in the early Tommotian (Kouchinsky et al., 2007; Maloof et al., 2010a; Maloof et al., 2005), are all present in the Zavkhan Terrane strata, increasing confidence in the use of $\delta^{13}C$ chemostratigraphic profiles as a tool for global correlation.

Here, we map late Ediacaran and early Cambrian records of $\delta^{13}C$ variability from Mongolia onto the Moroccan $\delta^{13}C$ record, which is constrained with absolute U/Pb ages from Morocco (Maloof et al., 2010b; Maloof et al., 2005) and Oman (Bowring et al., 2007). Although Morocco lacks fossils in the earliest Cambrian, it has a very expanded $\delta^{13}C$ curve from four localities with four Chemical Abrasion Isotope Dissolution Thermal

Ionization Mass Spectrometry (CA-ID-TIMS) U/Pb zircon ages on ash beds of 525.343 ± 0.088 Ma (Maloof et al., 2005, 2010a), 524.837 W 0.092 Ma (Maloof et al., 2010a), 523.17 ± 0.16 Ma (Maloof et al., 2010a), and 520.93 ± 0.14 Ma (Landing et al., 1998; Compston et al., 1992; Maloof et al., 2010a). The age from the E-C boundary is a CA-ID-TIMS U/Pb zircon age on an ash bed from Oman dated at 541.00 ± 0.29 Ma (Bowring et al., 2007; Gradstein et al., 2012).

Although there is some uncertainty in precise chemostratigraphic correlation between the Mongolia and Morocco composite curves, large-scale uncertainty is mitigated by the unambiguous end-Ediacaran negative excursion and the end Nemakit-Daldynian positive excursion. High frequency $\delta^{13}C$ oscillations during the earliest Cambrian are book-ended by these two easily identifiable chemostratigraphic markers that are preserved in both Mongolia and Morocco. Following Kouchinsky et al. (2007) and Maloof et al. (2010a), we assign the positive excursions numbers 2 through 6 (1 is the positive excursion during the end-Ediacaran). It is interesting that both in Mongolia and Morocco, there appear to be additional minor excursion between 1p and 2p, 3p and 4p, and 4p and 5p, suggesting that the carbon cycle was oscillating even more rapidly than previously thought during the earliest Cambrian.

This refined age model results in a couple important new interpretations about the age of the strata in the Zavkhan Terrane. The first is that the Bayangol Fm is entirely Nemakit-Daldynian in age rather than extending into the Tommotian as was previously suggested. The evidence supporting this interpretation is the very high $\delta^{13}C$ values of ~7‰ near the top of the measured sections of the Bayangol Fm in Bayan, Khunkher, and Orolgo gorges. The only two times during the early Cambrian that the $\delta^{13}C$ values are

this high is during the middle to late Nemakit-Daldynian. A second important point is that there is a second very high $\delta^{13}C$ excursion that begins in the uppermost Bayangol Fm and reaches values of 8‰ in the lower Salaagol Fm. The level of peak values is most clearly documented at Orolgo Gorge but is reproduced in other measured sections of the Salaagol Fm as well (Figs. 4.8 and 4.9).

This second very high $\delta^{13}C$ peak coincides with the FAD of archaeocyaths in the Zavkhan Terrane. Correlating this $\delta^{13}C$ excursion with the excursion at the Nemakit-Daldynian to Tommotian boundary distinguishes the archaeocyaths in the lower to middle Salaagol Fm as among the earliest documented archaeocyaths globally. The $\delta^{13}C$ values between the two high peaks in Mongolia are not as low as the -2 to -1‰ values in Morocco, which we interpret representing a small unconformity in the conglomerate beds just below the base of the Salaagol Fm.

Unfortunately the $\delta^{13}C$ values of -2 to 0‰ of the upper Salaagol Fm are not diagnostic of $\delta^{13}C$ values of any one member in the early Cambrian, and are consistent with a Tommotian, Atdabanian, or a Botomian age. Here we discuss two possible age models for the upper Salaagol Fm. The first age model is that the Salaagol Fm is Nemakit-Daldynian to Tommotian in age with relatively continuous strata. This age model is based, in part, on the similarity between Sr isotope values from Tommotian strata in Siberia (Derry et al., 1994; Kaufman et al., 1996) and from the upper Salaagol Fm (Brasier et al., 1996b). It is also based on the complete lack of any trilobite fossils (whole or disarticulated) in the upper Salaagol and Khairkhan fms, which would be expected if these units were Atdabanian or Botomian in age.

However, this age model is in conflict with the archaeocyath biostratigraphy from the Zavkhan Terrane, which uses a few archaeocyath species that are thought to be diagnostic of the Atdabanian and Botomian stages. Most of the archaeocyaths collected by Kruse et al. (1996) from the Salaagol Fm range from the Tommotian to Botomian in age; however, there are a few species that include *Tabulacyathellus bidzhaensis*, *Archaeopharetra marginata*, *Couberticyathus Lepidus, Robustocyathellus abundans, Orbicyathus mongolicus,* and *Ladaecyathus melnikovae,* that are thought to be restricted just to the Atdabanian and/or Botomian (Paleobiology Database). We emphasize that the age ranges for these specimens were calibrated in just Siberia, and thus it is possible that globally these specimens have a longer stratigraphic extent. The second age model for the Salaagol Fm, which is based on the robustness of using these few archaeocyth species for biostratigraphy, requires there to be a 6-10 million year unconformity in the medium sandstone to pebble conglomerate beds of the middle-upper Salaagol Fm (Fig. 4.9).

The second age model necessitates a multi-stage subsidence history in which the margin subsides for ~15 million years, there is a hiatus for 6-10 million years, and then subsides again for a few million years during deposition of the upper Salaagol and Khairkhan fms. The 6-10 million year hiatus in subsidence could reflect either slab break off or the passing of a peripheral forebulge before the final obduction of the allochthonous flysch of the Khairkhan Fm. The subsidence history for the first age model is much simpler, with a margin that is subsiding for 16-20 million years before the final collision of the Khantaishir-Dariv Arc. With a lack of trilobites, Tommotian-like Sr values, and a simpler subsidence mechanism, we prefer the first age model for the upper Salaagol and Khairkhan fms (Fig. 4.11). We suggest that the few archaeocyath species

from the upper Salaagol Fm that are thought to be diagnostic of the Atdabanian or Botomian were either misidentified or have longer stratigraphic ranges than was previously thought.

4.5.4. Refined biostratigraphy

By placing the previously described fossil horizons in an accurate sequence and chemostratigraphic framework, a new composite biostratigraphic range chart for ichnofossils and body fossils is compiled for the Zavkhan Terrane (Fig. 4.12). Additionally, this work establishes the necessary framework for more detailed paleontological studies in new sections from across the basin.

One important result is that this work helps resolve the long-standing problem of understanding the relative timing of the FAD of *T. pedum*, the FAD of SSFs, and the negative excursion that is associated with the E-C boundary. By adhering strictly to the GSSP definition of the boundary as the horizon that coincides with the FAD of *T. pedum* (Landing, 1994), the E-C boundary in the Zavkhan Terrane would be placed between members BG3 and BG4 (Fig. 4.12), contradicting other lines of evidence that suggest the boundary is much lower. These lines of evidence include 1) the FAD of *T. pedum* is ~275 m above the large negative carbon isotope excursion, which has been commonly used as a secondary chronostratigraphic marker (Brasier et al., 1996b; Grotzinger et al., 1995; Maloof et al., 2010a; Maloof et al., 2005; Peng et al., 2012; Zhu et al., 2006), in the Zuun-Arts Fm, 2) the FAD of *T. pedum* is ~250 m above the FAD of SSFs, and 3) the FAD of *T. pedum* is stratigraphically above the FAD of *Rusophycus*, which inverts the normal ichnofossil biostratigraphy (Crimes, 1987; Crimes, 1992; MacNaughton and Narbonne, 1999). The facies dependence and rarity of *T. pedum* in the Zavkhan Terrane

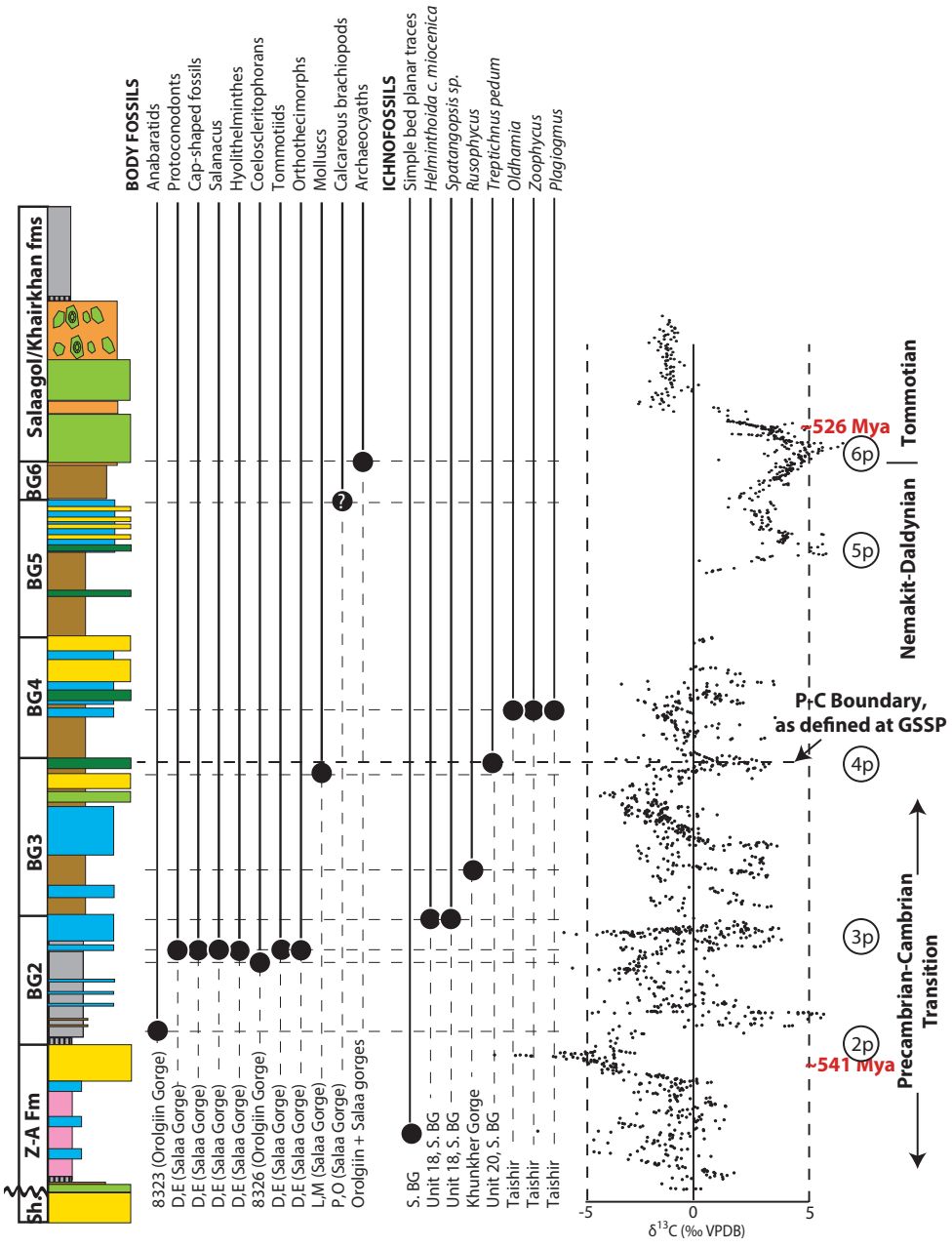

Figure 4.12. Composite SSF and ichnofossil biostratigraphic range chart with revised carbon isotope chemostratigraphic age model.

FADs in the fossil record are from previous workers (Brasier et al., 1996b; Endonzhamts and Lkhasuren, 1988; Esakova and Zhegallo, 1996; Khomentovsky and Gibsher, 1996; Korobov and Missarzhevsky, 1977; Voronin et al., 1982). Marker beds and section locations are listed below each circled FAD. Bold red line marks a depositional hiatus. Generic and higher group assignments used here are consistent with those from Maloof et al. (2010a) and references therein.

provide further support for reassessing the E-C boundary with a marker that is not as facies dependent as the first evolutionary appearance of the behavior represented by *T. pedum*.

We were not able to reproduce any of the previous claims that the FAD of SSFs is in the basal Zuun-Arts Fm, and we attribute the previous placement to misidentifying the phosphatic shales at the basal Bayangol Fm as those at the basal Zuun-Arts Fm. With the FAD of SSFs shifted stratigraphically up into the basal Bayangol Fm, globally, the FAD of SSFs and *T. pedum* only occur stratigraphically above the large negative carbon isotope excursion at the top of the E-C boundary (Brasier et al., 1990; Knoll et al., 1995b; Kouchinsky et al., 2001; Kouchinsky et al., 2007; Zhou et al., 1997). The one section globally that is a possible exception to this is the section at Khorbusuonka River (Knoll et al., 1995a).

Many of the SSF FAD horizons in the Zavkhan Terrane (tommotiids, orthothecimorphs, hyolithelminths, cap-shaped fossils, protoconodonts, *Salanacus*) are from beds "D" and "E" in the Salaa Gorge (Esakova and Zhegallo, 1996; Voronin et al., 1982). With the revised correlations and age model presented here, we place these between positive excursions 2p and 3p (Figs. 4.8 and 4.12) instead of between 1p and 2p (Maloof et al., 2010a). Other important fossils for calibrating biostratigraphic ranges globally are the molluscs *Watsonella* and *Aldanella* (Li et al., 2011; Parkhaev, 2007; Parkhaev et al., 2011; Rozanov et al., 2008; Steiner et al., 2007); however, more recently the FADs of both taxa have been shown to be diachronous both locally and globally (Landing et al., 2013). *Watsonella* has only been documented in one SSF horizon in the

upper Bayangol Fm at Salaa Gorge, whereas *Aldanella* has not been found in the Zavkhan Terrane.

4.5.5. Global origination rates during the earliest Cambrian

With the revised mapping, stratigraphy, and age model we have adjusted the FADs of SSFs in Mongolia. Previously, early Cambrian origination has been assessed with global FADs of SSFs (Maloof et al., 2010a); however, because these compilations have been limited to three localities, namely Siberia, China, and Mongolia, updating the age model or occurrence data for any one region causes adjustments to apparent global origination rates. Fig. 4.13 combines the new data from Mongolia with data from China and Siberia to show globally the number of SSF genera that first appear in each time bin of 2 million years.

The global compilation of fossil occurrence data still shows pulses of the first appearances of new genera during the earliest Cambrian. One possibility is that these peaks of fossil first appearances reflect peaks of diversification. Another possibility is that these fossil first appearance peaks instead reflect regional or global sedimentation patterns and/or taphonomic biases. The regional distribution of FADs for each peak as shown in Fig. 4.13 demonstrates that each of the three peaks is dominated by one region. This pattern suggests that periods of deposition and the facies dependence of phosphatized fossils are the primary controllers of the FAD peaks in Fig. 4.13. For example, in Mongolia, nearly all of the SSFs are in the lower to middle Bayangol Fm that contain phosphatic limestone beds, whereas SSFs are rare in the upper Bayangol Fm which consists almost entirely fine to medium grained sandstone, which are not the appropriate facies to preserve phosphatized SSFs. This lack of appropriate facies is most

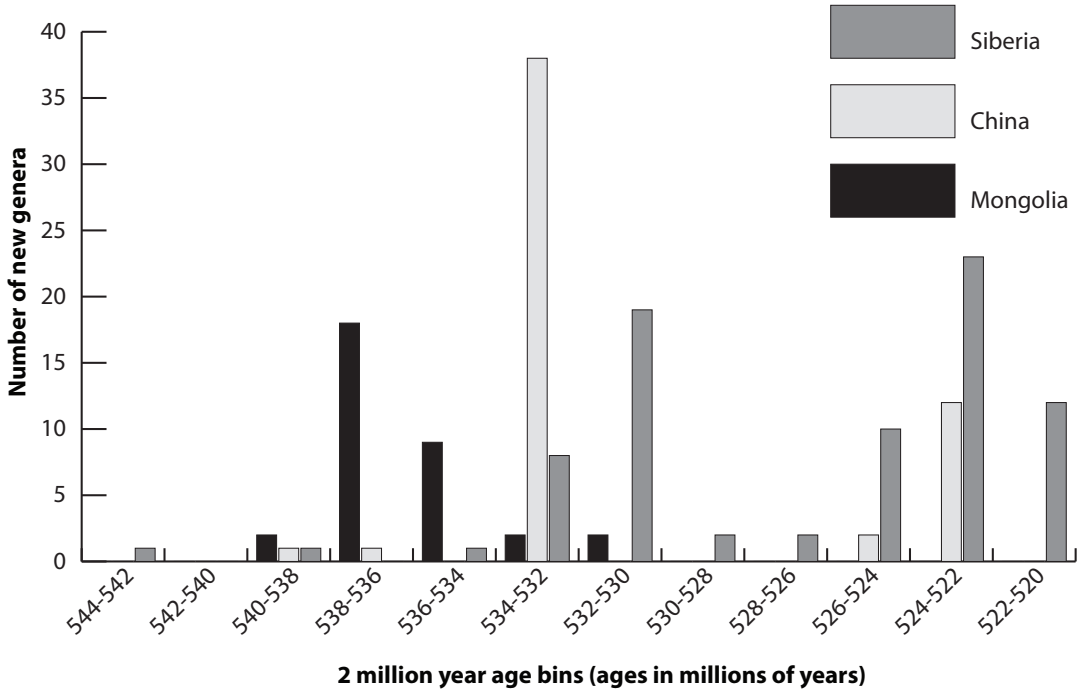

Figure 4.13. Number of new genera appearing in two million year time bins with revised age model from Mongolia.
Data from China and Siberia are modified from Maloof et al. (2010a).

likely due to the fact that these units were being deposited during the closure of the foreland basin rather than due to the closure of the phosphatization window at the end of the early Cambrian (Porter, 2004).

The second pulse of fossil FAD is due almost entirely to a huge number of FADs from China. These fossils come from the phosphatic limestone of the Zhongyicun Member. The apparent large spike in FADs in the Zhongyicun Member is due in part to

three major disconformities in the strata: one at the E-C boundary, the one in the lower Dahai Member, and one at the top contact of the Dahai Member (Steiner et al., 2007). An erosional surface at the top of the Dengying Formation has been observed in the Meishucun section (He et al., 1988; Qian et al., 1996). The result is that, particularly in the southern sections of Yunnan Province, the Daibu Member and portions of the Zhongyicun Member are missing (Steiner et al., 2007). In the overlying Nemakit-Daldynian to Tommotian upper Zhongyicun and lower Dahai members, there are also several disconformities, erosional surfaces, and phosphatic hardgrounds including a sub-Tommotian one in the sequence (Qian and Bengtson, 1989; Steiner et al., 2007; Yang et al., 2014), which helps to explain the dearth of FADs during the late Nemakit-Daldynian. There is another major disconformity at the boundary between the Dahai Member and the overlying Shiyantou Fm. In the Meishucun section, one of the key fossil localities in this compilation, most of the Dahai Member is missing due to non-deposition or later erosion. As SSF FADs from new sections in S. China continue to be added to this compilation and as regional and global correlations continue to be refined, the pulsed pattern of global FADs will most certainly change.

Finally, in many of the fossiliferous Siberian sections, there is a sub-Tommotian unconformity (Khomentovsky and Karlova, 1993; Knoll et al., 1995b; Zhu et al., 2001). We suggest that the apparent pulses of fossil first appearances are the result of intervals of non-deposition in the sections included in this compilation and do not represent global evolutionary patterns; FADs will not be found during periods in which sediment is not deposited. Charles Darwin (1859) suggested that the apparently rapid appearance of

fossils found in Cambrian strata was a product of the incompleteness in the stratigraphic record—at a smaller scale, this indeed may be the case.

4.5.6. Implications for early Cambrian carbon isotope variability

The large-amplitude, high-frequency excursions of inorganic $\delta^{13}C$ values that accompany the Cambrian radiation have long perplexed geologists. Brasier and Lindsay (2001) suggest that the $\delta^{13}C$ excursions are modulated by sea level change, which, in effect, change rates of organic carbon burial. They suggest that the positive excursions are the result of marine transgressions and the increase in the burial of organic matter, and the negative excursions are the result of regressions and the reduced rates of organic matter burial. Kirschvink and Raub (2003) offer an alternative methane fuse hypothesis in which the $\delta^{13}C$ excursions are attributed to the periodic release of large volumes of methane gas, which they attributed to seismic activity, sediment failure, or sediment erosion. Similarly, Maloof et al. (2005) invoke Paleocene-Eocene Thermal Maximum-like rapid (<100,000 years) releases of methane or organic carbon to explain the high-frequency negative excursions in the earliest Cambrian. Squire et al. (2006) elaborated on this hypothesis by suggesting that the periodic release of methane trapped in sedimentary rocks was the consequence of rapid erosion of the Transgondwanan Super-mountain. Maloof et al. (2010a) modified their earlier hypothesis for the drivers of geochemical change by stating that the rapidity and magnitude of the early Cambrian $\delta^{13}C$ excursions require volcanic outgassing that are up to an order of magnitude larger than modern fluxes and a 2.25 times increase in seafloor spreading during the early Cambrian. More recently, Schrag et al. (2013) suggested that the burial of authigenic carbonate was an important sink of carbon in anoxic oceans, and that the advent of bioturbation or

variations in surface redox could have resulted in fluctuations in the size of this additional carbon sink.

Coupled sequence and chemostratigraphy in Mongolia demonstrate that the negative $\delta^{13}C$ excursions occur predominantly in HSTs to LSTs and the positive $\delta^{13}C$ excursions occur in TSTs to HSTs. None of the hypotheses described above provide direct explanations for a mechanistic link between eustatic sea level change and the isotopic variations. If a weathering process is invoked, the isotopic variability indicates differential weathering of nutrients (i.e., phosphorous) that lead to organic carbon burial versus silicate weathering that leads to carbonate burial. Alternatively, nutrient availability due to recycling on the continental shelf or slope might explain carbon isotope changes linked to sea level. It is also possible that authigenic carbonate may have varied with sea level changes due to differential organic burial and anaerobic oxidation in slope sediments (Schrag et al., 2013). On the other hand, the sequence architecture in the Zavkhan Terrane could have been driven by regional tectonic forces that have no bearing on the global carbon cycle. However, large-scale sequence boundaries in the Zavkhan Terrane occur at roughly the same frequency as positive $\delta^{13}C$ excursions. Using the same calibration points for the positive excursions as Maloof et al. (2010a) and assuming constant rates of sedimentation between the excursions, we estimate the lag time between a maximum flooding surface and a positive excursion between the TST and HST as being between 200,000 and 500,000 years. These rates are highly dependent on the choice of calibration points for the positive excursions, and will continue to be refined as more early Cambrian ash horizons are dated globally. If there were high latitude glaciers during the late Ediacaran and early Cambrian, the large-scale sequences could be consistent with

Milankovitch cycles (Baode et al., 1986; Chumakov and Elston, 1989; Chumakov, 2011a; Chumakov, 2011b; Etemad-Saeed et al., 2015; Hebert et al., 2010; Meert and Van der Voo, 1994; Rice et al., 2011; Stodt et al., 2011; Torsvik et al., 1996; Zhu and Wang, 2011). Nonetheless, the repeating nature and scale of the oscillation, together with evidence of changing redox conditions (Schröder and Grotzinger, 2007; Wille et al., 2008), are suggestive of a forcing intrinsic to the carbon cycle, rather than external forcings such as volcanic or methane release.

4.6. Conclusion

A wide range of causes to explain the Cambrian radiation have been presented (review by Marshall, 2006); however, the strength of any of these explanations is limited by a precise calibration of rates of geochemical and biological change. Understanding the feedbacks between the radiation of animals and associated geochemical and environmental changes requires a precise age model and accurately calibrated fossil record. With new geological mapping, sequence stratigraphy, and a chemostratigraphic age model, we place previous SSF and ichnofossil finds into an accurate geological and temporal framework.

The new age model refines the age constraints on the Bayangol Fm to deposition entirely within the Nemakit-Daldynian. The Nemakit-Daldynian – Tommotian boundary is in the lower Salaagol Fm, coinciding with the FAD of archaeocyaths in the Zavkhan Terrane. The lack of trilobite fossils and Sr isotope chemostratigraphy suggest that the middle to upper Salaagol Fm is Tommotian in age rather than Atdabanian or Botomian as was previously suggested based on the identification of archaeocyath species with poorly constrained age ranges.

The FAD of SSFs in the Zavkhan Terrane is moved stratigraphically hundreds of meters up into the Bayangol Fm. With one possible exception (Knoll et al., 1995a), the FAD of SSFS and the FAD of *T. pedum* globally occurs above the nadir of the negative carbon isotope excursion at the base of the Cambrian. The FADs of tommotiids, orthothecimorphs, hyolithelminths, cap-shaped fossils, protoconodonts, and *Salanacus* are moved up to just below the positive $\delta^{13}C$ peak 3p. We demonstrate that with the new data from Monglia, there are still three pulses of fossil first appearances. We suggest that the pulsed nature of these first appearances is largely the result of surges in regional sedimentation and limited phosphatization windows in the sections in Mongolia, China, and Siberia rather than global evolutionary tempos. Rates of global origination and diversification during this evolutionarily critical transition remains an important problem for paleontologists and geologists, and future global correlations should include confidence intervals that take into account regional and local sampling biases.

With integrated sequence stratigraphy and high-resolution $\delta^{13}C$ chemostratigraphy, we show that the large $\delta^{13}C$ excursions and major sequence boundaries occur at roughly the same frequency in the Zavkhan Terrane, providing potential stratigraphic evidence that the high frequency carbon isotope excursions in the earliest Cambrian could have been modulated by global sea level change and corresponding weathering and burial events. Using a refined age model, we estimate that the lag time between maximum flooding surfaces and positive $\delta^{13}C$ excursions is 200,000-500,000 years. Combined, these data provide parameters and testable hypotheses to better constrain the relationships between biological and environmental change during this major transition in life.

4.7. Acknowledgements

We would like to thank A. Bayasgalan, B. Altantsetseg, S. Oyungerel, D. Oyun and S. Lkhagva-Ochir with logistical assistance in Mongolia. We would like to thank our field assistants G. Sarantuya, J. Chuluunbaatar, M. Delger, M. Jugder, A. Dorj, O. Dandar, U. Khuchitbaatar, A. Rooney, D. Bradley, S. Moon, C. Dwyer, R. Anderson, and E. Smith for the tremendous help in the field and lab. We thank J. Creveling and D. Jones for insightful comments and help with some of the initial fieldwork. We thank S. Porter, M. Zhu, E. Sperling, and A. Maloof for detailed and thoughtful reviews. We thank C. Bucholz for useful discussions. We thank S. Manley and G. Eischeid for the use of and assistance in laboratories at Harvard University. We thank NASA MIT Astrobiology node, NASA Exobiology, and NSF GRF to E. Smith for financial support.

4.8. References

Babcock, L.E., Peng, S., Zhu, M., Xiao, S. and Ahlberg, P., 2014. Proposed reassessment of the Cambrian GSSP. Journal of African Earth Sciences, 98: 3-10.

Baode, G., Ruitang, W., Hambrey, M. and Wuchen, G., 1986. Glacial sediments and erosional pavements near the Cambrian—Precambrian boundary in western Henan Province, China. Journal of the Geological Society, 143(2): 311-323.

Bezzubtsev, V.V., 1963. On the Precambrian-Cambrian stratigraphy of the Dzabkhan River Basin. Materials on the Geology of MPR, Gostopotekhizdat: 29-42.

Bold, U., Macdonald, F.A., Smith, E.F., Crowley, J.L. and Minjin, C., 2013. Elevating the Neoproterozoic Tsagaan-Olom Formation to a Group. Mongolian Geoscientist, 39(5).

Bowring, S.A., Grotzinger, J.P., Condon, D.J., Ramezani, J., Newall, M.J. and Allen, P.A., 2007. Geochronologic constraints on the chronostratigraphic framework of the Neoproterozoic Huqf Supergroup, Sultanate of Oman. American Journal of Science, 307(10): 1097-1145.

Brasier, M., Khomentovsky, V. and Corfield, R., 1993. Stable isotopic calibration of the earliest skeletal fossil assemblages in eastern Siberia (Precambrian-Cambrian boundary). Terra Nova, 5(3): 225-232.

Brasier, M., Shields, G., Kuleshov, V. and Zhegallo, E., 1996. Integrated chemo-and biostratigraphic calibration of early animal evolution: Neoproterozoic–early Cambrian of southwest Mongolia. Geological Magazine, 133(04): 445-485.

Brasier, M.D. and Lindsay, J.F., 2001. Did supercontinental amalgamation trigger the "Cambrian Explosion". The ecology of the Cambrian radiation: 69-89.

Brasier, M.D., Magaritz, M., Corfield, R., Huilin, L., Xiche, W., Lin, O., Zhiwen, J., Hamdi, B., Tinggui, H. and Fraser, A., 1990. The carbon-and oxygen-isotope record of the Precambrian–Cambrian boundary interval in China and Iran and their correlation. Geological Magazine, 127(04): 319-332.

Buatois, L.A., Almond, J. and Germs, G.J., 2013. Environmental tolerance and range offset of Treptichnus pedum: Implications for the recognition of the Ediacaran-Cambrian boundary. Geology, 41(4): 519-522.

Bucholz, C.E., Jagoutz, O., Schmidt, M.W. and Sambuu, O., 2014. Phlogopite-and clinopyroxene-dominated fractional crystallization of an alkaline primitive melt: petrology and mineral chemistry of the Dariv Igneous Complex, Western Mongolia. Contributions to Mineralogy and Petrology, 167(4): 1-28.

Calver, C., Crowley, J., Wingate, M., Evans, D., Raub, T. and Schmitz, M., 2013. Globally synchronous Marinoan deglaciation indicated by U-Pb geochronology of the Cottons Breccia, Tasmania, Australia. Geology, 41(10): 1127-1130.

Calver, C.R., Black, L.P., Everard, J.L. and Seymour, D.B., 2004. U-Pb zircon age constraints on late Neoproterozoic glaciation in Tasmania. Geology, 32(10): 893-896.

Chumakov, N. and Elston, D., 1989. The paradox of Late Proterozoic glaciations at low latitudes. Episodes, 12(2): 115-&.

Chumakov, N.M., 2011a. Glacial deposits of the Baykonur Formation, Kazakhstan and Kyrgyzstan. Geological Society, London, Memoirs, 36(1): 303-307.

Chumakov, N.M., 2011b. Glacial deposits of the Bokson Group, East Sayan Mountains, Buryatian Republic, Russian Federation. Geological Society, London, Memoirs, 36(1): 285-288.

Condon, D., Zhu, M.Y., Bowring, S., Wang, W., Yang, A.H. and Jin, Y.G., 2005. U-Pb ages from the Neoproterozoic Doushantuo Formation, China. Science, 308(5718): 95-98.

Corsetti, F.A. and Hagadorn, J.W., 2000. Precambrian-Cambrian transition: Death Valley, United States. Geology, 28(4): 299-302.

Crimes, P.T., 1987. Trace fossils and correlation of late Precambrian and early Cambrian strata. Geological Magazine, 124(02): 97-119.

Crimes, T.P., 1992. The record of trace fossils across the Proterozoic—Cambrian boundary, Origin and early evolution of the Metazoa. Springer, pp. 177-202.

Darwin, C.R., 1859. On the origin of species by means of natural selection, or the preservation of favoured races in the struggle for life. Murray, London.

Derry, L., Brasier, M., Corfield, R.e.a., Rozanov, A.Y. and Zhuravlev, A.Y., 1994. Sr and C isotopes in Lower Cambrian carbonates from the Siberian craton: a paleoenvironmental record during the 'Cambrian explosion'. Earth and Planetary Science Letters, 128(3): 671-681.

Dorjnamjaa, D. and Bat-Ireedui, Y., 1991. The Precambrian of Mongolia. Ulaanbaatar: Geological Institute of the Mongolian Academy of Sciences.

Dorjnamjaa, D., Bat-Ireedui, Y.A., Dashdavaa, Z. and Soelmaa, D., 1993. Precambrian-Cambrian Geology of the Dzavkhan Zone. Earth Sciences Department. Oxford, pp. 36.

Edel, J.B., Schulmann, K., Hanžl, P. and Lexa, O., 2014. Paleomagnetic and structural constraints on 90° anticlockwise rotation in SW Mongolia during the Permo–Triassic: Implications for Altaid oroclinal bending. Preliminary paleomagnetic results. Journal of Asian Earth Sciences, 94: 157-171.

Endonzhamts, Z. and Lkhasuren, B., 1988. Stratigraphy of the transitional beds between the Precambrian and Cambrian in the Zavkhan zone. , Pozdniy Dokembriy i Ranniy Paleozoy Sibiri, Izdatelstvo Instituta Geologii i Geofiziki, pp. 150-162.

Erwin, D.H., 1994. Early introduction of major morphological innovations. Acta Paleontologica Polonica, 38(3): 4.

Erwin, D.H., Laflamme, M., Tweedt, S.M., Sperling, E.A., Pisani, D. and Peterson, K.J., 2011. The Cambrian conundrum: early divergence and later ecological success in the early history of animals. Science, 334(6059): 1091-1097.

Esakova, N.V. and Zhegallo, E.A., 1996. Stratigrafaya i fauna nizhnego Kembriya Mongolii (Lower Cambrian stratigraphy and fauna of Mongolia). Sovmestnaya Sovetsko-Mongol'skaya Paleontologicheskaya Ekspeditsiya, 46: 208.

Etemad-Saeed, N., Hosseini-Barzi, M., Adabi, M.H., Miller, N.R., Sadeghi, A., Houshmandzadeh, A. and Stockli, D.F., 2015. Evidence for ca. 560Ma Ediacaran glaciation in the Kahar Formation, central Alborz Mountains, northern Iran. Gondwana Research.

Gehling, J.G., Jensen, S., Droser, M.L., Myrow, P.M. and Narbonne, G.M., 2001. Burrowing below the basal Cambrian GSSP, Fortune Head, Newfoundland. Geological Magazine, 138(02): 213-218.

Geyer, G., 2005. The Fish River Subgroup in Namibia: stratigraphy, depositional environments and the Proterozoic–Cambrian boundary problem revisited. Geological Magazine, 142(05): 465-498.

Geyer, G. and Uchman, A., 1995. Ichnofossil assemblages from the Nama Group (Neoproterozoic-Lower Cambrian) in Namibia and the Proterozoic-Cambrian boundary problem revisited. Beringeria Special Issue, 2: 175-202.

Gibsher, A. and Khomentovsky, V., 1990. The section of the Tsagaan Oloom and Bayan Gol Formations of the Vendian–Lower Cambrian in the Dzabkhan zone of Mongolia. The Late Precambrian and Early Paleozoic of Siberia. Institut Geologii I Geofiziki, Sibirskoe Otdelenie, Akademiya Nauk SSSR, Novosibirsk: 79-91.

Gibsher, A.S., Bat-Ireedui, Y.A., Balakhonov, I.G. and Efremenko, D.E. (Editors), 1991. The Bayan Gol reference section of the Vendian-Lower Cambrian in central Mongolia. Late Precambrian and Early Paleozoic of Siberia. Siberian Platform and its framework. Ob'edinennyy Institut Geologii, Geofiziki i Mineralogii, Sibierskoe Otdelenie, Akademiya Nauk SSSR, Novosibirsk, 151 pp.

Gibson, T., Myrow, P., Macdonald, F., Minjin, C. and Gehrels, G., 2013. Depositional history, tectonics, and detrital zircon geochronology of Ordovician and Devonian strata in southwestern Mongolia. Geological Society of America Bulletin, 125(5-6): 877-893.

Goldring, R. and Jensen, S., 1996. Trace fossils and biofabrics at the Precambrian–Cambrian boundary interval in western Mongolia. Geological Magazine, 133(04): 403-415.

Gradstein, F.M., Ogg, G. and Schmitz, M., 2012. The Geologic Time Scale 2012 2-Volume Set. Elsevier.

Grotzinger, J.P., Bowring, S.A., Saylor, B.Z. and Kaufman, A.J., 1995. Biostratigraphic and geochronologic constraints on early animal evolution. Science: 598-598.

He, T., Shen, L. and Yan, J., 1988. A new understanding on Meishucun Sinian-Cambrian Boundary Section in Jinning, Yunnan Journal of Chengdu University of Technology (Science & Technology Edition), 3: 005.

Hebert, C.L., Kaufman, A.J., Penniston-Dorland, S.C. and Martin, A.J., 2010. Radiometric and stratigraphic constraints on terminal Ediacaran (post-Gaskiers) glaciation and metazoan evolution. Precambrian Research, 182(4): 402-412.

Hoffman, P., 1967. Algal stromatolites: use in stratigraphic correlation and paleocurrent determination. Science, 157(3792): 1043-1045.

Jahn, B.-M., Litvinovsky, B., Zanvilevich, A. and Reichow, M., 2009. Peralkaline granitoid magmatism in the Mongolian–Transbaikalian Belt: evolution, petrogenesis and tectonic significance. Lithos, 113(3): 521-539.

Johnston, D., Macdonald, F., Gill, B., Hoffman, P. and Schrag, D., 2012. Uncovering the Neoproterozoic carbon cycle. Nature, 483(7389): 320-323.

Kaufman, A.J., Knoll, A.H., Semikhatov, M.A., Grotzinger, J.P., Jacobsen, S.B. and Adams, W., 1996. Integrated chronostratigraphy of Proterozoic–Cambrian boundary beds in the western Anabar region, northern Siberia. Geological Magazine, 133(05): 509-533.

Khomentovsky, V. and Gibsher, A., 1996. The Neoproterozoic–lower Cambrian in northern Govi-Altay, western Mongolia: regional setting, lithostratigraphy and biostratigraphy. Geological Magazine, 133(04): 371-390.

Khomentovsky, V. and Karlova, G., 1993. Biostratigraphy of the Vendian-Cambrian beds and the lower Cambrian boundary in Siberia. Geological Magazine, 130(01): 29-45.

Kirschvink, J. and Raub, T., 2003. A methane fuse for the Cambrian explosion: true polar wander. CR Geosci, 335: 71-83.

Kirschvink, J.L., Magaritz, M., Ripperdan, R.L., Zhuravlev, A.Y. and Rozanov, A.Y., 1991. The Precambrian-Cambrian boundary: magnetostratigraphy and carbon isotopes resolve correlation problems between Siberia, Morocco, and South China. GSA today, 1(4): 69-91.

Knoll, A.H., Grotzinger, J.P., Kaufman, A.J. and Kolosov, P., 1995a. Integrated approaches to terminal Proterozoic stratigraphy: an example from the Olenek Uplift, northeastern Siberia. Precambrian Research, 73(1): 251-270.

Knoll, A.H., Kaufman, A.J., Semikhatov, M.A., Grotzinger, J.P. and Adams, W., 1995b. Sizing up the sub-Tommotian unconformity in Siberia. Geology, 23(12): 1139-1143.

Korobov, M. and Missarzhevsky, V., 1977. O pogranichnykh sloyakh kembriya i dokembriya Zapadnoy Mongolii (khrebet Khasagt-Khairkhan). Bespozvonochnye paleozoya Mongolii: Sovmestnaya Sovestsko-Mongol'skaya Paleontologicheskaya Ekspeditsiya, Trudy, 5: 7-9.

Kouchinsky, A., Bengtson, S., Missarzhevsky, V.V., Pelechaty, S., Torssander, P. and Val'kov, A.K., 2001. Carbon isotope stratigraphy and the problem of a pre-Tommotian Stage in Siberia. Geological Magazine, 138(04): 387-396.

Kouchinsky, A., Bengtson, S., Pavlov, V., Runnegar, B., Torssander, P., Young, E. and Ziegler, K., 2007. Carbon isotope stratigraphy of the Precambrian–Cambrian Sukharikha River section, northwestern Siberian platform. Geological Magazine, 144(04): 609-618.

Kröner, A., Lehmann, J., Schulmann, K., Demoux, A., Lexa, O., Tomurhuu, D., Štípská, P., Liu, D. and Wingate, M.T., 2010. Lithostratigraphic and geochronological constraints on the evolution of the Central Asian Orogenic Belt in SW Mongolia: Early Paleozoic rifting followed by late Paleozoic accretion. American Journal of Science, 310(7): 523-574.

Kruse, P.D., Gandin, A., Debrenne, F. and Wood, R., 1996. Early Cambrian bioconstructions in the Zavkhan Basin of western Mongolia. Geological Magazine, 133(04): 429-444.

Landing, E., 1994. Precambrian-Cambrian boundary global stratotype ratified and a new perspective of Cambrian time. Geology, 22(2): 179-182.

Landing, E., Geyer, G., Brasier, M.D. and Bowring, S.A., 2013. Cambrian evolutionary radiation: context, correlation, and chronostratigraphy—overcoming deficiencies of the first appearance datum (FAD) concept. Earth-Science Reviews, 123: 133-172.

Lehmann, J., Schulmann, K., Lexa, O., Corsini, M., Kroner, A., Stipska, P., Tomurhuu, D. and Otgonbator, D., 2010. Structural constraints on the evolution of the Central Asian Orogenic Belt in SW Mongolia. American Journal of Science, 310(7): 575-628.

Levashova, N.M., Kalugin, V.M., Gibsher, A.S., Yff, J., Ryabinin, A.B., Meert, J. and Malone, S.J., 2010. The origin of the Baydaric microcontinent, Mongolia: Constraints from paleomagnetism and geochronology. Tectonophysics, 485(1-4): 306-320.

Li, D., Ling, H.-F., Jiang, S.-Y., Pan, J.-Y., Chen, Y.-Q., Cai, Y.-F. and Feng, H.-Z., 2009. New carbon isotope stratigraphy of the Ediacaran–Cambrian boundary interval from SW China: implications for global correlation. Geological Magazine, 146(04): 465-484.

Li, G., Zhao, X., Gubanov, A., Zhu, M. and Na, L., 2011. Early Cambrian mollusc Watsonella crosbyi: a potential GSSP index fossil for the base of the Cambrian Stage 2. Acta Geologica Sinica (English Edition), 85(2): 309-319.

Lindsay, J., Brasier, M., Dorjnamjaa, D., Goldring, R., Kruse, P. and Wood, R., 1996a. Facies and sequence controls on the appearance of the Cambrian biota in southwestern Mongolia: implications for the Precambrian–Cambrian boundary. Geological Magazine, 133(04): 417-428.

Lindsay, J., Brasier, M., Shields, G., Khomentovsky, V. and Bat-Ireedui, Y., 1996b. Glacial facies associations in a Neoproterozoic back-arc setting, Zavkhan Basin, western Mongolia. Geological Magazine, 133(04): 391-402.

Macdonald, F.A., 2011. The Tsagaan Oloom Formation, southwestern Mongolia. Geological Society, London, Memoirs, 36(1): 331-337.

Macdonald, F.A., Jones, D.S. and Schrag, D.P., 2009. Stratigraphic and tectonic implications of a new glacial diamictite-cap carbonate couplet in southwestern Mongolia. Geology, 37: 123-126.

Macdonald, F.A., Schmitz, M.D., Crowley, J.L., Roots, C.F., Jones, D.S., Maloof, A.C., Strauss, J.V., Cohen, P.A., Johnston, D.T. and Schrag, D.P., 2010. Calibrating the cryogenian. Science, 327(5970): 1241-1243.

MacNaughton, R.B. and Narbonne, G.M., 1999. Evolution and ecology of Neoproterozoic-Lower Cambrian trace fossils, NW Canada. Palaios: 97-115.

Maloof, A.C., Porter, S.M., Moore, J.L., Dudás, F.Ö., Bowring, S.A., Higgins, J.A., Fike, D.A. and Eddy, M.P., 2010a. The earliest Cambrian record of animals and ocean geochemical change. Geological Society of America Bulletin, 122(11-12): 1731-1774.

Maloof, A.C., Ramezani, J., Bowring, S.A., Fike, D.A., Porter, S.M. and Mazouad, M., 2010b. Constraints on early Cambrian carbon cycling from the duration of the Nemakit-Daldynian–Tommotian boundary δ13C shift, Morocco. Geology, 38(7): 623-626.

Maloof, A.C., Schrag, D.P., Crowley, J.L. and Bowring, S.A., 2005. An expanded record of Early Cambrian carbon cycling from the Anti-Atlas Margin, Morocco. Canadian Journal of Earth Sciences, 42(12): 2195-2216.

Markova, N., Korobov, M. and Zhuravleva, Z., 1972. K voprosu o vend-kembriyskikh otlozheniyakh Yugo-Zapadnoy Mongolii (On the problem of the Vendian-

Cambrian deposits of southwestern Mongolia). Bulleten'Moskovskogo obshchestva ispytateley prirody, Otdel geologicheskiy, 47(1): 57-70.

Marshall, C.R., 2006. Explaining the Cambrian "explosion" of animals. Annu. Rev. Earth Planet. Sci., 34: 355-384.

Meert, J.G. and Van der Voo, R., 1994. The Neoproterozoic (1000–540 Ma) glacial intervals: no more snowball earth? Earth and Planetary Science Letters, 123(1): 1-13.

Mullins, H.T., Gardulski, A.F., Wise, S.W. and Applegate, J., 1987. Middle Miocene oceanographic event in the eastern Gulf of Mexico: implications for seismic stratigraphic succession and Loop Current/Gulf Stream circulation. Geological Society of America Bulletin, 98(6): 702-713.

Narbonne, G.M., Kaufman, A.J. and Knoll, A.H., 1994. Integrated chemostratigraphy and biostratigraphy of the Windermere Supergroup, northwestern Canada: Implications for Neoproterozoic correlations and the early evolution of animals. Geological Society of America Bulletin, 106(10): 1281-1292.

Parkhaev, P.Y., 2007. Shell chirality in Cambrian gastropods and sinistral members of the genus Aldanella Vostokova, 1962. Paleontological Journal, 41(3): 233-240.

Parkhaev, P.Y., Karlova, G. and Rozanov, A.Y., 2011. Taxonomy, stratigraphy and biogeography of Aldanella attleborensis–a possible candidate for defining the base of Cambrian Stage 2. Museum of Northern Arizona Bulletin, 67: 298-300.

Peng, S., Babcock, L. and Cooper, R., 2012. The Cambrian Period. The geologic time scale, 2: 437-488.

Porter, S.M., 2004. Closing the phosphatization window: testing for the influence of taphonomic megabias on the pattern of small shelly fossil decline. Palaios, 19(2): 178-183.

Porter, S.M., 2007. Seawater chemistry and early carbonate biomineralization. Science, 316(5829): 1302-1302.

Qian, Y. and Bengtson, S., 1989. Paleontology and biostratigraphy of the Early Cambrian Meishucunian stage in Yunnan province, South China.

Qian, Y., Zhu, M., He, T. and Jiang, Z., 1996. New investigation of Precambrian-Cambrian boundary sections in eastern Yunnan Acta Micropalaontologica Sinica 03.

Repina, L. and Rozanov, A.Y., 1992. Cambrian of Siberia.

Rice, A.H.N., Edwards, M.B., Hansen, T.A., Arnaud, E. and Halverson, G.P., 2011. Glaciogenic rocks of the Neoproterozoic Smalfjord and Mortensnes formations, Vestertana Group, E. Finnmark, Norway. Geological Society, London, Memoirs, 36(1): 593-602.

Rooney, A.D., Macdonald, F.A., Strauss, J.V., Dudás, F.Ö., Hallmann, C. and Selby, D., 2014. Re-Os geochronology and coupled Os-Sr isotope constraints on the Sturtian snowball Earth. Proceedings of the National Academy of Sciences, 111(1): 51-56.

Rozanov, A.Y., Khomentovsky, V., Shabanov, Y.Y., Karlova, G., Varlamov, A., Luchinina, V., Demidenko, Y.E., Parkhaev, P.Y., Korovnikov, I. and Skorlotova, N., 2008. To the problem of stage subdivision of the Lower Cambrian. Stratigraphy and geological correlation, 16(1): 1-19.

Ruzhentsev, S.V. and Burashnikov, V.V., 1996. Tectonics of the western Mongolian Salairides. Geotectonics, 29(5): 379-394.

Schrag, D.P., Higgins, J.A., Macdonald, F.A. and Johnston, D.T., 2013. Authigenic carbonate and the history of the global carbon cycle. science, 339(6119): 540-543.

Schröder, S. and Grotzinger, J., 2007. Evidence for anoxia at the Ediacaran–Cambrian boundary: the record of redox-sensitive trace elements and rare earth elements in Oman. Journal of the Geological Society, 164(1): 175-187.

Shields, G.A., Brasier, M.D., Stille, P. and Dorjnamjaa, D.-i., 2002. Factors contributing to high δ13C values in Cryogenian limestones of western Mongolia. Earth and Planetary Science Letters, 196(3): 99-111.

Shields-Zhou, G., Hill, A. and Macgabhann, B., 2012. The Cryogenian Period. The Geologic Time Scale: 393-411.

Spence, G.H. and Tucker, M.E., 1997. Genesis of limestone megabreccias and their significance in carbonate sequence stratigraphic models: a review. Sedimentary Geology, 112(3): 163-193.

Squire, R.J., Campbell, I.H., Allen, C.M. and Wilson, C.J., 2006. Did the Transgondwanan Supermountain trigger the explosive radiation of animals on Earth? Earth and Planetary Science Letters, 250(1): 116-133.

Steiner, M., Li, G., Qian, Y., Zhu, M. and Erdtmann, B.-D., 2007. Neoproterozoic to early Cambrian small shelly fossil assemblages and a revised biostratigraphic correlation of the Yangtze Platform (China). Paleogeography, Paleoclimatology, Paleoecology, 254(1): 67-99.

Stodt, F., Rice, A.H.N., Björklund, L., Bax, G., Halverson, G.P. and Pharaoh, T., 2011. Evidence of late Neoproterozoic glaciation in the Caledonides of NW Scandinavia. Geological Society, London, Memoirs, 36(1): 603-612.

Torsvik, T., Smethurst, M., Meert, J.G., Van der Voo, R., McKerrow, W., Brasier, M., Sturt, B. and Walderhaug, H., 1996. Continental break-up and collision in the Neoproterozoic and Paleozoic—a tale of Baltica and Laurentia. Earth-Science Reviews, 40(3): 229-258.

Vail, P.R., Mitchum Jr, R. and Thompson III, S., 1977. Seismic Stratigraphy and Global Changes of Sea Level: Part 4. Global Cycles of Relative Changes of Sea Level.:

Section 2. Application of Seismic Reflection Configuration to Stratigraphic Interpretation.

Valentine, J.W., 2002. Prelude to the Cambrian Explosion. Annual Review of Earth and Planetary Sciences, 30(1): 285-306.

Van Wagoner, J.C., Mitchum, R., Campion, K. and Rahmanian, V., 1990. Siliciclastic sequence stratigraphy in well logs, cores, and outcrops: concepts for high-resolution correlation of time and facies.

Voronin, Y.I., Voronova, L.G., Girgor'eva, N.V., Drozdova, N.A., Zhegallo, E.A., Zhuravlev, A.Y., Ragozina, A.L., Rozanov, A.Y., Sayutina, T.A., Sysoev, V.A. and Fonin, V.D., 1982. The Precambrian/Cambrian boundary in the geosynclinal areas (the reference section of Salaany-Gol, MPR). Trudy Sovmestnoy Sovetsoko-Mongol'skoy Paleontologicheskoy Ekspeditsii, 18. Akademia Nauk SSSR, Moscow, 150 pp.

Wilhem, C., Windley, B.F. and Stampfli, G.M., 2012. The Altaids of Central Asia: A tectonic and evolutionary innovative review. Earth-Science Reviews, 113(3): 303-341.

Wille, M., Nägler, T.F., Lehmann, B., Schröder, S. and Kramers, J.D., 2008. Hydrogen sulphide release to surface waters at the Precambrian/Cambrian boundary. Nature, 453(7196): 767-769.

Wood, R., Zhuravlev, A.Y. and Anaaz, C.T., 1993. The ecology of Lower Cambrian buildups from Zuune Arts, Mongolia: implications for early metazoan reef evolution. Sedimentology, 40(5): 829-858.

Yang, B., Steiner, M., Li, G. and Keupp, H., 2014. Terreneuvian small shelly faunas of East Yunnan (South China) and their biostratigraphic implications. Paleogeography, Paleoclimatology, Paleoecology, 398: 28-58.

Yarmolyuk, V., Kovalenko, V., Anisimova, I., Sal'nikova, E., Kovach, V., Kozakov, I., Kozlovsky, A., Kudryashova, E., Kotov, A. and Plotkina, Y.V., 2008. Late Riphean alkali granites of the Zabhan microcontinent: evidence for the timing of Rodinia breakup and formation of microcontinents in the Central Asian Fold Belt, Doklady Earth Sciences. Springer, pp. 583-588.

Zhao, Y., Song, B. and Zhang, S., 2006. The Central Mongolian microcontinent: Its Yangtze affinity and tectonic implications, Abst.-vol., Symposium on continental growth and orogeny in Asia Taipei Taiwan March, pp. 19-26.

Zhegallo, L. and Zhuravlev, A.Y., 1991. Guidebook for the International excursion to the Vendian-Cambrian deposits of the Dzvkhan Zone of Mongolia, Unpublished guidebook. Paleontological Institute, Moscow, pp. 24.

Zhou, C., Zhang, J., Li, G. and Yu, Z., 1997. Carbon and oxygen isotopic record of the Early Cambrian from the Xiaotan Section, Yunnan, South China. Scientia geologica sinica, 32(02): 201-211.

Zhu, M., Li, G., Zhang, J. and Michael, S., 2001. Early Cambrian stratigraphy of east Yunnan, southwestern China: a synthesis.

Zhu, M., Strauss, H. and Shields, G.A., 2007. From snowball earth to the Cambrian bioradiation: calibration of Ediacaran–Cambrian earth history in South China. Paleogeography, Paleoclimatology, Paleoecology, 254(1): 1-6.

Zhu, M. and Wang, H., 2011. Neoproterozoic glaciogenic diamictites of the Tarim Block, NW China. Geological Society, London, Memoirs, 36(1): 367-378.

Zhu, M.-Y., Babcock, L.E. and Peng, S.-C., 2006. Advances in Cambrian stratigraphy and paleontology: integrating correlation techniques, paleobiology, taphonomy and paleoenvironmental reconstruction. Paleoworld, 15(3): 217-222.

APPENDICES

Appendix A1. Supplement to Chapter 2: Carbon and oxygen isotopic measurements for the Horse Thief Springs Formation and Beck Spring Dolomite

Stratigraphic meter	d13C	d18O	Unit
Beck Canyon, Kingston Range			
61.5	0.2484	-6.9948	HTS Fm
62	1.8544	-7.5739	HTS Fm
62.5	1.9104	-5.2626	HTS Fm
63	1.9814	-5.3091	HTS Fm
63.5	1.4604	-5.3279	HTS Fm
64	2.2844	-6.8988	HTS Fm
64.5	2.3474	-5.6249	HTS Fm
65	1.1574	-4.7399	HTS Fm
65.5	-1.1776	-5.7080	HTS Fm
66	-2.0656	-6.0555	HTS Fm
66.5	-2.6426	-3.5818	HTS Fm
67.2	-4.0756	-4.6330	HTS Fm
70.1	-6.0756	-6.2703	HTS Fm
77.6	-4.0536	-2.8186	HTS Fm
78	-4.8086	-6.3128	HTS Fm
78.8	-4.1776	-4.1342	HTS Fm
79.5	-4.0356	-4.6637	HTS Fm
137.5	1.1404	-4.8696	HTS Fm
138	0.4214	-5.6407	HTS Fm
138.5	0.8804	-6.0644	HTS Fm
139	0.8154	-6.1129	HTS Fm
139.5	0.9924	-5.8476	HTS Fm
140	1.2204	-6.7711	HTS Fm
140.5	1.7884	-4.5251	HTS Fm
141	1.7134	-5.1329	HTS Fm
141.5	2.0134	-4.7894	HTS Fm
142	1.8944	-5.2052	HTS Fm
142.5	1.9594	-5.1695	HTS Fm
143	1.7794	-6.1663	HTS Fm
143.5	1.7334	-4.7271	HTS Fm
144	1.6324	-5.4992	HTS Fm
144.5	1.5644	-4.9488	HTS Fm
145	1.2964	-5.1765	HTS Fm
145.5	1.2614	-5.8555	HTS Fm

146	0.4294	-8.9369	HTS Fm
147	-3.1596	-19.0819	HTS Fm
151.5	-0.2996	-9.3883	HTS Fm
153	-3.8516	-9.0171	HTS Fm
154.3	-3.7066	-7.6442	HTS Fm
156.1	-3.9766	-7.8323	HTS Fm
256.1	0.8314	-6.4069	HTS Fm
257.4	0.1014	-9.4328	HTS Fm
258.8	-0.4116	-9.8535	HTS Fm
267	1.6434	-6.2722	HTS Fm
267.5	2.1614	-5.0409	HTS Fm
268	2.1134	-5.6694	HTS Fm
268.5	2.9384	-4.2767	HTS Fm
270	2.0874	-6.3841	HTS Fm
270.5	2.7494	-5.3883	HTS Fm
271	2.5794	-6.0634	HTS Fm
271.5	2.2374	-11.9075	HTS Fm
272	2.1614	-5.5566	HTS Fm
273.7	2.8494	-5.0973	HTS Fm
277.1	3.2615	-2.2338	HTS Fm
277.5	1.9435	-3.0891	HTS Fm
279.5	3.9695	-3.4603	HTS Fm
281	2.3465	-3.8008	HTS Fm
281.5	2.5115	-3.2970	HTS Fm
283	2.7215	-1.9636	HTS Fm
283.8	3.1345	-2.8822	HTS Fm
285	3.1995	-2.1487	HTS Fm
286	3.2655	-1.8211	HTS Fm
286.8	3.0295	-2.4269	HTS Fm
291	3.8665	-3.4177	HTS Fm
291.5	4.7885	-2.3328	HTS Fm
292	5.1705	-2.0626	HTS Fm
292.5	5.4735	-2.0953	HTS Fm
293	5.6750	-1.2687	HTS Fm
294	4.5815	-3.4840	HTS Fm
294.5	4.2235	-4.5610	HTS Fm
295	3.9315	-4.3323	HTS Fm
296	4.7620	-3.4464	HTS Fm
300.5	3.8825	-2.9663	HTS Fm
301.5	3.7025	-3.0000	HTS Fm
302.9	3.6135	-2.9634	HTS Fm
303.5	3.5965	-3.8117	HTS Fm
305.5	3.6915	-2.9931	HTS Fm
307	3.8275	-2.2645	HTS Fm
307.5	3.5905	-2.5615	HTS Fm
308	3.4165	-2.7496	HTS Fm
308.5	3.9635	-2.4734	HTS Fm
310	3.6425	-2.9743	HTS Fm
311	3.8365	-1.9824	HTS Fm

313	4.0555	-2.7238	HTS Fm
316	3.3985	-2.0062	HTS Fm
316.5	3.9195	-0.4986	HTS Fm
317	4.3195	-0.8659	HTS Fm
320.8	3.7725	-2.1547	HTS Fm
321.9	2.9455	-1.9775	HTS Fm
323	3.7265	-0.8619	HTS Fm
323.5	3.1815	-0.9965	HTS Fm
324	3.5585	-2.0468	HTS Fm
325	2.5655	-2.5981	HTS Fm
326	2.3155	-1.7627	HTS Fm
327	3.5065	-0.7540	HTS Fm
328	2.9905	0.8387	HTS Fm
350.8	-3.0350	-3.9973	HTS Fm
351.8	-3.4220	-3.3816	HTS Fm
353	-4.0120	-3.6894	HTS Fm
353.5	-3.6220	-2.8104	HTS Fm
354	-3.5080	-3.5528	HTS Fm
355	-4.1490	-2.6243	HTS Fm
428.7	2.1460	-1.8127	HTS Fm
440	3.2840	-2.2987	HTS Fm
441.1	3.6490	-2.5560	HTS Fm
442	1.6960	-2.5709	HTS Fm
443	3.4450	-2.8659	HTS Fm
444	3.0990	-3.3301	HTS Fm
445	-3.8507	-18.0886	HTS Fm
455	-2.8857	-4.6087	HTS Fm
456	-2.6537	-7.4169	HTS Fm
457.5	-1.0397	-11.9841	HTS Fm
458	1.4193	-9.3412	HTS Fm
458.5	3.4653	-3.0101	HTS Fm
459	2.5693	-5.0571	HTS Fm
459.5	-0.7877	-8.2890	HTS Fm
478	-1.0177	-3.3467	BSD
478.5	-0.2157	-3.9683	BSD
479	0.1113	-6.2806	BSD
480	-0.2747	-7.6505	BSD
481	0.0073	-7.6436	BSD
482	-0.6467	-8.6513	BSD
Silurian Hills (base of BSD = N 35.5307, W 116.0945)			
9.1	-4.9667	-15.3001	HTS Fm
9.4	-4.7837	-16.6127	HTS Fm
12.7	-2.1407	-19.6228	HTS Fm
15.3	-0.8787	-15.6773	HTS Fm
15.8	-2.8427	-16.5860	HTS Fm
16.5	-2.6247	-19.5694	HTS Fm
18.5	-2.8997	-19.2200	HTS Fm
23	-1.6317	-17.4877	HTS Fm
45.6	-2.4307	-18.4825	HTS Fm

53	2.6683	-17.4521	HTS Fm
55	3.8823	-16.1781	HTS Fm
56	2.3473	-16.7631	HTS Fm
65.1	3.2063	-18.5944	HTS Fm
65.7	-0.1687	-22.0133	HTS Fm
74	3.5783	-16.5889	HTS Fm
80.1	-2.9487	-16.9245	HTS Fm
82.5	-1.2257	-18.2073	HTS Fm
91.6	0.4543	-22.3202	HTS Fm
103.4	3.2983	-18.8923	HTS Fm
105.7	1.5663	-18.5300	HTS Fm
113.6	-2.4957	-15.5327	HTS Fm
131.5	-1.5447	-20.2177	HTS Fm
224.3	0.0983	-19.5357	HTS Fm
228.3	0.1803	-19.7921	HTS Fm
234.2	-0.0197	-20.6869	HTS Fm
426.5	-2.5557	-16.4850	BSD?
427.1	-2.7357	-14.8933	BSD?
430	-4.5157	-18.0381	BSD?
430.7	-4.1387	-19.8723	BSD?
576.4	-5.4037	-18.7112	BSD?
582.5	-6.2877	-18.6092	BSD?
594	-5.4047	-18.2667	BSD?
594.5	-5.0517	-16.7463	BSD?
595	-3.8757	-15.8495	BSD?
595.6	-2.7670	-15.9337	BSD?
609.5	-3.0170	-17.7679	BSD?
623	-3.6700	-19.3467	BSD?
624	2.9700	-15.9683	BSD?
624.5	2.9090	-14.8953	BSD?
625	4.0570	-11.4625	BSD?
625.6	2.9230	-12.1000	BSD?
626	3.1030	-15.5160	BSD?
626.5	1.4090	-15.3902	BSD?
627.7	3.3710	-15.6842	BSD?
630	2.5410	-14.9735	BSD?
630.5	3.4960	-15.4774	BSD?
631	3.1450	-16.2336	BSD?
631.5	3.2190	-15.3823	BSD?
632	5.2300	-14.6261	BSD?
632.3	3.8400	-14.2549	BSD?
633	4.9720	-16.0485	BSD?
633.5	4.3810	-14.3143	BSD?
634	5.7380	-15.1398	BSD?
634.5	5.8450	-13.6045	BSD?
635	5.5490	-13.9183	BSD?
637	5.1980	-12.2979	BSD?
637.5	4.7150	-11.7961	BSD?
638	6.3600	-15.8604	BSD?

638.1	4.4600	-17.8748	BSD?
638.5	2.1650	-17.9065	BSD?
Happy Canyon, Panamint Mountains (N 36.08428' W 117.09411')			
1.5	1.6894	-9.7639	HTS Fm
2.8	2.1164	-7.7080	HTS Fm
7.7	1.5104	-9.5501	HTS Fm
9	2.7114	-7.0279	BSD
13.5	2.5054	-8.0524	BSD
15.5	2.3264	-7.3397	BSD
17.9	1.7104	-5.6936	BSD
20	2.7544	-4.6097	BSD
22	3.4574	-2.9378	BSD
24	3.1284	-2.4548	BSD
26	3.2604	-2.4944	BSD
28	3.8934	-2.4261	BSD
30	4.4694	-1.2591	BSD
32	4.6044	-1.6867	BSD
34	2.6694	-3.9920	BSD
36	4.1094	-3.0210	BSD
38	4.6154	-2.5627	BSD
40	4.6684	-1.8559	BSD
42	4.3544	-1.9559	BSD
45	3.5264	-2.6508	BSD
47	3.7734	-2.6508	BSD
51	3.6174	-2.5231	BSD
53	1.9944	-2.3103	BSD
56	3.5604	-2.5033	BSD
59.3	2.9404	-6.1123	BSD
61	3.8324	-1.9599	BSD
63	4.0074	-1.6797	BSD
65	3.0324	-1.9074	BSD
67	2.5454	-1.6649	BSD
69	2.1244	-2.3271	BSD
71	2.0004	-2.9636	BSD
73	2.4514	-2.3182	BSD
75	2.3514	-2.3489	BSD
78	2.1074	-3.4991	BSD
85	1.6654	-3.9425	BSD
88	2.0034	-3.2120	BSD
91	2.8384	-2.6874	BSD
94	1.2594	-3.7149	BSD
97	2.0894	-3.0665	BSD
100	2.0454	-4.0900	BSD
103.7	1.3304	-5.0957	BSD
109.5	3.2074	-4.9235	BSD
112	1.8944	-6.2727	BSD
114	2.6584	-5.3333	BSD
117	3.0144	-4.2959	BSD
120	2.2854	-4.7562	BSD

123	3.1594	-4.0158	BSD
126	2.6664	-3.7842	BSD
129	3.0124	-3.0606	BSD
132	2.7944	-3.4407	BSD
135	2.6714	-4.2464	BSD
138	2.9934	-3.7782	BSD
Saratoga Springs, Southern Ibex Hills (N 35.6866, W 116.4176)			
6.1	2.6510	-5.0762	HTS Fm
8.1	2.5510	-5.1277	HTS Fm
10.1	2.1460	-4.2141	HTS Fm
10.1	2.0790	-4.2437	HTS Fm
11.8	0.3470	-5.6840	HTS Fm
12.3	0.5330	-3.9418	HTS Fm
16.3	-1.8650	-2.6956	HTS Fm
17.3	-3.1880	0.0136	HTS Fm
31.2	-4.4220	-5.2188	HTS Fm
33.7	-4.3310	-5.2623	HTS Fm
33.7	-4.4080	-5.3177	HTS Fm
34.5	-4.4600	-4.6337	HTS Fm
60.3	0.3886	-5.2173	HTS Fm
65	0.6026	-6.4735	HTS Fm
71	0.0146	-5.7825	HTS Fm
74	-2.4124	-6.6754	HTS Fm
76	-2.4524	-5.5420	HTS Fm
78	-2.9714	-5.3787	HTS Fm
106.5	-1.7994	-8.6640	BSD
109.3	-1.4554	-9.8370	BSD
110.9	0.7126	-7.9533	BSD
115.9	-1.6794	-4.1483	BSD
117.8	-1.6924	-6.5536	BSD
120.2	-1.4704	-9.2678	BSD
121.7	-2.7364	-8.6828	BSD
127.6	-0.1134	-4.6086	BSD
129.5	-1.4064	-6.2676	BSD
132.7	-0.1334	-7.8028	BSD
140.9	0.9286	-7.7919	BSD
142.1	2.2876	-11.5227	BSD
144.6	2.1586	-13.0095	BSD
160.8	0.6396	-6.5190	BSD
164.4	0.9626	-2.6279	BSD
167	1.1436	-4.4730	BSD
167.4	1.0016	-2.5942	BSD
171	1.0616	-1.8499	BSD
173.8	1.6206	-5.2797	BSD
176.7	1.4906	-4.1572	BSD
177.4	1.8056	-3.6959	BSD
179.9	1.7766	-3.5217	BSD
184	2.0366	-2.5893	BSD
185.7	2.1196	-2.5853	BSD

189.5	1.4436	-3.9404	BSD
194.1	1.2826	-2.5487	BSD
196.3	1.6506	-4.7947	BSD
197.9	1.6706	-3.0476	BSD
202.1	2.4366	-3.0357	BSD
203.4	2.1626	-4.0800	BSD
205.8	1.8666	-3.8751	BSD
208.1	2.2006	-3.4485	BSD
210.7	2.5046	-3.2584	BSD
212.2	2.0086	-3.4514	BSD
214.5	1.7196	-2.1626	BSD
216.6	2.4816	-3.4148	BSD
219.6	3.2666	-3.9444	BSD
222.4	2.4496	-2.2092	BSD
226	2.9536	-3.5484	BSD
231.1	1.2506	-1.5232	BSD
234.4	1.7026	-1.8390	BSD
237	0.9086	-3.1644	BSD
240.1	1.9846	-7.0486	BSD
242.9	1.1136	-4.7155	BSD
246.2	1.3096	-3.0743	BSD
252.2	1.2886	-4.9273	BSD
272.8	2.4623	-6.3983	BSD
274.8	0.5633	-2.6933	BSD
276.8	2.1623	-3.4149	BSD
278.8	1.3383	-4.4394	BSD
281.1	0.8513	-1.5500	BSD
284.4	2.1023	-4.0148	BSD
286.7	2.6133	-5.8697	BSD
288.7	2.7463	-7.0724	BSD
290.7	0.6063	-5.2689	BSD
293.6	1.4523	-7.7970	BSD
296.5	0.0133	-3.9039	BSD
299.1	-0.5768	-4.0860	BSD
302.3	0.2363	-7.4278	BSD
303.9	0.6373	-3.7119	BSD
307.8	-0.5398	-5.9430	BSD
310	2.1933	-1.8836	BSD
310.6	1.9243	-2.7735	BSD
316	1.1183	-3.7109	BSD
318.9	1.1953	-2.1142	BSD
320.9	-0.0708	-2.2023	BSD
322.4	0.8503	-2.3023	BSD
324	0.7973	-3.4327	BSD
326.2	-0.0068	-1.5777	BSD
327.8	-0.2168	-2.6082	BSD
328.8	1.2703	-8.9759	BSD
332	1.2103	-3.0417	BSD
335.2	0.7693	-3.3436	BSD

337.3	0.6003	-2.5686	BSD
340.4	-0.2528	-2.9447	BSD
342.8	2.4163	-3.9524	BSD
346.6	2.1063	-4.0445	BSD
351.1	1.1293	-2.3577	BSD
355.9	1.8383	-1.3224	BSD
361.3	0.9523	-3.1041	BSD
368.9	1.0533	-2.3726	BSD
374.4	1.2283	-2.5696	BSD
377.6	2.7383	-3.4862	BSD
380	2.2293	-1.8925	BSD
382.2	2.2312	-3.0607	BSD
384.5	1.6322	-4.1525	BSD
386.4	1.9332	-3.1478	BSD
388.3	2.0792	-1.4987	BSD
390.3	1.8402	-4.5237	BSD
393	1.2852	-2.4242	BSD
394.6	3.2772	-4.7375	BSD
396.5	3.1812	-3.1775	BSD
399	3.0202	-2.5291	BSD
401	4.1512	-1.3106	BSD
406.6	1.8162	-3.1131	BSD
407.1	1.5332	-2.4093	BSD
408.1	1.3372	-3.9901	BSD
409.2	0.7542	-7.9416	BSD
409.7	1.7982	-10.2955	BSD
412.1	2.0412	-4.7909	BSD
413.8	1.6322	-5.0542	BSD
414.8	2.0312	-5.0374	BSD
415.8	3.0322	-4.4831	BSD
416.9	3.0282	-3.0092	BSD
417.3	1.3192	-3.6645	BSD
417.8	3.2022	-2.9053	BSD
418.8	3.4862	-2.9290	BSD
419.8	3.4772	-4.6088	BSD
421.7	2.5672	-6.2569	BSD
422.1	2.0303	-5.1739	BSD
427	-0.5867	-10.7963	BSD
428.5	-2.0827	-8.4672	BSD
429.3	-3.4897	-6.5241	BSD
430.8	-1.6847	-7.3803	BSD
433	-2.1607	-8.4484	BSD
434.3	-3.1737	-8.7829	BSD
Alexander Hills (only additional samples from top of section)			
0	4.0260	-0.3281	BSD
1	3.5460	-1.3526	BSD
2	3.4340	-1.9247	BSD
3	3.3460	-1.9188	BSD
4	1.8670	-2.3137	BSD

5	0.4580	-3.7550	BSD
6	0.3790	-4.9359	BSD
7	0.8320	-4.6636	BSD
8	0.4470	-5.4496	BSD
9	-1.0070	-3.6342	BSD
14	2.4420	-3.9905	BSD
15	2.1100	-3.4669	BSD
16	1.5680	-5.6842	BSD
17	0.4960	-9.3417	BSD
18	1.1580	-11.1690	BSD
19	0.9840	-10.0128	BSD
20	0.8960	-7.5273	BSD
21	0.7900	-6.0653	BSD
29	-0.1030	-5.2348	BSD
30	1.0560	-5.7000	BSD
31	0.8490	-4.9883	BSD
32	1.9000	-5.8901	BSD
33	1.2950	-5.1843	BSD
34	1.3370	-4.8854	BSD
35	1.1760	-5.8257	BSD
36	1.0860	-5.4664	BSD
Black Mountains (Base of BSD = N 35.9266, W 116.653; Base of carbonate at top of section = N 35.9156, W 116.6486)			
1	-0.3639	-4.5643	BSD
5	0.7261	-4.5693	BSD
10	3.9051	-4.5663	BSD
15	5.5991	-4.5653	BSD
22	4.7221	-4.5703	BSD
27	4.2191	-4.5673	BSD
30	5.3071	-4.5633	BSD
35	4.5411	-4.5673	BSD
40	4.5581	-4.5653	BSD
45	5.4401	-4.5683	BSD
50	5.0551	-4.5604	BSD
56	5.4531	-4.5663	BSD
60	5.1531	-4.5663	BSD
70	5.3491	-4.5613	BSD
75	3.6761	-4.5613	BSD
81	3.9161	-4.5712	BSD
88	4.0271	-4.5465	BSD
94	4.3371	-4.5594	BSD
99	4.8701	-4.5683	BSD
105	2.7011	-4.5653	BSD
113	3.1301	-4.5643	BSD
120	3.0901	-4.5584	BSD
126	3.0721	-4.5643	BSD
132	4.0371	-4.5613	BSD
140	3.1081	-4.5574	BSD
146	1.6461	-4.5613	BSD

151	3.0741	-4.5653	BSD
156	4.1501	-4.5623	BSD
167	3.7481	-4.5604	BSD
172	3.5621	-4.5673	BSD
175	3.5981	-4.5524	BSD
182	3.0341	-4.5534	BSD
192	2.8281	-4.5643	BSD
200	2.7361	-4.5683	BSD
209	2.9241	-4.5653	BSD
212	2.1171	-4.5534	BSD
216	2.7371	-4.5584	BSD
223	-0.6069	-4.5594	BSD
223	-1.5169	-4.5693	BSD
228	-1.4939	-4.5663	BSD
229	-2.0169	-4.5554	BSD
248.5	-3.2607	-8.1754	BSD(top)
249	1.1713	-8.1774	BSD(top)
250	1.3743	-8.1685	BSD(top)
251	1.4073	-8.1754	BSD(top)
251.5	0.4853	-8.1844	BSD(top)
253.6	1.4253	-6.7669	BSD(top)
254.2	-4.0217	-3.1787	BSD(top)
257.1	-1.6797	-8.4675	BSD(top)
258	-0.8637	-8.0072	BSD(top)
259	-1.3297	-6.9946	BSD(top)
260.2	-1.9307	-4.3507	BSD(top)
261	-1.3897	-15.9220	BSD(top)
262.4	-0.6137	-14.3571	BSD(top)
264	-2.2267	-8.3586	BSD(top)
266.6	-1.0787	-17.1118	BSD(top)
267.5	-1.5247	-11.7587	BSD(top)
268.5	-0.7217	-5.4543	BSD(top)
270	-0.6827	-13.5207	BSD(top)
271	-0.6807	-10.5600	BSD(top)
272.5	-0.6567	-15.9300	BSD(top)
274	0.9883	-8.0725	BSD(top)
275	1.4363	-7.4529	BSD(top)
276	1.0373	-7.8310	BSD(top)
277.2	-1.2537	-8.4991	BSD(top)
277.6	-0.5817	-5.0109	KP1
277.8	-0.8247	-6.1858	KP1
278.5	-0.5957	-5.2544	KP1
279.2	-1.0457	-5.3247	KP1
279.7	-2.7477	-4.4764	KP1
280.1	-2.5017	-6.9569	KP1
281.2	-2.5917	-7.2757	KP1

Appendix A2. Supplement to Chapter 2: Detrital zircon sample information and data from reference materials used for LA-ICPMS analyzes

Samples E1309-0 and -1 are from the pebble conglomerate developed above the unconformity defining the base of TU2; both clasts and matrix were processed. Sample F1302 and F1108 are from medium-grained sandstone beds in the middle (Saddle Peak Hills) and upper (Alexander Hills) parts of the Horse Thief Springs Formation, respectively. Two samples from the Beck Spring Dolomite (E1101-92.2, -293.7) are from pebble conglomerate beds at Saratoga Springs. The three KP1 samples are very fine to fine-grained sandstones from Alexander Hills (F1106, F1107) and Saratoga Springs (F1342). Samples from the lower part of TU3 include a sandy limestone from the Virgin Spring Limestone (VSL3-6.8) in the Saddle Peak Hills, a light green and pink, poorly sorted pebble conglomerate from KP2 (E1201) in the Saddle Peak Hills, a coarse sandstone from the top of KP2 (F1343) at Saratoga Springs. F1102 is a sample of KP3 from Sperry Wash (not shown in Fig. 2.7). F1345-188 and E1351-191 are samples from pebble conglomerate beds in the Silurian Hills.

Analysis was performed in 19 experiments in 5 sessions. Zircons were ablated with laser spots of 25 μm or 30 μm (wide using fluence and pulse rates of 5 J/cm^2 and 10 Hz, respectively, during a 45 second analysis (15 sec gas blank, 30 sec ablation) that excavated a pit ~25 μm deep. Ablated material was carried by a 1.2 L/min He gas stream to the nebulizer flow of the plasma. For experiments 1 and 2, dwell times were 5 microseconds for Si and Zr, 200 microseconds for ^{49}Ti and ^{207}Pb, 40 microseconds for

^{202}Hg, ^{204}Pb, ^{206}Pb, ^{208}Pb, ^{238}U, ^{232}Th and 10 microseconds for all other HFSE and REE. For all other experiments, dwell times were the same except for 80 microseconds for ^{206}Pb and ^{238}U.

Background count rates for each analyte were obtained prior to each spot analysis and subtracted from the raw count rate for each analyte. Ablation pits that appear to have intersected glass or mineral inclusions were identified by time-resolved data that show large fluctuations in Ti or P. U-Pb dates from these analyzes are considered valid if the time-resolved U-Pb ratios appear to have been unaffected by the inclusions. Analyzes that appear contaminated by common Pb were rejected based on an intensity of mass 204 above baseline. For concentration calculations, background-subtracted count rates for each analyte were internally normalized to ^{29}Si and calibrated with respect to NIST SRM-610 and -612 glasses as the primary standards. Temperature was calculated from the Ti-in-zircon thermometer (Watson et al., 2006). Because there are no constraints on the activity of TiO_2 in the source rocks, an average value in crustal rocks of 0.8 was used.

For U-Pb and ^{207}Pb-^{206}Pb dates, instrumental fractionation of the background-subtracted ratios was corrected and dates were calibrated with respect to interspersed measurements of the Plešovice zircon standard (Sláma et al., 2008). Two analyzes of Plešovice were done for every 10 analyzes of unknown zircon; a polynomial fit to the standard analyzes yields each sample-specific fractionation factor. Signals at mass 204 were indistinguishable from zero following subtraction of mercury backgrounds measured during the gas blank (<1000 cps ^{202}Hg), and thus dates are reported without common Pb correction. Radiogenic isotope ratio and age error propagation for all analyzes includes uncertainty contributions from counting statistics and background

subtraction. For spot analyzes that are individually interpreted (e.g., detrital zircon analyzes), the uncertainty from the standard calibration is propagated into the error on each date. This uncertainty is the standard deviation of the time-varying U-Pb fractionation factor and the standard error of the mean of the time-invariant, smaller ^{207}Pb-^{206}Pb fractionation factor. Standard calibration uncertainties for ^{207}Pb-^{206}Pb dates ranged from 0.4% to 1.6% (2σ). Standard calibration uncertainties for ^{206}Pb-^{238}U dates ranged from 2.0% to 9.3% (2σ). Age interpretations are based on ^{207}Pb-^{206}Pb dates. Analyzes with >20% discordance are not considered. Errors on the dates from individual analyzes are given at 2σ. Detrital zircon age histograms were generated with Isoplot (Ludwig, 2008). To better highlight stratigraphic provenance changes within TU2 in and to avoid smoothing of data, each sample was normalized individually.

Two zircon secondary reference materials were treated as unknowns to assess accuracy, interspersed as groups of two analyzes for every 20 unknown analyzes. Weighted mean dates are calculated using Isoplot 3.0 (Ludwig, 2003) from errors on individual dates that do not include the standard calibration uncertainties. However, errors on weighted mean dates include the standard calibration uncertainties within each experiment. FC-1 zircon (1098 Ma from unpublished CA-TIMS data, Boise State University) and Seiland zircon (530 Ma from unpublished CA-TIMS data, Boise State University) yielded accurate dates.

Appendix A3. Supplement to Chapter 2: Detrital zircon LA-ICPMS data

LA-ICPMS data from sample E1101-92.2									
	Dates (Ma)								
	208Pb*	±2s	207Pb*	±2s	207Pb*	±2s	206Pb*	±2s	%
Analysis	232Th	(Ma)	206Pb*	(Ma)	235U	(Ma)	238U*	(Ma)	disc.
E1101-92.2	1224	88	1159	79	1181	45	1193	55	3
E1101-92.2	1491	98	1410	33	1442	40	1463	64	4
E1101-92.2	1237	82	1349	26	1289	31	1253	46	8
E1101-92.2	1539	111	1677	36	1634	40	1601	64	5
E1101-92.2	3223	326	3093	44	3092	53	3089	115	0
E1101-92.2	1363	98	1429	23	1404	40	1387	63	3
E1101-92.2	2529	198	2504	44	2476	47	2443	88	3
E1101-92.2	1353	161	1365	102	1294	57	1252	64	9
E1101-92.2	1143	78	1195	48	1094	43	1044	57	14
E1101-92.2	3150	211	3261	20	3205	46	3116	112	6
E1101-92.2	1194	82	1335	76	1248	45	1198	53	11
E1101-92.2	1410	108	1383	45	1404	41	1418	61	3
E1101-92.2	2272	148	1787	31	1787	43	1787	76	0
E1101-92.2	1530	97	1284	49	1227	46	1195	64	8
E1101-92.2	1471	136	1153	109	1198	58	1223	68	7
E1101-92.2	1915	121	1490	39	1471	41	1457	64	2
E1101-92.2	3280	198	2484	39	2474	50	2461	100	1
E1101-92.2	3601	259	2644	33	2632	48	2616	100	1
E1101-92.2	2330	156	1800	34	1758	44	1722	73	5
E1101-92.2	1976	158	1578	88	1489	58	1427	73	11
E1101-92.2	2428	166	1726	39	1765	45	1798	77	5
E1101-92.2	1970	126	1495	41	1447	34	1414	49	6
E1101-92.2	3617	231	2631	33	2631	46	2631	96	0
E1101-92.2	2204	155	1614	44	1581	40	1556	60	4
E1101-92.2	2479	160	1792	58	1786	50	1781	77	1
E1101-92.2	1640	127	1451	42	1389	43	1349	64	8
E1101-92.2	2152	144	1809	31	1777	40	1750	67	4
E1101-92.2	1604	110	1238	66	1175	42	1141	53	9
E1101-92.2	2024	144	1476	57	1486	44	1492	64	1
E1101-92.2	1644	105	1243	33	1232	34	1225	49	2
E1101-92.2	1570	102	1247	50	1223	40	1209	55	3
E1101-92.2	1346	150	1216	44	1173	39	1150	54	6
E1101-92.2	2484	162	1926	32	1884	39	1845	68	5
E1101-92.2	3512	220	2557	37	2534	46	2507	92	2
E1101-92.2	2009	128	1757	48	1620	38	1516	52	15
E1101-92.2	2558	159	1872	34	1880	41	1887	71	1
E1101-92.2	1961	125	1469	41	1450	39	1437	58	2
E1101-92.2	1625	111	1128	91	1176	53	1202	67	7

E1101-92.2	1898	141	1481	45	1504	55	1520	89	3
E1101-92.2	2382	159	1809	35	1746	46	1694	77	7
E1101-92.2	2467	188	1807	59	1784	50	1765	76	3
E1101-92.2	1796	121	1442	44	1405	39	1380	57	5
E1101-92.2	2160	160	1591	57	1521	45	1470	64	8
E1101-92.2	2449	161	1805	31	1783	42	1764	72	3
E1101-92.2	1971	126	1450	34	1427	40	1412	62	3
E1101-92.2	2066	166	1372	65	1399	52	1418	75	4
E1101-92.2	2399	149	1863	42	1790	50	1729	83	8
E1101-92.2	1993	156	1454	106	1447	62	1442	74	1
E1101-92.2	3196	210	2481	69	2523	72	2574	139	5
E1101-92.2	1115	103	1252	94	1242	55	1236	66	1
E1101-92.2	1558	99	1258	40	1241	44	1231	64	2
E1101-92.2	3003	219	2541	25	2545	53	2548	114	0
E1101-92.2	2229	151	1857	39	1879	42	1900	73	-2
E1101-92.2	1347	98	1169	73	1194	41	1208	51	-3
E1101-92.2	1891	132	1734	34	1743	37	1751	62	-1
E1101-92.2	1968	140	1767	30	1764	42	1763	73	0
E1101-92.2	1269	89	1215	40	1208	37	1203	53	1
E1101-92.2	1479	115	1446	64	1443	44	1441	59	0
E1101-92.2	2732	197	2744	56	2636	60	2497	111	9
E1101-92.2	1153	78	1202	50	1167	36	1149	47	4
E1101-92.2	1820	121	1784	23	1786	38	1787	68	0
E1101-92.2	1272	95	1224	36	1223	35	1222	51	0
E1101-92.2	1256	83	1260	62	1224	38	1204	48	4
E1101-92.2	1336	139	1768	72	1688	53	1624	73	8
E1101-92.2	1288	93	1331	75	1327	44	1325	54	0
E1101-92.2	1250	87	1187	69	1193	40	1197	50	-1
E1101-92.2	1531	105	1434	39	1434	38	1435	59	0
E1101-92.2	1528	110	1722	29	1621	48	1545	79	10
E1101-92.2	1930	132	1806	28	1764	39	1729	66	4
E1101-92.2	1525	104	1438	34	1420	34	1408	51	2
E1101-92.2	1364	91	1216	55	1245	38	1262	52	-4
E1101-92.2	2150	168	1730	46	1745	43	1758	69	-2
E1101-92.2	1898	146	1676	37	1656	54	1641	91	2
E1101-92.2	2394	155	2067	27	2090	40	2114	77	-2
E1101-92.2	2118	145	1731	35	1748	43	1763	74	-2
E1101-92.2	1081	98	1306	37	1237	35	1197	49	8
E1101-92.2	1274	123	1368	69	1376	42	1381	53	-1
E1101-92.2	2449	201	2606	23	2557	33	2496	67	4
E1101-92.2	1576	136	1692	35	1684	30	1678	46	1
E1101-92.2	1729	146	1769	33	1778	35	1785	59	-1
E1101-92.2	1811	156	1792	36	1790	39	1788	65	0
E1101-92.2	1565	136	1606	29	1595	40	1587	67	1
E1101-92.2	1623	140	1634	51	1605	40	1583	57	3
E1101-92.2	1557	141	1470	27	1492	34	1508	56	-3
E1101-92.2	1519	136	1444	51	1395	45	1363	65	6
E1101-92.2	1570	136	1683	56	1558	40	1467	53	13
E1101-92.2	1858	157	1701	44	1727	46	1748	77	-3
E1101-92.2	2856	323	1852	102	1846	85	1840	131	1

E1101-92.2	2593	208	2418	40	2355	47	2282	88	6
E1101-92.2	1980	163	1809	45	1799	57	1792	99	1
E1101-92.2	1944	178	1774	50	1770	41	1766	63	0
E1101-92.2	2716	222	2543	37	2501	48	2448	96	4
E1101-92.2	2091	180	1770	49	1790	48	1807	80	-2
E1101-92.2	3087	248	2757	42	2774	47	2797	97	-1
E1101-92.2	1806	154	1639	44	1653	48	1665	79	-2
E1101-92.2	1929	199	1718	44	1786	50	1845	87	-7
E1101-92.2	2069	191	1835	42	1899	57	1959	105	-7
E1101-92.2	1294	145	1595	51	1523	37	1472	50	8
E1101-92.2	1786	146	1743	34	1754	35	1763	57	-1
E1101-92.2	1450	149	1725	39	1581	37	1475	54	15
E1101-92.2	1226	102	1193	57	1241	35	1269	45	-6
E1101-92.2	1093	98	1382	70	1253	40	1180	46	15
E1101-92.2	1604	137	1650	31	1705	34	1750	58	-6
E1101-92.2	1659	147	1466	65	1448	48	1435	67	2
E1101-92.2	2338	264	2213	50	2138	87	2062	164	7
E1101-92.2	1839	171	1793	55	1708	48	1640	71	9
E1101-92.2	2057	178	1770	51	1745	50	1724	81	3
E1101-92.2	2332	288	2348	112	2213	101	2070	162	12
E1101-92.2	1722	146	1448	50	1480	47	1503	74	-4
E1101-92.2	1669	142	1453	50	1465	43	1473	64	-1
E1101-92.2	1683	172	1450	109	1442	65	1438	79	1
E1101-92.2	1297	118	1169	135	1234	64	1271	68	-9
E1101-92.2	1402	122	1393	40	1379	30	1369	42	2
E1101-92.2	2938	245	2585	31	2636	51	2703	114	-5
E1101-92.2	1286	116	1226	44	1222	35	1221	49	0
E1101-92.2	1802	152	1749	58	1740	46	1732	68	1
E1101-92.2	1489	126	1377	34	1387	38	1394	59	-1
E1101-92.2	1772	160	1744	41	1716	47	1694	77	3
E1101-92.2	1285	108	1222	87	1216	49	1212	58	1
E1101-92.2	2286	202	2577	28	2512	39	2433	77	6
E1101-92.2	1028	98	1221	57	1203	39	1193	51	2
LA-ICPMS									
	Dates (Ma)								
	208Pb*	**±2s**	**207Pb***	**±2s**	**207Pb***	**±2s**	**206Pb***	**±2s**	**%**
Analysis	**232Th**	**(Ma)**	**206Pb***	**(Ma)**	**235U**	**(Ma)**	**238U***	**(Ma)**	**disc.**
E1101-293.7	2997	235	3107	22	3090	42	3063	101	1
E1101-293.7	3376	275	3102	30	3040	41	2947	89	5
E1101-293.7	3128	253	3084	21	3117	46	3168	113	-3
E1101-293.7	3391	270	2944	30	2929	45	2908	102	1
E1101-293.7	2582	224	2904	41	2754	48	2554	91	12
E1101-293.7	2837	221	2845	17	2803	39	2746	88	3
E1101-293.7	3350	275	2703	70	2601	78	2472	146	9
E1101-293.7	3212	270	2651	32	2660	48	2672	104	-1
E1101-293.7	3292	262	2643	26	2655	41	2671	89	-1
E1101-293.7	3163	244	2539	50	2562	55	2591	108	-2
E1101-293.7	2485	207	2523	34	2516	42	2508	83	1
E1101-293.7	2838	293	2506	37	2497	48	2485	96	1

E1101-293.7	2695	276	2468	42	2383	49	2284	92	7
E1101-293.7	2811	230	2382	36	2408	44	2438	87	-2
E1101-293.7	2168	172	2084	32	2083	41	2083	77	0
E1101-293.7	2907	271	2076	28	2088	42	2100	79	-1
E1101-293.7	3125	427	2060	95	2070	66	2080	92	-1
E1101-293.7	2332	225	1940	76	1831	49	1738	61	10
E1101-293.7	2144	169	1856	24	1824	39	1797	69	3
E1101-293.7	2154	180	1849	37	1765	40	1694	64	8
E1101-293.7	2209	182	1847	54	1854	41	1860	61	-1
E1101-293.7	1884	163	1839	39	1852	36	1864	59	-1
E1101-293.7	2312	207	1826	33	1858	43	1887	78	-3
E1101-293.7	2488	218	1820	51	1840	51	1858	87	-2
E1101-293.7	1768	139	1816	32	1779	38	1747	64	4
E1101-293.7	1927	153	1809	37	1802	36	1796	60	1
E1101-293.7	2137	173	1808	30	1786	38	1768	65	2
E1101-293.7	2004	156	1802	36	1779	41	1759	69	2
E1101-293.7	2041	165	1797	42	1763	41	1734	67	4
E1101-293.7	2318	276	1790	33	1740	61	1699	105	5
E1101-293.7	2247	194	1788	52	1810	46	1829	75	-2
E1101-293.7	1881	154	1783	29	1751	38	1725	65	3
E1101-293.7	2339	190	1775	38	1766	46	1759	78	1
E1101-293.7	1781	149	1772	27	1800	36	1824	63	-3
E1101-293.7	1555	150	1771	41	1726	39	1690	62	5
E1101-293.7	1833	149	1755	67	1760	43	1763	56	0
E1101-293.7	1636	132	1712	31	1701	38	1692	65	1
E1101-293.7	1719	148	1703	25	1740	41	1771	73	-4
E1101-293.7	1847	162	1697	32	1695	31	1694	49	0
E1101-293.7	2194	171	1682	32	1608	33	1553	52	8
E1101-293.7	1941	180	1653	38	1661	38	1666	62	-1
E1101-293.7	1683	198	1645	38	1596	45	1559	73	5
E1101-293.7	1394	122	1632	38	1511	63	1426	100	13
E1101-293.7	2185	189	1629	49	1677	45	1716	72	-5
E1101-293.7	1984	171	1619	46	1586	48	1562	75	3
E1101-293.7	2116	196	1550	49	1501	36	1465	49	5
E1101-293.7	1948	162	1516	39	1486	38	1465	59	3
E1101-293.7	1734	146	1498	55	1452	42	1421	59	5
E1101-293.7	1476	124	1490	49	1483	37	1479	52	1
E1101-293.7	1740	155	1479	63	1494	49	1504	71	-2
E1101-293.7	1779	180	1473	55	1490	41	1502	58	-2
E1101-293.7	1769	148	1471	30	1438	42	1415	67	4
E1101-293.7	1936	165	1467	54	1493	40	1511	57	-3
E1101-293.7	1751	146	1464	58	1390	40	1343	52	8
E1101-293.7	1376	120	1451	37	1428	33	1412	48	3
E1101-293.7	1714	145	1451	40	1442	34	1436	49	1
E1101-293.7	1514	125	1448	40	1460	34	1468	50	-1
E1101-293.7	1746	145	1447	50	1455	39	1460	57	-1
E1101-293.7	1796	181	1446	77	1465	45	1477	56	-2
E1101-293.7	1939	161	1446	36	1465	34	1479	53	-2
E1101-293.7	1670	142	1445	35	1416	39	1397	59	3
E1101-293.7	1918	168	1437	39	1458	35	1473	53	-3

E1101-293.7	1400	116	1428	24	1419	35	1413	55	1
E1101-293.7	1821	155	1426	57	1462	39	1487	53	-4
E1101-293.7	1679	180	1420	79	1386	48	1364	60	4
E1101-293.7	1410	117	1419	38	1430	31	1438	46	-1
E1101-293.7	1669	145	1414	50	1436	39	1451	56	-3
E1101-293.7	1441	137	1412	71	1436	44	1453	57	-3
E1101-293.7	1407	113	1404	27	1412	27	1417	41	-1
E1101-293.7	1783	163	1394	49	1456	39	1498	58	-7
E1101-293.7	1724	144	1392	41	1375	33	1365	47	2
E1101-293.7	1654	143	1389	43	1337	47	1305	70	6
E1101-293.7	1403	121	1389	65	1389	39	1389	48	0
E1101-293.7	1667	143	1387	45	1322	33	1283	44	7
E1101-293.7	1439	130	1384	46	1320	43	1281	62	7
E1101-293.7	1264	110	1383	77	1353	41	1333	44	4
E1101-293.7	1259	160	1381	39	1323	40	1287	59	7
E1101-293.7	1725	146	1381	41	1432	34	1467	50	-6
E1101-293.7	1427	210	1377	156	1260	71	1193	60	13
E1101-293.7	1649	144	1357	73	1324	47	1304	61	4
E1101-293.7	1706	146	1350	58	1381	43	1400	61	-4
E1101-293.7	1557	165	1317	87	1259	45	1225	49	7
E1101-293.7	1541	136	1303	30	1293	30	1286	45	1
E1101-293.7	1697	140	1298	53	1267	38	1249	52	4
E1101-293.7	1482	125	1297	47	1212	38	1165	51	10
E1101-293.7	1627	137	1290	68	1322	40	1341	51	-4
E1101-293.7	1431	196	1277	66	1247	46	1230	60	4
E1101-293.7	1471	129	1256	53	1208	35	1182	44	6
E1101-293.7	1223	105	1249	44	1220	31	1204	42	4
E1101-293.7	1318	296	1247	33	1234	28	1226	40	2
E1101-293.7	1432	124	1247	63	1218	35	1202	41	4
E1101-293.7	1610	145	1226	82	1205	45	1193	52	3
E1101-293.7	1452	125	1226	59	1207	38	1197	49	2
E1101-293.7	1292	113	1224	37	1247	33	1261	48	-3
E1101-293.7	1512	129	1218	79	1199	45	1188	54	2
E1101-293.7	1638	154	1206	53	1231	41	1245	57	-3
E1101-293.7	1481	141	1205	88	1200	47	1197	55	1
E1101-293.7	1208	129	1202	113	1215	55	1223	57	-2
E1101-293.7	1530	149	1198	61	1191	39	1188	51	1
E1101-293.7	1429	296	1194	36	1199	31	1202	43	-1
E1101-293.7	1262	102	1193	52	1193	35	1193	47	0
E1101-293.7	1573	129	1185	79	1195	43	1200	52	-1
E1101-293.7	1161	100	1146	46	1172	33	1186	46	-3
E1101-293.7	1579	164	1131	115	1168	52	1189	50	-5
E1101-293.7	1391	124	1098	93	1154	44	1184	46	-8
LA-ICPMS									
	Dates (Ma)								
	208Pb*	**±2s**	**207Pb***	**±2s**	**207Pb***	**±2s**	**206Pb***	**±2s**	**%**
Analysis	**232Th**	**(Ma)**	**206Pb***	**(Ma)**	**235U**	**(Ma)**	**238U***	**(Ma)**	**disc.**
E1201	1559	142	2343	43	2184	57	2018	101	14
E1201	1400	89	1819	35	1726	49	1650	82	9

E1201	1596	96	1816	39	1741	52	1680	87	7
E1201	1643	96	1805	35	1745	50	1695	85	6
E1201	1727	101	1802	34	1772	47	1746	81	3
E1201	1551	106	1799	36	1760	53	1728	92	4
E1201	1731	117	1786	25	1770	48	1756	86	2
E1201	1797	105	1783	38	1752	59	1725	102	3
E1201	1405	121	1781	39	1662	77	1570	127	12
E1201	1656	97	1775	32	1669	50	1586	83	11
E1201	1527	106	1775	35	1726	58	1686	101	5
E1201	1836	111	1774	38	1738	53	1708	91	4
E1201	1297	90	1771	34	1638	58	1536	94	13
E1201	1564	92	1769	34	1676	46	1603	74	9
E1201	1385	81	1751	25	1684	43	1631	72	7
E1201	1302	89	1737	30	1638	46	1563	74	10
E1201	1388	92	1736	55	1603	65	1504	100	13
E1201	1114	134	1728	29	1624	64	1545	106	11
E1201	1108	98	1718	32	1568	43	1460	67	15
E1201	1452	89	1712	66	1635	52	1576	75	8
E1201	1433	111	1683	45	1542	85	1440	136	14
E1201	1528	87	1505	63	1417	49	1359	67	10
E1201	1141	66	1157	64	1195	46	1216	63	-5
E1201	1271	70	1153	86	1166	54	1172	69	-2
LA-ICPMS									
	Dates (Ma)								
	208Pb*	**±2s**	**207Pb***	**±2s**	**207Pb***	**±2s**	**206Pb***	**±2s**	**%**
Analysis	**232Th**	**(Ma)**	**206Pb***	**(Ma)**	**235U**	**(Ma)**	**238U***	**(Ma)**	**disc.**
E1309-0	3636	334	3100	34	3083	63	3056	150	1
E1309-0	3442	321	3063	28	3029	51	2978	118	3
E1309-0	3614	412	2878	54	2711	63	2492	119	13
E1309-0	3453	337	2728	30	2735	52	2744	115	-1
E1309-0	3054	311	2644	38	2587	57	2515	117	5
E1309-0	1900	187	2447	33	2395	51	2335	101	5
E1309-0	2191	228	2407	36	2426	51	2449	103	-2
E1309-0	1876	227	2301	37	2178	55	2051	100	11
E1309-0	1857	203	2023	67	2026	48	2029	70	0
E1309-0	2019	198	1883	32	1905	42	1924	75	-2
E1309-0	2225	264	1875	33	1745	65	1639	110	13
E1309-0	3790	1667	1860	351	1721	192	1609	178	13
E1309-0	2293	261	1839	64	1852	56	1863	90	-1
E1309-0	1748	182	1829	43	1775	50	1730	84	5
E1309-0	2329	252	1828	44	1795	56	1767	95	3
E1309-0	1502	215	1827	53	1761	48	1706	74	7
E1309-0	1903	197	1818	43	1815	50	1812	85	0
E1309-0	2112	215	1815	39	1773	55	1738	95	4
E1309-0	2005	199	1799	26	1807	36	1814	63	-1
E1309-0	2062	199	1798	33	1786	45	1776	79	1
E1309-0	1780	180	1793	38	1781	41	1771	68	1
E1309-0	2181	233	1792	45	1817	57	1839	100	-3
E1309-0	1065	186	1785	30	1735	42	1693	71	5

E1309-0	2115	231	1784	81	1753	58	1726	80	3
E1309-0	2043	212	1782	42	1807	42	1830	70	-3
E1309-0	1660	170	1780	46	1670	51	1583	80	11
E1309-0	1846	186	1779	45	1785	51	1790	86	-1
E1309-0	1620	168	1774	38	1786	37	1796	62	-1
E1309-0	2088	215	1766	37	1747	46	1732	78	2
E1309-0	1820	199	1765	40	1798	50	1827	89	-3
E1309-0	2181	222	1754	47	1803	45	1846	75	-5
E1309-0	2192	230	1745	35	1762	47	1777	82	-2
E1309-0	1618	173	1731	31	1754	41	1773	70	-2
E1309-0	1732	187	1729	54	1669	56	1621	89	6
E1309-0	2206	214	1728	56	1693	60	1665	97	4
E1309-0	1771	211	1727	88	1616	59	1532	75	11
E1309-0	2189	225	1713	39	1755	43	1791	73	-5
E1309-0	1678	177	1712	50	1736	48	1756	79	-3
E1309-0	2074	226	1696	25	1690	43	1686	74	1
E1309-0	2225	255	1694	63	1653	53	1621	78	4
E1309-0	1858	264	1682	40	1583	69	1510	112	10
E1309-0	2120	199	1674	44	1687	51	1697	85	-1
E1309-0	1685	169	1670	60	1632	50	1603	75	4
E1309-0	2151	246	1651	36	1642	41	1635	68	1
E1309-0	2075	218	1642	58	1635	48	1630	73	1
E1309-0	2077	216	1630	41	1685	52	1730	90	-6
E1309-0	1772	212	1619	49	1626	50	1631	80	-1
E1309-0	1924	204	1595	65	1585	53	1577	78	1
E1309-0	1777	169	1489	43	1496	45	1500	70	-1
E1309-0	1803	185	1481	42	1497	39	1508	60	-2
E1309-0	1966	208	1478	77	1488	53	1495	72	-1
E1309-0	1382	153	1477	43	1502	43	1520	68	-3
E1309-0	1796	169	1462	43	1484	49	1500	79	-3
E1309-0	1726	184	1459	36	1446	45	1438	71	1
E1309-0	1736	183	1459	38	1475	45	1486	71	-2
E1309-0	1654	166	1456	45	1438	50	1426	77	2
E1309-0	1485	161	1455	57	1466	49	1474	73	-1
E1309-0	1679	175	1439	40	1406	43	1385	66	4
E1309-0	1625	167	1436	39	1421	50	1412	79	2
E1309-0	1725	179	1428	56	1451	56	1466	87	-3
E1309-0	1619	210	1426	94	1339	55	1285	65	10
E1309-0	1635	169	1400	39	1375	50	1359	77	3
E1309-0	1676	175	1391	60	1388	56	1387	83	0
E1309-0	1260	128	1362	34	1327	36	1305	54	4
E1309-0	1341	153	1342	61	1241	48	1183	64	12
E1309-0	1602	170	1331	83	1337	59	1341	81	-1
E1309-0	1646	176	1310	42	1330	43	1343	66	-2
E1309-0	1141	127	1306	46	1233	34	1191	45	9
E1309-0	1522	180	1304	131	1280	66	1266	69	3
E1309-0	1430	148	1292	72	1241	46	1211	59	6
E1309-0	1457	157	1290	103	1227	53	1191	58	8
E1309-0	1442	151	1281	38	1225	37	1193	53	7
E1309-0	1198	154	1281	105	1244	54	1222	60	5

E1309-0	1195	142	1279	89	1251	48	1235	54	3
E1309-0	1626	168	1277	47	1314	42	1337	62	-5
E1309-0	1158	126	1267	59	1253	37	1245	48	2
E1309-0	1415	180	1240	97	1195	61	1170	76	6
E1309-0	1472	148	1225	54	1224	44	1223	62	0
E1309-0	1305	149	1220	161	1202	72	1193	65	2
E1309-0	1479	151	1217	49	1219	38	1220	52	0
E1309-0	1126	127	1203	74	1221	44	1231	55	-2
E1309-0	1531	162	1201	88	1215	55	1222	70	-2
E1309-0	1465	157	1195	72	1220	42	1234	53	-3
E1309-0	1487	159	1188	34	1144	40	1120	58	6
E1309-0	1490	161	1183	48	1215	39	1233	55	-4
E1309-0	1181	132	1179	57	1225	41	1251	57	-6
E1309-0	1155	127	1177	55	1211	35	1230	46	-4
E1309-0	520	94	1169	105	1201	56	1219	66	-4
E1309-0	1382	152	1159	66	1147	42	1140	53	2
E1309-0	1473	159	1150	75	1133	47	1123	60	2
E1309-0	1200	122	1150	39	1144	36	1141	51	1
E1309-0	1341	163	1143	118	1110	53	1094	51	4
E1309-0	1477	172	1132	86	1181	45	1208	54	-7
E1309-0	1370	146	1107	47	1125	33	1134	45	-2
E1309-0	1446	160	1106	46	1175	35	1213	50	-10
E1309-0	983	142	1095	40	1001	45	959	60	12
E1309-0	1191	122	1089	70	1067	40	1056	47	3
E1309-0	1304	138	1082	60	1147	41	1181	56	-9
E1309-0	1278	139	1069	97	1036	52	1021	61	5
E1309-0	1322	148	1054	57	1085	40	1101	54	-4
E1309-0	1034	116	1019	66	1055	40	1072	51	-5
LA-ICPMS									
	Dates (Ma)								
	208Pb*	**±2s**	**207Pb***	**±2s**	**207Pb***	**±2s**	**206Pb***	**±2s**	**%**
Analysis	**232Th**	**(Ma)**	**206Pb***	**(Ma)**	**235U**	**(Ma)**	**238U***	**(Ma)**	**disc.**
E1309-1	3516	347	2892	26	2904	40	2921	92	-1
E1309-1	3354	380	2666	51	2618	46	2556	80	4
E1309-1	3182	314	2600	32	2597	58	2594	127	0
E1309-1	3268	334	2535	31	2537	45	2539	95	0
E1309-1	3031	285	2517	28	2561	35	2617	72	-4
E1309-1	3118	301	2491	50	2400	44	2294	73	8
E1309-1	3077	293	2457	38	2464	51	2473	102	-1
E1309-1	2878	271	2365	33	2353	37	2340	71	1
E1309-1	2922	276	2362	41	2348	41	2332	73	1
E1309-1	2295	226	1917	36	1867	44	1823	76	5
E1309-1	2481	238	1882	41	1910	55	1935	99	-3
E1309-1	2171	240	1882	67	1849	53	1819	80	3
E1309-1	2003	198	1863	28	1873	31	1881	54	-1
E1309-1	2410	232	1855	37	1883	41	1908	72	-3
E1309-1	2335	226	1849	64	1823	53	1800	81	3
E1309-1	2304	228	1849	49	1844	59	1840	103	1
E1309-1	2505	265	1849	49	1856	48	1863	80	-1

E1309-1	2168	208	1848	42	1880	39	1909	66	-3
E1309-1	2182	220	1831	45	1849	54	1866	94	-2
E1309-1	2073	208	1822	41	1772	46	1730	75	5
E1309-1	2231	217	1820	48	1859	39	1894	62	-4
E1309-1	2105	236	1811	37	1790	39	1772	64	2
E1309-1	2484	245	1804	37	1768	43	1738	72	4
E1309-1	2078	198	1799	45	1759	42	1726	66	4
E1309-1	2414	234	1797	21	1779	38	1763	68	2
E1309-1	2372	238	1796	26	1778	41	1762	73	2
E1309-1	2134	206	1795	38	1804	42	1811	71	-1
E1309-1	2162	210	1790	53	1708	51	1643	79	8
E1309-1	2189	216	1789	57	1804	55	1817	91	-2
E1309-1	1924	222	1778	46	1773	57	1769	99	1
E1309-1	2158	241	1778	33	1787	54	1795	97	-1
E1309-1	2286	226	1774	49	1812	48	1846	81	-4
E1309-1	2185	216	1773	42	1769	49	1765	83	0
E1309-1	2227	230	1766	45	1778	51	1789	87	-1
E1309-1	1904	187	1761	31	1785	41	1807	71	-3
E1309-1	2164	210	1717	33	1718	34	1718	56	0
E1309-1	2053	219	1713	42	1738	40	1760	65	-3
E1309-1	2088	216	1702	37	1740	46	1771	80	-4
E1309-1	2083	200	1691	50	1705	43	1717	67	-1
E1309-1	2184	215	1687	40	1722	40	1750	66	-4
E1309-1	1556	159	1664	68	1621	47	1588	64	5
E1309-1	2004	197	1644	43	1657	37	1667	57	-1
E1309-1	2139	241	1634	128	1541	69	1475	69	10
E1309-1	1960	193	1622	53	1603	53	1589	83	2
E1309-1	2097	200	1610	80	1564	55	1530	74	5
E1309-1	2070	212	1610	68	1505	44	1431	54	11
E1309-1	1996	205	1610	58	1573	54	1545	83	4
E1309-1	2002	197	1596	49	1608	44	1617	68	-1
E1309-1	2010	197	1587	64	1578	45	1571	62	1
E1309-1	1987	198	1584	56	1620	54	1647	87	-4
E1309-1	2147	216	1582	45	1582	34	1582	49	0
E1309-1	1951	202	1577	61	1537	45	1508	62	4
E1309-1	2001	194	1575	61	1571	54	1569	83	0
E1309-1	2059	203	1558	27	1567	34	1574	55	-1
E1309-1	2010	191	1537	56	1567	51	1589	80	-3
E1309-1	1999	198	1522	67	1560	47	1589	67	-4
E1309-1	1439	142	1518	23	1488	30	1467	48	3
E1309-1	1586	182	1504	53	1445	52	1405	77	7
E1309-1	1834	184	1486	47	1454	44	1432	67	4
E1309-1	1712	168	1486	58	1423	42	1382	56	7
E1309-1	1740	178	1481	52	1456	43	1438	62	3
E1309-1	1942	216	1477	89	1468	53	1462	65	1
E1309-1	1765	175	1466	46	1430	36	1407	51	4
E1309-1	1462	144	1464	25	1484	35	1499	57	-2
E1309-1	1269	136	1462	37	1437	35	1421	53	3
E1309-1	1759	178	1459	57	1452	45	1447	65	1
E1309-1	1812	178	1458	60	1473	54	1484	83	-2

E1309-1	2026	204	1457	64	1499	51	1529	75	-5
E1309-1	1773	185	1453	106	1462	62	1468	76	-1
E1309-1	1872	193	1447	54	1422	38	1405	52	3
E1309-1	1762	182	1443	61	1436	47	1431	67	1
E1309-1	1833	182	1442	55	1471	46	1491	68	-3
E1309-1	1467	144	1434	38	1458	31	1475	46	-3
E1309-1	1897	190	1428	69	1477	48	1511	67	-6
E1309-1	1755	172	1425	47	1363	41	1323	58	7
E1309-1	1773	176	1397	44	1412	41	1423	63	-2
E1309-1	1676	166	1395	53	1343	40	1311	55	6
E1309-1	1328	138	1392	47	1355	35	1331	48	4
E1309-1	1610	157	1385	55	1388	38	1391	52	0
E1309-1	1473	164	1383	103	1433	54	1466	61	-6
E1309-1	1597	160	1365	31	1344	34	1331	51	2
E1309-1	1463	149	1356	80	1272	43	1223	46	10
E1309-1	1637	162	1355	51	1336	38	1325	53	2
E1309-1	1290	136	1355	60	1329	39	1313	51	3
E1309-1	2083	262	1351	88	1323	55	1306	70	3
E1309-1	1763	203	1334	86	1347	89	1355	136	-2
E1309-1	1451	148	1326	85	1204	50	1137	58	14
E1309-1	1593	169	1316	53	1318	43	1319	62	0
E1309-1	1473	146	1297	39	1335	33	1359	48	-5
E1309-1	1518	150	1293	52	1236	46	1204	64	7
E1309-1	1297	129	1293	26	1335	27	1362	41	-5
E1309-1	1677	165	1285	43	1226	32	1193	43	7
E1309-1	1524	151	1281	35	1238	40	1214	58	5
E1309-1	1762	209	1279	71	1302	40	1316	49	-3
E1309-1	1584	154	1271	78	1251	51	1240	66	2
E1309-1	1773	195	1270	95	1335	52	1376	62	-8
E1309-1	1565	163	1268	86	1207	46	1173	52	7
E1309-1	1609	167	1268	42	1285	36	1295	52	-2
E1309-1	1505	157	1257	55	1259	54	1261	79	0
E1309-1	1396	137	1253	43	1239	36	1232	50	2
E1309-1	1509	151	1248	62	1239	43	1234	58	1
E1309-1	1609	158	1247	72	1249	42	1251	51	0
E1309-1	1536	159	1241	50	1242	33	1242	43	0
E1309-1	1502	162	1238	105	1214	50	1200	50	3
E1309-1	1560	158	1230	47	1230	35	1230	48	0
E1309-1	1635	161	1222	47	1265	32	1290	44	-6
E1309-1	1608	163	1220	64	1254	44	1274	60	-4
E1309-1	1492	152	1215	60	1199	38	1191	49	2
E1309-1	1644	169	1211	43	1200	32	1194	44	1
E1309-1	1408	147	1209	85	1231	47	1244	57	-3
E1309-1	1556	156	1197	57	1208	40	1214	54	-1
E1309-1	1586	162	1193	46	1176	32	1166	41	2
E1309-1	1534	158	1192	67	1221	42	1238	54	-4
E1309-1	1553	149	1191	92	1208	47	1217	53	-2
E1309-1	1426	142	1187	50	1217	38	1234	52	-4
E1309-1	1508	160	1187	63	1195	43	1199	57	-1
E1309-1	1485	145	1181	49	1214	36	1233	49	-4

E1309-1	1311	138	1180	48	1195	33	1203	45	-2
E1309-1	1494	162	1179	121	1225	57	1251	58	-6
E1309-1	1436	139	1174	44	1187	36	1195	50	-2
E1309-1	1178	126	1161	49	1177	32	1185	42	-2
E1309-1	1574	177	1161	58	1138	34	1126	42	3
E1309-1	1572	161	1159	66	1175	38	1184	47	-2
E1309-1	1659	196	1139	151	1171	60	1188	44	-4
E1309-1	1561	172	1136	35	1149	31	1156	44	-2
E1309-1	1269	135	1121	63	1100	40	1089	50	3
E1309-1	1012	104	1115	44	1076	35	1057	47	5
E1309-1	1305	135	1071	47	1086	38	1094	52	-2
E1309-1	1058	118	1041	47	1066	33	1079	44	-4
LA-ICPMS									
	Dates (Ma)								
	208Pb*	**±2s**	**207Pb***	**±2s**	**207Pb***	**±2s**	**206Pb***	**±2s**	**%**
Analysis	**232Th**	**(Ma)**	**206Pb***	**(Ma)**	**235U**	**(Ma)**	**238U***	**(Ma)**	**disc.**
E1351-191	3635	499	2986	26	2966	69	2937	164	2
E1351-191	3362	453	3027	32	2964	71	2873	164	5
E1351-191	3181	436	2697	29	2717	69	2743	158	-2
E1351-191	3008	433	2798	29	2758	69	2704	155	3
E1351-191	2870	406	2544	30	2497	73	2439	155	4
E1351-191	2079	156	2393	30	2388	54	2383	112	0
E1351-191	2271	169	2476	36	2362	62	2232	122	10
E1351-191	2515	343	1899	47	1935	66	1969	122	-4
E1351-191	2291	322	1945	31	1954	58	1962	109	-1
E1351-191	2369	319	1894	36	1878	64	1864	117	2
E1351-191	2186	300	1882	48	1870	66	1859	117	1
E1351-191	2160	304	1782	39	1818	63	1850	115	-4
E1351-191	2210	311	1880	36	1863	62	1849	113	2
E1351-191	2244	298	1801	35	1824	64	1844	117	-2
E1351-191	2344	345	1814	31	1828	63	1839	115	-1
E1351-191	2158	305	1818	35	1818	60	1818	108	0
E1351-191	2147	301	1895	50	1854	67	1818	116	4
E1351-191	2021	297	1856	22	1835	58	1816	107	2
E1351-191	2132	305	1808	35	1809	57	1809	102	0
E1351-191	2271	338	1690	57	1750	65	1801	112	-7
E1351-191	2222	330	1783	33	1791	68	1798	123	-1
E1351-191	1657	135	1887	76	1838	51	1795	68	5
E1351-191	2021	298	1765	33	1774	65	1783	117	-1
E1351-191	1531	112	1823	31	1797	45	1775	79	3
E1351-191	1531	127	1794	43	1778	51	1765	86	2
E1351-191	2271	334	1752	38	1755	67	1758	119	0
E1351-191	2026	288	1721	32	1740	58	1756	104	-2
E1351-191	2097	312	1715	34	1737	61	1755	109	-2
E1351-191	1984	287	1742	41	1748	61	1753	106	-1
E1351-191	2242	329	1779	37	1762	66	1747	117	2
E1351-191	2083	299	1762	24	1754	56	1747	100	1
E1351-191	2041	305	1697	38	1722	58	1743	102	-3
E1351-191	2088	314	1757	42	1749	65	1742	114	1

E1351-191	1489	116	1766	36	1750	47	1737	80	2
E1351-191	2162	300	1703	33	1721	59	1736	104	-2
E1351-191	2198	326	1820	33	1774	62	1735	109	5
E1351-191	1539	115	1733	40	1731	42	1730	70	0
E1351-191	2232	338	1819	32	1767	62	1723	110	5
E1351-191	1633	124	1817	37	1765	52	1722	89	5
E1351-191	1707	257	1721	35	1719	67	1718	118	0
E1351-191	1656	240	1918	211	1804	114	1707	101	11
E1351-191	1485	112	1727	40	1716	43	1707	72	1
E1351-191	2067	280	1618	50	1641	58	1659	97	-3
E1351-191	1959	275	1742	59	1694	59	1655	93	5
E1351-191	2023	300	1704	50	1676	67	1654	112	3
E1351-191	1755	260	1632	40	1611	60	1595	100	2
E1351-191	1882	257	1565	26	1578	54	1588	93	-1
E1351-191	1807	271	1569	28	1572	59	1574	101	0
E1351-191	1909	287	1607	31	1565	63	1534	105	5
E1351-191	1807	257	1465	37	1484	54	1497	88	-2
E1351-191	1656	229	1481	39	1490	55	1496	90	-1
E1351-191	1818	264	1480	69	1486	57	1491	84	-1
E1351-191	1826	248	1429	49	1464	57	1487	92	-4
E1351-191	1790	256	1472	28	1481	51	1487	86	-1
E1351-191	1725	254	1467	54	1477	66	1485	105	-1
E1351-191	1798	275	1422	51	1458	64	1483	103	-4
E1351-191	1754	240	1469	70	1477	66	1483	101	-1
E1351-191	1815	274	1500	48	1490	59	1483	95	1
E1351-191	1593	279	1375	79	1436	63	1478	95	-7
E1351-191	1748	244	1349	59	1421	59	1470	92	-9
E1351-191	1791	259	1724	47	1576	60	1467	92	15
E1351-191	1772	292	1571	117	1509	76	1466	97	7
E1351-191	1667	220	1404	48	1439	61	1462	99	-4
E1351-191	1735	242	1452	41	1457	59	1460	96	0
E1351-191	1753	238	1442	50	1451	57	1457	89	-1
E1351-191	1858	262	1504	37	1475	54	1454	86	3
E1351-191	1755	255	1425	41	1442	68	1453	111	-2
E1351-191	1849	256	1441	41	1446	59	1449	95	-1
E1351-191	1511	225	1464	35	1451	61	1443	99	1
E1351-191	1818	271	1467	52	1451	65	1440	103	2
E1351-191	1675	250	1406	50	1426	61	1439	97	-2
E1351-191	1772	257	1415	43	1427	60	1436	96	-1
E1351-191	1721	241	1454	56	1443	59	1435	91	1
E1351-191	1740	250	1536	66	1476	62	1434	93	7
E1351-191	1641	246	1374	54	1409	61	1433	96	-4
E1351-191	1618	236	1406	39	1422	55	1433	89	-2
E1351-191	1651	259	1567	111	1486	75	1430	96	9
E1351-191	1700	259	1461	64	1434	62	1416	92	3
E1351-191	1393	139	1418	69	1415	54	1413	77	0
E1351-191	1734	252	1391	34	1404	58	1413	94	-2
E1351-191	1687	243	1469	47	1426	65	1397	102	5
E1351-191	1672	236	1502	76	1439	60	1397	85	7
E1351-191	1941	312	1518	63	1442	67	1392	100	8

E1351-191	1547	255	1489	92	1430	66	1390	89	7
E1351-191	1621	264	1574	171	1461	91	1385	92	12
E1351-191	1679	245	1335	56	1357	70	1371	110	-3
E1351-191	1562	217	1247	52	1320	60	1366	95	-10
E1351-191	1641	228	1324	53	1347	60	1362	93	-3
E1351-191	1647	251	1400	49	1372	60	1354	92	3
E1351-191	1588	219	1325	38	1339	53	1347	83	-2
E1351-191	1590	212	1420	54	1375	56	1345	83	5
E1351-191	1577	231	1282	54	1320	56	1343	86	-5
E1351-191	1540	224	1322	31	1332	50	1338	80	-1
E1351-191	1578	246	1296	38	1317	61	1330	97	-3
E1351-191	1681	245	1281	47	1298	49	1308	74	-2
E1351-191	1469	197	1232	53	1277	55	1304	83	-6
E1351-191	1479	206	1269	49	1287	53	1297	81	-2
E1351-191	1427	195	1209	61	1258	58	1287	87	-6
E1351-191	1323	229	1286	125	1281	77	1278	97	1
E1351-191	1557	228	1354	53	1307	52	1278	76	6
E1351-191	1495	201	1247	53	1262	56	1271	85	-2
E1351-191	1576	218	1250	95	1261	61	1268	79	-1
E1351-191	1582	222	1224	55	1248	53	1262	78	-3
E1351-191	1517	208	1251	62	1253	55	1254	80	0
E1351-191	1595	251	1326	35	1277	56	1249	85	6
E1351-191	1526	219	1280	47	1260	56	1248	84	2
E1351-191	1569	217	1339	38	1280	51	1244	76	7
E1351-191	1626	242	1243	45	1243	53	1242	79	0
E1351-191	1450	211	1258	48	1247	53	1240	79	1
E1351-191	1393	215	1178	41	1213	72	1233	111	-5
E1351-191	1467	209	1284	55	1251	51	1231	73	4
E1351-191	1374	214	1226	93	1224	62	1222	82	0
E1351-191	1543	242	1235	75	1222	65	1215	93	2
E1351-191	1581	221	1159	63	1193	53	1212	76	-5
E1351-191	1423	208	1279	40	1235	50	1210	74	5
E1351-191	1355	204	1259	50	1227	52	1209	75	4
E1351-191	1500	237	1204	56	1203	60	1202	88	0
E1351-191	1431	223	1223	97	1205	66	1194	87	2
E1351-191	1515	238	1291	64	1227	62	1191	88	8
E1351-191	1154	95	1180	95	1184	57	1185	71	0
E1351-191	1612	268	1333	126	1234	67	1177	73	12
E1351-191	1187	177	1223	32	1189	54	1171	80	4
E1351-191	1120	99	1264	77	1201	44	1166	52	8
LA-ICPMS									
	Dates (Ma)								
	208Pb*	**±2s**	**207Pb***	**±2s**	**207Pb***	**±2s**	**206Pb***	**±2s**	**%**
Analysis	**232Th**	**(Ma)**	**206Pb***	**(Ma)**	**235U**	**(Ma)**	**238U***	**(Ma)**	**disc.**
F901-10.0	1572	156	1803	22	1819	31	1832	54	-2
F901-10.0	1909	128	1783	42	1807	37	1828	60	-3
F901-10.0	1344	240	1549	81	1508	64	1480	92	4
F901-10.0	1430	109	1476	47	1383	43	1324	62	10
F901-10.0	1376	234	1413	215	1308	91	1245	60	12

F901-10.0	1104	124	1409	50	1402	36	1397	49	1
F901-10.0	1132	194	1298	102	1329	59	1348	74	-4
F901-10.0	1047	116	1280	84	1232	43	1204	45	6
F901-10.0	1103	73	1220	37	1157	33	1124	46	8
F901-10.0	1092	187	1208	147	1219	68	1226	68	-1
F901-10.0	1071	167	1193	53	1238	39	1263	54	-6
LA-ICPMS									
	Dates (Ma)								
	208Pb*	**±2s**	**207Pb***	**±2s**	**207Pb***	**±2s**	**206Pb***	**±2s**	**%**
Analysis	**232Th**	**(Ma)**	**206Pb***	**(Ma)**	**235U**	**(Ma)**	**238U***	**(Ma)**	**disc.**
F1102	1927	121	1954	64	1837	62	1735	97	11
F1102	1585	99	1946	84	1863	73	1790	112	8
F1102	1629	143	1842	47	1809	71	1780	125	3
F1102	1599	95	1744	40	1733	55	1724	94	1
F1102	1759	126	1682	193	1558	96	1469	79	13
F1102	1565	112	1681	56	1654	55	1632	87	3
F1102	1565	105	1649	59	1690	52	1723	83	-5
F1102	1839	104	1607	42	1576	51	1553	82	3
F1102	1488	101	1499	72	1470	61	1450	88	3
F1102	1494	94	1492	59	1439	59	1403	88	6
F1102	1287	79	1477	30	1383	42	1323	63	10
F1102	1508	95	1477	41	1378	41	1316	60	11
F1102	1599	114	1475	68	1407	57	1363	80	8
F1102	1429	82	1472	59	1442	52	1421	76	3
F1102	1547	89	1452	45	1410	54	1382	83	5
F1102	1249	82	1445	70	1420	51	1404	71	3
F1102	1278	81	1435	64	1392	51	1364	71	5
F1102	1249	81	1426	104	1407	63	1395	78	2
F1102	1507	88	1414	45	1350	44	1310	64	7
F1102	1312	94	1405	87	1406	55	1406	71	0
F1102	2127	259	1405	44	1409	48	1411	74	0
F1102	1367	107	1362	162	1275	73	1223	62	10
F1102	1167	71	1340	68	1296	51	1269	69	5
F1102	1167	79	1340	72	1322	49	1310	66	2
F1102	1001	63	1309	72	1181	49	1112	60	15
F1102	1325	83	1306	62	1217	49	1167	65	11
F1102	1253	71	1299	73	1202	51	1149	65	12
F1102	1133	68	1290	62	1189	44	1135	57	12
F1102	1103	69	1260	74	1195	51	1160	66	8
F1102	1201	73	1259	63	1320	52	1357	76	-8
F1102	1273	75	1237	88	1229	60	1224	79	1
F1102	1069	62	1230	43	1167	41	1133	58	8
F1102	1105	67	1229	48	1194	42	1174	59	4
F1102	1398	87	1217	59	1195	48	1182	66	3
F1102	1108	67	1209	66	1162	44	1137	56	6
F1102	1074	59	1188	74	1166	49	1154	63	3
F1102	1112	67	1144	103	1169	56	1182	66	-3
F1102	1166	74	1128	102	1195	55	1233	66	-9
F1102	1276	105	1128	81	1196	54	1234	73	-9

F1102	930	66	1012	75	1058	47	1081	60	-7
LA-ICPMS									
	Dates (Ma)								
	208Pb*	**±2s**	**207Pb***	**±2s**	**207Pb***	**±2s**	**206Pb***	**±2s**	**%**
Analysis	**232Th**	**(Ma)**	**206Pb***	**(Ma)**	**235U**	**(Ma)**	**238U***	**(Ma)**	**disc.**
F1105	2552	452	1792	55	1841	66	1885	116	-5
F1105	1741	271	1394	78	1450	63	1489	94	-7
F1105	1509	244	1280	153	1205	64	1164	49	9
F1105	1306	219	1118	122	1143	92	1156	127	-3
LA-ICPMS									
	Dates (Ma)								
	208Pb*	**±2s**	**207Pb***	**±2s**	**207Pb***	**±2s**	**206Pb***	**±2s**	**%**
Analysis	**232Th**	**(Ma)**	**206Pb***	**(Ma)**	**235U**	**(Ma)**	**238U***	**(Ma)**	**disc.**
F1106	1622	100	1891	57	1815	52	1750	81	7
F1106	1690	119	1887	28	1845	45	1807	81	4
F1106	1554	116	1837	27	1807	51	1781	91	3
F1106	1810	112	1828	41	1739	39	1665	61	9
F1106	1861	109	1807	36	1776	38	1749	62	3
F1106	1888	114	1800	53	1782	45	1768	70	2
F1106	1665	111	1790	33	1803	50	1815	90	-1
F1106	1476	95	1781	43	1734	40	1696	62	5
F1106	1618	107	1726	26	1713	39	1702	68	1
F1106	1527	108	1704	30	1685	36	1669	60	2
F1106	1620	126	1691	34	1694	50	1697	87	0
F1106	1706	120	1631	88	1625	55	1620	69	1
F1106	1655	127	1630	48	1543	40	1481	57	9
F1106	1427	89	1498	34	1485	35	1475	54	2
F1106	1569	95	1493	53	1455	37	1430	50	4
F1106	1486	98	1481	52	1457	49	1441	74	3
F1106	1676	153	1479	106	1481	65	1482	83	0
F1106	1543	90	1478	36	1436	36	1408	55	5
F1106	1470	85	1461	41	1416	37	1386	55	5
F1106	1327	85	1461	65	1402	44	1364	57	7
F1106	1362	83	1451	42	1385	49	1343	73	7
F1106	1558	133	1451	101	1520	54	1570	61	-8
F1106	1223	76	1444	51	1362	37	1310	50	9
F1106	1575	100	1441	51	1466	47	1483	72	-3
F1106	1405	86	1431	25	1385	35	1356	54	5
F1106	1236	81	1426	44	1356	43	1313	63	8
F1106	1419	85	1424	42	1391	34	1369	48	4
F1106	1310	91	1418	57	1400	41	1387	57	2
F1106	1564	121	1414	47	1494	54	1551	89	-10
F1106	1376	95	1398	92	1360	55	1336	66	4
F1106	1417	95	1330	49	1337	39	1341	56	-1
F1106	1239	80	1324	65	1320	44	1318	59	0
F1106	1313	103	1303	48	1310	45	1315	67	-1
F1106	1126	80	1287	82	1229	43	1195	46	7
F1106	1387	97	1287	61	1247	39	1224	49	5

F1106	1030	75	1279	46	1198	41	1153	56	10
F1106	2388	926	1267	48	1261	34	1257	46	1
F1106	1026	62	1266	46	1180	33	1134	42	10
F1106	1253	79	1256	44	1212	32	1187	42	5
F1106	1064	66	1253	54	1196	33	1164	41	7
F1106	1085	68	1238	50	1195	34	1171	44	5
F1106	1231	77	1230	42	1208	38	1195	54	3
F1106	1084	64	1226	61	1156	32	1120	35	9
F1106	1153	70	1223	53	1222	39	1221	53	0
F1106	1126	74	1222	62	1197	37	1183	46	3
F1106	1136	76	1220	43	1172	35	1147	47	6
F1106	1205	74	1207	42	1199	38	1195	53	1
F1106	1046	87	1187	123	1118	51	1083	42	9
F1106	1155	70	1185	45	1174	30	1169	40	1
F1106	1068	71	1138	60	1126	34	1120	41	2
LA-ICPMS									
	Dates (Ma)								
	208Pb*	**±2s**	**207Pb***	**±2s**	**207Pb***	**±2s**	**206Pb***	**±2s**	**%**
Analysis	**232Th**	**(Ma)**	**206Pb***	**(Ma)**	**235U**	**(Ma)**	**238U***	**(Ma)**	**disc.**
F1107	3099	579	2683	59	2700	67	2722	137	-1
F1107	2275	384	2600	39	2565	55	2521	112	3
F1107	2364	173	2525	27	2463	46	2389	94	5
F1107	2303	232	2356	47	2239	73	2113	136	10
F1107	1790	209	1917	57	1773	58	1653	89	14
F1107	1937	185	1887	51	1851	52	1819	86	4
F1107	1890	301	1869	65	1843	55	1819	86	3
F1107	1976	201	1859	86	1806	66	1760	95	5
F1107	2030	323	1850	89	1904	85	1954	144	-6
F1107	1628	268	1849	58	1860	48	1869	76	-1
F1107	2050	208	1826	81	1826	62	1825	93	0
F1107	1870	182	1823	40	1784	45	1750	76	4
F1107	2153	385	1817	74	1849	63	1878	100	-3
F1107	1945	332	1801	73	1774	79	1752	130	3
F1107	1763	283	1796	68	1847	61	1892	100	-5
F1107	1386	251	1795	68	1715	51	1650	70	8
F1107	1924	234	1795	63	1757	52	1726	78	4
F1107	2096	129	1762	37	1731	46	1705	77	3
F1107	2174	125	1759	30	1724	46	1695	79	4
F1107	1938	112	1751	26	1727	37	1708	64	2
F1107	1574	223	1719	35	1633	71	1567	119	9
F1107	1836	298	1714	79	1729	58	1741	83	-2
F1107	1702	166	1713	61	1642	49	1587	70	7
F1107	1704	285	1699	66	1713	63	1724	102	-1
F1107	1360	219	1674	65	1661	47	1650	65	1
F1107	1930	145	1644	32	1640	52	1637	88	0
F1107	2058	129	1592	41	1495	44	1428	66	10
F1107	1662	276	1582	70	1519	56	1475	80	7
F1107	1743	281	1554	87	1631	64	1692	94	-9
F1107	1626	100	1552	50	1447	42	1377	59	11

F1107	1770	197	1550	148	1449	78	1382	80	11
F1107	1227	207	1536	68	1463	49	1413	66	8
F1107	2027	114	1535	33	1595	43	1640	73	-7
F1107	1440	96	1517	67	1445	46	1398	60	8
F1107	1699	275	1514	74	1495	51	1481	70	2
F1107	1644	172	1508	79	1467	50	1439	62	5
F1107	1768	111	1505	57	1488	43	1476	62	2
F1107	1163	228	1489	120	1398	64	1340	68	10
F1107	1434	140	1480	44	1419	38	1379	55	7
F1107	1471	140	1474	45	1467	51	1462	79	1
F1107	1607	101	1472	42	1488	41	1499	64	-2
F1107	1273	204	1456	61	1451	48	1448	69	1
F1107	1489	157	1455	57	1482	56	1501	88	-3
F1107	1606	207	1455	167	1385	77	1340	61	8
F1107	1134	165	1450	57	1401	40	1368	53	6
F1107	1756	111	1448	41	1477	52	1497	85	-3
F1107	1852	105	1440	60	1431	52	1425	76	1
F1107	1866	113	1439	51	1412	45	1394	66	3
F1107	1346	249	1436	131	1357	65	1307	63	9
F1107	1105	205	1431	117	1372	61	1334	64	7
F1107	1492	153	1429	53	1452	49	1467	74	-3
F1107	1775	127	1429	72	1378	53	1345	72	6
F1107	1415	148	1424	89	1398	45	1382	47	3
F1107	1268	133	1423	47	1429	40	1434	59	-1
F1107	1583	169	1422	41	1451	45	1470	72	-3
F1107	1842	138	1422	67	1448	48	1465	67	-3
F1107	1985	206	1419	55	1394	48	1378	70	3
F1107	1240	204	1404	63	1338	47	1297	63	8
F1107	1512	166	1400	85	1458	61	1499	87	-7
F1107	1729	305	1375	167	1430	95	1467	116	-7
F1107	1352	224	1373	85	1391	59	1402	81	-2
F1107	1172	140	1372	82	1362	47	1356	56	1
F1107	1527	155	1356	49	1336	34	1323	46	2
F1107	1246	131	1354	57	1311	42	1284	57	5
F1107	1224	149	1353	64	1291	44	1254	58	7
F1107	1661	103	1341	47	1336	42	1333	61	1
F1107	1485	162	1316	73	1374	61	1412	91	-7
F1107	1517	95	1293	69	1206	49	1157	63	10
F1107	1484	244	1285	126	1349	74	1390	94	-8
F1107	1111	110	1284	51	1264	37	1252	50	2
F1107	1418	226	1276	57	1284	49	1289	71	-1
F1107	1277	135	1271	71	1294	62	1308	91	-3
F1107	1271	75	1263	30	1266	42	1268	65	0
F1107	1318	226	1246	86	1296	74	1326	108	-6
F1107	1301	142	1243	105	1230	62	1222	76	2
F1107	1475	92	1234	49	1250	42	1258	60	-2
F1107	1332	140	1217	71	1242	46	1256	60	-3
F1107	1571	110	1216	74	1199	45	1190	56	2
F1107	959	96	1215	43	1177	41	1157	58	5
F1107	1240	75	1213	32	1207	35	1203	51	1

F1107	970	158	1204	48	1193	34	1188	45	1
F1107	1288	91	1204	86	1213	48	1218	57	-1
F1107	1593	174	1199	108	1212	57	1219	65	-2
F1107	1397	231	1190	73	1237	57	1265	81	-6
F1107	1111	119	1188	54	1199	34	1204	44	-1
F1107	1517	94	1180	53	1192	37	1199	49	-2
F1107	1345	103	1168	80	1207	50	1230	66	-5
F1107	1152	145	1148	90	1141	46	1137	52	1
F1107	1212	205	1090	99	1160	49	1199	56	-10
LA-ICPMS									
	Dates (Ma)								
	208Pb*	**±2s**	**207Pb***	**±2s**	**207Pb***	**±2s**	**206Pb***	**±2s**	**%**
Analysis	**232Th**	**(Ma)**	**206Pb***	**(Ma)**	**235U**	**(Ma)**	**238U***	**(Ma)**	**disc.**
F1108	3644	331	2870	26	2867	48	2863	109	0
F1108	3570	312	2797	26	2765	41	2720	89	3
F1108	3734	333	2795	32	2805	43	2819	92	-1
F1108	3560	315	2693	30	2670	51	2640	110	2
F1108	2874	258	2595	24	2555	37	2506	76	3
F1108	3619	322	2576	46	2662	54	2777	115	-8
F1108	2648	239	2449	38	2395	44	2333	83	5
F1108	3245	378	2382	25	2301	46	2212	90	7
F1108	2834	281	2000	70	1876	46	1765	57	12
F1108	2521	229	1958	25	1890	32	1829	56	7
F1108	2239	200	1931	31	1893	40	1859	70	4
F1108	2427	241	1929	38	1924	36	1919	59	0
F1108	2265	215	1855	41	1795	45	1745	73	6
F1108	1702	166	1854	57	1768	40	1696	53	9
F1108	2414	216	1850	38	1819	40	1793	66	3
F1108	1786	162	1844	26	1812	31	1785	53	3
F1108	2448	238	1839	37	1803	39	1772	65	4
F1108	2012	207	1835	50	1857	46	1875	75	-2
F1108	2230	206	1832	33	1800	40	1773	68	3
F1108	2507	344	1829	92	1725	71	1641	99	10
F1108	2548	317	1822	103	1781	73	1746	100	4
F1108	2554	232	1819	54	1821	47	1823	75	0
F1108	2372	217	1814	43	1797	53	1782	91	2
F1108	1755	168	1811	31	1801	32	1793	54	1
F1108	1910	178	1810	35	1751	34	1702	53	6
F1108	2028	203	1807	49	1743	39	1689	58	7
F1108	2409	225	1795	40	1819	40	1839	68	-2
F1108	1939	181	1789	47	1769	43	1752	69	2
F1108	2228	200	1782	51	1743	40	1712	58	4
F1108	1904	187	1777	38	1790	40	1801	68	-1
F1108	1941	195	1775	33	1776	34	1777	56	0
F1108	2229	204	1749	46	1710	37	1678	55	4
F1108	2370	218	1745	41	1777	42	1803	71	-3
F1108	2295	203	1740	36	1758	39	1773	66	-2
F1108	2214	203	1738	44	1724	45	1713	74	1
F1108	2410	222	1730	40	1764	44	1793	76	-4

F1108	1959	187	1726	32	1746	36	1763	61	-2
F1108	2076	199	1725	47	1681	37	1645	54	5
F1108	2093	199	1719	46	1682	41	1652	63	4
F1108	1831	176	1699	43	1720	37	1738	59	-2
F1108	2274	200	1694	27	1705	32	1714	55	-1
F1108	1936	179	1691	31	1718	34	1740	57	-3
F1108	1388	146	1685	110	1549	63	1451	68	14
F1108	1843	172	1670	32	1665	36	1662	58	0
F1108	2195	201	1656	43	1628	39	1607	61	3
F1108	1918	177	1656	64	1520	38	1424	43	14
F1108	2030	186	1653	64	1631	45	1614	62	2
F1108	1458	146	1623	96	1550	47	1497	39	8
F1108	1987	193	1623	51	1604	41	1590	61	2
F1108	2152	194	1622	42	1629	34	1635	52	-1
F1108	1806	165	1588	39	1576	34	1567	50	1
F1108	1960	188	1564	70	1518	48	1485	64	5
F1108	1866	186	1564	63	1577	43	1586	59	-1
F1108	2016	187	1558	41	1533	35	1515	52	3
F1108	2175	217	1545	73	1574	52	1595	74	-3
F1108	2127	196	1545	37	1553	44	1560	71	-1
F1108	2027	200	1535	56	1450	38	1392	49	9
F1108	1932	190	1533	59	1491	46	1462	65	5
F1108	2061	195	1500	41	1511	37	1518	57	-1
F1108	1841	181	1493	64	1454	40	1428	50	4
F1108	1597	156	1489	32	1495	31	1499	47	-1
F1108	1789	161	1489	40	1466	36	1451	53	3
F1108	1694	157	1488	47	1460	41	1442	60	3
F1108	1959	202	1479	75	1442	52	1417	69	4
F1108	1886	174	1478	46	1454	32	1438	43	3
F1108	1845	198	1472	59	1435	43	1409	60	4
F1108	2066	188	1466	51	1458	40	1453	58	1
F1108	1439	134	1463	55	1443	39	1429	53	2
F1108	1753	170	1459	67	1419	46	1393	62	4
F1108	1863	175	1453	57	1489	52	1515	80	-4
F1108	1315	125	1420	44	1367	29	1334	38	6
F1108	1719	201	1413	61	1357	45	1322	61	6
F1108	1853	173	1410	46	1443	39	1465	58	-4
F1108	1838	167	1392	42	1419	37	1437	56	-3
F1108	1523	145	1377	45	1380	34	1382	48	0
F1108	1803	174	1374	44	1312	31	1274	41	7
F1108	1751	162	1372	66	1354	41	1343	51	2
F1108	1777	161	1367	36	1353	40	1344	60	2
F1108	1328	137	1367	46	1328	38	1304	53	5
F1108	1641	166	1357	109	1246	54	1183	53	13
F1108	1862	188	1354	55	1364	39	1370	54	-1
F1108	1279	132	1349	58	1337	39	1329	52	1
F1108	1218	119	1340	131	1298	66	1273	68	5
F1108	1461	140	1321	56	1303	40	1291	55	2
F1108	1602	147	1295	56	1264	40	1246	54	4
F1108	1590	158	1259	50	1239	32	1228	41	2

F1108	1600	144	1252	42	1201	28	1173	36	6
F1108	1619	156	1242	59	1203	46	1182	62	5
F1108	1577	146	1241	98	1235	47	1231	47	1
F1108	1556	139	1235	51	1214	31	1203	39	3
F1108	1176	121	1230	88	1226	46	1223	51	1
F1108	1578	152	1216	107	1185	53	1168	58	4
F1108	1078	104	1199	30	1134	26	1100	35	8
F1108	1210	131	1184	53	1177	39	1174	53	1
F1108	1568	155	1182	48	1190	40	1194	57	-1
LA-ICPMS									
	Dates (Ma)								
	208Pb*	**±2s**	**207Pb***	**±2s**	**207Pb***	**±2s**	**206Pb***	**±2s**	**%**
Analysis	**232Th**	**(Ma)**	**206Pb***	**(Ma)**	**235U**	**(Ma)**	**238U***	**(Ma)**	**disc.**
F1302	2473	156	2037	22	2009	39	1982	72	3
F1302	2194	431	1911	59	1934	72	1955	128	-2
F1302	2089	377	1901	59	1875	50	1851	77	3
F1302	2199	398	1897	74	1909	76	1921	129	-1
F1302	2138	141	1884	32	1872	48	1861	87	1
F1302	1967	252	1873	68	1903	61	1931	100	-3
F1302	1539	215	1869	27	1820	32	1776	55	5
F1302	2247	386	1867	87	1852	71	1839	109	2
F1302	2126	141	1861	49	1865	44	1869	72	0
F1302	2096	259	1858	63	1843	57	1830	91	1
F1302	1827	230	1855	47	1878	39	1898	61	-2
F1302	1826	238	1848	43	1891	55	1930	100	-4
F1302	1981	269	1839	49	1782	40	1734	59	6
F1302	1638	207	1817	34	1786	30	1760	48	3
F1302	2118	270	1801	35	1864	67	1921	127	-7
F1302	1838	240	1792	74	1757	54	1728	77	4
F1302	1976	273	1787	45	1736	48	1694	77	5
F1302	1681	312	1780	135	1706	86	1646	106	8
F1302	1868	337	1712	84	1730	66	1745	100	-2
F1302	1572	203	1663	43	1643	41	1627	64	2
F1302	1399	289	1660	71	1618	73	1586	114	4
F1302	1093	176	1623	53	1538	53	1478	81	9
F1302	1744	230	1565	52	1567	45	1568	69	0
F1302	1596	301	1540	70	1495	58	1465	83	5
F1302	1462	272	1530	123	1462	75	1415	91	7
F1302	1821	122	1514	56	1548	46	1573	68	-4
F1302	1721	318	1505	93	1505	62	1505	83	0
F1302	1765	310	1495	88	1528	69	1552	102	-4
F1302	1255	175	1494	75	1439	45	1403	55	6
F1302	1589	203	1488	48	1493	42	1497	63	-1
F1302	1582	108	1471	33	1469	34	1468	53	0
F1302	1797	322	1465	125	1484	74	1498	91	-2
F1302	1598	211	1461	78	1444	46	1433	56	2
F1302	1769	332	1459	59	1434	54	1417	81	3
F1302	1641	205	1457	53	1413	46	1384	66	5
F1302	1425	185	1454	47	1472	37	1484	54	-2

F1302	1461	195	1431	42	1434	49	1437	77	0
F1302	896	145	1428	65	1483	49	1521	72	-6
F1302	1762	316	1427	66	1475	50	1509	73	-6
F1302	1575	308	1418	60	1496	71	1552	117	-9
F1302	1613	224	1409	102	1388	54	1374	60	3
F1302	1516	196	1405	59	1352	45	1318	61	6
F1302	1463	194	1397	86	1400	63	1401	89	0
F1302	1424	180	1384	47	1372	36	1365	51	1
F1302	1636	120	1378	53	1423	45	1453	67	-5
F1302	1198	221	1358	107	1278	54	1231	55	9
F1302	1710	309	1340	83	1423	61	1479	88	-10
F1302	1499	273	1317	88	1302	64	1293	87	2
F1302	1438	202	1289	73	1221	38	1182	41	8
F1302	1161	147	1265	41	1245	38	1234	54	2
F1302	1403	182	1251	91	1214	52	1193	62	5
F1302	1099	158	1221	79	1227	44	1230	53	-1
F1302	1482	302	1218	143	1209	61	1204	51	1
F1302	1027	189	1212	48	1204	33	1200	44	1
F1302	1031	178	1194	64	1115	48	1075	63	10
F1302	1447	268	1178	82	1243	60	1281	84	-9
LA-ICPMS									
	Dates (Ma)								
	208Pb*	**±2s**	**207Pb***	**±2s**	**207Pb***	**±2s**	**206Pb***	**±2s**	**%**
Analysis	**232Th**	**(Ma)**	**206Pb***	**(Ma)**	**235U**	**(Ma)**	**238U***	**(Ma)**	**disc.**
F1342	3103	203	2853	42	2829	60	2795	130	2
F1342	3241	207	2793	45	2842	62	2911	137	-4
F1342	2598	177	2736	34	2705	34	2662	64	3
F1342	2643	181	2449	29	2365	45	2270	88	7
F1342	1769	146	1905	73	1906	63	1907	101	0
F1342	2121	182	1883	53	1911	45	1937	73	-3
F1342	2059	156	1880	60	1821	57	1770	91	6
F1342	2101	186	1875	64	1814	60	1762	94	6
F1342	1590	120	1858	46	1882	46	1904	77	-2
F1342	2014	150	1842	34	1772	42	1714	70	7
F1342	1667	127	1832	38	1843	53	1853	95	-1
F1342	1488	160	1827	33	1768	46	1718	79	6
F1342	1535	101	1806	35	1779	38	1757	63	3
F1342	2170	145	1789	23	1780	41	1773	74	1
F1342	2091	155	1781	40	1761	48	1744	81	2
F1342	2001	158	1771	52	1770	53	1769	88	0
F1342	1627	110	1768	26	1770	31	1771	53	0
F1342	1507	120	1739	35	1695	35	1659	55	5
F1342	1511	123	1736	35	1707	44	1683	73	3
F1342	1444	106	1724	20	1693	36	1667	62	3
F1342	1833	141	1717	42	1695	47	1678	78	2
F1342	1981	146	1695	48	1674	38	1657	56	2
F1342	1615	113	1656	23	1685	39	1708	69	-3
F1342	1443	103	1642	32	1632	34	1624	55	1
F1342	1844	141	1627	73	1618	66	1611	101	1

F1342	1435	104	1625	33	1610	35	1599	56	2
F1342	1903	125	1611	36	1619	39	1625	64	-1
F1342	1622	137	1529	47	1487	49	1458	75	5
F1342	1308	92	1523	64	1544	44	1560	62	-2
F1342	1589	106	1507	41	1476	38	1454	56	4
F1342	1642	115	1493	58	1478	57	1468	87	2
F1342	1628	128	1480	46	1480	55	1479	87	0
F1342	1291	92	1478	35	1364	32	1292	45	13
F1342	1648	130	1475	56	1435	49	1409	71	4
F1342	1719	124	1471	51	1485	50	1494	78	-2
F1342	1700	131	1468	45	1478	43	1484	67	-1
F1342	1541	113	1467	47	1450	38	1438	55	2
F1342	1283	194	1465	40	1403	53	1362	82	7
F1342	1447	100	1461	47	1461	33	1461	45	0
F1342	1318	98	1461	58	1429	44	1407	60	4
F1342	1715	130	1454	35	1441	31	1431	46	2
F1342	1642	117	1454	51	1480	49	1499	77	-3
F1342	1278	94	1443	32	1444	30	1445	46	0
F1342	1668	135	1441	59	1425	46	1415	64	2
F1342	1558	111	1439	55	1395	42	1366	58	5
F1342	1658	133	1437	41	1426	37	1419	56	1
F1342	1676	148	1436	58	1433	57	1430	87	0
F1342	1838	174	1431	90	1429	46	1427	48	0
F1342	1595	122	1431	46	1405	34	1388	48	3
F1342	1615	116	1429	53	1451	51	1466	78	-3
F1342	1357	95	1427	55	1440	44	1449	64	-2
F1342	920	71	1419	44	1308	35	1242	47	12
F1342	1088	107	1408	25	1295	49	1228	74	13
F1342	1219	90	1403	35	1438	33	1462	50	-4
F1342	1656	181	1376	61	1403	63	1422	97	-3
F1342	1176	103	1372	75	1395	52	1410	72	-3
F1342	1627	118	1371	52	1392	39	1406	55	-3
F1342	1479	127	1369	73	1368	53	1368	74	0
F1342	1217	117	1329	77	1236	47	1183	57	11
F1342	1195	100	1314	63	1335	47	1349	66	-3
F1342	1132	86	1311	40	1331	32	1343	47	-2
F1342	1129	90	1310	45	1311	39	1312	57	0
F1342	1554	139	1300	68	1324	40	1339	51	-3
F1342	1277	89	1294	39	1274	35	1263	50	2
F1342	1409	105	1285	40	1241	41	1215	59	5
F1342	1079	100	1284	53	1252	37	1233	48	4
F1342	1135	89	1282	46	1243	44	1220	63	5
F1342	1311	118	1272	80	1235	66	1214	92	5
F1342	1286	112	1268	61	1244	41	1230	54	3
F1342	1160	82	1264	40	1273	38	1279	56	-1
F1342	1246	117	1256	79	1167	77	1120	106	11
F1342	1405	98	1251	53	1236	46	1227	65	2
F1342	1427	105	1250	40	1248	37	1246	54	0
F1342	1084	74	1250	54	1222	36	1206	46	4
F1342	1432	105	1241	67	1190	38	1163	45	6

F1342	1355	137	1240	77	1234	43	1230	52	1
F1342	1418	124	1240	59	1237	45	1235	62	0
F1342	1338	103	1236	76	1230	48	1227	61	1
F1342	1378	101	1229	52	1229	40	1230	56	0
F1342	1481	106	1224	47	1223	33	1222	45	0
F1342	1048	70	1222	37	1225	36	1227	52	0
F1342	1380	107	1222	74	1180	61	1158	84	5
F1342	1153	89	1222	58	1234	46	1241	64	-2
F1342	946	94	1218	81	1174	40	1150	42	6
F1342	1331	107	1214	42	1258	63	1284	98	-6
F1342	1063	74	1212	50	1272	35	1308	48	-8
F1342	1238	89	1202	67	1199	41	1197	51	0
F1342	1386	100	1201	34	1230	38	1247	58	-4
F1342	1348	103	1196	48	1182	45	1175	65	2
F1342	1066	83	1196	54	1186	31	1181	38	1
F1342	1085	78	1194	36	1160	27	1142	36	4
F1342	1232	87	1191	39	1177	34	1170	47	2
F1342	1325	89	1191	33	1154	25	1135	33	5
F1342	1061	95	1186	53	1168	36	1157	46	2
F1342	1052	79	1186	37	1199	40	1207	59	-2
F1342	1435	103	1181	57	1199	37	1209	48	-2
F1342	988	74	1165	57	1130	39	1113	50	5
F1342	1326	117	1165	91	1187	48	1199	55	-3
LA-ICPMS									
	Dates (Ma)								
	208Pb*	**±2s**	**207Pb***	**±2s**	**207Pb***	**±2s**	**206Pb***	**±2s**	**%**
Analysis	**232Th**	**(Ma)**	**206Pb***	**(Ma)**	**235U**	**(Ma)**	**238U***	**(Ma)**	**disc.**
F1343	1383	130	1230	57	1146	39	1103	49	10
F1343	1513	145	1263	48	1245	42	1235	59	2
F1343	1737	183	1447	51	1431	50	1420	75	2
F1343	1631	151	1370	39	1342	40	1325	60	3
F1343	1836	184	1486	69	1505	47	1519	65	-2
F1343	1521	142	1262	36	1233	38	1216	55	4
F1343	1534	142	1258	37	1241	40	1232	59	2
F1343	2207	207	1852	30	1832	52	1814	93	2
F1343	1824	168	1483	36	1467	46	1457	73	2
F1343	1823	181	1378	44	1359	41	1347	61	2
F1343	2494	236	1796	34	1808	45	1818	79	-1
F1343	2407	223	1847	35	1855	48	1863	85	-1
F1343	1980	179	1500	39	1470	40	1449	61	3
F1343	2660	405	1855	65	1816	51	1781	75	4
F1343	2378	265	1791	38	1802	49	1811	86	-1
F1343	3470	312	2584	67	2547	66	2499	122	3
F1343	1738	168	1351	53	1336	41	1326	58	2
F1343	1723	160	1355	42	1283	38	1239	54	9
F1343	1864	168	1407	39	1396	41	1389	62	1
F1343	2420	217	1780	41	1736	40	1700	63	4
F1343	2427	268	1764	47	1741	45	1722	73	2
F1343	1625	170	1229	41	1240	46	1246	68	-1

F1343	1538	175	1241	64	1247	52	1250	73	-1
F1343	1626	150	1304	49	1284	39	1272	54	2
F1343	2276	211	1770	42	1798	45	1823	76	-3
F1343	2265	205	1792	36	1794	45	1796	79	0
F1343	1770	203	1399	60	1409	52	1415	77	-1
F1343	1466	176	1163	66	1189	45	1204	60	-3
F1343	1718	170	1341	49	1356	48	1366	73	-2
F1343	1572	147	1274	47	1242	39	1223	54	4
F1343	2235	206	1816	44	1751	43	1697	67	7
F1343	2141	195	1681	35	1686	38	1691	63	-1
F1343	2282	219	1787	39	1784	53	1781	92	0
F1343	1771	198	1500	64	1461	57	1435	84	4
F1343	2358	225	1838	67	1851	70	1862	119	-1
F1343	1632	170	1182	66	1194	43	1200	56	-1
F1343	1680	178	1310	60	1326	50	1336	72	-2
F1343	2130	195	1616	62	1517	51	1448	72	10
F1343	1871	180	1517	53	1445	55	1397	82	8
F1343	1897	179	1455	38	1425	40	1406	61	3
F1343	2028	195	1645	71	1579	55	1529	78	7
F1343	2294	212	1846	45	1846	48	1846	81	0
F1343	1855	170	1473	61	1426	49	1394	70	5
F1343	1623	163	1315	65	1264	47	1234	63	6
F1343	1905	187	1441	52	1453	48	1462	73	-1
F1343	2213	254	1747	53	1727	51	1711	81	2
F1343	2178	200	1744	50	1756	48	1766	77	-1
F1343	1791	187	1364	59	1341	44	1326	61	3
F1343	1776	231	1466	69	1415	47	1382	61	6
F1343	2302	205	1818	40	1810	53	1803	92	1
F1343	1574	149	1269	70	1233	48	1212	63	4
F1343	2178	429	1661	147	1661	87	1661	103	0
F1343	2309	222	1806	41	1846	41	1880	69	-4
F1343	2397	217	1866	29	1873	48	1880	87	-1
F1343	2174	203	1800	30	1800	44	1800	77	0
F1343	1594	151	1241	50	1272	38	1290	54	-4
F1343	3750	365	2941	38	2889	47	2815	99	4
F1343	1726	166	1459	52	1473	44	1482	66	-2
F1343	2123	187	1870	26	1894	41	1916	76	-2
F1343	1363	148	1208	56	1155	42	1127	55	7
F1343	1510	199	1260	116	1267	66	1272	79	-1
F1343	1666	153	1443	32	1487	44	1518	73	-5
F1343	1386	132	1212	58	1210	43	1208	58	0
F1343	2183	191	1965	34	2021	40	2077	73	-6
F1343	1839	236	1635	94	1620	56	1608	67	2
F1343	2080	194	1706	60	1774	50	1833	79	-7
F1343	1535	217	1354	87	1392	57	1416	77	-5
F1343	1443	176	1323	39	1366	50	1393	80	-5
F1343	1442	214	1291	47	1310	39	1323	56	-2
F1343	1757	167	1759	31	1731	47	1709	82	3
F1343	2018	736	1571	94	1533	63	1506	82	4
F1343	1527	179	1471	52	1472	51	1473	78	0

F1343	1368	173	1329	70	1345	48	1355	65	-2
F1343	1878	180	1780	39	1809	45	1834	77	-3
F1343	1823	177	1713	49	1754	43	1789	68	-4
F1343	1890	208	1792	43	1777	50	1765	84	2
F1343	2829	316	2600	51	2564	53	2519	100	3
F1343	1707	210	1721	40	1741	44	1758	74	-2
F1343	1198	132	1264	151	1228	66	1207	56	4
F1343	1445	159	1448	57	1459	55	1467	84	-1
F1343	1672	191	1828	45	1796	55	1769	94	3
F1343	1255	115	1399	54	1348	42	1316	58	6
F1343	1598	148	1634	42	1664	48	1688	81	-3
F1343	2741	410	2623	54	2629	54	2637	101	-1
F1343	1428	162	1487	81	1432	52	1396	67	6
F1343	2009	378	1921	78	1862	57	1810	80	6
F1343	1453	131	1422	35	1450	46	1468	74	-3
LA-ICPMS									
	Dates (Ma)								
	208Pb*	**±2s**	**207Pb***	**±2s**	**207Pb***	**±2s**	**206Pb***	**±2s**	**%**
Analysis	**232Th**	**(Ma)**	**206Pb***	**(Ma)**	**235U**	**(Ma)**	**238U***	**(Ma)**	**disc.**
F1345-188	4442	400	3045	29	3079	52	3132	126	-3
F1345-188	3010	272	3109	27	3080	53	3035	126	2
F1345-188	3895	358	3052	33	3005	52	2936	117	4
F1345-188	3799	366	2875	38	2868	49	2859	106	1
F1345-188	3517	344	2806	21	2808	50	2812	115	0
F1345-188	2809	269	2650	31	2677	53	2714	117	-2
F1345-188	3325	310	2544	28	2532	50	2516	106	1
F1345-188	2635	252	2448	28	2442	55	2434	117	1
F1345-188	2482	271	2353	44	2359	61	2365	122	0
F1345-188	2258	221	1873	39	1910	47	1945	84	-4
F1345-188	2911	331	1831	57	1890	67	1944	121	-6
F1345-188	2414	251	1765	30	1812	43	1854	78	-5
F1345-188	1924	190	1789	33	1820	44	1847	79	-3
F1345-188	1873	188	1827	37	1834	42	1841	73	-1
F1345-188	2286	218	1823	30	1830	38	1836	67	-1
F1345-188	2463	241	1772	31	1805	44	1834	79	-4
F1345-188	1885	191	1800	22	1812	41	1824	75	-1
F1345-188	2306	224	1753	35	1781	49	1806	87	-3
F1345-188	1837	180	1787	27	1795	45	1803	81	-1
F1345-188	2289	234	1816	48	1808	60	1801	103	1
F1345-188	1815	170	1835	38	1814	48	1797	82	2
F1345-188	2641	268	1922	61	1853	57	1791	91	7
F1345-188	2330	226	1802	35	1791	48	1782	83	1
F1345-188	1790	182	1811	43	1792	60	1777	104	2
F1345-188	2448	234	1856	30	1811	45	1772	77	5
F1345-188	2201	212	1806	33	1785	48	1768	83	2
F1345-188	2347	239	1811	36	1784	47	1761	80	3
F1345-188	2437	233	1698	33	1732	42	1761	73	-4
F1345-188	2293	222	1762	37	1757	36	1753	59	1
F1345-188	2148	207	1792	35	1767	43	1746	72	3

F1345-188	2509	244	1766	47	1754	49	1743	81	1
F1345-188	2275	233	1800	43	1765	53	1735	90	4
F1345-188	2405	236	1757	33	1741	42	1728	72	2
F1345-188	1984	258	1740	32	1722	42	1707	71	2
F1345-188	1912	259	1748	148	1725	88	1706	104	2
F1345-188	1734	185	1676	32	1683	45	1688	77	-1
F1345-188	2284	222	1786	34	1728	43	1681	71	6
F1345-188	2463	250	1809	48	1731	46	1667	72	8
F1345-188	1828	184	1622	38	1646	42	1665	70	-3
F1345-188	2151	215	1687	29	1671	41	1659	70	2
F1345-188	2297	220	1785	32	1710	42	1650	70	8
F1345-188	2295	230	1713	31	1667	55	1631	93	5
F1345-188	2250	215	1623	42	1620	48	1619	78	0
F1345-188	2264	248	1758	46	1666	60	1594	97	9
F1345-188	1713	194	1721	18	1636	48	1571	81	9
F1345-188	1619	165	1811	26	1675	50	1570	83	13
F1345-188	1779	180	1530	41	1538	42	1544	66	-1
F1345-188	1867	184	1461	37	1506	48	1538	79	-5
F1345-188	1780	201	1493	63	1511	50	1523	74	-2
F1345-188	1585	165	1431	38	1485	41	1523	67	-6
F1345-188	1785	196	1594	48	1553	48	1523	74	4
F1345-188	1865	181	1514	57	1518	53	1521	81	0
F1345-188	1912	190	1504	36	1491	41	1482	64	1
F1345-188	1996	212	1468	67	1473	44	1476	59	-1
F1345-188	1956	193	1450	52	1463	47	1472	71	-2
F1345-188	1769	174	1429	44	1449	50	1463	79	-2
F1345-188	1711	184	1367	82	1417	64	1450	93	-6
F1345-188	2095	219	1399	54	1427	45	1447	67	-3
F1345-188	2072	207	1461	31	1451	38	1444	60	1
F1345-188	1453	148	1407	35	1429	40	1444	63	-3
F1345-188	1494	199	1339	74	1401	53	1441	75	-8
F1345-188	1795	197	1523	55	1469	52	1433	77	6
F1345-188	1620	178	1445	79	1438	52	1432	69	1
F1345-188	1856	188	1442	61	1436	58	1432	88	1
F1345-188	1455	158	1434	54	1429	49	1426	73	1
F1345-188	1754	184	1413	74	1420	52	1425	71	-1
F1345-188	1874	200	1443	40	1430	43	1421	66	2
F1345-188	2041	197	1501	47	1453	45	1421	66	5
F1345-188	1759	184	1455	41	1434	48	1420	74	2
F1345-188	1359	132	1393	33	1409	38	1420	59	-2
F1345-188	1971	193	1424	48	1422	41	1420	60	0
F1345-188	1969	194	1429	48	1419	43	1412	64	1
F1345-188	1302	127	1458	68	1423	49	1400	68	4
F1345-188	1432	160	1422	57	1408	45	1399	63	2
F1345-188	1968	196	1394	58	1384	47	1378	67	1
F1345-188	1724	183	1387	65	1380	47	1375	65	1
F1345-188	1908	195	1511	46	1425	39	1368	55	10
F1345-188	1919	226	1368	63	1364	42	1361	56	0
F1345-188	1571	155	1415	49	1378	44	1355	65	4
F1345-188	1784	182	1435	69	1376	43	1339	54	7

F1345-188	1657	180	1325	40	1332	41	1336	62	-1
F1345-188	1720	173	1397	40	1359	48	1335	74	4
F1345-188	1604	164	1308	41	1322	42	1330	64	-2
F1345-188	1735	173	1297	50	1313	39	1323	56	-2
F1345-188	1689	165	1279	31	1295	38	1304	58	-2
F1345-188	1559	159	1269	48	1289	43	1301	63	-3
F1345-188	1358	137	1243	41	1273	44	1292	67	-4
F1345-188	1381	138	1368	85	1320	48	1291	56	6
F1345-188	1344	136	1236	30	1260	43	1274	66	-3
F1345-188	1572	171	1213	72	1251	42	1273	54	-5
F1345-188	1547	163	1308	87	1282	50	1266	60	3
F1345-188	1559	159	1179	62	1231	57	1261	84	-7
F1345-188	1538	153	1208	38	1239	38	1257	56	-4
F1345-188	1646	166	1159	65	1218	48	1252	68	-8
F1345-188	1379	141	1248	83	1246	49	1245	61	0
F1345-188	1662	174	1203	70	1226	50	1239	69	-3
F1345-188	1472	157	1198	85	1220	50	1233	62	-3
F1345-188	1327	134	1244	55	1235	40	1231	54	1
F1345-188	1584	157	1213	64	1224	48	1229	66	-1
F1345-188	1573	154	1111	77	1184	49	1225	66	-10
F1345-188	1630	163	1257	130	1236	63	1223	65	3
F1345-188	1682	177	1280	67	1243	49	1221	66	5
F1345-188	1256	126	1210	80	1212	43	1213	51	0
F1345-188	1536	159	1219	56	1215	37	1213	49	1
F1345-188	1533	156	1245	52	1223	38	1211	51	3
F1345-188	1593	153	1226	56	1215	45	1209	62	1
F1345-188	1633	171	1264	48	1228	51	1207	74	5
F1345-188	1410	152	1149	99	1186	49	1207	54	-5
F1345-188	1437	149	1183	49	1197	45	1205	64	-2
F1345-188	1504	149	1275	50	1228	37	1201	50	6
F1345-188	1646	173	1192	59	1196	47	1198	65	-1
F1345-188	1409	147	1178	57	1186	40	1191	54	-1
F1345-188	1289	156	1201	54	1193	42	1188	58	1
F1345-188	1499	154	1256	60	1201	45	1171	60	7
F1345-188	1580	163	1273	45	1207	39	1170	54	8
F1345-188	1322	135	1171	77	1164	53	1160	69	1
F1345-188	1338	127	1219	31	1180	38	1159	56	5
F1345-188	1566	165	1168	100	1162	47	1159	49	1
LA-ICPMS									
	Apparent ages (Ma)								
	208Pb*	**±2s**	**207Pb***	**±2s**	**207Pb***	**±2s**	**206Pb***	**±2s**	**%**
Analysis	**232Th**	**(Ma)**	**206Pb***	**(Ma)**	**235U**	**(Ma)**	**238U***	**(Ma)**	**disc.**
VSL3-5	2665	225	2995	28	2980	48	2958	111	1
VSL3-5	5277	2015	2925	94	2860	86	2769	156	5
VSL3-5	2839	248	2543	43	2574	69	2613	149	-3
VSL3-5	2163	196	2506	35	2488	50	2466	101	2
VSL3-5	2772	293	2444	49	2471	63	2503	127	-2
VSL3-5	2377	216	2151	71	2084	62	2018	98	6
VSL3-5	1840	155	1994	44	1952	42	1912	68	4

VSL3-5	3708	1943	1990	229	1854	146	1735	173	13
VSL3-5	2107	152	1914	43	1858	54	1808	93	6
VSL3-5	2107	169	1851	36	1819	44	1791	75	3
VSL3-5	2066	195	1843	61	1808	57	1777	90	4
VSL3-5	1573	151	1806	35	1665	37	1556	57	14
VSL3-5	1976	182	1805	42	1743	48	1692	79	6
VSL3-5	1953	149	1792	23	1747	37	1710	64	5
VSL3-5	2040	187	1780	60	1754	71	1732	119	3
VSL3-5	2216	292	1776	49	1737	85	1706	149	4
VSL3-5	1679	156	1774	27	1817	41	1856	74	-5
VSL3-5	11908	8339	1769	333	1773	337	1776	556	0
VSL3-5	1918	167	1757	51	1695	56	1646	90	6
VSL3-5	1562	136	1747	49	1740	50	1734	82	1
VSL3-5	1945	147	1744	50	1705	62	1673	104	4
VSL3-5	1940	148	1743	30	1729	52	1718	91	1
VSL3-5	1702	157	1742	31	1714	44	1692	75	3
VSL3-5	1568	157	1740	71	1708	58	1681	86	3
VSL3-5	1940	182	1730	33	1695	56	1667	97	4
VSL3-5	1922	151	1730	39	1705	43	1686	71	3
VSL3-5	1896	145	1722	29	1673	55	1635	95	5
VSL3-5	1948	153	1688	38	1658	47	1635	78	3
VSL3-5	1789	139	1682	39	1640	53	1607	89	4
VSL3-5	1929	147	1675	48	1665	52	1658	85	1
VSL3-5	1635	142	1663	54	1591	47	1537	70	8
VSL3-5	1935	158	1657	36	1708	50	1749	87	-6
VSL3-5	1487	131	1554	43	1539	39	1528	59	2
VSL3-5	1720	198	1520	75	1462	67	1422	98	6
VSL3-5	1554	130	1510	65	1385	65	1305	93	14
VSL3-5	1861	166	1506	57	1511	60	1515	94	-1
VSL3-5	1271	120	1505	41	1499	37	1494	55	1
VSL3-5	1629	118	1482	42	1442	42	1415	64	5
VSL3-5	1708	128	1480	34	1425	51	1389	80	6
VSL3-5	1349	116	1446	23	1456	31	1463	51	-1
VSL3-5	1736	145	1443	67	1487	59	1518	91	-5
VSL3-5	1593	166	1436	76	1362	52	1315	68	8
VSL3-5	1598	149	1427	51	1463	51	1488	80	-4
VSL3-5	1575	176	1419	76	1315	51	1252	65	12
VSL3-5	1699	175	1417	79	1455	67	1481	100	-5
VSL3-5	1374	150	1411	75	1406	48	1403	63	1
VSL3-5	1510	146	1406	52	1311	48	1254	68	11
VSL3-5	1593	126	1405	77	1434	48	1454	63	-3
VSL3-5	1200	110	1403	57	1406	36	1408	47	0
VSL3-5	1203	107	1397	47	1363	36	1342	50	4
VSL3-5	1139	106	1377	87	1283	50	1227	57	11
VSL3-5	1579	125	1363	57	1320	45	1294	63	5
VSL3-5	1249	117	1363	78	1363	48	1364	61	0
VSL3-5	1500	122	1361	70	1344	52	1333	71	2
VSL3-5	1215	109	1345	43	1350	39	1353	57	-1
VSL3-5	1413	122	1342	68	1310	48	1291	65	4
VSL3-5	1429	145	1338	139	1259	67	1214	64	9

VSL3-5	1441	112	1337	45	1299	44	1276	65	5
VSL3-5	1547	154	1324	60	1325	52	1325	75	0
VSL3-5	385	2203	1314	73	1220	57	1167	76	11
VSL3-5	1415	129	1279	63	1189	57	1140	78	11
VSL3-5	1309	129	1269	53	1251	42	1240	58	2
VSL3-5	1249	112	1267	51	1192	52	1151	73	9
VSL3-5	1407	115	1265	64	1228	46	1207	61	5
VSL3-5	1337	104	1256	50	1216	49	1194	69	5
VSL3-5	1321	120	1249	88	1168	60	1125	76	10
VSL3-5	1396	111	1232	58	1224	43	1220	59	1
VSL3-5	1113	102	1229	53	1243	42	1252	60	-2
VSL3-5	1119	108	1221	52	1229	39	1233	54	-1
VSL3-5	1409	138	1219	67	1192	48	1177	63	3
VSL3-5	1292	125	1216	60	1243	44	1259	62	-4
VSL3-5	1323	103	1211	54	1208	40	1207	54	0
VSL3-5	1166	105	1210	51	1144	46	1110	63	8
VSL3-5	1355	137	1200	74	1195	48	1192	62	1
VSL3-5	1350	109	1193	58	1184	52	1180	74	1
VSL3-5	1457	128	1185	77	1198	50	1206	64	-2
VSL3-5	1309	104	1183	77	1178	62	1176	86	1
VSL3-5	1323	104	1180	60	1159	39	1148	50	3
VSL3-5	1256	158	1145	107	1095	65	1069	80	7
VSL3-5	3870	2366	1137	135	1209	72	1250	87	-10
VSL3-5	1047	114	1116	96	1153	55	1173	68	-5
VSL3-5	1233	107	1111	64	1074	37	1056	44	5
LA-ICPMS									
	Dates (Ma)								
	208Pb*	**±2s**	**207Pb***	**±2s**	**207Pb***	**±2s**	**206Pb***	**±2s**	**%**
Analysis	**232Th**	**(Ma)**	**206Pb***	**(Ma)**	**235U**	**(Ma)**	**238U***	**(Ma)**	**disc.**
VSL3-6.8	2348	436	2103	137	2092	88	2080	109	1
VSL3-6.8	2144	406	2007	49	1866	58	1742	95	13
VSL3-6.8	1781	332	1920	89	1841	60	1773	79	8
VSL3-6.8	1618	291	1800	62	1818	44	1834	63	-2
VSL3-6.8	2361	147	1789	36	1802	40	1813	69	-1
VSL3-6.8	2045	265	1773	72	1782	51	1789	71	-1
VSL3-6.8	1568	192	1756	49	1748	40	1741	60	1
VSL3-6.8	1994	353	1755	64	1751	63	1747	103	0
VSL3-6.8	2208	264	1731	52	1731	46	1732	73	0
VSL3-6.8	2032	222	1723	57	1645	59	1586	92	8
VSL3-6.8	1487	272	1674	116	1538	67	1441	74	14
VSL3-6.8	1590	279	1661	56	1685	46	1705	72	-3
VSL3-6.8	1989	499	1656	194	1542	108	1461	115	12
VSL3-6.8	1750	238	1626	226	1496	102	1405	58	14
VSL3-6.8	2073	383	1552	112	1501	68	1465	83	6
VSL3-6.8	1731	231	1542	97	1507	53	1482	59	4
VSL3-6.8	1924	312	1532	65	1522	50	1515	71	1
VSL3-6.8	1570	212	1529	137	1427	72	1360	74	11
VSL3-6.8	1660	194	1528	51	1475	52	1438	79	6
VSL3-6.8	1636	284	1523	65	1447	43	1395	54	8

VSL3-6.8	1768	289	1522	56	1465	81	1426	128	6
VSL3-6.8	1910	110	1502	34	1461	42	1432	66	5
VSL3-6.8	1743	223	1490	69	1503	46	1512	62	-1
VSL3-6.8	1486	260	1485	56	1475	46	1468	67	1
VSL3-6.8	1640	221	1478	92	1475	53	1472	62	0
VSL3-6.8	1924	363	1478	92	1530	57	1567	74	-6
VSL3-6.8	1472	257	1472	81	1451	67	1437	97	2
VSL3-6.8	1584	199	1467	53	1422	33	1393	40	5
VSL3-6.8	1784	129	1466	86	1368	51	1306	61	11
VSL3-6.8	1547	194	1452	48	1416	42	1391	61	4
VSL3-6.8	1908	135	1443	72	1435	48	1430	63	1
VSL3-6.8	1356	170	1432	100	1296	51	1215	50	15
VSL3-6.8	1677	203	1428	43	1408	43	1394	65	2
VSL3-6.8	1396	252	1421	59	1473	43	1510	62	-6
VSL3-6.8	1550	221	1392	120	1368	69	1353	82	3
VSL3-6.8	1767	110	1360	54	1365	49	1369	73	-1
VSL3-6.8	1522	195	1353	82	1336	61	1326	84	2
VSL3-6.8	1791	266	1347	160	1396	86	1429	98	-6
VSL3-6.8	1673	104	1328	34	1268	41	1233	61	7
VSL3-6.8	1484	288	1322	136	1194	93	1124	116	15
VSL3-6.8	1306	249	1322	117	1238	62	1190	68	10
VSL3-6.8	1233	156	1321	49	1318	34	1316	46	0
VSL3-6.8	1692	198	1309	80	1337	65	1354	95	-3
VSL3-6.8	1547	257	1303	70	1283	58	1272	82	2
VSL3-6.8	1653	331	1303	207	1292	90	1285	71	1
VSL3-6.8	1541	282	1303	61	1273	39	1255	49	4
VSL3-6.8	1443	186	1302	101	1291	64	1284	83	1
VSL3-6.8	1357	172	1295	64	1235	42	1200	53	7
VSL3-6.8	1599	92	1282	47	1254	48	1239	70	3
VSL3-6.8	1158	210	1275	70	1234	40	1210	47	5
VSL3-6.8	1344	176	1274	108	1295	56	1308	63	-3
VSL3-6.8	1588	88	1271	39	1219	36	1189	50	6
VSL3-6.8	1654	110	1269	85	1218	50	1190	60	6
VSL3-6.8	1749	105	1264	57	1277	40	1285	53	-2
VSL3-6.8	1719	101	1263	39	1289	46	1305	70	-3
VSL3-6.8	1192	214	1258	98	1321	51	1359	58	-8
VSL3-6.8	1558	257	1251	86	1225	73	1211	102	3
VSL3-6.8	1492	82	1236	57	1194	40	1171	52	5
VSL3-6.8	1605	92	1222	37	1199	42	1186	61	3
VSL3-6.8	1451	243	1202	95	1246	45	1272	46	-6
VSL3-6.8	1371	260	1156	65	1181	59	1195	85	-3
VSL3-6.8	1329	246	1136	99	1161	68	1174	90	-3

Appendix A4. Supplement to Chapter 3: Carbon and oxygen isotopic methods and data tables for the Wood Canyon Formation in Death Valley, CA

Carbon ($\delta^{13}C$) and oxygen ($\delta^{18}O$) isotopic measurements were obtained on 218 samples from two sections of the lower member of the Wood Canyon Fm. Samples were micro-drilled along individual laminations, where visible, to obtain 5 to 20 mg of powder. Veins, fractures, and siliciclastic-rich areas were avoided. Carbonate $\delta^{13}C$ and $\delta^{18}O$ data were acquired simultaneously on a VG Optima dual inlet mass spectrometer at the Harvard University Laboratory for Geochemical Oceanography. Carbonate samples were reacted with orthophosphoric acid using a VG Isocarb preparation device, which includes a common acid bath with a magnetic stirrer. Approximately 1 mg of micro-drilled samples was reacted in the bath at 90°C. Evolved CO_2 was collected cryogenically and analyzed using an in-house reference gas. Potential memory effect resulting from the common acid-bath system was minimized by increasing the reaction time for dolomite samples. Memory effect is estimated at <0.1‰ based on variability of standards run after dolomite samples. Standard deviation (1σ) from standards was better than ± 0.1‰ for both $\delta^{13}C$ and $\delta^{18}O$. Carbonate $\delta^{13}C$ and $\delta^{18}O$ isotopic results are reported in per mil (‰) notation relative to V-PDB (Vienna-Pee Dee Belemnite) by using an in-house Cararra Marble standard that was calibrated against several NBS carbonate standards and cross-calibrated with other laboratories.

Boundary Canyon				Echo Canyon		
m corrected	**d13C**	**d180**		**m corrected**	**d13C**	**d180**
139.00	-2.07	-0.09		0.70	0.06	-9.75
139.10	-2.73	-0.30		1.30	0.27	-9.47

139.40	-2.78	0.35		1.70	0.28	-9.34
139.70	-2.73	1.03		2.00	0.64	-8.46
140.00	-2.81	-0.44		2.30	0.19	-9.46
140.10	-2.67	-0.10		2.60	0.57	-8.57
140.30	-2.31	0.78		3.10	0.42	-8.59
140.60	-2.55	0.03		3.50	-0.18	-9.27
140.90	-2.67	-0.18		4.80	-0.27	-8.35
141.30	-2.76	0.50		5.20	0.26	-8.77
141.50	-2.82	1.86		6.00	0.31	-8.74
141.80	-2.87	1.04		6.40	0.37	-7.81
142.10	-2.90	0.73		6.70	0.44	-7.69
142.50	-2.71	0.95		7.00	0.35	-7.99
142.80	-2.34	0.79		8.60	-0.10	-8.02
143.00	-2.33	0.85		18.10	0.24	-6.64
143.40	-2.28	-0.03		18.30	0.52	-6.41
143.60	-2.20	-0.04		18.70	0.37	-6.85
143.80	-2.44	0.59		19.50	0.12	-7.31
144.00	-1.89	0.28		20.10	-1.04	-7.47
144.40	-2.37	0.32		20.90	-0.48	-7.32
144.80	-2.17	0.47		21.30	-0.09	-8.68
145.00	-2.08	-0.20		21.50	-0.12	-7.89
145.20	-1.34	-0.36		22.00	-0.04	-7.32
145.60	-0.28	0.00		22.40	-0.12	-7.85
145.90	0.26	0.42		23.10	-0.24	-6.53
146.10	0.34	-0.30		23.50	-0.02	-7.56
146.50	0.99	0.41		23.80	-0.21	-8.47
147.40	1.96	-0.73		24.10	-0.42	-7.01
148.40	2.47	-0.66		24.60	0.11	-6.99
149.30	0.21	-0.76		24.90	0.28	-6.38
149.50	-0.02	-1.59		25.80	0.81	-7.17
149.80	-0.08	-1.60		26.50	0.78	-7.47
151.80	-0.37	-0.04		29.20	-0.54	-7.76
152.70	-1.38	-0.17		29.70	-0.73	-7.55
105.00	-3.55	-0.63		30.00	-0.84	-7.90
105.40	-3.82	-0.61		30.40	-0.77	-8.05
105.60	-3.71	-0.57		30.80	-0.77	-7.42
105.90	-3.34	-0.10		31.20	-0.90	-7.53
106.20	-3.01	-0.09		31.50	-1.23	-7.09
106.40	-3.01	0.23		31.80	-1.70	-8.40
106.60	-2.95	0.12		34.60	-2.03	-6.95
106.90	-2.76	0.02		35.00	-2.14	-7.34
107.40	-2.88	-0.04		35.50	-2.32	-6.90
107.60	-2.77	-0.65		36.00	-2.28	-7.26
108.00	-2.72	-0.40		36.20	-2.43	-6.84
108.20	-2.55	-1.69		36.50	-2.60	-7.17
110.00	-1.84	0.42		37.00	-2.58	-7.54
110.40	-2.52	-1.58		37.60	-2.51	-7.50
110.70	-2.36	0.31		38.00	-2.40	-6.95
111.00	-3.48	-0.34		38.40	-2.48	-6.05
111.20	-4.19	-2.57		39.00	-2.24	-7.82

33.60	-6.28	-6.14		39.70	-1.69	-7.00
33.20	-3.91	-6.43		40.00	-1.22	-6.46
33.00	-3.17	-6.99		40.50	-0.97	-6.26
32.60	-3.14	-8.04		41.00	-1.91	-7.16
32.30	-3.44	-7.64		41.50	-1.56	-6.46
32.00	-3.43	-9.15		42.00	-2.13	-6.12
31.50	-3.00	-7.75		42.50	-2.77	-6.66
31.20	-2.84	-8.32		42.80	-2.83	-6.26
30.90	-2.69	-8.01		43.00	-3.43	-6.69
30.50	-2.23	-6.81		43.70	-3.85	-6.11
29.90	-2.16	-6.86		44.00	-3.99	-7.32
29.60	-1.80	-6.46		44.30	-2.59	-6.39
29.30	-1.89	-7.42		44.70	-2.93	-6.28
29.00	-2.27	-6.53		45.00	-4.20	-7.19
28.50	-2.49	-6.84		45.40	-5.49	-6.77
28.30	-2.43	-7.03		46.00	-5.59	-6.60
28.00	-2.81	-7.22		47.00	-5.71	-6.81
27.70	-2.60	-7.05		47.40	-9.06	-6.04
27.30	-2.53	-6.75		158.00	-3.45	-7.18
27.00	-2.40	-7.06		158.40	-3.13	-7.22
26.60	-2.04	-7.76		158.80	-3.35	-7.72
26.30	-1.89	-7.57		159.40	-3.03	-7.12
26.00	-1.84	-7.09		159.80	-3.00	-6.97
25.80	-1.71	-7.89		160.20	-3.32	-7.26
25.50	-1.50	-7.77		160.50	-2.99	-7.57
25.20	-1.80	-7.39		232.00	-2.33	-9.56
24.90	-1.81	-7.36		232.30	-2.58	-7.84
24.60	-1.95	-8.01		232.50	-2.27	-6.85
24.40	-1.86	-7.47		232.70	-2.07	-6.15
24.00	-1.84	-7.46		233.20	-2.79	-8.83
23.80	-1.37	-7.21		233.50	-2.62	-8.45
23.40	-1.25	-7.82		235.60	-2.71	-13.19
22.60	-1.49	-8.25		235.90	-1.41	-10.28
22.20	-1.52	-7.43		236.40	-0.99	-11.23
22.00	-1.20	-6.87		236.70	-0.35	-9.28
21.70	-1.18	-7.78		237.00	-2.11	-14.05
21.40	-0.79	-6.11		237.40	0.04	-10.02
18.90	0.17	-7.11		238.00	1.67	-6.41
18.60	-0.09	-7.73		238.50	0.73	-9.15
18.30	-0.16	-8.39		238.80	1.42	-8.01
17.80	-0.28	-9.14		239.00	1.54	-7.96
17.50	-0.34	-8.97		239.90	1.05	-8.95
17.20	-0.31	-8.76		240.70	0.34	-8.97
17.00	-0.29	-8.63		241.00	-0.10	-8.58
16.70	-0.41	-9.03				
16.50	-0.34	-8.36				
16.00	-0.12	-8.39				
15.50	-0.23	-8.88				
15.30	0.03	-7.74				
14.90	0.19	-7.69				

14.60	0.41	-8.14				
14.30	0.38	-9.01				
14.00	0.60	-8.31				
13.80	0.66	-8.51				
13.50	0.46	-8.62				
13.20	0.46	-8.10				
12.90	0.57	-8.10				
12.70	0.78	-7.45				
12.50	0.97	-8.40				
12.00	0.43	-9.83				
11.30	0.37	-10.14				
6.80	0.32	-9.73				
6.50	0.58	-9.26				
4.40	1.57	-6.38				
4.20	0.76	-8.84				
3.50	0.94	-8.04				
3.20	0.73	-8.79				
3.00	1.52	-7.54				
2.80	0.66	-8.44				
2.50	0.31	-9.55				

Appendix A5. Supplement to Chapter 3: Carbon and oxygen isotopic methods and data tables for the Deep Spring Formation in Esmeralda County, NV

Carbon ($\delta^{13}C$) and oxygen ($\delta^{18}O$) isotopic measurements were obtained on 535 samples from two sections of the uppermost Reed Fm through Deep Spring Fm in Esmeralda County, NV. Samples were micro-drilled along individual laminations, where visible, to obtain 5 to 20 mg of powder. Veins, fractures, and siliciclastic-rich areas were avoided. Carbonate $\delta^{13}C$ and $\delta^{18}O$ data were acquired simultaneously on a VG Optima dual inlet mass spectrometer at the Harvard University Laboratory for Geochemical Oceanography. Carbonate samples were reacted with orthophosphoric acid using a VG Isocarb preparation device, which includes a common acid bath with a magnetic stirrer. Approximately 1 mg of micro-drilled samples was reacted in the bath at 90°C. Evolved CO_2 was collected cryogenically and analyzed using an in-house reference gas. Potential memory effect resulting from the common acid-bath system was minimized by increasing the reaction time for dolomite samples. Memory effect is estimated at <0.1‰ based on variability of standards run after dolomite samples. Standard deviation (1σ) from standards was better than ± 0.1‰ for both $\delta^{13}C$ and $\delta^{18}O$. Carbonate $\delta^{13}C$ and $\delta^{18}O$ isotopic results are reported in per mil (‰) notation relative to V-PDB (Vienna-Pee Dee Belemnite) by using an in-house Cararra Marble standard that was calibrated against several NBS carbonate standards and cross-calibrated with other laboratories.

E1511				E1512 (below E1426 and above E1425)		
m	**d13C**	**d18O**		**m**	**d13C**	**d18O**
0.10	1.48	-17.90		0.20	-2.12	-16.69
0.80	1.50	-17.78		1.00	-1.85	-16.36
2.00	2.06	-14.18		2.00	-2.16	-16.62
3.00	2.08	-12.98		3.00	-2.36	-18.13
4.00	2.77	-10.77		5.00	-2.34	-15.61
5.00	2.20	-16.53		6.00	-2.82	-15.70
6.00	1.98	-17.50		6.60	-2.19	-17.71
7.50	2.90	-18.66		8.00	-2.03	-16.85
9.00	3.69	-15.30		9.00	-2.37	-17.53
9.70	2.36	-17.74		10.00	-2.15	-17.42
11.00	3.33	-18.45		11.00	-2.37	-14.89
12.00	3.59	-16.72		11.60	-2.05	-16.31
13.00	3.04	-17.00		13.00	-2.42	-12.68
15.00	2.67	-14.97		14.00	-2.58	-18.08
16.00	3.14	-17.36		16.00	-2.45	-17.66
17.00	2.98	-17.55		17.00	-1.60	-14.87
18.00	3.00	-17.94		18.00	-2.39	-16.55
19.10	2.83	-17.57		19.00	-2.47	-16.26
20.00	3.24	-18.33		20.00	-1.73	-15.33
21.50	2.89	-17.92		21.00	-1.88	-15.31
23.00	2.71	-17.49		22.00	-1.11	-14.01
24.00	2.80	-17.38		23.00	-2.42	-15.55
25.00	2.75	-17.61		24.00	-1.86	-14.29
26.00	2.65	-19.08		25.00	-1.70	-15.85
27.00	2.34	-15.88		26.00	-2.66	-16.48
28.00	2.51	-18.46		27.00	-2.54	-14.24
29.00	2.67	-17.82		28.00	-1.06	-12.91
30.00	2.42	-16.12		29.00	-2.43	-14.74
31.00	2.32	-20.40		30.00	-2.36	-14.20
32.00	2.22	-19.77		31.00	-0.74	-12.73
33.00	1.64	-16.07		32.00	-2.70	-11.96
34.00	2.01	-15.62		33.00	-1.26	-13.97
35.00	1.99	-14.49		34.00	-2.47	-10.92
36.00	1.84	-19.76		35.00	-2.74	-12.09
37.00	1.89	-19.44		36.50	-2.39	-12.65
38.00	1.69	-20.04		37.50	0.22	-12.96
39.10	1.09	-19.68		39.00	-2.42	-15.44
40.00	1.78	-20.09		40.00	-2.86	-14.53
41.00	1.87	-20.89		41.00	-0.22	-13.70
42.00	1.64	-22.46		42.00	-1.72	-14.18
43.50	1.98	-16.71		43.00	-3.37	-14.32
45.00	2.14	-16.00				
46.00	1.68	-17.80				
47.00	2.58	-14.42				
48.00	1.70	-14.90				
49.00	1.18	-18.74				

50.00	1.81	-10.83				
51.00	0.94	-11.85				
52.00	-0.12	-16.52				
53.10	0.82	-12.32				
54.00	1.40	-12.83				
55.00	1.12	-14.16				
56.50	0.42	-17.18				
58.00	1.86	-13.87				
59.00	0.93	-18.12				
60.00	2.05	-19.78				
E1513 (Ru through basal DSFl)				**E1515 (Ru-DSFl transition beds)**		
-2.00	1.87	-11.59		0.10	1.94	-14.65
-1.00	1.88	-10.56		1.00	2.13	-13.91
2.60	1.50	-14.18		2.00	2.10	-14.26
3.00	2.30	-13.97		3.00	1.90	-14.23
3.80	3.15	-13.73		4.00	1.53	-15.30
5.00	3.39	-14.14		5.00	2.38	-15.77
6.00	3.18	-14.92		6.00	2.39	-15.72
7.00	3.01	-15.97		7.00	2.20	-15.68
8.00	3.51	-10.33		8.00	2.09	-13.17
10.00	2.41	-9.67		9.00	2.23	-14.01
11.00	2.77	-11.47		10.00	2.16	-13.17
12.00	2.21	-10.70		11.00	1.98	-12.91
13.00	2.28	-11.67		12.00	1.87	-13.09
14.00	3.62	-8.78		13.30	2.42	-16.41
15.00	1.89	-13.69		14.30	2.17	-14.89
32.00	1.95	-11.18		15.00	1.54	-14.53
17.00	2.57	-13.25		16.00	2.39	-16.08
18.00	2.45	-13.23		17.00	1.98	-16.44
19.00	2.37	-14.44		18.00	2.52	-19.50
20.00	1.91	-18.30		19.00	1.02	-16.98
20.3A	1.99	-15.80		20.00	2.04	-16.63
20.3B	1.86	-15.03		21.00	2.13	-20.38
21.00	1.55	-15.93		22A	1.45	-18.34
22.00	2.26	-12.42		22B	1.89	-14.65
23.00	2.06	-13.25		23.00	2.38	-12.19
24.00	2.13	-11.02		24.00	2.09	-12.82
25.00	2.04	-13.01		25.00	1.60	-22.30
26.00	1.94	-13.95		26.00	2.23	-19.41
27.00	2.15	-15.03		27.00	2.57	-17.51
29.00	2.31	-12.52		28.00	2.14	-17.12
30.00	1.91	-12.15		29.00	2.04	-16.92
31.00	1.67	-11.10		30.00	1.30	-16.93
33.00	2.00	-10.74				
34.00	1.90	-10.92				
35.00	1.94	-9.45				
36.00	1.90	-12.81				
38.00	2.61	-17.29				
38.00	2.59	-17.23				

39.00	2.34	-15.48				
40.00	2.06	-15.68				
41.00	2.71	-15.12				
42.00	2.14	-15.31				
43.00	2.43	-14.93				
44.00	2.35	-17.49				
44.5A	2.70	-15.62				
44.5B	2.21	-15.08				
45.00	2.39	-15.34				
46.00	2.33	-19.60				
47.00	1.90	-14.95				
48.00	2.26	-12.62				
49.00	1.80	-13.25				
50.00	2.12	-12.35				
51.00	1.47	-16.36				
53.00	2.94	-19.63				
54.00	2.71	-15.70				
55.00	2.32	-13.77				
56.00	1.97	-16.25				
57.00	1.61	-14.65				
58.00	1.91	-14.74				
59.00	0.63	-15.19				
60.00	1.09	-16.40				
61.00	0.95	-16.50				
62.00	1.35	-13.78				
63.00	0.47	-16.31				
64.00	1.40	-16.52				
65.00	1.44	-17.43				
E1421				**E1426**		
m corrected	d13C	d180		m corrected	d13C	d180
465.50	-3.62	-15.99		161.80	-2.97	-16.39
464.50	-3.40	-10.94		162.10	-2.89	-15.64
463.50	-2.82	-12.98		162.50	-3.21	-13.15
462.50	-2.75	-14.69		163.10	-3.05	-16.65
462.00	-2.49	-11.22		163.50	-2.98	-12.88
461.50	-3.06	-19.39		164.00	-3.19	-16.33
461.00	-2.30	-10.55		164.60	-3.03	-15.79
460.50	-2.20	-10.39		165.00	-2.92	-12.25
460.00	-2.56	-13.49		165.50	-2.13	-12.67
459.50	-2.86	-13.23		166.00	-2.94	-18.44
459.00	-2.64	-17.47		166.50	-2.73	-17.87
458.50	-2.32	-13.35		167.50	-2.85	-14.18
457.50	-2.78	-16.64		168.00	-3.01	-17.30
457.00	-2.50	-16.64		168.50	-3.02	-13.03
456.50	-2.79	-18.53		169.40	-3.24	-19.40
456.00	-2.85	-15.03		170.00	-2.82	-15.50
455.50	-2.32	-15.26		170.50	-2.50	-12.87
455.00	-2.42	-14.71		171.00	-2.94	-18.89
454.00	-2.08	-14.87		171.50	-2.61	-22.02

454.00	-2.16	-14.88		172.00	-2.94	-20.95
453.50	-2.15	-13.18		172.50	-2.63	-17.09
453.00	-2.54	-20.38		172.80	-2.11	-13.29
452.50	-2.76	-21.95		173.70	-2.65	-19.35
452.00	-2.86	-21.11		174.00	-3.09	-19.86
451.50	-2.41	-16.30		174.50	-2.94	-19.43
451.00	-2.12	-14.53		175.00	-2.78	-18.72
450.50	-2.61	-22.74		175.50	-3.00	-20.04
450.00	-2.37	-18.11		176.00	-2.96	-14.63
449.50	-2.23	-16.23		176.50	-2.35	-15.53
449.20	-2.26	-16.67		177.00	-3.09	-14.94
448.90	-2.44	-19.69		177.50	-2.34	-14.80
447.50	-2.15	-15.47		177.90	-3.21	-24.45
447.10	-2.15	-15.84		178.50	-2.32	-24.96
446.50	-2.36	-14.09		179.00	-3.35	-14.40
445.90	-2.28	-11.17		179.50	-2.60	-14.29
445.50	-2.42	-9.11		180.00	-2.38	-11.74
445.10	-2.62	-9.89		180.50	-2.51	-15.95
444.10	-2.36	-11.57		181.00	-2.67	-16.38
342.90	-5.80	-16.76		181.50	-2.46	-16.70
343.10	-5.85	-15.08		182.00	-3.04	-22.44
343.50	-6.42	-18.06		182.50	-3.32	-24.39
344.00	-6.41	-15.96		183.00	-3.01	-23.17
344.50	-6.43	-18.20		183.50	-2.99	-22.24
345.00	-6.38	-17.04		184.00	-3.24	-25.59
345.30	-6.81	-17.06		184.50	-2.55	-16.29
313.30	-4.91	-11.93		185.00	-3.17	-25.09
313.50	-6.35	-14.06		185.50	-3.03	-25.31
314.30	-6.17	-12.48		186.00	-2.47	-18.70
314.50	-6.01	-16.88		186.50	-3.10	-19.57
315.00	-5.72	-17.43		187.00	-2.72	-24.26
315.50	-5.56	-15.62		187.50	-2.84	-25.18
316.00	-5.24	-14.70		187.80	-1.45	-11.96
316.50	-5.00	-15.94		188.50	-2.37	-16.17
316.70	-4.39	-16.62		206.30	-1.11	-11.84
317.10	-4.38	-16.89		205.00	-2.24	-14.79
317.60	-3.57	-12.79		203.50	-2.34	-15.09
317.80	-3.06	-13.15		201.50	-2.39	-15.04
318.00	-3.95	-16.74		200.50	-2.27	-15.29
318.20	-4.27	-16.52		199.50	-2.33	-15.15
318.50	-3.18	-16.97		198.50	-2.47	-15.20
318.80	-3.62	-16.31		197.50	-2.42	-15.47
319.00	-4.36	-17.08		196.50	-2.40	-14.99
319.20	-5.09	-16.98		195.50	-2.41	-15.37
319.40	-4.94	-16.32		194.00	-2.50	-15.28
319.50	-4.97	-15.70		193.50	-2.53	-15.36
320.00	-4.59	-15.89		192.50	-2.42	-14.45
320.30	-6.22	-16.94		191.50	-2.46	-15.38
326.20	-5.34	-16.50		190.50	-2.42	-15.05
326.50	-5.24	-16.72		189.50	-2.56	-15.54

326.80	-3.89	-15.37				
327.00	-2.54	-16.10		**E1425**		
327.30	-3.54	-16.31		30.00	1.56	-17.96
327.50	-2.09	-16.05		29.50	2.33	-14.08
327.80	-2.57	-16.46		29.00	-0.39	-14.42
328.10	-4.11	-16.56		58.00	2.93	-8.26
328.30	-4.25	-16.47		28.50	0.12	-15.88
328.50	-4.45	-16.56		28.00	1.54	-14.60
328.80	-3.93	-15.84		26.80	-0.43	-15.71
329.20	-3.66	-17.01		25.00	1.36	-13.40
346.80	-7.14	-17.98		24.00	2.08	-14.37
352.10	-6.55	-17.45		23.00	2.09	-17.38
352.70	-6.00	-13.46		22.30	1.59	-18.74
353.50	-5.46	-13.68		21.70	1.87	-13.63
355.10	-6.84	-17.67		21.00	1.93	-12.84
355.10	-6.85	-17.66		20.00	2.05	-12.36
355.50	-7.42	-18.22		19.00	1.75	-16.66
356.50	-8.16	-18.00		18.00	1.62	-16.69
360.10	-6.38	-16.61		17.20	1.22	-17.03
360.60	-5.81	-16.17		16.50	2.18	-16.76
361.00	-7.24	-17.12		16.00	2.88	-13.68
361.00	-7.24	-17.11		15.30	3.24	-13.24
361.50	-9.47	-23.67		14.60	0.87	-13.07
362.00	-7.22	-17.16		13.50	2.75	-13.42
362.50	-6.55	-17.34		12.30	1.75	-15.76
365.50	-6.73	-17.35		11.70	2.40	-13.56
366.50	-6.17	-17.12		11.00	2.09	-12.96
367.00	-6.61	-17.23		10.30	2.30	-15.23
367.50	-6.57	-16.89		70.00	4.27	-16.13
368.00	-6.35	-15.16		69.50	1.67	-15.50
368.50	-6.76	-15.76		69.00	3.54	-18.80
369.00	-6.01	-16.06		68.60	3.50	-18.88
369.50	-6.44	-16.83		68.00	3.15	-19.77
371.20	-3.08	-9.68		67.00	2.82	-19.38
372.20	-6.50	-16.17		66.00	3.01	-18.76
372.80	-6.44	-14.89		64.00	2.87	-18.39
373.30	-4.23	-15.19		62.50	2.64	-13.74
329.50	-4.00	-15.85		61.50	2.14	-14.73
329.70	-2.74	-16.18		61.00	2.68	-13.34
329.90	-4.03	-16.11		60.50	2.82	-14.47
330.20	-4.04	-16.28		60.00	0.45	-9.67
330.50	-3.69	-16.16		59.50	3.07	-10.73
331.10	-3.81	-16.53		58.80	2.54	-10.70
331.50	-3.40	-12.23		57.00	2.26	-13.66
331.80	-4.55	-15.98		56.00	2.76	-14.91
332.00	-4.35	-15.72		55.50	2.39	-11.31
332.20	-4.69	-16.66		55.00	2.46	-7.73
332.50	-4.33	-16.00		54.50	1.95	-12.77
334.50	-5.90	-15.75		54.00	0.84	-13.41
342.10	-5.49	-18.11		53.00	2.29	-12.54

342.50	-5.72	-18.54		51.50	2.55	-13.56
401.40	-3.92	-14.18		51.00	1.94	-8.66
411.50	-1.38	-12.06		50.40	1.92	-9.74
413.00	0.04	-13.48		50.00	2.24	-11.36
443.50	-2.50	-12.75		49.50	2.38	-15.14
414.00	-0.71	-11.31		48.50	2.00	-11.09
415.50	-1.09	-12.02		47.50	2.08	-11.19
416.50	-1.95	-13.46		47.00	2.76	-13.51
468.00	-2.30	-7.62		46.60	3.12	-10.38
374.20	-6.75	-14.01		44.80	2.82	-14.02
376.00	-6.73	-16.82		44.00	3.09	-10.30
574.50	0.62	-7.83		42.80	-0.94	-13.44
573.50	0.53	-9.56		42.00	3.02	-14.22
572.50	0.57	-9.57		41.00	2.08	-14.61
571.50	0.55	-9.36		40.00	3.25	-15.17
570.50	0.51	-8.53		39.50	1.98	-14.75
569.50	0.31	-9.96		38.60	3.28	-14.20
568.70	-1.25	-6.22		38.00	1.06	-15.90
568.50	0.29	-9.23		36.50	3.25	-19.57
567.50	0.58	-10.56		35.90	3.22	-18.11
566.50	0.69	-10.00		33.00	1.94	-14.75
564.50	1.00	-10.12		32.50	1.66	-14.53
563.50	0.89	-10.46		32.00	0.89	-16.93
562.50	0.87	-9.64		31.60	2.39	-14.77
561.50	0.83	-10.06		31.00	1.27	-15.68
560.50	0.86	-10.05		30.50	1.62	-15.27
559.50	0.85	-9.39		9.60	2.49	-13.60
397.00	-3.45	-12.27		8.60	2.39	-16.56
397.50	-3.53	-12.15		8.00	2.88	-19.98
398.00	-3.45	-11.27		7.50	3.18	-19.45
399.30	-4.64	-12.59		6.40	3.35	-20.44
400.10	-3.92	-14.66		5.70	3.00	-20.20
400.50	-3.35	-13.48		5.30	3.76	-9.15
401.00	-3.50	-11.27		4.70	2.96	-22.56
410.90	-1.30	-13.49		4.00	3.04	-12.48
412.00	0.12	-14.43		3.50	0.35	-9.80
416.00	0.15	-14.51		2.50	-0.66	-21.15
418.00	-2.50	-12.54		1.40	2.46	-21.84
418.50	-1.34	-13.32		0.00	2.73	-17.69
419.50	-4.57	-13.07		0.50	1.51	-17.57
420.00	-1.63	-13.32		1.00	1.00	-19.71
420.50	-1.07	-11.93		1.40	2.51	-22.15
422.90	0.85	-14.23		83.50	1.47	-20.58
425.80	-0.13	-12.59		83.00	2.72	-19.54
557.50	0.84	-9.22		82.00	2.56	-20.71
556.50	0.72	-10.19		81.00	2.89	-15.33
555.50	0.82	-9.29		79.00	2.84	-16.30
554.50	0.74	-8.36		78.00	2.92	-15.40
553.90	1.19	-6.06		77.00	2.92	-15.58
393.00	-3.19	-11.97		76.50	3.11	-13.76

393.50	-3.66	-9.48		76.00	2.80	-11.53
394.00	-3.45	-9.11		75.50	3.16	-14.53
394.50	-3.52	-12.74		75.00	3.20	-14.25
395.00	-3.34	-11.87		74.50	3.07	-16.11
395.50	-3.69	-12.49		74.00	3.40	-11.55
396.00	-3.66	-12.33		73.50	3.42	-12.12
396.50	-3.18	-11.45		73.00	3.68	-17.69
378.10	-4.58	-14.96		72.50	4.08	-16.67
378.50	-4.58	-16.00		72.00	3.72	-16.04
379.00	-4.36	-13.38		71.50	3.94	-10.07
380.90	-4.47	-16.91		71.00	3.60	-19.62
381.60	-3.32	-13.83		70.50	4.14	-17.43
383.00	-2.95	-18.69		70.00	4.32	-16.57
383.50	-2.97	-17.03		69.50	1.83	-16.04
383.90	-3.46	-18.01		69.00	3.51	-18.84
385.00	-3.37	-15.69		68.60	3.50	-18.86
385.50	-3.26	-19.39		68.00	3.36	-18.30
386.00	-3.58	-15.67		67.00	3.09	-19.19
386.50	-3.65	-16.89				
387.00	-3.01	-13.52		**E1512**		
387.50	-3.29	-13.25		113.70	-2.12	-16.69
388.30	-2.63	-11.66		114.50	-1.85	-16.36
389.00	-2.92	-13.87		115.50	-2.16	-16.62
389.50	-1.90	-10.86		116.50	-2.36	-18.13
390.00	-2.62	-10.04		118.50	-2.34	-15.61
390.50	-3.16	-11.23		119.50	-2.82	-15.70
391.00	-3.35	-12.65		120.10	-2.19	-17.71
391.50	-3.70	-12.48		121.50	-2.03	-16.85
392.00	-3.42	-12.48		122.50	-2.37	-17.53
392.50	-3.61	-12.53		123.50	-2.15	-17.42
429.00	0.02	-11.56		124.50	-2.37	-14.89
429.50	0.64	-10.92		125.10	-2.05	-16.31
429.90	0.68	-12.02		126.50	-2.42	-12.68
431.20	1.37	-10.71		127.50	-2.58	-18.08
431.50	-0.35	-11.51		129.50	-2.45	-17.66
431.90	-0.27	-12.37		130.50	-1.60	-14.87
432.20	-3.10	-12.14		131.50	-2.39	-16.55
432.50	-0.27	-11.79		132.50	-2.47	-16.26
432.80	-0.88	-9.50		133.50	-1.73	-15.33
433.20	-0.22	-10.54		134.50	-1.88	-15.31
433.50	-0.95	-12.70		135.50	-1.11	-14.01
433.90	-1.39	-12.02		136.50	-2.42	-15.55
434.20	-1.40	-11.51		137.50	-1.86	-14.29
434.50	-1.44	-13.82		138.50	-1.70	-15.85
434.80	-2.82	-17.00		139.50	-2.66	-16.48
437.50	-1.48	-13.42		140.50	-2.54	-14.24
437.80	-3.56	-11.91		141.50	-1.06	-12.91
438.00	-1.83	-13.30		142.50	-2.43	-14.74
438.50	-3.32	-17.78		143.50	-2.36	-14.20
440.90	-2.80	-16.48		144.50	-0.74	-12.73

441.50	-2.82	-14.87		145.50	-2.70	-11.96
441.70	-2.55	-16.53		146.50	-1.26	-13.97
442.80	-2.50	-17.06		147.50	-2.47	-10.92
426.10	-0.24	-9.95		148.50	-2.74	-12.09
426.40	0.38	-11.55		150.00	-2.39	-12.65
427.00	0.39	-12.30		151.00	0.22	-12.96
427.20	-0.04	-12.06		152.50	-2.42	-15.44
427.40	-0.32	-11.16		153.50	-2.86	-14.53
428.60	-1.01	-12.15		154.50	-0.22	-13.70
				155.50	-1.72	-14.18
				156.50	-3.37	-14.32

Appendix A6. Supplement to Chapter 3: Carbon and oxygen isotope data from the Zuun-Arts Ridge and Khongor sections of the Zuun-Arts Formation in Western Mongolia

Data tables for additional sections of the Zuun-Arts Fm can be found in Appendix A7.

Khongor locality

height	m from base	$d^{13}C$	$d^{18}O$
598.0	12.0	-0.28	-4.12
603.0	17.0	-1.55	-3.65
605.0	19.0	-0.65	-3.69
607.0	21.0	-1.37	-5.74
609.0	23.0	-2.06	-6.52
615.0	29.0	0.06	-10.62
617.0	31.0	0.82	-9.25
619.0	33.0	0.67	-11.00
621.0	35.0	0.20	-8.41
623.0	37.0	1.05	-8.28
625.0	39.0	-0.88	-10.80
627.0	41.0	-0.61	-8.83
629.0	43.0	-0.30	-10.22
631.0	45.0	0.37	-13.74
633.0	47.0	-0.97	-8.68
635.0	49.0	-0.41	-9.42
637.0	51.0	-3.28	-14.89
639.0	53.0	-5.03	-10.10
643.0	57.0	-2.38	-8.96
655.0	69.0	-1.35	-8.49
657.0	71.0	-2.98	-8.07
659.0	73.0	-3.14	-8.93
661.0	75.0	-0.20	-9.01
663.0	77.0	-0.86	-8.79
665.0	79.0	-5.53	-11.34
667.0	81.0	-4.12	-11.44
669.0	83.0	-4.41	-10.65
671.0	85.0	-0.53	-10.63
673.0	87.0	-1.14	-10.60
678.0	92.0	-2.88	-12.05
680.0	94.0	-1.70	-10.28
682.0	96.0	0.19	-10.51
684.0	98.0	0.50	-9.79
692.0	106.0	-1.59	-12.69
694.0	108.0	0.74	-9.67
698.0	112.0	-1.23	-7.38
700.0	114.0	-1.52	-7.13

702.0	116.0	-2.46	-9.08
704.0	118.0	-0.29	-8.94
706.0	120.0	-1.41	-8.23
708.0	122.0	0.26	-8.06
710.0	124.0	-1.13	-7.87
712.0	126.0	-0.38	-8.26
714.0	128.0	0.56	-7.45
716.0	130.0	-1.81	-9.08
718.0	132.0	-0.34	-7.72
720.0	134.0	-1.25	-7.69
722.0	136.0	-0.08	-7.60
724.0	138.0	-3.52	-9.07
726.0	140.0	-1.11	-8.29
728.0	142.0	-1.07	-8.36
730.0	144.0	-4.27	-10.14
732.0	146.0	-1.76	-8.42
736.0	150.0	-1.65	-8.29
740.0	154.0	-0.31	-9.30
742.0	156.0	-4.11	-11.99
744.0	158.0	-1.22	-10.34
746.0	160.0	-0.70	-10.89
748.0	162.0	-2.33	-12.58
750.0	164.0	-2.41	-10.11
752.0	166.0	-1.38	-9.56
754.0	168.0	-4.45	-10.37
756.0	170.0	-3.01	-8.78
758.0	172.0	-1.33	-8.05
760.0	174.0	-3.71	-7.98
762.0	176.0	-2.97	-8.95
764.0	178.0	-0.74	-7.68
766.0	180.0	-2.70	-8.75
768.0	182.0	-3.61	-9.20
770.0	184.0	-2.57	-9.97
772.0	186.0	-2.00	-9.41
774.0	188.0	-1.25	-24.53
776.0	190.0	-2.54	-16.77
780.0	194.0	-1.29	-8.26
782.0	196.0	-1.85	-12.39
784.0	198.0	-2.15	-30.96
786.0	200.0	-4.08	-27.36
788.0	202.0	-4.54	-14.33
790.0	204.0	-4.04	-10.92
798.0	212.0	-4.01	-10.29
804.0	218.0	-6.51	-22.66
806.0	220.0	-4.14	-10.58
808.0	222.0	-3.94	-10.85
810.0	224.0	-3.97	-11.58
812.0	226.0	-3.98	-8.78
814.0	228.0	-4.08	-16.27
816.0	230.0	-4.22	-24.62

818.0	232.0	-4.64	-11.01
820.0	234.0	-4.30	-17.45
822.0	236.0	-4.78	-9.03
824.0	238.0	-6.99	-10.23
826.0	240.0	-6.80	-15.90
828.0	242.0	-5.37	-11.78
830.0	244.0	-3.73	-10.12
832.0	246.0	-3.83	-8.04

Zuun-Arts Ridge locality

height	from base	$d^{13}C$	$d^{18}O$
17.0	9.0	-1.75	-3.76
20.0	12.0	0.52	-6.03
27.0	19.0	4.70	-14.51
33.0	25.0	6.46	-11.77
36.5	28.5	5.40	-11.98
40.0	32.0	3.74	-13.21
42.0	34.0	4.22	-11.54
50.0	42.0	2.85	-7.45
53.0	45.0	5.62	-10.47
55.0	47.0	5.96	-7.34
60.0	52.0	4.38	-9.15
64.0	56.0	5.25	-8.17
68.0	60.0	1.08	-13.13
74.0	66.0	2.16	-8.43
78.0	70.0	2.71	-10.44
81.0	73.0	2.59	-11.20
86.0	78.0	2.96	-11.02
90.0	82.0	2.74	-8.43
94.0	86.0	0.61	-9.01
98.0	90.0	1.30	-10.50
102.0	94.0	0.87	-10.65
106.0	98.0	-0.86	-9.42
112.0	104.0	-0.04	-10.13
114.0	106.0	-0.95	-10.26
118.0	110.0	0.41	-9.21
122.0	114.0	0.23	-9.64
124.0	116.0	-0.03	-8.26
126.0	118.0	-0.49	-8.34
128.0	120.0	-1.24	-10.76
130.0	122.0	-1.49	-9.11
132.0	124.0	-1.66	-10.81
134.0	126.0	-2.44	-10.83
138.0	130.0	-2.80	-8.14
140.0	132.0	0.95	-8.11
142.0	134.0	1.38	-10.13
146.0	138.0	-1.50	-8.33
148.0	140.0	-0.57	-8.72

150.0	142.0	-1.47	-11.51
152.0	144.0	-0.70	-10.82
154.0	146.0	-1.62	-9.97
156.0	148.0	-1.09	-8.16
160.0	152.0	-2.04	-8.52
162.0	154.0	-2.51	-10.19
166.0	158.0	-3.49	-9.89
170.0	162.0	-3.54	-11.82
174.0	166.0	-4.77	-9.17
178.0	170.0	-4.73	-10.84
182.0	174.0	-4.38	-10.64
186.0	178.0	-3.49	-11.40
190.0	182.0	-3.53	-13.52
194.0	186.0	-3.29	-18.36
198.0	190.0	-3.49	-15.40
202.0	194.0	-4.25	-11.04
206.0	198.0	-4.11	-12.33

Appendix A7. Supplement to Chapter 4: Carbon and oxygen isotopic measurements for the Zuun-Arts, Bayangol, and Salaagol formations

The following data tables include GPS coordinates for measured sections and carbon and oxygen isotope measurements. These tables are organized by locality. Additional data on the taxon and references for the different Mongolia SSF fossil horizons, the carbon isotope peaks used to construct the age model, and the revised global FADs can be found in the supplementary material of Smith et al., accepted.

GPS coordinates for the bases of measured sections.

Section	Locality		Lat		Lon
E1113	Taishir	N	46.701	E	96.577
E1114	Taishir	N	46.697	E	96.576
E1115	Taishir	N	46.709	E	96.538
E1117	Taishir	N	46.702	E	96.575
E1325	SE Taishir	N	46.623	E	96.664
E1215	KTN	N	46.634	E	96.796
E1216	KTN	N	46.698	E	96.863
E1123	SE of Bayan Gorge	N	46.653	E	96.494
E1129	Bayan Gorge	N	46.712	E	96.312
E1126	Bayan Gorge	N	46.740	E	96.332
F1120	Bayan Gorge	N	46.707	E	96.311
E1130	Bayan Gorge	N	46.694	E	96.308
D706	Bayan Gorge	N	46.688	E	96.288
E1207	SE Khukh-Davaa	N	47.124	E	95.404
E1209	SE Khukh-Davaa	N	47.103	E	95.448
E1328	SE Khukh-Davaa	N	46.979	E	95.556
E1329	SE Khukh-Davaa	N	46.977	E	95.555
E1331	SE Khukh-Davaa	N	46.976	E	95.568
F874	Salaa and Tsagaan gorges	N	46.821	E	95.802
D718	Salaa and Tsagaan gorges	N	46.815	E	95.798
D720	Salaa and Tsagaan gorges	N	46.835	E	95.780
F1131	Salaa and Tsagaan gorges	N	46.813	E	95.771
E1109	Salaa and Tsagaan gorges	N	46.836	E	95.744
E1211	NE Khukh-Davaa	N	47.189	E	95.424
E1212	NE Khukh-Davaa	N	47.204	E	95.390
E1138	Khunkher Gorge	N	46.750	E	95.970
E1220	Orolgo Gorge	N	46.791	E	95.608

F708	Khongor	N	46.663	E	96.255
F721	Zuun-Arts Ridge	N	47.311	E	96.476

Taishir locality

m corrected	d13C	d18O	section	Fm
0.5	-2.886	-8.174	E1113	BG
2	-3.942	-9.520	E1113	BG
5.8	-3.644	-10.751	E1113	BG
14.5	1.433	-11.074	E1113	BG
17.6	0.337	-8.409	E1113	BG
20.6	1.571	-10.616	E1113	BG
23.6	-0.906	-9.167	E1113	BG
26.6	-0.046	-10.083	E1113	BG
29.6	-1.293	-10.479	E1113	BG
34	-2.686	-10.610	E1113	BG
34.6	-1.530	-10.638	E1113	BG
39.4	-1.943	-7.862	E1113	BG
42.4	-1.999	-9.005	E1113	BG
49	-2.221	-10.024	E1113	BG
50.9	-1.795	-7.555	E1113	BG
54.5	-2.649	-8.632	E1113	BG
57.6	-1.909	-6.340	E1113	BG
61	-2.777	-10.545	E1113	BG
62.8	-2.112	-9.250	E1113	BG
65.8	0.835	-9.195	E1113	BG
68.8	-2.839	-8.972	E1113	BG
71.8	-2.465	-9.502	E1113	BG
74.8	-3.297	-8.098	E1113	BG
77	-2.383	-11.303	E1113	BG
77.8	-0.576	-6.516	E1113	BG
78.6	-2.835	-8.902	E1113	BG
81.6	-1.786	-5.531	E1113	BG
93.7	-1.833	-10.423	E1117	BG
96.2	-1.860	-10.072	E1117	BG
98.2	-1.646	-9.312	E1117	BG
100.2	-1.425	-9.468	E1117	BG
102.2	-1.667	-9.303	E1117	BG
104.2	-1.238	-7.892	E1117	BG
106.2	-0.656	-9.366	E1117	BG
108.2	-0.850	-7.846	E1117	BG
110.2	0.541	-8.975	E1117	BG
112.2	0.431	-9.247	E1117	BG
114.2	0.953	-12.532	E1117	BG
116.2	1.306	-12.636	E1117	BG
118.2	1.558	-10.412	E1117	BG
120.2	2.290	-8.187	E1117	BG
122.2	1.202	-13.582	E1117	BG
126.2	2.398	-8.586	E1117	BG

128.2	1.800	-11.582	E1117	BG
130.2	0.957	-8.414	E1117	BG
132.2	1.145	-9.756	E1117	BG
134.2	-0.102	-8.450	E1117	BG
136.2	-0.522	-7.418	E1117	BG
140.2	-0.823	-7.764	E1117	BG
142.2	-0.642	-9.909	E1117	BG
144.2	-1.909	-9.312	E1117	BG
146.2	-1.713	-10.000	E1117	BG
148.2	-2.119	-8.620	E1117	BG
150.2	-2.147	-8.173	E1117	BG
163.2	-1.670	-10.572	E1117	BG
165.2	-1.685	-9.448	E1117	BG
167.2	-2.041	-8.162	E1117	BG
179.2	-2.296	-8.136	E1117	BG
181.2	-2.659	-10.414	E1117	BG
183.2	-2.342	-8.732	E1117	BG
185.2	-2.602	-9.399	E1117	BG
187.2	-2.718	-8.490	E1117	BG
189.2	-2.242	-12.276	E1117	BG
191.2	-2.784	-12.703	E1117	BG
195.2	-1.677	-13.886	E1117	BG
196.2	-1.098	-13.397	E1117	BG
187.5	0.818	-15.659	E1115	BG
188.5	-1.371	-9.801	E1115	BG
189	-1.394	-10.011	E1115	BG
190	0.858	-17.068	E1115	BG
191	-1.145	-13.286	E1115	BG
192	-0.290	-15.197	E1115	BG
193	-1.343	-16.495	E1115	BG
223.5	-0.797	-10.520	E1115	BG
224.5	-1.285	-10.678	E1115	BG
228.3	-0.526	-10.345	E1115	BG
230	-0.676	-10.490	E1115	BG
232	-1.866	-10.665	E1115	BG
236.6	-1.727	-11.667	E1115	BG
237.5	-2.419	-12.459	E1115	BG
240.5	-1.694	-12.104	E1115	BG
244	-1.220	-11.877	E1115	BG
248.7	-2.131	-10.770	E1115	BG
252	-1.704	-11.576	E1115	BG
253	-2.439	-11.802	E1115	BG
255	-1.615	-10.906	E1115	BG
256.3	-1.623	-10.029	E1115	BG
257.3	-2.400	-8.929	E1115	BG
258.3	-2.680	-9.208	E1115	BG
259.3	-2.742	-7.750	E1115	BG
299	-2.679	-12.993	E1115	BG
299.1	-2.295	-13.316	E1115	BG
333.9	-0.010	-12.652	E1115	BG

335	-0.497	-14.018	E1115	BG
336	0.031	-11.391	E1115	BG
337	0.698	-11.742	E1115	BG
346	0.801	-11.404	E1115	BG
349	1.068	-11.971	E1115	BG
352	0.295	-12.083	E1115	BG
354	0.352	-12.844	E1115	BG
-148.7	-3.367	-6.307	E1114	ZA
-148.3	-3.580	-6.939	E1114	ZA
-146.9	-2.127	-6.333	E1114	ZA
-141.1	-2.857	-11.450	E1114	ZA
-140.4	-2.138	-10.878	E1114	ZA
-139.8	-5.412	-11.048	E1114	ZA
-139.3	-2.872	-12.462	E1114	ZA
-138.8	-5.706	-12.028	E1114	ZA
-138.4	-5.379	-12.434	E1114	ZA
-137.6	-3.785	-19.169	E1114	ZA
-137	-5.654	-10.772	E1114	ZA
-136.6	-4.322	-11.320	E1114	ZA
-136.2	-7.170	-11.071	E1114	ZA
-135.7	-4.232	-11.517	E1114	ZA
-135.2	-2.623	-10.403	E1114	ZA
-134.6	-3.481	-11.045	E1114	ZA
-134.2	-4.236	-10.412	E1114	ZA
-133.7	-7.561	-10.133	E1114	ZA
-133.2	-7.767	-10.189	E1114	ZA
-132.2	-7.583	-10.390	E1114	ZA
-131.7	-5.719	-10.151	E1114	ZA
-131.2	-7.435	-10.355	E1114	ZA
-130.7	-9.038	-10.485	E1114	ZA
-130.2	-6.440	-9.774	E1114	ZA
-130	-4.953	-9.425	E1114	ZA
-129.2	-2.422	-9.612	E1114	ZA
-128.7	-1.925	-9.480	E1114	ZA
-127.7	-2.759	-9.974	E1114	ZA
-127.2	-3.269	-9.828	E1114	ZA
-126.7	-3.340	-10.927	E1114	ZA
-126.2	-3.046	-9.465	E1114	ZA
-125.5	-3.834	-9.267	E1114	ZA
-125.2	-4.092	-9.367	E1114	ZA
-124.2	-3.819	-9.925	E1114	ZA
-123.6	-2.543	-9.062	E1114	ZA
-123.2	-2.757	-9.969	E1114	ZA
-122.7	-2.398	-9.291	E1114	ZA
-122.2	-4.574	-9.305	E1114	ZA
-121.5	-4.865	-9.407	E1114	ZA
-120.6	-5.077	-9.474	E1114	ZA
-120.4	-5.109	-9.174	E1114	ZA
-119.8	-5.941	-11.068	E1114	ZA
-119	-5.678	-9.360	E1114	ZA

-118	-6.246	-11.126	E1114	ZA
-117.5	-6.068	-9.859	E1114	ZA
-117	-6.121	-9.967	E1114	ZA
-116.5	-3.942	-9.664	E1114	ZA
-116	-4.675	-9.625	E1114	ZA
-115.5	-5.025	-10.013	E1114	ZA
-115	-2.882	-9.631	E1114	ZA
-114.5	-4.498	-10.059	E1114	ZA
-114	-6.288	-9.575	E1114	ZA
-113.5	-6.056	-9.622	E1114	ZA
-113	-5.354	-10.490	E1114	ZA
-112.5	-5.128	-10.298	E1114	ZA
-112	-5.475	-9.698	E1114	ZA
-111.5	-4.591	-9.237	E1114	ZA
-111	-9.394	-9.938	E1114	ZA
-110.5	-5.123	-9.199	E1114	ZA
-110	-4.809	-9.387	E1114	ZA
-109.3	-5.596	-9.113	E1114	ZA
-109	-5.790	-9.108	E1114	ZA
-108.5	-7.269	-9.252	E1114	ZA
-108	-7.248	-9.832	E1114	ZA
-107.5	-5.265	-9.273	E1114	ZA
-107	-7.804	-9.691	E1114	ZA
-106.5	-5.151	-9.331	E1114	ZA
-106	-4.808	-9.636	E1114	ZA
-104.3	-7.427	-9.749	E1114	ZA
-103.9	-7.202	-9.522	E1114	ZA
-103	-4.478	-9.279	E1114	ZA
-101.8	-6.331	-9.207	E1114	ZA
-101.4	-5.420	-9.179	E1114	ZA
-100.7	-4.301	-9.407	E1114	ZA
-100.4	-3.077	-9.243	E1114	ZA
-99.8	-3.666	-8.999	E1114	ZA
-99.3	-3.916	-8.994	E1114	ZA
-97	-0.919	-8.780	E1114	ZA
-94.5	-1.954	-8.748	E1114	ZA
-94	-3.056	-9.068	E1114	ZA
-93.4	-2.649	-8.895	E1114	ZA
-93	-2.638	-8.790	E1114	ZA
-91.5	-4.643	-8.946	E1114	ZA
-91	-4.884	-9.199	E1114	ZA
-89.9	-3.268	-9.084	E1114	ZA
-89	-2.397	-9.037	E1114	ZA
-86.5	-2.555	-9.036	E1114	ZA
-85	-4.602	-9.341	E1114	ZA
-84	-4.637	-9.116	E1114	ZA
-83	-5.218	-12.526	E1114	ZA
-82	-1.338	-9.328	E1114	ZA
-81	-1.075	-10.357	E1114	ZA
-80	-2.972	-8.912	E1114	ZA

-79	-4.416	-10.310	E1114	ZA
-78	-1.604	-17.343	E1114	ZA
-77	-1.579	-9.947	E1114	ZA
-75.4	-5.318	-8.880	E1114	ZA
-75	-3.035	-9.911	E1114	ZA
-73.5	-1.939	-9.729	E1114	ZA
-71.1	-1.899	-9.722	E1114	ZA
-70	-0.029	-9.986	E1114	ZA
-69	0.221	-10.061	E1114	ZA
-67	0.235	-9.041	E1114	ZA
-66	-0.569	-9.198	E1114	ZA
-65	0.138	-8.765	E1114	ZA
-64	-0.677	-9.135	E1114	ZA
-63	1.562	-8.619	E1114	ZA
-62	-4.572	-9.421	E1114	ZA
-61	-3.553	-9.420	E1114	ZA
-60	-2.945	-9.470	E1114	ZA
-58	0.339	-9.331	E1114	ZA
-57	2.346	-8.744	E1114	ZA
-56	1.922	-8.662	E1114	ZA
-55	1.890	-8.943	E1114	ZA
-54	1.866	-9.005	E1114	ZA
-52	2.146	-8.636	E1114	ZA
-50	0.951	-9.205	E1114	ZA
-49	0.904	-9.185	E1114	ZA
-43	-2.162	-8.228	E1114	ZA
-40	-3.130	-9.226	E1114	ZA
-38	-2.239	-11.729	E1114	ZA
-36	-1.891	-15.948	E1114	ZA
-34	-3.352	-12.169	E1114	ZA
-30	-2.834	-13.824	E1114	ZA
-28	-1.077	-14.262	E1114	ZA
-26	0.678	-9.716	E1114	ZA
-24	2.355	-7.637	E1114	ZA
-20	1.103	-7.266	E1114	ZA
-32	-1.982	-14.513	E1114	ZA
-18	-0.851	-8.368	E1114	ZA
-15	-3.784	-8.923	E1114	ZA
-11	-0.455	-9.240	E1114	ZA
-9	-2.313	-9.567	E1114	ZA
-7	0.257	-10.688	E1114	ZA
-69	0.558	-9.769	E1114	ZA
-68	0.058	-9.067	E1114	ZA

SE Taishir

m	d13C	d18O	section	Fm
0	4.545	-6.611	E1325	SG
1	4.316	-8.978	E1325	SG

2	4.407	-6.371	E1325	SG
3	4.861	-9.081	E1325	SG
5	4.544	-10.446	E1325	SG
7	4.063	-9.827	E1325	SG
9	5.017	-1.478	E1325	SG
15	5.021	-0.834	E1325	SG
21	4.264	-8.124	E1325	SG
23	5.485	-5.259	E1325	SG
25	4.987	-6.962	E1325	SG
27	5.208	-7.059	E1325	SG
29	3.436	-7.328	E1325	SG
32	5.364	-1.598	E1325	SG
34	5.820	-7.800	E1325	SG
38	5.854	-2.295	E1325	SG
40	5.190	-5.792	E1325	SG
42	4.428	-2.436	E1325	SG
47	5.378	-5.126	E1325	SG
49	4.550	-4.794	E1325	SG
51	5.088	-1.582	E1325	SG
53	5.642	-2.761	E1325	SG
55	3.435	-3.701	E1325	SG
57	4.707	-6.600	E1325	SG
59	4.404	-2.441	E1325	SG
61	5.175	-4.811	E1325	SG
63	5.298	-7.889	E1325	SG
65	4.605	-7.264	E1325	SG
67	1.546	-4.857	E1325	SG
72	1.117	-3.719	E1325	SG
74	1.070	-4.382	E1325	SG
84	-1.291	-2.742	E1325	SG
86	-1.697	-1.459	E1325	SG
88	-1.533	-2.320	E1325	SG
90	-1.604	-1.951	E1325	SG
92	-1.631	-1.107	E1325	SG
94	-1.026	-6.165	E1325	SG
96	-1.315	-6.336	E1325	SG
98	-1.610	-1.808	E1325	SG
100	-1.356	-1.314	E1325	SG
102	-0.685	-0.685	E1325	SG
104	-1.417	-1.088	E1325	SG
106	-1.117	-1.099	E1325	SG
109	-1.141	-3.989	E1325	SG
111	-1.166	-1.435	E1325	SG
113	-2.197	-2.648	E1325	SG
115	-1.254	-4.721	E1325	SG
117	-1.441	-1.293	E1325	SG
119	-1.583	-1.340	E1325	SG
121	-1.363	-1.713	E1325	SG
123	-1.654	-9.730	E1325	SG
125	-1.078	-8.641	E1325	SG

128	-1.399	-9.035	E1325	SG
130	-1.052	-9.307	E1325	SG
132	-0.547	-4.721	E1325	SG
134	-1.444	-13.345	E1325	SG
136	-0.766	-7.187	E1325	SG
138	-1.335	-16.239	E1325	SG
140	-1.201	-10.360	E1325	SG
142	-1.568	-10.506	E1325	SG
144	-1.358	-14.438	E1325	SG
146	-1.389	-12.535	E1325	SG
150	-1.796	-11.429	E1325	SG
152	-1.418	-13.179	E1325	SG
154	-1.674	-14.780	E1325	SG
159	-2.229	-15.993	E1325	SG
161	-0.926	-12.396	E1325	SG
163	-1.183	-9.833	E1325	SG
165	-1.968	-14.174	E1325	SG
167	-1.499	-15.685	E1325	SG
169	-1.322	-14.648	E1325	SG
171	-0.862	-10.820	E1325	SG
173	-1.538	-12.933	E1325	SG
175	-1.714	-10.276	E1325	SG
177	-0.999	-13.418	E1325	SG

KTN

m corrected	d13C	d18O	section	Fm
48.5	-3.200	-12.104	E1216	ZA
49	-3.002	-11.828	E1216	ZA
49.5	-0.506	-11.160	E1216	ZA
50	-3.294	-10.829	E1216	ZA
50.5	-3.818	-14.311	E1216	ZA
52.5	-3.160	-12.319	E1216	ZA
53	-5.758	-20.181	E1216	ZA
54	-3.949	-13.216	E1216	ZA
55	-2.593	-11.091	E1216	ZA
57	-0.507	-11.187	E1216	ZA
58	-0.349	-9.887	E1216	ZA
59	-0.564	-9.897	E1216	ZA
60	-0.641	-10.977	E1216	ZA
60.5	-0.622	-11.113	E1216	ZA
61	-0.496	-11.501	E1216	ZA
61.5	1.705	-9.509	E1216	ZA
62	-2.146	-12.926	E1216	ZA
62.5	-2.143	-11.797	E1216	ZA
63	-1.539	-10.348	E1216	ZA
64	-2.085	-12.045	E1216	ZA
65	-3.477	-12.108	E1216	ZA
66	-3.450	-11.728	E1216	ZA

67	-4.673	-11.413	E1216	ZA
68	-6.842	-15.220	E1216	ZA
69	-6.118	-12.185	E1216	ZA
69.5	-6.416	-12.412	E1216	ZA
70	-7.496	-12.493	E1216	ZA
71	-5.691	-11.487	E1216	ZA
72	-5.741	-11.375	E1216	ZA
73	-5.964	-11.597	E1216	ZA
74	-5.995	-11.752	E1216	ZA
75	-5.266	-11.743	E1216	ZA
76	-5.215	-10.768	E1216	ZA
77	-4.321	-11.143	E1216	ZA
78	-4.047	-10.594	E1216	ZA
79	-4.473	-10.966	E1216	ZA
80	-3.201	-10.705	E1216	ZA
81	-2.448	-9.932	E1216	ZA
82	-3.084	-10.552	E1216	ZA
83	-3.368	-11.376	E1216	ZA
84	-3.407	-11.077	E1216	ZA
85	-3.180	-10.539	E1216	ZA
86	-3.479	-10.068	E1216	ZA
87	-3.505	-9.878	E1216	ZA
90	-1.935	-9.639	E1216	ZA
92	-2.673	-9.473	E1216	ZA
93	-2.945	-10.776	E1216	ZA
94	-2.889	-10.052	E1216	ZA
95	-3.423	-9.413	E1216	ZA
96	-3.796	-9.843	E1216	ZA
97	-4.748	-9.537	E1216	ZA
98	-4.798	-10.237	E1216	ZA
99	-5.534	-9.989	E1216	ZA
102	-2.003	-9.447	E1216	ZA
102.5	-2.921	-9.716	E1216	ZA
103	-2.271	-10.342	E1216	ZA
104	-3.022	-10.546	E1216	ZA
104.5	-4.597	-10.160	E1216	ZA
105	-4.332	-11.389	E1216	ZA
106	-4.028	-12.363	E1216	ZA
107	-5.085	-13.302	E1216	ZA
108	-2.738	-13.996	E1216	ZA
109	-6.488	-14.525	E1216	ZA
110	-5.778	-13.572	E1216	ZA
113	-5.902	-20.883	E1216	ZA
114	-6.392	-24.228	E1216	ZA
120	-5.456	-15.440	E1216	ZA
121	-6.672	-12.222	E1216	ZA
122	-5.432	-11.090	E1216	ZA
123	-3.423	-10.392	E1216	ZA
124	-5.308	-12.331	E1216	ZA
125	-4.889	-10.928	E1216	ZA

126	-5.033	-12.021	E1216	ZA
127	-5.735	-14.133	E1216	ZA
129	-5.195	-14.160	E1216	ZA
129.2	-3.540	-11.952	E1216	ZA
135	-4.037	-16.521	E1216	ZA
136	-3.573	-16.418	E1216	ZA
137	-4.230	-16.049	E1216	ZA
138	-4.215	-16.477	E1216	ZA
139	-4.241	-15.678	E1216	ZA
140	-4.271	-15.025	E1216	ZA
143	-3.427	-13.038	E1216	ZA
144	-3.541	-11.734	E1216	ZA
145	-3.831	-17.931	E1216	ZA
146	-3.913	-17.935	E1216	ZA
147	-3.313	-16.445	E1216	ZA
149	-3.765	-17.458	E1216	ZA
150	-2.311	-15.401	E1216	ZA
151	-1.005	-14.170	E1216	ZA
152	-1.812	-18.707	E1216	ZA
153	-1.053	-17.187	E1216	ZA
154	-0.323	-17.036	E1216	ZA
155	-0.801	-15.408	E1216	ZA
156	-1.426	-12.654	E1216	ZA
157	-3.157	-16.944	E1216	ZA
158	-1.402	-11.144	E1216	ZA
159	-1.915	-15.635	E1216	ZA
160	-0.772	-16.750	E1216	ZA
161	-0.943	-16.743	E1216	ZA
162	-0.428	-19.722	E1216	ZA
163	-1.236	-19.938	E1216	ZA
164	-2.682	-29.279	E1216	ZA
164	-0.106	-23.629	E1216	ZA
166	-3.440	-24.957	E1216	ZA
166	-2.757	-24.208	E1216	ZA
167	-2.836	-23.829	E1216	ZA
172	-2.976	-26.814	E1216	ZA
174	-0.896	-17.224	E1216	ZA
176	-2.785	-24.569	E1216	ZA
178	-0.048	-23.853	E1216	ZA
188	0.070	-12.123	E1215	BG
190.8	-0.202	-10.567	E1215	BG
194.5	-0.858	-9.561	E1215	BG
195	-0.428	-8.559	E1215	BG
196	-0.581	-10.810	E1215	BG
197	-0.680	-8.093	E1215	BG
198	-1.443	-11.285	E1215	BG
199	-2.578	-11.767	E1215	BG
200	-2.303	-11.490	E1215	BG
201	-2.213	-8.871	E1215	BG
202	-2.295	-11.707	E1215	BG

203	-1.214	-10.136	E1215	BG
204	-1.500	-9.238	E1215	BG
205	-2.516	-8.796	E1215	BG
206	-2.328	-11.374	E1215	BG
207.5	-2.347	-11.912	E1215	BG
208	-2.517	-9.623	E1215	BG
209	-2.491	-11.165	E1215	BG
210	-2.411	-9.707	E1215	BG
210.5	-2.819	-9.037	E1215	BG
211.5	-2.793	-11.811	E1215	BG
212	-2.541	-11.092	E1215	BG
212.5	-2.830	-9.568	E1215	BG
213.2	-2.877	-10.235	E1215	BG
214	-2.052	-11.776	E1215	BG
214.5	-2.274	-9.366	E1215	BG
215	-2.507	-10.434	E1215	BG
215.5	-1.743	-10.864	E1215	BG
216	-2.302	-10.664	E1215	BG
216.5	-2.965	-9.588	E1215	BG
217	-3.037	-9.734	E1215	BG
218	-1.553	-8.966	E1215	BG
218.5	-2.445	-12.967	E1215	BG
219	-2.588	-12.086	E1215	BG
219.1	-2.351	-10.994	E1215	BG
220	-2.298	-9.811	E1215	BG
221	-2.402	-13.138	E1215	BG
222	-2.782	-9.747	E1215	BG
223	-2.817	-8.838	E1215	BG
224	-2.633	-8.413	E1215	BG
231	-1.513	-8.533	E1215	BG
232	0.287	-8.971	E1215	BG
233	-0.185	-7.422	E1215	BG
234	0.863	-9.071	E1215	BG
235	1.712	-8.569	E1215	BG
236	0.314	-9.208	E1215	BG
238	0.933	-8.363	E1215	BG
239	-2.719	-8.870	E1215	BG
240	-3.919	-8.986	E1215	BG
241	-4.174	-9.509	E1215	BG
242	-3.812	-9.019	E1215	BG
243	-2.674	-9.942	E1215	BG
244	-4.045	-12.316	E1215	BG
248	-3.371	-11.753	E1215	BG
249	-2.786	-11.484	E1215	BG
251	-1.031	-12.191	E1215	BG
252	-0.619	-11.199	E1215	BG
253	-0.787	-10.982	E1215	BG
254	-1.107	-10.369	E1215	BG
255	-0.492	-10.913	E1215	BG
256	-0.677	-11.934	E1215	BG

257	-1.479	-11.094	E1215	BG
278	-0.633	-13.307	E1215	BG
279	-1.782	-13.132	E1215	BG
280	-2.018	-10.340	E1215	BG
281	-2.206	-11.194	E1215	BG
283	-2.518	-9.018	E1215	BG
284	-2.510	-10.442	E1215	BG
285	-0.686	-9.412	E1215	BG
286	-1.140	-9.456	E1215	BG
288	-1.378	-10.150	E1215	BG
289	-1.639	-9.140	E1215	BG
290	-1.467	-8.510	E1215	BG
291	1.070	-11.341	E1215	BG
292	1.677	-10.146	E1215	BG
293	1.356	-8.798	E1215	BG
294	1.348	-8.179	E1215	BG
326	-2.621	-13.865	E1215	BG
336	-2.418	-11.033	E1215	BG
347	-2.261	-13.276	E1215	BG

SE Bayan Gorge

m corrected	d13C	d18O	section	Fm
0	1.577	-8.094	E1123	ZA
1	1.991	-8.913	E1123	ZA
1.5	1.847	-7.944	E1123	ZA
4	1.564	-8.755	E1123	ZA
5	1.253	-8.571	E1123	ZA
6	1.350	-7.831	E1123	ZA
7	1.299	-8.414	E1123	ZA
8	0.991	-7.803	E1123	ZA
9	1.346	-7.381	E1123	ZA
10	1.178	-7.876	E1123	ZA
11	1.161	-7.810	E1123	ZA
12	1.706	-7.557	E1123	ZA
14	1.449	-7.611	E1123	ZA
15	-2.112	-8.223	E1123	ZA
16	1.099	-9.631	E1123	ZA
17	1.077	-7.902	E1123	ZA
18	1.956	-7.758	E1123	ZA
19	1.322	-7.910	E1123	ZA
20	0.153	-8.105	E1123	ZA
21	-1.591	-8.084	E1123	ZA
22	-1.405	-7.820	E1123	ZA
24	-1.042	-8.271	E1123	ZA
25	-0.200	-7.380	E1123	ZA
27	0.627	-8.184	E1123	ZA
29	0.479	-8.085	E1123	ZA
31	0.829	-7.700	E1123	ZA

33	0.259	-7.742	E1123	ZA
35	1.663	-7.625	E1123	ZA
37	0.354	-10.299	E1123	ZA
39	1.154	-7.971	E1123	ZA
41	-0.075	-8.766	E1123	ZA
43	-0.091	-8.306	E1123	ZA
45	0.542	-8.298	E1123	ZA
47	0.843	-8.275	E1123	ZA
49	-0.037	-8.361	E1123	ZA
51	-0.113	-8.019	E1123	ZA
53	-0.741	-8.574	E1123	ZA
55	-0.612	-8.047	E1123	ZA
57	-0.887	-8.582	E1123	ZA
59	-0.713	-8.082	E1123	ZA
61	-1.876	-9.376	E1123	ZA
63	-0.915	-9.117	E1123	ZA
65	-1.226	-9.283	E1123	ZA
67	-0.717	-9.000	E1123	ZA
69	-0.684	-8.826	E1123	ZA
71	-1.380	-9.169	E1123	ZA
73	-1.044	-8.457	E1123	ZA
75	-0.981	-8.658	E1123	ZA
77	-0.879	-8.798	E1123	ZA
79	-0.650	-8.675	E1123	ZA
81	-0.869	-8.848	E1123	ZA
83	-2.610	-8.341	E1123	ZA
86	-4.518	-8.528	E1123	ZA
88	-3.576	-8.934	E1123	ZA
90	-3.997	-7.853	E1123	ZA
92	-4.070	-8.325	E1123	ZA
94	-4.779	-8.024	E1123	ZA
96	-4.943	-8.366	E1123	ZA
97	-4.193	-7.117	E1123	ZA
99	-3.646	-7.713	E1123	ZA
101	-4.095	-8.064	E1123	ZA
103	-4.072	-8.899	E1123	ZA
105	-4.552	-9.694	E1123	ZA
106	-4.807	-8.285	E1123	ZA
149.6	-3.795	-11.775	E1123	BG
151	-1.310	-11.079	E1123	BG
153	-1.802	-11.636	E1123	BG
154	-1.732	-11.747	E1123	BG
157	-0.545	-11.585	E1123	BG
158	-3.085	-11.680	E1123	BG
164	-2.069	-11.657	E1123	BG
167	-2.707	-11.640	E1123	BG
168	-1.911	-11.550	E1123	BG
170	-2.148	-11.402	E1123	BG
171	-2.070	-10.943	E1123	BG
183	-2.449	-11.174	E1123	BG

202	-2.606	-11.041	E1123	BG
209	-2.759	-10.251	E1123	BG
211	-3.058	-9.515	E1123	BG
213	-3.031	-9.783	E1123	BG
221	-1.268	-8.096	E1123	BG
223	-1.989	-10.447	E1123	BG
225	-2.279	-8.037	E1123	BG
229	-3.355	-8.245	E1123	BG
233	-3.306	-8.598	E1123	BG
276	1.156	-12.174	E1123	BG
278	0.340	-11.759	E1123	BG
280	0.704	-11.550	E1123	BG
285	1.802	-12.926	E1123	BG
287	0.890	-12.611	E1123	BG
290	-0.063	-12.083	E1123	BG
292	0.225	-12.402	E1123	BG
293	0.156	-12.161	E1123	BG
295	-0.086	-12.096	E1123	BG
300	3.052	-11.840	E1123	BG
306.5	3.249	-11.576	E1123	BG
308	2.584	-11.515	E1123	BG
310	1.676	-10.207	E1123	BG
313	2.101	-11.017	E1123	BG
314	1.636	-8.323	E1123	BG
315	0.744	-10.365	E1123	BG
316	1.714	-7.645	E1123	BG
317	1.741	-9.678	E1123	BG
318	2.240	-8.365	E1123	BG
319	2.340	-7.530	E1123	BG
320	2.208	-7.491	E1123	BG
321	0.758	-8.835	E1123	BG
322	0.621	-7.979	E1123	BG
323	-0.437	-7.379	E1123	BG
324	-1.203	-8.358	E1123	BG
325	0.206	-6.881	E1123	BG
326	0.535	-7.241	E1123	BG
327	0.304	-7.350	E1123	BG
328	1.043	-7.919	E1123	BG
329	1.205	-7.585	E1123	BG
330	1.013	-8.448	E1123	BG
331	0.620	-7.474	E1123	BG
333	0.205	-7.855	E1123	BG
334	1.210	-7.340	E1123	BG
335	0.933	-8.111	E1123	BG
336	0.142	-8.782	E1123	BG
337	0.700	-7.648	E1123	BG
338	-0.068	-7.728	E1123	BG
339	-0.451	-7.447	E1123	BG
340	-0.732	-7.379	E1123	BG
341	-0.635	-7.283	E1123	BG

342	-0.722	-7.350	E1123	BG
343	-1.184	-7.746	E1123	BG
347	-2.607	-7.907	E1123	BG
348	-2.488	-7.986	E1123	BG
349	-2.187	-6.871	E1123	BG
350	-2.554	-7.762	E1123	BG
351	-2.586	-8.017	E1123	BG
352	-2.733	-7.781	E1123	BG
353	-2.642	-7.384	E1123	BG
354	-2.177	-7.223	E1123	BG
355	-2.359	-7.880	E1123	BG
356	-2.327	-7.465	E1123	BG
357	-2.520	-7.109	E1123	BG
358	-2.429	-7.060	E1123	BG
359	-2.362	-7.182	E1123	BG
360	-2.394	-7.229	E1123	BG
361	-2.340	-7.250	E1123	BG
362	-2.532	-7.456	E1123	BG
363	-2.848	-7.422	E1123	BG
364	-2.658	-8.137	E1123	BG
365	-2.959	-7.211	E1123	BG
366	-2.745	-7.656	E1123	BG
367	-2.742	-7.589	E1123	BG
369	-3.696	-12.545	E1123	BG
415	-1.152	-13.008	E1123	BG
416	-1.201	-13.037	E1123	BG
416	-1.043	-13.419	E1123	BG
418	-0.629	-10.570	E1123	BG
418.5	-1.600	-12.790	E1123	BG
423	-1.506	-13.240	E1123	BG
424	-0.939	-11.849	E1123	BG
425	-0.992	-11.907	E1123	BG
425	-1.053	-9.689	E1123	BG
426	-1.686	-12.220	E1123	BG
427	-1.834	-12.066	E1123	BG
428	-2.064	-12.529	E1123	BG
429	-1.676	-12.637	E1123	BG
430	0.847	-12.625	E1123	BG
431	0.679	-12.821	E1123	BG
432	2.211	-1.819	E1123	BG
432	1.139	-12.470	E1123	BG
433	-1.516	-12.586	E1123	BG
434	-1.568	-12.600	E1123	BG
434	-0.951	-12.296	E1123	BG
435	-1.813	-11.794	E1123	BG
436	-1.524	-12.545	E1123	BG
438	-1.391	-12.261	E1123	BG
439	-0.420	-12.312	E1123	BG
441	-1.436	-11.883	E1123	BG
442	-1.452	-11.820	E1123	BG

443	-0.255	-12.090	E1123	BG
444	1.683	-9.349	E1123	BG
445	2.278	-10.331	E1123	BG
446	2.954	-8.988	E1123	BG
447	0.677	-8.437	E1123	BG
448	0.614	-8.438	E1123	BG
448	-0.661	-9.007	E1123	BG
449	-1.779	-9.959	E1123	BG
450	-0.232	-10.302	E1123	BG
451	-0.477	-10.637	E1123	BG
452	-0.525	-10.683	E1123	BG
452	-0.664	-10.261	E1123	BG
453	-1.028	-11.585	E1123	BG
454	-0.366	-10.480	E1123	BG
455	-1.928	-12.355	E1123	BG
456	-2.049	-12.962	E1123	BG
457	-1.674	-12.974	E1123	BG
458	-1.950	-13.103	E1123	BG
459	-1.845	-14.134	E1123	BG
460	-1.915	-14.183	E1123	BG
460	-3.084	-12.491	E1123	BG
461	-3.374	-13.006	E1123	BG
462	-2.130	-14.455	E1123	BG
463	-3.926	-14.719	E1123	BG

Bayan Gorge

m corrected	d13C	d18O	section	Fm
-28.8	-4.230	-10.179	F1120	ZA
-27.3	-4.378	-10.244	F1120	ZA
-26.3	-5.210	-8.953	F1120	ZA
-25.9	-4.902	-8.916	F1120	ZA
-24.9	-5.023	-8.554	F1120	ZA
-23.9	-4.754	-8.972	F1120	ZA
-22.9	-4.811	-8.529	F1120	ZA
-21.9	-4.925	-8.245	F1120	ZA
-20.4	-6.011	-10.100	F1120	ZA
-19.5	-5.489	-9.884	F1120	ZA
-18.4	-4.644	-8.258	F1120	ZA
-17.3	-4.020	-13.408	F1120	ZA
-16.7	-4.389	-8.056	F1120	ZA
-15.4	-4.174	-8.022	F1120	ZA
-14.4	-4.386	-8.744	F1120	ZA
-13.4	-6.394	-9.082	F1120	ZA
-12.3	-7.948	-9.738	F1120	ZA
-11.3	-8.177	-9.436	F1120	ZA
-10	-7.426	-9.872	F1120	ZA
-8.9	-7.371	-8.788	F1120	ZA
-7.9	-5.244	-11.749	F1120	ZA

-6.9	-5.209	-9.841	F1120	ZA
-5.9	-5.538	-8.876	F1120	ZA
-3.9	-6.054	-10.319	F1120	ZA
-2.9	-5.122	-9.236	F1120	ZA
-1.7	-4.963	-9.913	F1120	ZA
-0.7	-4.939	-9.756	F1120	ZA
0	-4.768	-7.530	F1120	ZA
0.2	-0.362	-10.208	F1120	BG
0.4	-2.911	-10.481	F1120	BG
0.6	-3.129	-11.354	F1120	BG
0.9	-3.321	-11.742	F1120	BG
1.4	-3.901	-9.784	F1120	BG
2.5	-3.925	-12.647	F1120	BG
3.5	-4.058	-11.265	F1120	BG
5.1	-3.821	-11.912	F1120	BG
6.1	-4.059	-12.034	F1120	BG
7.4	-3.740	-11.524	F1120	BG
7.7	-3.002	-10.569	F1120	BG
13.8	1.128	-10.688	F1120	BG
14.2	2.615	-9.549	F1120	BG
15.2	1.085	-10.784	F1120	BG
15.9	-0.348	-10.496	F1120	BG
17.1	3.571	-10.999	F1120	BG
17.8	2.349	-10.905	F1120	BG
19.4	3.643	-11.098	F1120	BG
20.1	2.642	-10.625	F1120	BG
21.1	2.734	-10.753	F1120	BG
23.1	3.005	-10.585	F1120	BG
24.1	2.509	-10.467	F1120	BG
25.1	1.803	-10.758	F1120	BG
26.1	1.844	-10.749	F1120	BG
27.1	1.045	-10.831	F1120	BG
28.1	1.360	-10.752	F1120	BG
29.1	1.262	-10.692	F1120	BG
30.1	0.851	-10.459	F1120	BG
31.1	1.353	-10.582	F1120	BG
33.1	1.902	-10.294	F1120	BG
34.1	0.348	-10.329	F1120	BG
35.1	-1.381	-10.232	F1120	BG
36.1	-0.678	-10.329	F1120	BG
39.1	-1.127	-10.190	F1120	BG
40.1	-0.030	-10.268	F1120	BG
42.1	0.398	-10.261	F1120	BG
43.1	0.305	-9.986	F1120	BG
45.1	-0.430	-10.294	F1120	BG
46.1	-0.332	-9.917	F1120	BG
48.1	-0.689	-9.690	F1120	BG
48.6	-1.527	-10.352	F1120	BG
50.1	-1.710	-10.369	F1120	BG
51.1	-1.639	-9.184	F1120	BG

53.1	1.006	-10.536	F1120	BG
54.1	0.296	-10.230	F1120	BG
55.1	0.183	-10.153	F1120	BG
56.1	-1.514	-9.553	F1120	BG
57.1	-0.471	-9.648	F1120	BG
58.1	-1.967	-9.612	F1120	BG
59.1	-4.101	-9.790	F1120	BG
61.1	-3.636	-10.460	F1120	BG
63.1	-2.359	-9.669	F1120	BG
69.1	-3.326	-9.688	F1120	BG
71.1	-3.251	-9.554	F1120	BG
72.1	-2.752	-9.353	F1120	BG
73.1	-2.943	-9.639	F1120	BG
74.6	-2.950	-9.636	F1120	BG
77.3	-2.745	-8.531	F1120	BG
78.1	-2.685	-9.134	F1120	BG
81.1	-3.139	-8.950	F1120	BG
82.1	-2.724	-8.844	F1120	BG
84.1	-2.942	-9.172	F1120	BG
87.1	-2.742	-8.649	F1120	BG
88.1	-2.537	-8.233	F1120	BG
89.1	-2.389	-7.893	F1120	BG
90.1	-2.702	-8.274	F1120	BG
91.1	-2.673	-8.097	F1120	BG
92.1	-2.444	-8.272	F1120	BG
93.4	-2.050	-8.610	F1120	BG
94.3	-1.631	-7.516	F1120	BG
96.1	-2.420	-7.704	F1120	BG
97.1	-2.633	-7.736	F1120	BG
98.1	-2.649	-9.047	F1120	BG
99.1	-3.489	-9.018	F1120	BG
100.1	-3.422	-8.174	F1120	BG
101.1	-3.023	-7.623	F1120	BG
102.1	-3.569	-8.140	F1120	BG
103.1	-3.319	-9.315	F1120	BG
113.2	-3.434	-8.126	F1121	BG
114.1	-1.939	-8.502	F1121	BG
115.1	-1.889	-8.385	F1121	BG
116.1	-2.612	-10.158	F1121	BG
117.1	-2.441	-8.892	F1121	BG
118.1	-3.796	-10.123	F1121	BG
119.1	-4.708	-10.452	F1121	BG
119.6	-5.687	-10.561	F1121	BG
120.1	-4.021	-10.935	F1121	BG
121.1	-3.035	-10.609	F1121	BG
121.4	-2.671	-10.590	F1121	BG
121.6	-3.224	-10.432	F1121	BG
121.9	-3.568	-10.710	F1121	BG
122.1	-6.279	-9.447	F1121	BG
122.3	-4.424	-10.460	F1121	BG

122.5	-3.421	-10.500	F1121	BG
122.7	-3.313	-10.222	F1121	BG
123.1	-3.430	-10.229	F1121	BG
123.3	-3.024	-10.528	F1121	BG
123.5	-4.222	-9.926	F1121	BG
123.7	-3.895	-10.260	F1121	BG
123.9	-1.347	-8.394	F1121	BG
124.1	-1.052	-8.267	F1121	BG
124.3	0.080	-9.856	F1121	BG
124.5	-1.971	-8.271	F1121	BG
124.7	-0.296	-7.331	F1121	BG
124.9	-0.833	-9.637	F1121	BG
125.1	-1.448	-10.360	F1121	BG
125.3	-1.578	-9.155	F1121	BG
125.5	-0.183	-7.926	F1121	BG
125.7	-0.515	-8.849	F1121	BG
125.9	-0.786	-8.365	F1121	BG
126.1	-1.403	-9.044	F1121	BG
126.3	-0.196	-9.654	F1121	BG
126.5	-0.932	-8.570	F1121	BG
126.7	-1.603	-9.348	F1121	BG
126.9	-1.114	-9.224	F1121	BG
127.1	-1.199	-7.878	F1121	BG
127.3	-1.346	-9.265	F1121	BG
127.5	1.585	-7.200	F1121	BG
127.7	1.035	-9.035	F1121	BG
127.9	-0.358	-9.878	F1121	BG
128.1	-0.939	-8.152	F1121	BG
128.3	-0.291	-7.821	F1121	BG
128.5	-0.600	-10.512	F1121	BG
140.6	-0.600	-10.951	F1121	BG
141.6	-2.003	-12.458	F1121	BG
142.6	-1.231	-10.678	F1121	BG
143.6	-1.133	-13.259	F1121	BG
178.6	-0.609	-10.612	F1121	BG
180.1	-1.095	-11.842	F1121	BG
192.1	-2.398	-10.292	F1121	BG
192.6	-3.380	-12.019	F1121	BG
194.1	-2.353	-11.731	F1121	BG
195.1	-1.907	-11.652	F1121	BG
196.1	-2.168	-12.142	F1121	BG
197.1	-1.786	-12.611	F1121	BG
198.1	-1.713	-11.856	F1121	BG
199.1	-1.266	-8.767	F1121	BG
200.1	-1.406	-10.036	F1121	BG
201.1	-1.359	-11.150	F1121	BG
202.1	-1.331	-12.122	F1121	BG
203.1	-1.517	-11.603	F1121	BG
204.1	-1.347	-10.409	F1121	BG
205.1	-2.228	-12.679	F1121	BG

206.1	-2.327	-11.346	F1121	BG
207.1	-1.445	-10.399	F1121	BG
208.1	-2.330	-11.153	F1121	BG
209.1	-1.782	-9.389	F1121	BG
210.1	-2.313	-12.161	F1121	BG
212.1	-2.376	-12.537	F1121	BG
213.1	-2.051	-10.908	F1121	BG
214.1	-2.423	-11.018	F1121	BG
216.1	-2.310	-9.437	F1121	BG
217.1	-2.230	-9.447	F1121	BG
219.1	-2.316	-9.233	F1121	BG
221.1	-1.381	-7.890	F1121	BG
222.1	-1.500	-5.866	F1121	BG
223.1	-0.828	-6.683	F1121	BG
224.1	-1.345	-8.256	F1121	BG
225.1	-0.835	-9.309	F1121	BG
226.1	-0.680	-8.819	F1121	BG
227.1	-1.785	-7.743	F1121	BG
228.1	-2.102	-7.479	F1121	BG
229.1	-2.044	-8.251	F1121	BG
230.1	-2.137	-9.923	F1121	BG
231.1	-1.649	-9.393	F1121	BG
233.1	-1.445	-9.174	F1121	BG
234.1	-1.475	-8.922	F1121	BG
235.1	-1.429	-9.300	F1121	BG
236.1	-1.871	-7.974	F1121	BG
238.1	-1.934	-7.949	F1121	BG
240.1	-1.981	-8.679	F1121	BG
242.1	-2.842	-9.674	F1121	BG
244.1	-3.247	-12.001	F1121	BG
246.1	-3.924	-12.043	F1121	BG
248.1	-4.541	-13.083	F1121	BG
250.1	-4.092	-12.842	F1121	BG
252.1	-3.867	-12.001	F1121	BG
254.1	-4.346	-13.553	F1121	BG
255.1	-3.945	-12.532	F1121	BG
299.7	-0.797	-12.077	F1121	BG
300.4	-0.633	-11.318	F1121	BG
301.7	-1.300	-9.387	F1121	BG
303.4	-1.995	-9.747	F1121	BG
303.9	-1.623	-10.066	F1121	BG
304.6	-1.145	-9.511	F1121	BG
306.6	-1.558	-11.169	F1121	BG
308.1	-1.428	-10.794	F1121	BG
310.1	-2.326	-10.240	F1121	BG
312.1	-2.218	-10.221	F1121	BG
314.1	1.174	-10.271	F1121	BG
315.1	2.461	-9.577	F1121	BG
316.1	2.351	-8.150	F1121	BG
317.6	0.385	-7.240	F1121	BG

319.1	-0.437	-8.092	F1121	BG
320.1	-1.762	-11.895	F1121	BG
321.1	-3.311	-9.223	F1121	BG
322.1	-2.187	-8.381	F1121	BG
323.1	-3.797	-11.110	F1121	BG
325.1	-2.738	-13.994	F1121	BG
593	-0.149	-16.036	E1130	BG
596	-0.311	-15.418	E1130	BG
596.5	0.038	-13.931	E1130	BG
597	-0.076	-14.994	E1130	BG
601	-0.727	-13.902	E1130	BG
611	0.427	-14.952	E1130	BG
612	0.164	-15.994	E1130	BG
617	0.483	-15.256	E1130	BG
618	0.853	-14.860	E1130	BG
622	-1.126	-15.890	E1130	BG
645	1.807	-14.163	E1130	BG
592	-0.055	-15.649	E1130	BG
705.1	4.130	-10.820	D706	BG
706	4.310	-10.660	D706	BG
707.4	4.200	-10.860	D706	BG
708	4.170	-11.580	D706	BG
710	4.240	-10.650	D706	BG
711	4.340	-10.630	D706	BG
712	4.250	-11.400	D706	BG
713	4.280	-10.610	D706	BG
714.5	4.030	-9.940	D706	BG
715	4.340	-9.830	D706	BG
716	4.420	-9.950	D706	BG
717	4.610	-10.020	D706	BG
718	4.210	-11.850	D706	BG
719	4.190	-9.520	D706	BG
720	4.220	-9.870	D706	BG
721.3	4.220	-11.310	D706	BG
722	4.270	-11.370	D706	BG
723.2	4.200	-13.940	D706	BG
724	3.930	-14.440	D706	BG
725	3.690	-15.620	D706	BG
730.2	5.140	-12.920	D706	BG
731	5.020	-13.780	D706	BG
733	4.410	-14.750	D706	BG
734	4.320	-12.360	D706	BG
735	4.330	-12.560	D706	BG
736	4.870	-12.580	D706	BG
737	4.080	-12.460	D706	BG
738	3.840	-12.300	D706	BG
739	5.120	-11.850	D706	BG
741	3.940	-12.060	D706	BG
742.2	4.050	-12.060	D706	BG
743	4.080	-10.940	D706	BG

744.2	3.740	-12.210	D706	BG
745	4.110	-11.280	D706	BG
746	4.170	-11.690	D706	BG
747	4.230	-11.170	D706	BG
748	4.090	-11.960	D706	BG
749.5	3.810	-11.880	D706	BG
750.5	4.210	-8.850	D706	BG
751.8	4.180	-10.760	D706	BG
753	4.400	-10.900	D706	BG
754	4.740	-9.590	D706	BG
755	4.240	-11.640	D706	BG
756.5	3.940	-11.270	D706	BG
758	3.930	-11.500	D706	BG
759	4.330	-10.230	D706	BG
760.5	4.350	-9.030	D706	BG
763	4.210	-10.010	D706	BG
764.5	4.340	-11.730	D706	BG
766	4.620	-9.100	D706	BG
767	4.250	-9.980	D706	BG
-202	1.402	-8.614	E1129	ZA
-201.5	1.735	-9.421	E1129	ZA
-201	-0.022	-9.263	E1129	ZA
-200.5	1.650	-8.778	E1129	ZA
-200.4	-0.622	-13.444	E1129	ZA
-200	1.265	-8.909	E1129	ZA
-199.5	0.695	-9.556	E1129	ZA
-199	1.384	-16.411	E1129	ZA
-198.5	0.725	-10.979	E1129	ZA
-198	1.144	-9.317	E1129	ZA
-197.5	1.306	-8.957	E1129	ZA
-197	1.126	-8.317	E1129	ZA
-196.5	0.806	-9.003	E1129	ZA
-196	0.834	-9.845	E1129	ZA
-195.5	0.875	-8.677	E1129	ZA
-195	-0.024	-9.370	E1129	ZA
-194.5	-1.049	-8.549	E1129	ZA
-194	-0.767	-8.567	E1129	ZA
-193.5	1.180	-7.640	E1129	ZA
-193	0.706	-8.360	E1129	ZA
-192.5	0.915	-8.119	E1129	ZA
-192	0.063	-8.337	E1129	ZA
-191.5	-0.523	-9.383	E1129	ZA
-191	0.008	-9.346	E1129	ZA
-190.5	-2.128	-7.278	E1129	ZA
-190	0.254	-8.371	E1129	ZA
-189.5	0.017	-9.744	E1129	ZA
-189	-0.709	-8.724	E1129	ZA
-188.5	-0.164	-9.548	E1129	ZA
-188	0.488	-8.396	E1129	ZA
-187.5	-0.144	-8.643	E1129	ZA

-187	0.083	-9.414	E1129	ZA
-186.5	0.742	-9.525	E1129	ZA
-185	-0.773	-8.230	E1129	ZA
-184.5	-0.823	-7.658	E1129	ZA
-184	-0.564	-9.403	E1129	ZA
-183.5	-0.627	-9.882	E1129	ZA
-183	0.344	-9.806	E1129	ZA
-182.5	-2.091	-8.557	E1129	ZA
-182	-0.832	-9.300	E1129	ZA
-181.5	-0.867	-8.352	E1129	ZA
-181	-0.911	-9.220	E1129	ZA
-180.5	-1.234	-9.276	E1129	ZA
-180	-1.349	-9.261	E1129	ZA
-179.5	-0.764	-9.435	E1129	ZA
-179	-1.704	-10.374	E1129	ZA
-178.5	-1.135	-7.634	E1129	ZA
-178	-1.963	-10.046	E1129	ZA
-177.5	-1.908	-9.565	E1129	ZA
-177	-1.953	-10.284	E1129	ZA
-176	-1.021	-8.493	E1129	ZA
-175.5	-1.131	-6.868	E1129	ZA
-175	-2.252	-8.955	E1129	ZA
-174.5	-1.971	-9.836	E1129	ZA
-174	-2.978	-9.899	E1129	ZA
-173.5	-2.223	-9.739	E1129	ZA
-173	-2.488	-9.790	E1129	ZA
-172.5	-1.986	-9.857	E1129	ZA
-172	-2.425	-9.880	E1129	ZA
-171.5	-0.627	-9.327	E1129	ZA
-171	-1.757	-9.193	E1129	ZA
-170.5	-1.749	-9.831	E1129	ZA
-170	-1.711	-9.271	E1129	ZA
-169.5	-0.961	-9.287	E1129	ZA
-168.5	-2.527	-9.559	E1129	ZA
-167.5	-2.991	-8.706	E1129	ZA
-167	-1.372	-9.007	E1129	ZA
-166.5	-0.770	-9.576	E1129	ZA
-166	-1.160	-9.125	E1129	ZA
-165.5	-3.340	-10.277	E1129	ZA
-165	-2.486	-8.391	E1129	ZA
-164.5	-2.096	-8.057	E1129	ZA
-164	-1.680	-9.914	E1129	ZA
-163.5	-1.937	-8.933	E1129	ZA
-163	-2.528	-9.398	E1129	ZA
-162.5	-1.771	-8.006	E1129	ZA
-162	-0.463	-8.401	E1129	ZA
-161.5	0.284	-7.936	E1129	ZA
-161	0.249	-8.332	E1129	ZA
-160.5	0.281	-8.274	E1129	ZA
-160	-0.320	-7.834	E1129	ZA

-159.5	-0.369	-8.170	E1129	ZA
-159	-1.397	-8.157	E1129	ZA
-158	0.432	-8.128	E1129	ZA
-157.5	0.776	-8.191	E1129	ZA
-157	0.908	-7.889	E1129	ZA
-156.5	0.355	-8.493	E1129	ZA
-156	0.221	-8.060	E1129	ZA
-155.5	-0.468	-8.050	E1129	ZA
-155	-0.907	-7.737	E1129	ZA
-126.5	-3.830	-9.498	E1129	ZA
-126	-2.646	-10.423	E1129	ZA
-125.5	-1.316	-9.038	E1129	ZA
-125	-1.831	-8.176	E1129	ZA
-124.5	-0.616	-7.962	E1129	ZA
-124	-3.013	-9.775	E1129	ZA
-123.5	-0.579	-8.124	E1129	ZA
-123	-2.667	-8.964	E1129	ZA
-122.5	-2.720	-8.738	E1129	ZA
-122	-2.128	-7.789	E1129	ZA
-121.5	-2.354	-8.314	E1129	ZA
-121	-0.692	-8.870	E1129	ZA
-120.5	-0.274	-9.094	E1129	ZA
-120	-1.219	-9.255	E1129	ZA
-119.5	-1.163	-8.544	E1129	ZA
-116.5	-3.285	-7.907	E1129	ZA
-116	-1.172	-8.240	E1129	ZA
-115.5	-0.090	-8.883	E1129	ZA
-115	0.089	-8.122	E1129	ZA
-114.5	-0.598	-8.362	E1129	ZA
-114	-2.940	-11.104	E1129	ZA
-113.5	-2.364	-8.698	E1129	ZA
-113	-1.358	-8.186	E1129	ZA
-110.5	-1.160	-16.949	E1129	ZA
-110	-1.232	-9.002	E1129	ZA
-109.5	-1.185	-9.846	E1129	ZA
-109	-0.209	-8.996	E1129	ZA
-108.5	-0.149	-7.953	E1129	ZA
-108	-0.315	-8.593	E1129	ZA
-107.5	-0.322	-9.457	E1129	ZA
-106.5	0.775	-7.855	E1129	ZA
-105.5	0.219	-8.508	E1129	ZA
-105	1.560	-8.640	E1129	ZA
-104.5	0.682	-8.437	E1129	ZA
-104	0.536	-8.550	E1129	ZA
-103.5	-0.643	-8.778	E1129	ZA
-103	-1.531	-11.459	E1129	ZA
-102.5	-2.471	-11.233	E1129	ZA
-102	-3.302	-9.983	E1129	ZA
-101.5	-2.603	-13.040	E1129	ZA
-100.5	-0.495	-8.132	E1129	ZA

-100	-0.588	-6.163	E1129	ZA
-97.5	-0.812	-8.353	E1129	ZA
-97	-1.293	-8.602	E1129	ZA
-96	-1.187	-8.197	E1129	ZA
-95.5	0.511	-10.968	E1129	ZA
-95	-0.562	-8.580	E1129	ZA
-94.5	-1.392	-9.170	E1129	ZA
-94	-0.201	-8.133	E1129	ZA
-93.5	0.081	-8.717	E1129	ZA
-92.5	-1.735	-8.922	E1129	ZA
-92	-1.479	-9.952	E1129	ZA
-91.5	-1.157	-9.344	E1129	ZA
-91	-2.044	-9.217	E1129	ZA
-90.5	-2.011	-10.500	E1129	ZA
-90	0.671	-9.397	E1129	ZA
-89.5	0.700	-10.538	E1129	ZA
-89	0.834	-10.402	E1129	ZA
-88.5	1.207	-9.049	E1129	ZA
-88	0.424	-9.582	E1129	ZA
-87.5	-1.197	-8.856	E1129	ZA
-86.5	-1.464	-8.786	E1129	ZA
-86	-1.845	-9.852	E1129	ZA
-85.5	-1.831	-8.415	E1129	ZA
-85	0.184	-10.244	E1129	ZA
-84.5	-1.325	-9.788	E1129	ZA
-84	-0.512	-10.484	E1129	ZA
-83.5	-0.058	-8.381	E1129	ZA
-82.5	-0.089	-9.530	E1129	ZA
-82	-0.182	-9.697	E1129	ZA
-81.5	-1.159	-8.830	E1129	ZA
-81	-1.458	-9.065	E1129	ZA
-80.5	-1.900	-10.027	E1129	ZA
-80	-1.728	-8.396	E1129	ZA
-79.5	0.183	-10.317	E1129	ZA
-79	0.701	-9.831	E1129	ZA
-78.5	0.732	-10.456	E1129	ZA
-77.5	0.688	-11.173	E1129	ZA
-76.5	1.182	-9.062	E1129	ZA
-75.5	0.381	-9.951	E1129	ZA
-74.5	0.212	-10.316	E1129	ZA
-73.5	0.736	-8.166	E1129	ZA
-72.5	0.461	-10.152	E1129	ZA
-71.5	0.422	-9.114	E1129	ZA
-70.5	-0.858	-7.656	E1129	ZA
-69.5	0.524	-8.239	E1129	ZA
-68.5	0.133	-7.624	E1129	ZA
-67.5	-1.553	-9.649	E1129	ZA
-66.5	-1.088	-8.210	E1129	ZA
-65.5	-2.826	-8.423	E1129	ZA
-64.5	-1.041	-7.512	E1129	ZA

-63.5	-1.446	-7.738	E1129	ZA
-62.5	-0.025	-7.927	E1129	ZA
-61.5	0.609	-8.331	E1129	ZA
-60.5	0.452	-7.769	E1129	ZA
-59.5	-1.035	-8.512	E1129	ZA
-58.5	-1.152	-7.302	E1129	ZA
-57.5	-0.341	-13.063	E1129	ZA
-56.5	-1.533	-8.438	E1129	ZA
-55.5	-0.635	-7.801	E1129	ZA
-54.5	-0.625	-8.098	E1129	ZA
-53.5	-1.081	-8.329	E1129	ZA
-52.5	-1.528	-7.799	E1129	ZA
-51.5	-2.059	-8.020	E1129	ZA
-50.5	-2.536	-8.610	E1129	ZA
-49.5	-2.095	-9.419	E1129	ZA
-48.5	-1.761	-9.662	E1129	ZA
-47.5	-1.022	-7.810	E1129	ZA
-46.5	0.083	-9.503	E1129	ZA
-42.5	-1.338	-8.188	E1129	ZA
-41.5	-1.506	-8.770	E1129	ZA
-40.5	-1.668	-8.555	E1129	ZA
-39.5	-2.307	-8.079	E1129	ZA
-38.5	-1.851	-8.036	E1129	ZA
-37.5	-2.300	-7.099	E1129	ZA
-36.5	-2.310	-7.535	E1129	ZA
-35.5	-2.907	-7.731	E1129	ZA
-34.5	-3.167	-9.204	E1129	ZA
-33.5	-3.096	-8.932	E1129	ZA
-32.5	-3.102	-8.545	E1129	ZA
-31.5	-3.453	-7.639	E1129	ZA
-30.5	-3.975	-8.008	E1129	ZA
-29.5	-3.899	-8.414	E1129	ZA
-26.5	-5.256	-9.184	E1129	ZA
-25.5	-4.359	-7.352	E1129	ZA
-24.5	-4.464	-7.416	E1129	ZA
-23.5	-4.974	-5.067	E1129	ZA
-22.5	-4.261	-7.584	E1129	ZA
-21.5	-4.375	-8.111	E1129	ZA
-20.5	-3.580	-7.666	E1129	ZA
-19.5	-4.409	-7.832	E1129	ZA
-18.5	-3.224	-8.191	E1129	ZA
-17.5	-3.588	-8.229	E1129	ZA
-16.5	-3.573	-7.703	E1129	ZA
-15.5	-4.216	-8.866	E1129	ZA
-14.5	-4.450	-9.010	E1129	ZA
-13.5	-7.730	-6.756	E1129	ZA
-12.5	-7.749	-9.131	E1129	ZA
-11.5	-8.252	-8.051	E1129	ZA
-10.5	-5.787	-8.648	E1129	ZA
-9.5	-5.179	-8.063	E1129	ZA

-8.5	-7.597	-10.961	E1129	ZA
-7.5	-7.927	-11.208	E1129	ZA
-6.5	-5.314	-11.133	E1129	ZA
-3.5	-5.423	-11.468	E1129	ZA
-3	-5.554	-9.489	E1129	ZA
-2.5	-3.797	-11.430	E1129	ZA
-1.5	-4.985	-8.742	E1129	ZA
0	-3.742	-12.475	E1129	ZA

SE Khukh-Davaa

m corrected	d13C	d18O	section	Fm
0.4	1.6115	-3.85423905	E1209	ZA
0.6	1.6005	-4.230383568	E1209	ZA
1	-1.2575	-2.428849295	E1209	ZA
1.2	2.4955	-4.596629547	E1209	ZA
1.5	2.5625	-3.117787676	E1209	ZA
2	2.3825	-4.315511012	E1209	ZA
2.5	2.5715	-2.747582282	E1209	ZA
3	2.3595	-3.345454096	E1209	ZA
3.5	2.7075	-2.883192279	E1209	ZA
4	2.6395	-3.20291512	E1209	ZA
4.5	2.8125	-3.021771839	E1209	ZA
5	2.2825	-3.843350656	E1209	ZA
5.5	1.9635	-4.723330859	E1209	ZA
6	2.1945	-0.542187577	E1209	ZA
6.5	2.8215	-1.504325662	E1209	ZA
7	2.5955	-2.505068052	E1209	ZA
8	2.3155	-2.840628557	E1209	ZA
8.5	1.5945	-9.563716902	E1209	ZA
9	-0.0255	-2.198213314	E1209	ZA
10	1.8695	-3.402865627	E1209	ZA
10.5	2.7295	-3.472155407	E1209	ZA
11	3.0655	-1.826028211	E1209	ZA
11.5	2.2205	-2.568418708	E1209	ZA
12	1.1786	-1.611130908	E1209	ZA
12.5	1.8096	-2.081707498	E1209	ZA
13	1.8156	-1.348225687	E1209	ZA
14	3.1836	-0.468245484	E1209	ZA
15	3.8186	-0.704820589	E1209	ZA
16.5	-1.9274	-3.615981193	E1209	ZA
16.8	-0.6474	-3.404152438	E1209	ZA
17	-0.7214	-6.171784212	E1209	ZA
17.5	-1.7024	-2.447953477	E1209	ZA
18	-1.7784	-3.182029201	E1209	ZA
18.5	-1.6044	-3.846221232	E1209	ZA
19	-1.9034	-4.6430537	E1209	ZA
19.2	-2.0344	-3.119074487	E1209	ZA
19.5	-1.8314	-3.524914625	E1209	ZA

20	-2.1894	-4.630581539	E1209	ZA
20.5	-2.1024	-2.103484286	E1209	ZA
21	-2.1004	-3.29823806	E1209	ZA
21.9	-2.1734	-4.126745855	E1209	ZA
22	-1.7664	-3.14481069	E1209	ZA
22.5	-2.1054	-5.416525612	E1209	ZA
23	-2.5354	-2.713234348	E1209	ZA
27	0.8406	-6.11932195	E1209	ZA
28	1.1126	-4.932487008	E1209	ZA
28.5	1.2756	-4.825582777	E1209	ZA
29	1.1156	-6.204449394	E1209	ZA
29.5	1.7856	-5.662999258	E1209	ZA
30	1.3366	-4.800836427	E1209	ZA
30.5	1.0956	-5.09878248	E1209	ZA
30.8	0.6146	-4.927537738	E1209	ZA
31	1.1096	-6.443994061	E1209	ZA
31.5	1.2636	-8.089131403	E1209	ZA
32	0.9576	-6.857753031	E1209	ZA
32.5	1.2146	-6.022316258	E1209	ZA
33	1.3976	-7.141841128	E1209	ZA
33.5	1.0736	-6.591482306	E1209	ZA
34	0.5596	-8.215832715	E1209	ZA
35.5	-0.6424	-13.74119772	E1209	ZA
36	2.2236	-21.22152438	E1209	ZA
37.5	2.7886	-21.12550854	E1209	ZA
38	2.8586	-20.28908191	E1209	ZA
38.5	3.7716	-11.68428112	E1209	ZA
42	2.8766	-11.41207127	E1209	ZA
42.5	2.4696	-9.816426627	E1209	ZA
43	2.6506	-9.187869339	E1209	ZA
43.5	2.7016	-7.821870824	E1209	ZA
46	3.7896	-11.26458302	E1209	ZA
46.5	4.5976	-11.36257857	E1209	ZA
48	2.9366	-7.920856224	E1209	ZA
49	3.5236	-10.057951	E1209	ZA
50	5.0476	-8.532585994	E1209	ZA
51	5.1126	-9.962925019	E1209	ZA
52	5.4296	-14.55782727	E1209	ZA
53	5.3746	-9.052259342	E1209	ZA
54	5.2616	-8.275223954	E1209	ZA
55	4.9206	-9.874828013	E1209	ZA
56	4.8136	-14.65780252	E1209	ZA
57	5.1816	-10.3677753	E1209	ZA
58	5.3466	-8.310462757	E1209	ZA
59	4.9526	-9.093437268	E1209	ZA
60	5.6526	-8.004597872	E1209	ZA
61	3.0146	-14.80192527	E1209	ZA
62	5.3846	-11.1691611	E1209	ZA
63	5.2086	-11.15431329	E1209	ZA
64	4.9276	-12.97366493	E1209	ZA

66	5.9796	-12.25206137	E1209	ZA
67	5.4896	-11.27804504	E1209	ZA
67.2	5.7476	-12.15406583	E1209	ZA
68	5.5776	-11.72941846	E1209	ZA
69	5.1986	-12.2085078	E1209	ZA
70	1.3676	-11.83533284	E1209	ZA
71	4.9486	-11.57005197	E1209	ZA
72	5.3736	-11.67002722	E1209	ZA
73	4.3626	-9.882350903	E1209	ZA
74	4.9236	-11.54629547	E1209	ZA
76	4.4196	-7.9372878	E1209	ZA
77	4.0766	-10.75045286	E1209	ZA
78	6.15	-9.463414289	E1209	ZA
79	3.975	-19.4342136	E1209	ZA
80	3.288	-11.84401315	E1209	ZA
80.1	2.974	-10.765	E1209	ZA
81	3.070	-12.072	E1209	ZA
82	4.051	-13.816	E1209	ZA
83	3.532	-14.781	E1209	ZA
84	6.551	-21.742	E1209	ZA
87	2.982	-11.864	E1209	ZA
88	2.749	-13.859	E1209	ZA
89	2.847	-13.057	E1209	ZA
90	2.952	-14.040	E1209	ZA
91	3.057	-12.910	E1209	ZA
91.2	2.119	-10.581	E1209	ZA
92	2.851	-10.583	E1209	ZA
93	2.614	-10.182	E1209	ZA
94	2.758	-10.950	E1209	ZA
95	2.995	-11.531	E1209	ZA
96	3.890	-29.500	E1209	ZA
98	2.815	-17.209	E1209	ZA
100	2.902	-20.976	E1209	ZA
102	2.775	-10.549	E1209	ZA
105	2.735	-9.644	E1209	ZA
106	2.617	-10.919	E1209	ZA
110	2.673	-9.717	E1209	ZA
114	1.781	-12.961	E1209	ZA
134	1.008	-13.630	E1209	ZA
136	0.808	-10.222	E1209	ZA
138	0.750	-10.346	E1209	ZA
140	0.719	-11.581	E1209	ZA
142	-2.200	-17.958	E1209	ZA
144	-1.936	-17.068	E1209	ZA
146	-0.403	-17.281	E1209	ZA
148	-1.163	-18.660	E1209	ZA
150	-2.130	-17.307	E1209	ZA
152	-5.770	-8.203	E1209	ZA
153	-7.458	-14.775	E1209	ZA
154	-7.116	-16.787	E1209	ZA

156	-4.513	-17.519	E1209	ZA
158	-3.417	-17.176	E1209	ZA
160	-1.174	-15.711	E1209	ZA
162	-0.103	-15.876	E1209	ZA
164	-0.040	-15.542	E1209	ZA
166	-0.018	-16.694	E1209	ZA
168	-0.764	-17.102	E1209	ZA
170	-0.804	-17.300	E1209	ZA
172	-1.059	-20.365	E1209	ZA
174	-1.204	-21.429	E1209	ZA
176	-1.989	-19.161	E1209	ZA
178	-1.928	-18.421	E1209	ZA
180	-2.391	-18.984	E1209	ZA
182	-3.125	-15.895	E1209	ZA
184	-2.935	-20.647	E1209	ZA
186	-3.839	-17.805	E1209	ZA
188	-3.878	-12.706	E1209	ZA
190	-4.116	-12.671	E1209	ZA
192	-3.316	-21.290	E1209	ZA
196	-5.114	-16.928	E1209	ZA
198	-7.799	-21.654	E1209	ZA
200	-6.623	-22.412	E1209	ZA
201	-6.119	-14.746	E1209	ZA
202	-5.146	-14.323	E1209	ZA
204	-5.735	-19.527	E1209	ZA
206	-3.738	-14.806	E1209	ZA
208	-4.686	-19.151	E1209	ZA
210	-5.471	-16.298	E1209	ZA
212	-4.819	-19.747	E1209	ZA
214	-4.831	-18.349	E1209	ZA
216	-4.014	-15.054	E1209	ZA
218	-3.647	-13.582	E1209	ZA
220	-3.390	-12.667	E1209	ZA
222	-3.439	-13.124	E1209	ZA
224	-3.963	-12.450	E1209	ZA
226	-2.841	-12.968	E1209	ZA
228	-4.373	-12.667	E1209	ZA
230	-4.572	-18.044	E1209	ZA
232	-4.767	-16.102	E1209	ZA
234	-6.644	-16.866	E1209	ZA
236	-4.838	-13.905	E1209	ZA
238	-4.092	-11.207	E1209	ZA
240	-2.339	-13.318	E1209	ZA
241.5	-3.337	-11.831	E1209	ZA
243	-4.409	-9.029	E1209	ZA
245	-6.275	-15.193	E1209	ZA
247	-7.704	-11.712	E1209	ZA
249	-4.657	-14.597	E1209	ZA
252	-6.244	-14.389	E1209	ZA
254	-6.716	-13.193	E1209	ZA

256	-5.524	-13.941	E1209	ZA
258	-5.411	-12.461	E1209	ZA
260	-4.492	-18.303	E1209	ZA
262	-4.405	-18.721	E1209	ZA
260	-3.140	-12.548	E1207	BG
261	-3.873	-14.442	E1207	BG
262	-4.930	-13.464	E1207	BG
264	3.082	-15.893	E1207	BG
265	3.308	-15.653	E1207	BG
267	2.990	-13.976	E1207	BG
268	-1.826	-15.061	E1207	BG
274	-4.641	-15.486	E1207	BG
311	-3.249	-15.048	E1207	BG
319	-4.349	-15.052	E1207	BG
343.5	-2.751	-15.060	E1207	BG
486.5	-3.663	-11.521	E1207	BG
493	-1.224	-13.117	E1207	BG
494	-0.292	-13.941	E1207	BG
495	-0.852	-15.296	E1207	BG
496	0.536	-12.487	E1207	BG
497	-1.355	-19.128	E1207	BG
508	-3.153	-14.009	E1207	BG
519	0.416	-12.399	E1207	BG
524.4	-0.797	-15.393	E1207	BG
525.5	-0.596	-15.549	E1207	BG
526	-0.644	-14.679	E1207	BG
526.5	0.621	-13.668	E1207	BG
526.7	0.822	-13.403	E1207	BG
527.2	0.778	-13.720	E1207	BG
528	0.017	-13.628	E1207	BG
528.3	1.079	-11.911	E1207	BG
528.9	0.750	-13.733	E1207	BG
529	0.644	-14.209	E1207	BG
530	2.844	-13.327	E1207	BG
530.5	2.778	-13.386	E1207	BG
530.7	3.081	-13.585	E1207	BG
530.8	2.204	-13.607	E1207	BG
531.1	1.998	-13.536	E1207	BG
531.5	1.425	-13.944	E1207	BG
532.5	1.009	-11.806	E1207	BG
533.5	0.850	-11.969	E1207	BG
534	0.666	-12.762	E1207	BG
535	3.249	-15.711	E1207	BG
536	3.502	-12.933	E1207	BG
537	4.075	-13.035	E1207	BG
538	3.480	-16.024	E1207	BG
540	3.676	-11.649	E1207	BG
541	2.583	-11.552	E1207	BG
542	1.150	-8.906	E1207	BG
543	1.231	-9.066	E1207	BG

544	2.832	-9.936	E1207	BG
545	3.151	-12.247	E1207	BG
546	3.001	-12.204	E1207	BG
547	3.615	-16.999	E1207	BG
547	3.552	-16.998	E1207	BG
548	3.946	-11.328	E1207	BG
549	3.667	-14.041	E1207	BG
550	2.329	-14.737	E1207	BG
551	2.336	-15.711	E1207	BG
552	1.994	-13.675	E1207	BG
553	1.987	-14.112	E1207	BG
554	2.395	-14.100	E1207	BG
556	2.271	-18.704	E1207	BG
557	1.844	-17.055	E1207	BG
576	3.401	-16.784	E1207	BG
577	3.587	-14.410	E1207	BG
578	3.021	-14.641	E1207	BG
579	2.785	-15.614	E1207	BG
580	2.189	-10.534	E1207	BG
581	1.558	-13.435	E1207	BG
582	2.167	-16.611	E1207	BG
583	1.650	-9.801	E1207	BG
584	2.235	-9.248	E1207	BG
585	1.920	-14.961	E1207	BG
592	1.954	-21.145	E1207	BG
594	1.809	-19.390	E1207	BG
595	1.060	-21.853	E1207	BG
596	0.952	-19.885	E1207	BG
597	0.894	-13.464	E1207	BG
598	1.264	-16.442	E1207	BG
600	0.691	-12.570	E1207	BG
601	0.810	-8.787	E1207	BG
602	-0.319	-17.987	E1207	BG
620	2.618	-14.806	E1207	BG
623	2.175	-22.177	E1207	BG
625	3.135	-14.140	E1207	BG
630	2.622	-22.539	E1207	BG
631	2.559	-19.834	E1207	BG
632	3.219	-20.329	E1207	BG
633	3.051	-20.735	E1207	BG
635	3.129	-14.544	E1207	BG
636	2.332	-13.382	E1207	BG
637	3.058	-12.200	E1207	BG
638	3.149	-10.560	E1207	BG
639	3.195	-9.551	E1207	BG
640	2.846	-11.329	E1207	BG
641	2.684	-12.477	E1207	BG
651	0.700	-11.947	E1207	BG
652	3.403	-16.187	E1207	BG
654	3.870	-9.634	E1207	BG

655	3.427	-11.747	E1207	BG
656	2.864	-11.917	E1207	BG
657	2.526	-11.571	E1207	BG
658	3.589	-10.028	E1207	BG
659	3.340	-12.377	E1207	BG
660	2.914	-11.378	E1207	BG
661	2.920	-15.226	E1207	BG
662	3.005	-12.788	E1207	BG
663	3.232	-9.314	E1207	BG
664	0.561	-10.811	E1207	BG
665	0.166	-8.765	E1207	BG
666	0.118	-11.875	E1207	BG
667	0.342	-9.758	E1207	BG
668	-0.315	-12.910	E1207	BG
670	-0.399	-11.192	E1207	BG
671	-0.076	-14.195	E1207	BG
672	0.122	-10.596	E1207	BG
673	-0.072	-9.448	E1207	BG
674	-0.328	-11.628	E1207	BG
675	-0.266	-10.208	E1207	BG
686	-1.417	-12.144	E1207	BG
687	-1.957	-17.857	E1207	BG
713	-1.866	-15.088	E1207	BG
721	-2.772	-19.866	E1207	BG
723	-3.202	-10.038	E1207	BG
725	-3.341	-11.635	E1207	BG
727	-3.040	-20.525	E1207	BG
729	-3.356	-11.374	E1207	BG
731	-3.282	-12.731	E1207	BG
733	-3.232	-24.227	E1207	BG
735	-3.179	-14.306	E1207	BG
737	-3.333	-20.112	E1207	BG
739	-3.326	-14.347	E1207	BG
741	-3.060	-14.856	E1207	BG
743	-3.238	-12.871	E1207	BG
745	-3.193	-16.005	E1207	BG
747	-3.515	-11.129	E1207	BG
749	-3.491	-19.425	E1207	BG
751	-2.271	-22.346	E1207	BG
753	-2.811	-14.900	E1207	BG
755	-1.902	-17.148	E1207	BG
757	-2.892	-14.096	E1207	BG
759	-3.053	-12.782	E1207	BG
761	-2.935	-18.053	E1207	BG
763.5	-2.904	-16.436	E1207	BG
765	-1.863	-17.415	E1207	BG
767	-2.263	-16.903	E1207	BG
769	-2.328	-20.542	E1207	BG
771	-1.157	-25.707	E1207	BG
773	-3.493	-16.893	E1207	BG

775	-1.993	-15.004	E1207	BG
781	-2.992	-17.241	E1207	BG
783	-2.354	-14.527	E1207	BG
784	-3.024	-20.724	E1207	BG
785	-2.002	-14.770	E1207	BG
795	-0.786	-21.678	E1207	BG
797	-1.885	-17.929	E1207	BG
798	-1.901	-18.665	E1207	BG
799	-1.256	-19.258	E1207	BG
801	1.091	-11.611	E1207	BG
805	-0.010	-15.199	E1207	BG
807	0.040	-16.481	E1207	BG
809	0.422	-15.691	E1207	BG
811	0.271	-15.946	E1207	BG
813	-0.092	-20.433	E1207	BG
815	-0.061	-16.245	E1207	BG
818	1.412	-16.763	E1207	BG
820	2.049	-18.389	E1207	BG
822	1.477	-15.684	E1207	BG
826	0.806	-16.024	E1207	BG
828	0.756	-14.667	E1207	BG
830	0.642	-15.089	E1207	BG
832	0.513	-16.073	E1207	BG
911.5	3.778	-16.043	E1207	BG
938	0.897	-12.677	E1207	BG
939	1.973	-12.082	E1207	BG
940	2.102	-14.717	E1207	BG
941	2.257	-14.518	E1207	BG
942	0.760	-9.727	E1207	BG
943	1.696	-12.952	E1207	BG
944	1.752	-16.053	E1207	BG
945	1.169	-24.719	E1207	BG
946	1.984	-12.413	E1207	BG
947	1.198	-25.026	E1207	BG
948.5	1.140	-19.379	E1207	BG
949	0.918	-29.102	E1207	BG
950	0.992	-27.168	E1207	BG
951	0.107	-25.518	E1207	BG
952	0.484	-13.847	E1207	BG
953	0.969	-11.841	E1207	BG
954	1.054	-16.652	E1207	BG
955	1.176	-11.790	E1207	BG
956	1.453	-14.572	E1207	BG
957	0.532	-15.731	E1207	BG
958	1.130	-13.281	E1207	BG
959	0.920	-16.134	E1207	BG
960	0.420	-17.745	E1207	BG
961	0.397	-19.339	E1207	BG
963	0.532	-17.150	E1207	BG
964	0.641	-17.823	E1207	BG

965	0.514	-12.477	E1207	BG
966	0.047	-18.256	E1207	BG
974.8	2.239	-14.110	E1207	BG
976	1.990	-10.158	E1207	BG
977	3.721	-10.522	E1207	BG
981.5	3.108	-15.550	E1207	BG
982	2.937	-11.877	E1207	BG
983	2.301	-12.413	E1207	BG
983.8	3.684	-11.186	E1207	BG
998	1.887	-14.214	E1207	BG
999	2.111	-14.607	E1207	BG
1000	1.511	-10.599	E1207	BG
1006	1.551	-10.707	E1207	BG
1007	0.211	-10.092	E1207	BG
1008	-0.236	-13.498	E1207	BG
1009	0.340	-10.272	E1207	BG
1010	0.944	-8.202	E1207	BG
1011	0.712	-9.253	E1207	BG
1012	-0.080	-8.343	E1207	BG
1013	0.006	-11.577	E1207	BG
119	-0.516	-13.961	E1329	SG
120	-0.990	-12.500	E1329	SG
121	-1.348	-15.180	E1329	SG
121.3	-1.189	-11.838	E1329	SG
122	-1.140	-13.588	E1329	SG
123	-0.793	-13.145	E1329	SG
123.3	-1.090	-8.380	E1329	SG
124	-1.032	-8.270	E1329	SG
127	-1.006	-15.087	E1329	SG
128	-0.868	-14.357	E1329	SG
129	-0.878	-9.356	E1329	SG
130	-1.006	-16.875	E1329	SG
131	-1.105	-18.355	E1329	SG
132	-1.054	-19.806	E1329	SG
133	-0.898	-17.684	E1329	SG
134	-0.964	-19.479	E1329	SG
136	-0.627	-18.482	E1329	SG
137	-0.763	-12.152	E1329	SG
138	-0.401	-9.149	E1329	SG
139	-0.375	-8.735	E1329	SG
140	-0.795	-7.975	E1329	SG
141	-0.815	-8.864	E1329	SG
142	-0.789	-13.257	E1329	SG
143	-0.980	-11.255	E1329	SG
144	-0.997	-12.069	E1329	SG
145	-0.853	-9.123	E1329	SG
146	-0.853	-9.742	E1329	SG
147	-1.066	-16.805	E1329	SG
148	-1.337	-15.475	E1329	SG
152	-1.408	-16.258	E1329	SG

154	-1.213	-14.534	E1329	SG
156	-1.387	-12.941	E1329	SG
158	-1.495	-15.765	E1329	SG
160	-1.224	-15.223	E1329	SG
162	-1.472	-14.611	E1329	SG
164	-1.184	-11.989	E1329	SG
166	-1.253	-15.203	E1329	SG
168	-1.201	-14.864	E1329	SG
170	-1.065	-15.011	E1329	SG
175	-1.563	-14.407	E1329	SG
177	-1.475	-14.496	E1329	SG
179	-1.373	-13.562	E1329	SG
185	-1.282	-15.920	E1329	SG
187	-1.326	-14.820	E1329	SG
191	-1.770	-15.484	E1329	SG
193.5	-1.023	-13.572	E1329	SG
194	-0.997	-15.696	E1329	SG
195	-1.642	-17.624	E1329	SG
197	-1.259	-17.991	E1329	SG
199	-1.404	-17.708	E1329	SG
201	1.116	-16.854	E1329	SG
203	0.277	-19.634	E1329	SG
164	0.058	-9.067	E1329	SG
160	-1.920	-13.022	E1340	SG
161	-1.703	-12.184	E1340	SG
162	-1.773	-5.418	E1340	SG
163	-1.480	-11.472	E1340	SG
164	-1.625	-7.382	E1340	SG
165	-1.011	-14.634	E1340	SG
166	-1.743	-12.070	E1340	SG
167	-1.865	-7.565	E1340	SG
168	-1.362	-15.488	E1340	SG
169	-2.043	-10.684	E1340	SG
170	-2.022	-12.723	E1340	SG
171	-1.784	-3.739	E1340	SG
172	-1.553	-7.288	E1340	SG
173	-1.900	-11.542	E1340	SG
174	-1.626	-9.881	E1340	SG
175	-1.578	-7.562	E1340	SG
176	-1.523	-11.229	E1340	SG
177	-1.463	-5.574	E1340	SG
178	-1.434	-9.247	E1340	SG
179	-1.900	-5.024	E1340	SG
180	-2.484	-7.364	E1340	SG
181	-2.183	-8.974	E1340	SG
183	-1.533	-11.747	E1340	SG
184	-1.454	-1.198	E1340	SG
185	-1.660	-12.875	E1340	SG
186	-1.669	-8.602	E1340	SG
158	-2.311	-15.120	E1340	SG

159	-1.889	-19.412	E1340	SG
188	-1.395	-17.888	E1340	SG
190	-1.248	-20.216	E1340	SG
191	-1.048	-13.300	E1340	SG
192	-2.378	-21.785	E1340	SG
194	-4.063	-17.505	E1340	SG
196	-1.648	-18.330	E1340	SG
197	-1.907	-14.707	E1340	SG
198	-1.928	-16.332	E1340	SG
199	-1.594	-15.787	E1340	SG
200	-1.631	-14.500	E1340	SG

Salaa and Tsagaan gorges

m corrected	d13C	d18O	section	Fm
32.2	0.928	-10.274	F874	ZA
34.2	1.125	-9.868	F874	ZA
36.2	1.777	-13.322	F874	ZA
38.2	1.829	-10.305	F874	ZA
40.2	1.334	-9.143	F874	ZA
42.2	0.381	-17.847	F874	ZA
44.2	0.743	-9.681	F874	ZA
46.2	0.445	-13.563	F874	ZA
48.2	1.211	-15.035	F874	ZA
50.2	0.517	-16.085	F874	ZA
52.2	-0.122	-14.158	F874	ZA
54.2	0.496	-12.972	F874	ZA
56.2	0.619	-15.856	F874	ZA
58.2	0.074	-12.774	F874	ZA
60.2	-0.365	-17.911	F874	ZA
62.2	-0.969	-13.471	F874	ZA
64.2	1.140	-10.597	F874	ZA
66.2	-0.689	-17.177	F874	ZA
68.2	-0.384	-15.034	F874	ZA
70.2	-0.889	-12.236	F874	ZA
72.2	-0.819	-14.800	F874	ZA
74.2	-0.585	-16.042	F874	ZA
76.2	0.131	-14.057	F874	ZA
78.2	1.663	-8.162	F874	ZA
80.2	-0.486	-12.267	F874	ZA
82.2	-0.012	-10.598	F874	ZA
84.2	-1.323	-12.333	F874	ZA
88.2	-0.484	-9.525	F874	ZA
91.2	-1.309	-6.559	F874	ZA
93.2	-0.604	-6.825	F874	ZA
95.2	-1.521	-6.277	F874	ZA
97.2	-1.207	-7.939	F874	ZA
99.2	-1.663	-6.589	F874	ZA

101.2	-1.662	-6.189	F874	ZA
103.2	-1.586	-6.305	F874	ZA
105.2	-1.599	-6.645	F874	ZA
107.2	-1.953	-6.419	F874	ZA
109.2	-2.098	-6.314	F874	ZA
111.2	-2.169	-6.134	F874	ZA
113.2	-2.254	-7.314	F874	ZA
115.2	-2.575	-7.164	F874	ZA
117.2	-3.365	-6.672	F874	ZA
119.2	-3.399	-6.618	F874	ZA
121.2	-3.860	-7.804	F874	ZA
181.0	-9.160	-10.830	D718	ZA
183.0	-6.600	-12.850	D718	ZA
185.0	-8.400	-10.830	D718	ZA
187.0	-7.470	-12.370	D718	ZA
189.0	-8.510	-9.760	D718	ZA
191.0	-6.420	-14.450	D718	ZA
193.0	-6.020	-12.400	D718	ZA
201.0	-3.960	-13.480	D718	ZA
203.0	-4.790	-13.960	D718	ZA
211.0	0.130	-14.120	D718	ZA
213.0	1.520	-14.730	D718	BG
217.0	0.120	-14.960	D718	BG
221.0	-0.010	-14.950	D718	BG
231.0	-1.370	-15.030	D718	BG
272.0	-0.350	-14.190	D718	BG
288.0	-0.790	-12.820	D718	BG
289.0	-0.570	-13.500	D718	BG
290.1	0.036	-8.985	D720	BG
292.0	0.172	-10.195	D720	BG
296.0	0.125	-8.722	D720	BG
298.0	-0.158	-8.231	D720	BG
300.0	0.228	-8.328	D720	BG
302.0	0.175	-10.032	D720	BG
304.0	-0.169	-8.570	D720	BG
306.0	-0.052	-8.709	D720	BG
308.0	0.249	-8.699	D720	BG
310.5	0.114	-8.220	D720	BG
312.0	0.333	-7.961	D720	BG
314.0	0.454	-8.924	D720	BG
323.0	0.393	-8.012	D720	BG
325.0	0.350	-7.535	D720	BG
327.0	0.276	-7.992	D720	BG
328.9	0.016	-15.400	D720	BG
329.0	0.564	-8.287	D720	BG
331.0	0.435	-9.950	D720	BG
335.0	0.799	-9.577	D720	BG
337.0	0.700	-8.552	D720	BG
339.0	1.380	-8.749	D720	BG
341.0	1.250	-8.917	D720	BG

343.0	1.545	-8.560	D720	BG
345.0	1.302	-8.199	D720	BG
356.0	2.235	-10.314	D720	BG
358.0	-0.654	-11.413	D720	BG
439.1	3.762	-11.219	D720	BG
440.0	4.065	-11.111	D720	BG
442.0	4.059	-11.089	D720	BG
444.2	3.574	-11.667	D720	BG
446.0	2.872	-12.288	D720	BG
452.0	3.448	-10.632	D720	BG
454.0	3.271	-10.325	D720	BG
460.0	-1.441	-10.282	D720	BG
464.5	2.501	-10.060	D720	BG
465.0	3.329	-10.291	D720	BG
467.0	1.876	-10.610	D720	BG
469.0	0.803	-9.611	D720	BG
471.0	1.296	-10.043	D720	BG
639.0	1.226	-15.914	D720	BG
659.0	-1.114	-16.513	D720	BG
666.5	-0.664	-15.169	D720	BG
687.5	-1.725	-11.842	D720	BG
688.5	-1.547	-10.287	D720	BG
691.0	-1.170	-9.867	D720	BG
693.0	-1.866	-11.030	D720	BG
694.5	-1.894	-14.499	D720	BG

NE Khukh Davaa

m corrected	d13C	d18O	section	Fm
0	-3.860	-33.008	E1211	BG
1	-3.129	-22.645	E1211	BG
2	-4.615	-12.883	E1211	BG
3	-3.295	-22.698	E1211	BG
4	-3.405	-17.847	E1211	BG
5	-3.337	-13.478	E1211	BG
6	-3.625	-18.749	E1211	BG
7	-3.213	-17.253	E1211	BG
8	-3.643	-16.296	E1211	BG
9	-5.873	-22.795	E1211	BG
152	-2.940	-19.756	E1211	BG
154	-3.011	-14.965	E1211	BG
156	-3.085	-17.860	E1211	BG
158	-3.129	-18.436	E1211	BG
160	-2.977	-14.832	E1211	BG
162	-2.174	-17.571	E1211	BG
166	-2.761	-18.714	E1211	BG
168	-2.534	-18.398	E1211	BG
170	-1.713	-18.689	E1211	BG
172	-0.699	-16.093	E1211	BG

174	-1.020	-14.318	E1211	BG
176	-0.461	-18.012	E1211	BG
178	0.259	-17.430	E1211	BG
180	0.464	-17.963	E1211	BG
182	-1.961	-10.790	E1211	BG
184	-1.873	-9.526	E1211	BG
186	-2.249	-10.298	E1211	BG
187.5	-0.803	-10.442	E1211	BG
188	1.483	-14.160	E1211	BG
190	0.272	-14.111	E1211	BG
192	0.527	-13.176	E1211	BG
194	0.353	-14.261	E1211	BG
300	2.760	-11.336	E1211	BG
301	3.363	-14.899	E1211	BG
304	3.339	-14.409	E1211	BG
305	3.414	-14.802	E1211	BG
307	2.987	-15.518	E1211	BG
308	2.585	-13.808	E1211	BG
309.5	1.999	-14.639	E1211	BG
310	2.688	-14.337	E1211	BG
311	1.711	-12.291	E1211	BG
312	2.159	-15.572	E1211	BG
313	2.295	-10.633	E1211	BG
314	2.393	-12.476	E1211	BG
315	2.063	-10.963	E1211	BG
316	1.666	-11.999	E1211	BG
317	1.705	-16.314	E1211	BG
318	0.943	-9.870	E1211	BG
319	0.185	-9.168	E1211	BG
320	0.595	-14.803	E1211	BG
321	0.753	-11.392	E1211	BG
322	0.226	-8.611	E1211	BG
322.7	0.114	-14.430	E1211	BG
323	-0.140	-13.173	E1211	BG
324	0.101	-13.874	E1211	BG
325	0.032	-14.573	E1211	BG
326	-0.591	-15.076	E1211	BG
327	-1.083	-15.913	E1211	BG
327.2	-0.320	-15.703	E1211	BG
330	0.445	-17.196	E1211	BG
369.5	2.292	-16.249	E1211	BG
370	1.313	-13.792	E1211	BG
371	2.384	-8.382	E1211	BG
372	1.632	-8.268	E1211	BG
374	0.452	-11.004	E1211	BG
375	2.136	-15.854	E1211	BG
378	0.349	-15.351	E1211	BG
380	0.583	-10.845	E1211	BG
382	0.219	-11.107	E1211	BG
384	1.628	-12.446	E1211	BG

386	-0.585	-11.751	E1211	BG
389.5	-0.547	-18.443	E1211	BG
392	-0.570	-12.448	E1211	BG
394	-0.969	-11.832	E1211	BG
396	-0.399	-10.666	E1211	BG
398	-0.336	-9.001	E1211	BG
400	-0.651	-8.707	E1211	BG
402	-0.873	-9.686	E1211	BG
403.5	-0.814	-8.260	E1211	BG
406	-1.540	-11.241	E1211	BG
408	-1.137	-13.614	E1211	BG
410	-1.326	-15.735	E1211	BG
411	-1.009	-14.454	E1211	BG
412	-1.642	-13.845	E1211	BG
414	-1.606	-10.762	E1211	BG
416	-1.690	-12.759	E1211	BG
416	-1.698	-12.776	E1211	BG
417.5	-1.632	-11.045	E1211	BG
420	-1.521	-15.746	E1211	BG
423	-1.746	-12.558	E1211	BG
425	-1.617	-12.035	E1211	BG
427	-1.665	-12.916	E1211	BG
429	-1.648	-14.580	E1211	BG
431	-1.579	-10.410	E1211	BG
433	-1.400	-14.663	E1211	BG
434	-0.379	-9.858	E1211	BG
435	-0.798	-12.459	E1211	BG
438	-2.037	-12.813	E1211	BG
440	-1.876	-12.581	E1211	BG
443	-2.063	-10.038	E1211	BG
501	2.457	-16.952	E1211	BG
502	3.099	-16.479	E1211	BG
504	2.516	-17.690	E1211	BG
505.5	2.748	-17.298	E1211	BG
506	2.815	-16.944	E1211	BG
508	3.294	-18.606	E1211	BG
513	3.222	-18.177	E1211	BG
514	3.484	-18.740	E1211	BG
517	2.319	-18.697	E1211	BG
520.5	2.888	-18.813	E1211	BG
523	2.671	-17.396	E1211	BG
524	1.823	-16.277	E1211	BG
525	2.085	-16.949	E1211	BG
526	1.016	-12.485	E1211	BG
528	1.924	-17.276	E1211	BG
530	1.604	-9.769	E1211	BG
531	1.251	-9.240	E1211	BG
532	-0.502	-16.525	E1211	BG
532.5	-0.224	-17.365	E1211	BG
532.8	0.177	-17.978	E1211	BG

533	-0.588	-16.362	E1211	BG
565	1.658	-19.754	E1211	BG
566	3.104	-18.281	E1211	BG
567	1.736	-19.216	E1211	BG
568	3.276	-17.200	E1211	BG
569	1.065	-12.932	E1211	BG
571	-0.061	-10.975	E1211	BG
572	-0.041	-10.911	E1211	BG
574	-2.483	-10.259	E1211	BG
575	-0.344	-10.313	E1211	BG
577	-0.401	-11.579	E1211	BG
579	0.024	-9.381	E1211	BG
581	-0.042	-10.555	E1211	BG
583	0.095	-10.333	E1211	BG
585	-0.605	-10.395	E1211	BG
587	-0.891	-10.979	E1211	BG
589	1.036	-9.455	E1211	BG
592	0.488	-8.349	E1211	BG
594	0.777	-10.216	E1211	BG
596	2.089	-16.385	E1211	BG
598	1.094	-13.446	E1211	BG
600	-0.080	-33.059	E1211	BG
602	-0.428	-13.652	E1211	BG
604	-0.986	-15.911	E1211	BG
606	-1.469	-13.391	E1211	BG
608	-1.451	-13.045	E1211	BG
611	-1.826	-9.053	E1211	BG
612	-1.496	-9.588	E1211	BG
613	-1.786	-11.070	E1211	BG
614	-1.460	-17.346	E1211	BG
615	-1.830	-9.008	E1211	BG
616	-1.587	-15.601	E1211	BG
618	-1.520	-9.383	E1211	BG
620	-0.135	-9.659	E1211	BG
622	-0.266	-12.225	E1211	BG
624	-0.390	-13.710	E1211	BG
628	-2.010	-10.436	E1211	BG
632	-1.881	-13.477	E1211	BG
636	-1.470	-14.134	E1211	BG
639	-1.956	-11.816	E1211	BG
643	-2.410	-8.479	E1211	BG
645	-2.453	-8.695	E1211	BG
648	-2.755	-9.350	E1211	BG
671	-2.241	-9.484	E1211	BG
682	-3.541	-11.853	E1211	BG
685	-0.547	-15.833	E1211	BG
688	-2.291	-14.783	E1211	BG

Khunkher Gorge

Appendix A7

m corrected	d13C	d18O	section	Fm
0	-0.804	-13.685	E1138	BG
2	-2.257	-12.296	E1139	BG
5	-2.448	-14.407	E1140	BG
6	-5.260	-9.348	E1141	BG
7	0.530	-20.280	E1142	BG
12	-1.799	-15.459	E1143	BG
13	-1.386	-15.400	E1144	BG
19	-3.123	-13.919	E1145	BG
22	-3.959	-10.635	E1146	BG
25	-4.814	-9.303	E1147	BG
27	-4.610	-9.693	E1148	BG
29	-4.307	-14.167	E1149	BG
30	-6.797	-9.665	E1150	BG
31	-3.285	-12.691	E1151	BG
32	-3.252	-14.228	E1152	BG
50	-2.601	-17.465	E1153	BG
58	0.311	-12.718	E1154	BG
59	-0.792	-11.821	E1155	BG
63	-1.887	-11.195	E1156	BG
64	-2.524	-12.226	E1157	BG
66	-2.706	-11.453	E1158	BG
68.5	-1.979	-10.929	E1159	BG
70	-2.520	-11.022	E1160	BG
72	-3.085	-11.084	E1161	BG
73	-2.971	-11.131	E1162	BG
74	-3.296	-11.668	E1163	BG
75	-2.759	-10.532	E1164	BG
76	-2.888	-10.698	E1165	BG
77	-3.295	-11.160	E1166	BG
79	-2.776	-10.954	E1167	BG
84	-2.634	-10.594	E1168	BG
85	-3.408	-11.320	E1169	BG
92.5	-3.347	-11.515	E1170	BG
95	-2.856	-11.136	E1171	BG
98	-2.179	-10.611	E1172	BG
99	-1.677	-12.722	E1173	BG
106	-1.892	-10.633	E1174	BG
107	-1.787	-10.758	E1175	BG
108	-1.708	-9.978	E1176	BG
118	-3.368	-9.485	E1177	BG
120	-1.945	-10.567	E1178	BG
121	-2.754	-9.987	E1179	BG
123	-3.277	-10.441	E1180	BG
128	-3.136	-9.686	E1181	BG
129.5	-3.577	-11.109	E1182	BG
132	-1.282	-10.989	E1183	BG
134	-0.687	-9.022	E1184	BG
138	-2.828	-11.005	E1185	BG
140	-2.264	-11.647	E1186	BG

146	-1.345	-8.726	E1187	BG
148	-1.821	-9.892	E1188	BG
151	-2.216	-10.046	E1189	BG
152	-2.337	-9.537	E1190	BG
154	-2.431	-12.732	E1191	BG
156	-2.257	-8.984	E1192	BG
158	-2.167	-9.580	E1193	BG
161	-0.755	-9.655	E1194	BG
162	0.048	-9.362	E1195	BG
164	0.122	-9.267	E1196	BG
166	-0.498	-8.295	E1197	BG
168	-0.873	-8.106	E1198	BG
170	-0.292	-8.798	E1199	BG
172	0.182	-7.377	E1200	BG
177	2.087	-12.367	E1201	BG
180	0.800	-10.765	E1202	BG
190	1.764	-10.078	E1203	BG
192	0.157	-11.478	E1204	BG
197	0.555	-11.996	E1205	BG
199	-0.552	-12.429	E1206	BG
201	0.231	-11.241	E1207	BG
203	-1.531	-10.648	E1208	BG
205	1.654	-10.753	E1209	BG
207	0.607	-11.242	E1210	BG
209	0.333	-10.833	E1211	BG
211	0.816	-10.470	E1212	BG
213	0.733	-7.200	E1213	BG
215	0.968	-10.962	E1214	BG
217	2.316	-9.733	E1215	BG
217	2.277	-9.752	E1216	BG
219	3.144	-9.157	E1217	BG
221	2.596	-8.825	E1218	BG
223	-0.671	-7.877	E1219	BG
225	0.372	-15.569	E1220	BG
225	0.297	-15.545	E1221	BG
227	0.903	-9.387	E1222	BG
228	2.332	-9.908	E1223	BG
229	3.472	-13.366	E1224	BG
232	4.497	-14.501	E1225	BG
237	3.264	-11.353	E1226	BG
246	-0.708	-14.965	E1227	BG
296.5	-2.245	-15.995	E1228	BG
324	-1.692	-11.161	E1229	BG
326	-2.043	-10.997	E1230	BG
327	-2.469	-11.011	E1231	BG
328	-1.688	-10.237	E1232	BG
331	-2.941	-10.063	E1233	BG
334	-2.382	-9.794	E1234	BG
336	-2.062	-9.745	E1235	BG
336	-2.029	-9.898	E1236	BG

337.5	-1.958	-9.907	E1237	BG
339	-1.775	-9.468	E1238	BG
340.5	2.235	-1.871	E1239	BG
342.5	-1.217	-9.732	E1240	BG
345	-1.570	-10.775	E1241	BG
346	-1.347	-10.818	E1242	BG
348	-1.395	-9.717	E1243	BG
349	-1.431	-9.723	E1244	BG
349	-1.668	-9.546	E1245	BG
352	-1.645	-10.027	E1246	BG
355	0.879	-5.276	E1247	BG
356	-1.966	-9.669	E1248	BG
357	-1.820	-11.332	E1249	BG
358	-1.932	-10.526	E1250	BG
359	-1.208	-9.897	E1251	BG
360	-1.269	-8.759	E1252	BG
361	-1.547	-8.622	E1253	BG
362	-1.811	-10.704	E1254	BG
363	-1.859	-9.285	E1255	BG
364	-1.983	-8.839	E1256	BG
365	-1.900	-10.170	E1257	BG
366	-2.161	-8.817	E1258	BG
367	-2.076	-8.529	E1259	BG
417	-2.692	-12.481	E1260	BG
418	-2.830	-10.098	E1261	BG
419	-2.588	-11.492	E1262	BG
420	-2.777	-11.731	E1263	BG
421	-2.648	-14.852	E1264	BG
422	-2.471	-13.131	E1265	BG
423	-2.965	-15.107	E1266	BG
424	-3.233	-15.568	E1267	BG
563	-1.130	-16.306	E1268	BG
588	0.678	-17.215	E1269	BG
603	0.469	-16.140	E1270	BG
603.5	0.232	-15.669	E1271	BG
618	-1.144	-17.675	E1272	BG
634	-0.978	-17.708	E1273	BG
635	-1.142	-15.992	E1274	BG
645	-0.892	-13.410	E1275	BG
646	-1.286	-13.782	E1276	BG
654.5	-1.773	-15.479	E1277	BG
660	3.124	-15.292	E1278	BG
661	3.634	-15.277	E1279	BG
676	-1.422	-14.568	E1280	BG
677	-0.676	-15.466	E1281	BG
678	-1.526	-13.891	E1282	BG
679	-1.612	-10.330	E1283	BG
680	-1.784	-9.188	E1284	BG
681	-1.123	-12.703	E1285	BG
683	-1.261	-11.688	E1286	BG

686	-1.662	-10.744	E1287	BG
687	-1.334	-15.919	E1288	BG
688	-1.442	-9.410	E1289	BG
694	0.896	-13.464	E1290	BG
695	0.844	-13.252	E1291	BG
702.5	-0.883	-13.807	E1292	BG
703	-0.275	-13.374	E1293	BG
703.5	-0.420	-13.203	E1294	BG
704.5	0.960	-15.129	E1295	BG
705.5	0.524	-15.154	E1296	BG
706.5	0.606	-17.374	E1297	BG
707.5	1.482	-14.104	E1298	BG
708.5	2.339	-17.248	E1299	BG
777	-0.216	-15.749	E1300	BG
778	-0.400	-15.558	E1301	BG
779	-0.497	-17.430	E1302	BG
792	0.607	-14.752	E1303	BG
792.7	0.584	-16.075	E1304	BG
793	0.677	-14.086	E1305	BG
793.1	0.698	-15.585	E1306	BG
793.8	0.733	-14.683	E1307	BG
794.6	0.427	-15.079	E1308	BG
795	0.633	-17.175	E1309	BG
796	0.591	-16.603	E1310	BG
803	0.823	-20.816	E1311	BG
804	0.859	-14.102	E1312	BG
805	0.794	-15.844	E1313	BG
834	-0.151	-13.561	E1314	BG
849	1.476	-14.350	E1315	BG
855	1.927	-15.139	E1316	BG
892	5.870	-14.651	E1317	BG
937	2.826	-14.357	E1318	BG
941	2.514	-14.885	E1319	BG
1065	4.170	-13.016	E1320	BG
1066	4.336	-12.449	E1321	BG
1067	4.410	-12.769	E1322	BG
1068	4.762	-12.964	E1323	BG
1069	5.031	-12.940	E1324	BG
1070	5.352	-10.003	E1325	BG
1071	5.933	-12.722	E1326	BG
1073	5.346	-12.828	E1327	BG
1074	5.427	-10.384	E1328	BG

Orolgo Gorge

m corrected	d13C	d18O	section	Fm
53	-2.482	-11.899	E1220	BG
54	-2.564	-12.360	E1220	BG
56	-3.070	-12.247	E1220	BG

57	-4.138	-11.350	E1220	BG
78.5	2.285	-11.190	E1220	BG
80	-0.545	-11.551	E1220	BG
81	-0.525	-10.287	E1220	BG
82	1.939	-11.124	E1220	BG
83	4.233	-10.908	E1220	BG
84	4.442	-10.424	E1220	BG
84.1	4.604	-9.548	E1220	BG
85	0.038	-10.928	E1220	BG
85.5	3.139	-9.642	E1220	BG
86	1.276	-10.893	E1220	BG
87	0.300	-11.306	E1220	BG
91	2.646	-11.453	E1220	BG
91.8	2.028	-9.199	E1220	BG
93	2.801	-11.385	E1220	BG
107	1.643	-10.380	E1220	BG
108	5.337	-10.104	E1220	BG
109	2.835	-10.279	E1220	BG
110	2.776	-10.685	E1220	BG
112	3.142	-10.902	E1220	BG
124	5.951	-9.869	E1220	BG
125	5.492	-9.436	E1220	BG
126	6.089	-9.568	E1220	BG
127	4.868	-8.743	E1220	BG
128	5.538	-9.463	E1220	BG
129	5.759	-9.494	E1220	BG
130	6.797	-8.720	E1220	BG
131	6.764	-9.887	E1220	BG
132	4.864	-9.651	E1220	BG
133	4.420	-9.781	E1220	BG
135	5.363	-8.397	E1220	BG
137.5	0.619	-9.286	E1220	BG
137.65	-1.677	-10.800	E1220	BG
138	-1.065	-11.601	E1220	BG
138.5	-0.631	-10.797	E1220	BG
139	-1.889	-11.476	E1220	BG
139.5	-2.307	-11.652	E1220	BG
139.7	-2.131	-11.446	E1220	BG
140	-2.091	-11.539	E1220	BG
140.5	-2.046	-11.483	E1220	BG
141	-2.105	-11.660	E1220	BG
141.5	-1.959	-11.378	E1220	BG
142	-1.783	-11.443	E1220	BG
143	-0.749	-11.145	E1220	BG
144	-1.116	-8.440	E1220	BG
145	-1.817	-11.139	E1220	BG
146	-1.961	-8.035	E1220	BG
147	-0.964	-7.512	E1220	BG
148	-0.394	-9.542	E1220	BG
149	-0.811	-11.248	E1220	BG

150	-0.454	-10.746	E1220	BG
151	-1.661	-11.433	E1220	BG
152	-1.053	-12.119	E1220	BG
153	-0.287	-11.959	E1220	BG
154	-0.132	-11.933	E1220	BG
156	1.430	-11.968	E1220	BG
157	0.354	-11.266	E1220	BG
375.5	-0.884	-13.464	E1220	BG
377	0.309	-12.879	E1220	BG
378	0.634	-13.986	E1220	BG
379	0.685	-13.589	E1220	BG
380	0.090	-13.974	E1220	BG
381	-0.560	-13.926	E1220	BG
382	-1.339	-14.016	E1220	BG
386	-0.043	-12.467	E1220	BG
387	-0.832	-14.087	E1220	BG
392	2.156	-13.902	E1220	BG
393	2.403	-14.102	E1220	BG
394	1.367	-13.269	E1220	BG
395	0.658	-14.073	E1220	BG
406	-0.815	-14.073	E1220	BG
407	-0.827	-13.878	E1220	BG
408	-0.784	-13.104	E1220	BG
409	-0.912	-10.440	E1220	BG
410	-0.273	-12.713	E1220	BG
412	1.834	-13.628	E1220	BG
414	2.138	-13.421	E1220	BG
416	2.163	-13.369	E1220	BG
417	2.204	-13.534	E1220	BG
418	2.193	-13.430	E1220	BG
419	2.155	-13.428	E1220	BG
420	2.402	-13.179	E1220	BG
421	2.168	-13.483	E1220	BG
422	2.506	-13.252	E1220	BG
423	2.172	-12.938	E1220	BG
424	2.859	-13.548	E1220	BG
425	2.488	-13.354	E1220	BG
426	2.822	-13.610	E1220	BG
428.5	0.512	-13.792	E1220	BG
454	-0.551	-13.556	E1220	BG
456	-1.428	-14.414	E1220	BG
471	-1.461	-13.183	E1220	BG
473	-1.736	-13.524	E1220	BG
475	-1.815	-13.750	E1220	BG
477	-1.128	-11.040	E1220	BG
479	-1.093	-11.192	E1220	BG
481	-1.322	-12.445	E1220	BG
483	-1.793	-11.282	E1220	BG
485	-0.911	-12.774	E1220	BG
487	-1.061	-11.965	E1220	BG

489	-1.326	-12.425	E1220	BG
491	-1.530	-12.564	E1220	BG
493	-0.812	-10.982	E1220	BG
495	-1.117	-12.331	E1220	BG
497	-0.845	-12.359	E1220	BG
499	1.355	-8.195	E1220	BG
501	2.612	-12.584	E1220	BG
503	2.901	-12.619	E1220	BG
505	-0.008	-12.532	E1220	BG
507	1.562	-12.337	E1220	BG
520	-0.874	-12.658	E1220	BG
523	-1.547	-12.496	E1220	BG
525	-1.513	-11.869	E1220	BG
527	-1.337	-12.813	E1220	BG
529	-1.814	-10.925	E1220	BG
538	0.127	-13.029	E1220	BG
539	-0.857	-13.552	E1220	BG
541	-0.728	-12.698	E1220	BG
543	-0.314	-12.793	E1220	BG
545	-0.879	-13.223	E1220	BG
547	-0.674	-12.095	E1220	BG
549	-0.173	-8.463	E1220	BG
551	0.122	-8.606	E1220	BG
552	-0.366	-13.005	E1220	BG
555	-0.463	-13.009	E1220	BG
557	-0.565	-14.322	E1220	BG
584.5	0.075	-14.645	E1220	BG
586	0.096	-14.805	E1220	BG
587	-0.303	-15.214	E1220	BG
589	1.016	-14.625	E1220	BG
591	0.062	-14.967	E1220	BG
598.5	-0.383	-14.360	E1220	BG
605	0.342	-13.745	E1220	BG
668.5	-3.133	-13.741	E1220	BG
674	-0.793	-13.593	E1220	BG
676.5	-0.683	-13.496	E1220	BG
686	-0.756	-13.266	E1220	BG
687	-1.681	-13.295	E1220	BG
689	2.680	-13.268	E1220	BG
690	-0.325	-12.935	E1220	BG
692	-0.653	-12.873	E1220	BG
694	-0.812	-12.034	E1220	BG
695.5	-1.210	-12.001	E1220	BG
707	-0.491	-12.202	E1220	BG
709	-0.171	-12.478	E1220	BG
714	-0.362	-11.808	E1220	BG
722.9	0.761	-9.491	E1220	BG
724	1.299	-5.170	E1220	BG
728	0.197	-9.458	E1220	BG
730	1.809	-9.128	E1220	BG

732	0.521	-8.473	E1220	BG
734	1.015	-7.427	E1220	BG
739	0.416	-9.271	E1220	BG
743	0.068	-7.393	E1220	BG
744	-0.247	-7.002	E1220	BG
745	-0.052	-6.587	E1220	BG
748	-0.671	-7.920	E1220	BG
750	-0.865	-7.238	E1220	BG
757	-0.564	-8.436	E1220	BG
760	-0.451	-6.504	E1220	BG
761	-0.945	-6.894	E1220	BG
763	-1.400	-7.758	E1220	BG
765	-0.520	-7.792	E1220	BG
766	-0.389	-7.396	E1220	BG
767	-1.003	-7.219	E1220	BG
769	-1.530	-7.165	E1220	BG
769	-1.594	-7.288	E1220	BG
771	-0.564	-7.808	E1220	BG
773	-0.278	-7.902	E1220	BG
775	-0.871	-7.333	E1220	BG
777	-0.926	-7.371	E1220	BG
779	-0.966	-8.201	E1220	BG
781	-0.947	-7.162	E1220	BG
783	-0.992	-7.280	E1220	BG
785	-1.129	-7.332	E1220	BG
787	-1.155	-7.769	E1220	BG
789	-1.429	-7.637	E1220	BG
791	-1.329	-7.501	E1220	BG
793	-1.387	-7.306	E1220	BG
795	-1.166	-7.067	E1220	BG
796	-1.220	-7.423	E1220	BG
798	-1.345	-8.236	E1220	BG
799	-1.166	-8.223	E1220	BG
801	-0.935	-8.415	E1220	BG
802	-0.664	-7.456	E1220	BG
803	-0.849	-7.918	E1220	BG
804	-0.909	-8.264	E1220	BG
806	-1.079	-8.099	E1220	BG
807	-1.333	-8.056	E1220	BG
808	-1.942	-8.136	E1220	BG
810	-0.771	-7.568	E1220	BG
811	-0.851	-7.731	E1220	BG
812	-0.960	-7.444	E1220	BG
813	-0.812	-7.316	E1220	BG
814	-0.234	-7.399	E1220	BG
815	-0.182	-7.215	E1220	BG
816	0.093	-6.907	E1220	BG
817	-0.273	-7.141	E1220	BG
818	-1.375	-9.431	E1220	BG
819	-1.137	-9.367	E1220	BG

821	-0.263	-8.711	E1220	BG
822	0.349	-6.010	E1220	BG
823	-0.834	-7.569	E1220	BG
825	-0.829	-8.405	E1220	BG
830	-0.365	-8.121	E1220	BG
832	0.529	-9.108	E1220	BG
834	1.006	-10.068	E1220	BG
836	0.540	-10.168	E1220	BG
838	1.675	-8.057	E1220	BG
839	1.729	-8.783	E1220	BG
927	-0.075	-13.215	E1220	BG
930.5	0.347	-12.870	E1220	BG
932	0.388	-12.018	E1220	BG
934	0.187	-12.673	E1220	BG
936	0.335	-12.236	E1220	BG
938	0.774	-13.005	E1220	BG
940	0.758	-12.292	E1220	BG
996	0.510	-12.655	E1220	BG
998	0.777	-12.638	E1220	BG
999	0.800	-12.382	E1220	BG
1000	0.807	-11.779	E1220	BG
1001	1.069	-11.465	E1220	BG
1002	1.171	-10.815	E1220	BG
1004	1.824	-12.340	E1220	BG
1016	2.661	-11.502	E1220	BG
1017	0.167	-13.554	E1220	BG
1018	3.262	-10.765	E1220	BG
1019	3.123	-11.773	E1220	BG
1020	3.217	-10.143	E1220	BG
1022	2.996	-10.514	E1220	BG
1023	2.914	-10.972	E1220	BG
1024	3.544	-9.067	E1220	BG
1025	3.640	-9.890	E1220	BG
1026	4.874	-10.173	E1220	BG
1027	6.061	-9.773	E1220	BG
1028	5.857	-10.573	E1220	BG
1029	6.202	-10.501	E1220	BG
1030	5.608	-9.952	E1220	BG
1035	5.463	-10.884	E1220	BG
1044	5.495	-11.039	E1220	BG
1045	5.811	-10.712	E1220	BG
1052	6.035	-11.023	E1220	BG
1053	4.874	-10.869	E1220	BG
1054	3.176	-8.301	E1220	BG
1055	4.139	-10.800	E1220	BG
1056	4.157	-10.751	E1220	BG
1057	3.969	-10.702	E1220	BG
1058	4.003	-12.118	E1220	BG
1059	3.914	-12.726	E1220	BG
1060	4.189	-9.439	E1220	BG

1061	4.236	-9.320	E1220	BG
1063	4.068	-10.281	E1220	BG
1064	4.245	-10.584	E1220	BG
1065	4.197	-9.819	E1220	BG
1066	4.167	-10.319	E1220	BG
1067	4.340	-10.038	E1220	BG
1068	4.269	-10.274	E1220	BG
1069	4.380	-10.125	E1220	BG
1070	4.289	-9.852	E1220	BG
1071	4.269	-9.932	E1220	BG
1072	4.159	-10.207	E1220	BG
1073	4.153	-9.849	E1220	BG
1074	4.312	-9.775	E1220	BG
1075	6.070	-10.096	E1220	BG
1076	5.997	-9.884	E1220	BG
1077	4.578	-10.149	E1220	BG
1078	4.397	-10.052	E1220	BG
1079	4.142	-9.797	E1220	BG
1080	4.003	-10.794	E1220	BG
1081	3.949	-10.052	E1220	BG
1082	4.255	-10.299	E1220	BG
1084	3.955	-10.011	E1220	BG
1086	3.519	-10.327	E1220	BG
1087	3.038	-10.889	E1220	BG
1088	3.206	-11.313	E1220	BG
1089	3.589	-11.260	E1220	BG
1092	3.098	-11.319	E1220	BG
1094	3.115	-10.893	E1220	BG
1095.5	3.372	-11.411	E1220	BG
1099	3.442	-11.778	E1220	BG
1100	2.726	-11.976	E1220	BG
1103	3.168	-11.807	E1220	BG
1104.5	2.647	-12.244	E1220	BG
1106.6	3.555	-12.333	E1220	BG
1110	3.139	-12.482	E1220	BG
1112	3.492	-10.576	E1220	BG
1116	3.451	-11.894	E1220	BG
1118	3.160	-9.299	E1220	BG
1120	2.875	-7.822	E1220	BG
1122	2.807	-9.315	E1220	BG
1124	2.874	-9.971	E1220	BG
1125	2.814	-9.239	E1220	BG
1127	3.391	-8.859	E1220	BG
1129	3.055	-9.029	E1220	BG
1131	2.781	-10.063	E1220	BG
1133	2.649	-10.199	E1220	BG
1134	3.411	-9.743	E1220	BG
1136	2.338	-12.614	E1220	BG
1162	1.595	-11.850	E1220	BG
1164.5	2.087	-12.943	E1220	BG

1167.5	2.101	-13.643	E1220	BG
1169	2.126	-12.372	E1220	BG
1171	2.105	-12.237	E1220	BG
1179	2.170	-11.999	E1220	BG
1181	2.296	-12.295	E1220	BG
1207.5	3.493	-12.223	E1220	SG
1210	4.398	-11.067	E1220	SG
1211	4.189	-10.036	E1220	SG
1213	4.309	-11.925	E1220	SG
1215	4.401	-9.765	E1220	SG
1225.5	3.259	-13.386	E1220	SG
1226	4.079	-8.896	E1220	SG
1226.5	3.554	-12.276	E1220	SG
1229	3.747	-10.198	E1220	SG
1232	3.980	-11.861	E1220	SG
1234	3.699	-12.299	E1220	SG
1236.5	3.991	-12.693	E1220	SG
1238	3.861	-13.075	E1220	SG
1240	4.016	-11.302	E1220	SG
1242	4.044	-9.846	E1220	SG
1245	4.140	-12.464	E1220	SG
1247	4.273	-12.284	E1220	SG
1250	4.375	-10.869	E1220	SG
1250.7	4.423	-10.975	E1220	SG
1251.7	4.390	-10.853	E1220	SG
1253	4.376	-9.148	E1220	SG
1255.5	3.998	-14.094	E1220	SG
1257.8	4.347	-9.641	E1220	SG
1259.8	4.134	-10.207	E1220	SG
1262.8	4.461	-9.170	E1220	SG
1264	4.341	-10.214	E1220	SG
1265.8	4.620	-9.906	E1220	SG
1267.6	4.315	-11.593	E1220	SG
1269.5	4.608	-9.395	E1220	SG
1272	4.203	-10.611	E1220	SG
1274	4.018	-12.706	E1220	SG
1278	4.479	-9.750	E1220	SG
1280	4.386	-10.419	E1220	SG
1282	4.562	-9.048	E1220	SG
1284	4.690	-8.402	E1220	SG
1286	4.697	-8.797	E1220	SG
1288	4.592	-9.278	E1220	SG
1290	4.532	-9.896	E1220	SG
1292	5.080	-9.302	E1220	SG
1294	5.168	-10.033	E1220	SG
1296	5.108	-9.614	E1220	SG
1298	5.086	-9.511	E1220	SG
1300	5.029	-9.539	E1220	SG
1302	4.460	-9.233	E1220	SG
1304	5.024	-8.700	E1220	SG

1305.3	4.981	-8.324	E1220	SG
1307	4.907	-8.742	E1220	SG
1310	4.944	-9.472	E1220	SG
1312	5.020	-8.911	E1220	SG
1314	5.199	-9.371	E1220	SG
1316	4.902	-8.100	E1220	SG
1318	4.897	-9.029	E1220	SG
1320	4.689	-8.863	E1220	SG
1322	4.658	-7.344	E1220	SG
1326	5.287	-9.057	E1220	SG
1328	5.561	-9.273	E1220	SG
1330	4.973	-9.810	E1220	SG
1332	6.019	-8.393	E1220	SG
1336	5.228	-9.804	E1220	SG
1337.5	5.862	-10.465	E1220	SG
1340	6.435	-9.347	E1220	SG
1342	5.181	-11.893	E1220	SG
1343.5	6.033	-9.957	E1220	SG
1345	6.764	-10.334	E1220	SG
1347	5.430	-11.175	E1220	SG
1353	5.407	-11.045	E1220	SG
1358	7.005	-11.434	E1220	SG
1360	5.954	-8.649	E1220	SG
1364	4.827	-11.796	E1220	SG
1366	5.074	-12.283	E1220	SG
1366	5.002	-12.346	E1220	SG
1367	5.346	-14.025	E1220	SG
1373	4.478	-6.830	E1220	SG
1375	4.222	-11.683	E1220	SG
1376	4.557	-9.465	E1220	SG
1379	4.235	-10.410	E1220	SG
1381	4.409	-11.336	E1220	SG
1383	4.441	-9.059	E1220	SG
1385	4.454	-8.853	E1220	SG
1387	4.306	-12.365	E1220	SG
1396	4.145	-9.217	E1220	SG
1398	4.025	-10.220	E1220	SG
1399	4.017	-8.921	E1220	SG
1402	4.106	-8.845	E1220	SG
1404	3.889	-8.469	E1220	SG
1406	4.081	-8.753	E1220	SG
1408	4.082	-9.244	E1220	SG
1414	4.165	-10.617	E1220	SG
1416	4.115	-8.566	E1220	SG
1418	4.151	-10.372	E1220	SG
1420	3.746	-14.008	E1220	SG
1423	3.773	-11.350	E1220	SG
1425	3.792	-12.395	E1220	SG
1427	3.789	-10.066	E1220	SG
1429	2.905	-9.452	E1220	SG

1431	3.096	-11.462	E1220	SG
1433	3.731	-11.673	E1220	SG
1437	2.950	-11.158	E1220	SG
1439	2.673	-11.062	E1220	SG
1441	2.528	-9.591	E1220	SG
1443	2.141	-11.807	E1220	SG
1445	2.039	-12.013	E1220	SG
1447	1.732	-14.032	E1220	SG
1451	3.581	-12.133	E1220	SG
1454	3.207	-13.788	E1220	SG
1457	3.517	-12.356	E1220	SG
1461	3.581	-12.856	E1220	SG
1464	3.643	-12.619	E1220	SG
1466	3.843	-11.267	E1220	SG
1468	4.094	-11.041	E1220	SG
1471	4.089	-9.584	E1220	SG
1473	3.929	-9.781	E1220	SG
1475.5	3.664	-10.116	E1220	SG
1477	3.600	-8.914	E1220	SG
1479	3.691	-9.034	E1220	SG
1481	3.640	-7.508	E1220	SG
1483	3.579	-9.851	E1220	SG
1485	3.504	-9.019	E1220	SG
1487	3.620	-9.051	E1220	SG
1489	4.003	-8.764	E1220	SG
1491	3.476	-7.836	E1220	SG
1493	3.337	-9.004	E1220	SG
1495	3.294	-8.780	E1220	SG
1497	3.189	-7.245	E1220	SG
1499	3.138	-7.914	E1220	SG
1501	3.606	-6.902	E1220	SG
1503	3.794	-8.138	E1220	SG
1505	3.753	-8.906	E1220	SG
1506	5.261	-9.838	E1220	SG
1510	3.254	-9.621	E1220	SG
1512	3.285	-8.063	E1220	SG
1514	3.680	-9.688	E1220	SG
1516	3.884	-9.725	E1220	SG
1517	3.587	-9.996	E1220	SG
1521	3.135	-9.189	E1220	SG
1522	3.161	-9.679	E1220	SG
1523	2.951	-8.555	E1220	SG
1525	2.835	-9.683	E1220	SG
1528	2.733	-7.803	E1220	SG
1530	2.723	-7.575	E1220	SG
1532	2.648	-6.979	E1220	SG
1534	2.561	-8.534	E1220	SG
1536	2.624	-8.212	E1220	SG
1538	2.548	-8.146	E1220	SG
1540	2.426	-7.651	E1220	SG

1542	2.422	-9.372	E1220	SG
1545	2.120	-9.853	E1220	SG
1547	2.107	-8.366	E1220	SG
1550	2.128	-8.494	E1220	SG
1552	2.221	-8.819	E1220	SG
1554	2.250	-7.546	E1220	SG
1556	1.968	-7.686	E1220	SG
1558	2.322	-8.579	E1220	SG
1560	2.116	-8.783	E1220	SG
1562	2.082	-8.606	E1220	SG
1564	1.803	-8.175	E1220	SG
1566	1.642	-8.156	E1220	SG
1568	1.517	-9.500	E1220	SG
1570	1.759	-9.269	E1220	SG

Appendix A8. Engraved plates

Three intaglio drypoint prints. All prints were made on an intaglio press at the Bow and Arrow Press in Cambridge, MA. Each print is individually inked, wiped, and printed. The prints are of: A) Zircon grain, B) *Cloudina*, and C) The small shelly fossil, chancelloriid.